# Allqokirus australis (Sparassodonta, Metatheria) from the early Palaeocene of Tiupampa (Bolivia) and the rise of the metatherian carnivorous radiation in South America

Christian De Muizon, Sandrine Ladevèze, Charlène Selva, Robin Vignaud, Florent Goussard

geodiversitas

2018 • 40 • 16

# *Allqokirus australis* (Sparassodonta, Metatheria) from the early Palaeocene of Tiupampa (Bolivia) and the rise of the metatherian carnivorous radiation in South America

Christian de MUIZON, Sandrine LADEVÈZE, Charlène SELVA, Robin VIGNAUD & Florent GOUSSARD

art. 40 (16) — Published on 23 August 2018
www.geodiversitas.com

MUSÉUM
NATIONAL D'HISTOIRE NATURELLE
PUBLICATIONS SCIENTIFIQUES

Couverture / *Cover* :
Reconstitution de la tête d'*Allqokirus australis* en vue latérale (**haut**) et en vue antérolatérale (**bas**)/*Reconstruction of the head of* Allqokirus australis *in lateral view (**top**) and in anterolateral view (**bottom**).*

*Geodiversitas* est indexé dans / Geodiversitas *is indexed in:*
– Science Citation Index Expanded (SciSearch®)
– ISI Alerting Services®
– Current Contents® / Physical, Chemical, and Earth Sciences®
– Scopus®

*Geodiversitas* est distribué en version électronique par / Geodiversitas *is distributed electronically by:*
– BioOne® (http://www.bioone.org)

Les articles ainsi que les nouveautés nomenclaturales publiés dans *Geodiversitas* sont référencés par / *Articles and nomenclatural novelties published in* Geodiversitas *are referenced by:*
– ZooBank® (http://zoobank.org)

***Geodiversitas*** est une revue en flux continu publiée par les Publications scientifiques du Muséum, Paris
**Geodiversitas** *is a fast track journal published by the Museum Science Press, Paris*

Les Publications scientifiques du Muséum publient aussi / *The Museum Science Press also publish:*
***Adansonia***, ***Zoosystema***, ***Anthropozoologica***, ***European Journal of Taxonomy***, ***Naturae***.

Diffusion – Publications scientifiques Muséum national d'Histoire naturelle
CP 41 – 57 rue Cuvier F-75231 Paris cedex 05 (France)
Tél. : 33 (0)1 40 79 48 05 / Fax : 33 (0)1 40 79 38 40
diff.pub@mnhn.fr / http://sciencepress.mnhn.fr


ISSN (imprimé / *print*) : 1280-9659/ ISSN (électronique / *electronic*) : 1638-9395

# *Allqokirus australis* (Sparassodonta, Metatheria) from the early Palaeocene of Tiupampa (Bolivia) and the rise of the metatherian carnivorous radiation in South America

**Christian de MUIZON**
**Sandrine LADEVÈZE**
**Charlène SELVA**
**Robin VIGNAUD**
**Florent GOUSSARD**
CR2P (CNRS, MNHN, Sorbonne Université),
Département Origines et Évolution, Muséum national d'Histoire naturelle,
case postale 38, 57 rue Cuvier, F-75231 Paris cedex 05 (France)

Submitted on 15 January 2018 | accepted on 2 April 2018 | published on 23 August 2018

urn:lsid:zoobank.org:pub:12046AA5-049A-4443-A8DB-F0604DBDAFC1

Muizon C. de, Ladevèze S., Selva C., Vignaud R. & Goussard F. 2018. — *Allqokirus australis* (Sparassodonta, Metatheria) from the early Palaeocene of Tiupampa (Bolivia) and the rise of the metatherian carnivorous radiation in South America. *Geodiversitas* 40 (16): 363-459. https://doi.org/10.5252/geodiversitas2018v40a16. http://geodiversitas.com/40/16

**ABSTRACT**
The present paper describes a disarticulated skull of *Allqokirus australis* Marshall & Muizon, 1988, a basal sparassodont (Metatheria, Mammalia) from the early Palaeocene (*c.* 65 Ma.) of Tiupampa (Bolivia). The specimen includes the rostrum and palate with right premaxilla, both maxillae, left lacrimal, palatines and most upper teeth. The second largest element includes the frontals, the left squamosal, the parietals, the supraoccipital, the basisphenoid, the presphenoid, the alisphenoid, and part of the pterygoids. The nasals, basioccipital and exoccipitals are missing. Other elements are the left petrosal, the right jugal and squamosal, and both dentaries. The elements of the specimen allow for a good reconstruction of the skull, which is thoroughly described and compared to that of other sparassodonts and to the Tiupampa pucadelphyids, *Pucadelphys* and *Andinodelphys*. The dental morphology of *Allqokirus australis* is extremely similar to that of *Patene simpsoni* from the early Eocene of Itaboraí (Brazil) and presents distinct (although incipient) carnivorous adaptations. Furthermore, some characters of the ear region (e.g. medial process of the squamosal, deep groove for the internal carotid artery at the ventral apex of the petrosal) are also present in most other sparassodonts and in the pucadelphyids from the same locality. A parsimony analysis performed on the basis of a data matrix of 364 characters and 38 taxa placed *Allqokirus* in a sparassodont clade (the Mayulestidae) that also included *Mayulestes* and *Patene*. This family constitutes the sister group of all other sparassodonts. Our analysis also retrieved a large clade composed of the sparassodonts and the pucadelphyids, formally named Pucadelphyda n. superord. This superorder represents the large metatherian carnivorous radiation of the Tertiary of South America, which is first known at Tiupampa, and which started to diversify probably slightly earlier, during the late Cretacous in South America. So far, no representative of Pucadelphyda has been discovered in North America. At Tiupampa, *Allqokirus* and *Mayulestes* are the largest metatherians of the fauna and they fill the predaceous mammalian ecological niche. They are the earliest representatives of Sparassodonta, a successful metatherian carnivorous radiation which persisted in South America until the late Pliocene, i.e., during more than 63 Ma.

**KEY WORDS**
Metatheria,
Sparassodonta,
early Palaeocene,
Bolivia,
Phylogeny.

**RÉSUMÉ**
Allqokirus australis *(Sparassodonta, Metatheria) du Paléocène inférieur de Tiupampa (Bolivie) et l'essor de la radiation de métathériens carnivores en Amérique du Sud.*
Le présent article décrit un crâne désarticulé d'*Allqokirus australis* Marshall & Muizon, 1988, un sparassodonte (Metatheria, Mammalia) basal du Paléocène inférieur (*c.* 65 Ma.) de Tiupampa (Bolivie). Le spécimen comprend le rostre et le palais avec le prémaxillaire droit, les deux maxillaires, le lacrimal gauche, les palatins et la plupart des dents jugales. Le deuxième plus gros élément comprend les frontaux, le squamosal gauche, les pariétaux, le supraoccipital, le basisphénoïde, le présphénoïde, l'alisphénoïde et une partie des ptérygoïdes. Les nasaux, le basioccipital et les exoccipitaux manquent. Les autres éléments sont le pétreux gauche, le jugal et le squamosal droits et les deux dentaires. Les éléments du spécimen permettent une bonne reconstitution du crâne, lequel est décrit en détail et comparé à celui des autres sparassodontes ainsi qu'aux « didelphimorphes » de Tiupampa, *Pucadelphys* et *Andinodelphys*. La morphologie dentaire d'*Allqokirus australis* est extrêmement semblable à celle de *Patene simpsoni* de l'Éocène inférieur d'Itaboraí (Brésil) et présente de distinctes adaptations à la carnivorie, bien que celles-ci soient encore peu développées. De plus, certains caractères de la région auditive (processus médial du squamosal et profond sillon pour la carotide interne à l'apex de la face ventrale du pétreux) sont aussi présents chez la plupart des autres sparassodontes et chez les Pucadelphyidae de la même localité. L'analyse de parcimonie réalisée sur la base d'une matrice de données de 364 caractères et 38 taxons a inclus *Allqokirus* dans un clade de sparassodontes, les Mayulestidae, qui contient également *Mayulestes* et *Patene*. Cette famille constitue le groupe-frère de tous les autres sparassodontes. Notre analyse a aussi mis en évidence un grand clade comprenant les Sparassodonta et les Pucadelphyidae, clade formellement désigné sous le nom de Pucadelphyda n. superord. Ce superordre constitue la grande radiation de métathériens carnivores d'Amérique du Sud, connue pour la première fois à Tiupampa et qui a probablement commencé à se diversifier légèrement plus tôt, dans le Crétacé supérieur, en Amérique du Sud. Aucun représentant des Pucadelphyda n'a, pour l'instant, été découvert en Amérique du nord. À Tiupampa, *Allqokirus* et *Mayulestes* sont les plus grands métathériens de la faune et remplissent une niche écologique mammalienne de prédateurs. Ils sont les premiers représentants connus des Sparassodonta, une radiation métathérienne carnivore prospère, qui perdura jusqu'au Pliocène supérieur, c'est-à-dire durant au moins 63 Ma.

**MOTS CLÉS**
Metatheria,
Sparassodonta,
Paléocène inférieur,
Bolivie,
phylogénie.

## INTRODUCTION

Sparassodonts constitute a clade of predaceous metatherians, which occupied the carnivorous-predaceous ecological niche in South America during the Cenozoic (Marshall 1978, 1981; Babot *et al.* 2002; Argot 2004a; Forasiepi 2009). The earliest undisputed sparassodonts are from the early Eocene of Itaboraí (Brazil) (Marshall 1981) and the latest ones are from the late Pliocene of Catamarca and Buenos Aires (Argentina) (Riggs 1934; Marshall 1976a; Goin & Pascual 1987). In the early 1980s, the discovery of the Tiupampa mammal fauna in the Bolivian Andes greatly extended the knowledge of the South American Cenozoic mammal fauna down to the earliest Palaeocene, approximately 65 Ma ago, one Ma after the end of the Cretaceous (Marshall *et al.* 1983; Marshall & Muizon 1988; Muizon 1992; Gelfo *et al.* 2009; Woodburne *et al.* 2014a, b; Muizon *et al.* 1983, 2015; Goin *et al.* 2016). The fauna of Tiupampa (Tiupampan SALMA) includes *c.* 15 taxa of Metatheria and 12 taxa of Eutheria. While eutherian taxa of Tiupampa demonstrate closest affinities to the North American mammal faunas of the early Cenozoic, most of the Tiupampa metatherians are closely related to the South American faunas and even, in some cases, represent plausible morphological ancestors for some metatherian taxa of the late Palaeocene-early Eocene of Itaborai (Marshall & Muizon 1988; Muizon 1992). As a matter of fact, some isolated upper and lower molars of a relatively large (for the fauna) carnivorous metatherian, larger to much larger than those of the insectivorous metatherians of the fauna, were referred to a new taxon, *Allqokirus australis*, showing closer affinities with the sparassodont *Patene simpsoni* from Itaboraí (Brazil) than with any other South American metatherian (Marshall & Muizon 1988; Muizon 1992). In the 1990s, Muizon (1994, 1998) described *Mayulestes ferox*, a second relatively large (as compared to the other taxa of the fauna) carnivorous metatherian from Tiupampa and referred it to the superfamily Borhyaenoidea (*sensu* Muizon 1999), included by Forasiepi (2009) in the order Sparassodonta Ameghino, 1894. This interpretation was followed by Babot *et al.* (2002). Alternatively, other phylogenetic hypotheses have recovered the Tiupampan taxa (i.e., *Mayulestes, Pucadelphys*, and *Andinodelphys*) as a monophyletic stem group of Marsupialia and not specifically the sister taxon to Sparassodonta (e.g. Rougier *et al.* 1998; Babot 2005;

Forasiepi 2009 and derived matrices: Engelman & Croft 2014; Forasiepi *et al.* 2015; Suarez *et al.* 2015). Moreover, in a parsimony analysis that included mostly Recent marsupials (and no unequivocal sparassodonts), Horovitz & Sánchez-Villagra (2003) found a sister-group relationship between *Mayulestes* and *Pucadelphys*. A similar conclusion was obtained by Luo *et al.* (2003) in their analysis, which results in placing *Mayulestes, Pucadelphys* and *Andinodelphys* in the same clade. It is noteworthy that Luo *et al.*'s (2003) analysis did not include unequivocal sparassodonts either. The analysis performed by Ladevèze & Muizon (2007) was inconclusive since, of the two equally parsimonious trees obtained, one included *Mayulestes* in the same clade as *Notogale* and *Sallacyon* (the two other sparassodonts considered in their study), and the other placed *Mayulestes* as the sister taxon of a large clade including from base to top, borhyaenoids, *Asiatherium* + Gurlin Tsav skull, *Didelphodon* + *Pediomys*, pucadelphyids, didelphids, and Australidelphia. However, this study did not support a *Mayulestes-Pucadelphys-Andinodelphys* clade. Goin (2003) considered that the tooth morphology of *Mayulestes* was close to that of the North American Peradectoidea. Subsequently, Goin *et al.* (2016) in their history of South American metatherians, following the interpretation of Rougier *et al.* (1998), Forasiepi (2009), Engelman & Croft (2014), Forasiepi *et al.* (2015), and Suarez *et al.* (2015), did not include *Mayulestes* in Sparassodonta. It is noteworthy however that the three latter publications used the same data matrix as Forasiepi (2009) with almost no revision of the character list and taxa scorings, and consequently obtained the same result for the phylogenetic position of the Tiupampa metatherians. More innovative is the recent analysis of metatherian phylogeny presented by Wilson *et al.* (2016), which recovered four Tiupampa taxa (*Pucadelphys, Andinodelphys, Jaskhadelphys* and *Mayulestes*) and Bohyaenoidea as an early diverging clade, at the base of Marsupialiformes, with no close relationship with Peradectoidea (see discussion below in the phylogeny section).

Here, we describe a partial skull referred to *Allqokirus australis* from the site called "the Quarry" at Tiupampa, Bolivia (Marshall *et al.* 1995) (Fig. 1). This specimen, although not as complete as the holotype and single specimen of *Mayulestes ferox*, allows a fairly good reconstruction of the skull of *Allqokirus australis* and represents a new basis for comparisons between the two Tiupampa macrocarnivorous metatherians (*Allqokirus* and *Mayulestes*) on the one hand and post-Palaeocene sparassodonts on the other hand. We therefore intend to address here the discrepancy mentioned above on the affinities of these Tiupampa carnivorous metatherians having at hand all the Tiupampa specimens of *Pucadelphys*, *Andinodelphys*, *Mayulestes* and *Allqokirus*, which was not the case for most of the previous authors that have considered the phylogenetic relationships of *Mayulestes*. In addition, this study will also lead to consider the early stages of the evolutionary history of the South America metatherian carnivorous radiation.

### Faunal list of the Tiupampa metatherians

Infraclass METATHERIA Huxley, 1880
- Supercohort NOTOMETATHERIA Kirsch, Lapointe & Springer, 1997
  - Cohort "AMERIDELPHIA" Szalay, 1982
    - Superorder Pucadelphyda n.
      - Order SPARASSODONTA Ameghino, 1894
        - Family Mayulestidae Muizon, 1994
          - *Allqokirus australis* Marshall & Muizon, 1988
          - *Mayulestes ferox* Muizon, 1994
      - Order indet.
        - Family Pucadelphyidae Muizon, 1998
          - *Pucadelphys andinus* Marshall & Muizon, 1988
          - *Andinodelphys cochabambensis* Marshall & Muizon, 1988
          - *Mizquedelphys pilpinensis* Marshall & Muizon, 1988
  - Cohort "AMERIDELPHIA" incertae sedis
    - Family Peradectidae Crochet, 1979
      - *Peradectes* cf. *P. austrinum*
    - Family Jaskhadelphyidae Muizon, 1992
      - *Jaskhadelphys minutus* Marshall & Muizon, 1988
    - Family indet.
      - *Incadelphys antiquus* Marshall & Muizon, 1988
      - *Szalinia gracilis* Muizon & Cifelli, 2001
      - *Tiulordia floresi* Marshall & Muizon, 1988
  - Cohort AUSTRALIDELPHIA Szalay, 1982
    - Order POLYDOLOPIMORPHIA Archer, 1984
      - Family Sillustaniidae Crochet & Sigé, 1996
        - *Roberthoffstetteria nationalgeographica* Marshall, Muizon & Sigé, 1983
    - Order MICROBIOTHERIA Ameghino, 1889
      - Family Microbiotheriidae Ameghino, 1887
        - *Khasia cordillierensis* Marshall & Muizon, 1988

### Notes

In the Tiupampa faunal list provided by Muizon *et al.* (2015), because of an editorial lapsus, *Pucadelphys andinus*, *Andinodelphys cochabambensis,* and *Jaskhadelphys minutus* were inadvertently included in the Sparassodonta and not, as originally intended, in an indeterminate order. This error has been corrected here and a slightly modified classification is proposed.

The Polydolopimorphia are included here in the Australidelphia, following Goin *et al.* (2009; 2016); see also Sigé *et al.* (2009).

*Khasia* is referred here to the Microbiotheriidae rather than to the Pediomyidae *contra* Goin *et al.* (2016). Morphological arguments supporting this assignation are provided by Muizon *et al.* (2018).

## MATERIAL AND METHODS

The new specimen of *Allqokirus australis* (MNHC 8267) is a skull of a subadult individual with erupting M4/m4 and P3/p3. The skull is fragmented into seven parts (Fig. 1).

The rostrum and palate form one of the largest elements, which includes the right premaxilla, both maxillae, the left lacrimal and both palatines. The upper teeth are *in situ* and include: the roots of right I2-I5, the root of the right canine, the left canine, P1-M3 of both sides, and right M4. The second largest element includes the frontals, the left squamosal, the parietals, the supraoccipital, the basisphenoid, the presphenoid, the alisphenoid, and part of the pterygoids. The nasals are missing, but a distinct imprint of their most posterior part is observed on the anterior edge of the frontals at the level of the nasal-frontal suture; the basioccipital and exoccipitals are missing. On this element, part of the braincase is preserved, but the parietals have been displaced by post-mortem distortion and dip below the frontals. This distortion has been digitally corrected. The third element is formed by the right squamosal and jugal, and the fourth is the isolated left petrosal. The dentaries comprise the three last elements. The right dentary is complete and bears all its teeth, only missing the crown of i1 and the tip of the protoconid of m3. On the left dentary, the corpus and the ramus lack contact because of breakage. The corpus bears i4-m3 and a fragment of the paraconid of m4; the ramus preserves the coronoid process (missing the anterior base), the condyle, and the angular process.

Anatomical terminology for the description essentially follows Marshall & Muizon (1995) Wible (2003), Forasiepi (2009), and Muizon *et al.* (2015). Dental terminology follows Marshall & Muizon (1995). Lower incisor homology follows Hershkovitz (1982, 1995).

In the following description, closer comparisons are made with other sparassodonts, pucadelphyids (*Andinodelphys* and *Pucadelphys)* and didelphids, but occasional comparisons are also made with dasyurids, thylacinids, and stagodontids.

CT scanning of the seven parts of the specimen MNHC 8267 was performed at the X-ray Tomography Imagery Platform AST-RX (Accès Scientifique à la Tomographie par Rayons X) of the MNHN, using a GE Sensing and Inspection Technologies phoenix|x-ray v|tome|x L240-180 CT scanner. Data processing was undertaken at the 3D imaging facilities lab of the UMR 7207 CR2P (MNHN CNRS UPMC-Paris6). 2 scans were made with an isotropic voxel size of 0.03589524 mm, under a voltage of 100 kV and a current of 270 µA. The data were reconstructed using phoenix datos|x® 2.0 reconstruction software, then exported into a 16 bit TIFF image stack of 1548 and 1730 slices. Mimics® Innovation Suite v.18 (Materialise) was used for segmentation and 3D object rendering for export. Cinema 4D R17 (Maxon) was used for slight retrodeformation, symmetrisation, assembling of parts, reconstruction of missing parts, lighting, and final rendering.

Two versions of the skull are proposed. In Figure 5, the original seven elements have been assembled in order to reconstruct the general morphology of the skull. The parietals and the left lacrimal, which were not *in situ*, have been virtually placed in anatomical articulation with their neighbouring bones, and the rostrum has been virtually connected to the braincase. In Figure 6, a more complete reconstruction is provided, with symmetrisation of best preserved parts and simulation of some missing ones. The bones missing or incomplete on one side of the skull have been virtually replaced by the mirror image of the bone of the other side (i.e., premaxilla, lacrimal, jugal, petrosal, and dentary). The nasals and the medial part of the alveolar process of the premaxillae have been simulated; however, the exoccipital and basioccipital, which are totally missing (with no indication of their extension provided by the adjacent bones) have not been reconstructed.

## PARSIMONY ANALYSIS

A parsimony analysis was conducted to examine the phylogenetic relationships of the two putative sparassodonts from Tiupampa, namely *Allqokirus* and *Mayulestes*, with other sparassodonts and metatherians. The dataset matrix has been established mainly on the basis of that of Forasiepi *et al.* (2015), which we have reworked and for which we have coded new taxa and added new characters. Some characters of Forasiepi *et al.* (2015) have not been included in the present analysis, either because they were not relevant to our taxon sample or because they were redundant with other characters. In the present data matrix, 82 characters were added to that of Forasiepi *et al.* (2015). Some are new and some have been previously used by other authors; in this case, references are given (see list of characters and taxa; Appendices 1 and 2). The scorings are based on studied material and resulted in a significant revision and changes of some codings (changes are indicated in the character list). As a matter of fact, many specimens that were coded from indirect observations (literature, older osteological matrices) were misinterpreted for some features. Moreover, we removed some sparassodonts from the matrix since the resolution of the relationships within Sparassodonta is not the focus of the present study. However, we have retained representatives of the major sparassodont groups. Generally, the early diverging taxa and those with rather complete cranial remains have been retained in the present matrix. The revised and updated matrix is available in supplementary data — http://sciencepress.mnhn.fr/sites/default/files/documents/en/file1.nex) and in Morphobank (http://morphobank.org).

Our dataset contains a total of 364 osteological characters (102 dental, 16 mandibular, 124 cranial, 122 post-cranial), examined in three outgroup and 35 ingroup taxa (fossil and extant metatherians). The character list is given in Appendix 1. The three outgroup taxa are fossil eutherians, the sister group to Metatheria. They include *Prokennalestes* from the Early Cretaceous of Mongolia and which is known from upper and lower postcanine teeth, dentaries, and one petrosal (Kielan-Jaworowska & Dashzeveg 1989; Sigogneau-Russell *et al.* 1992; Wible *et al.* 2001). Other outgroup taxa are *Maelestes*, represented by the skull,

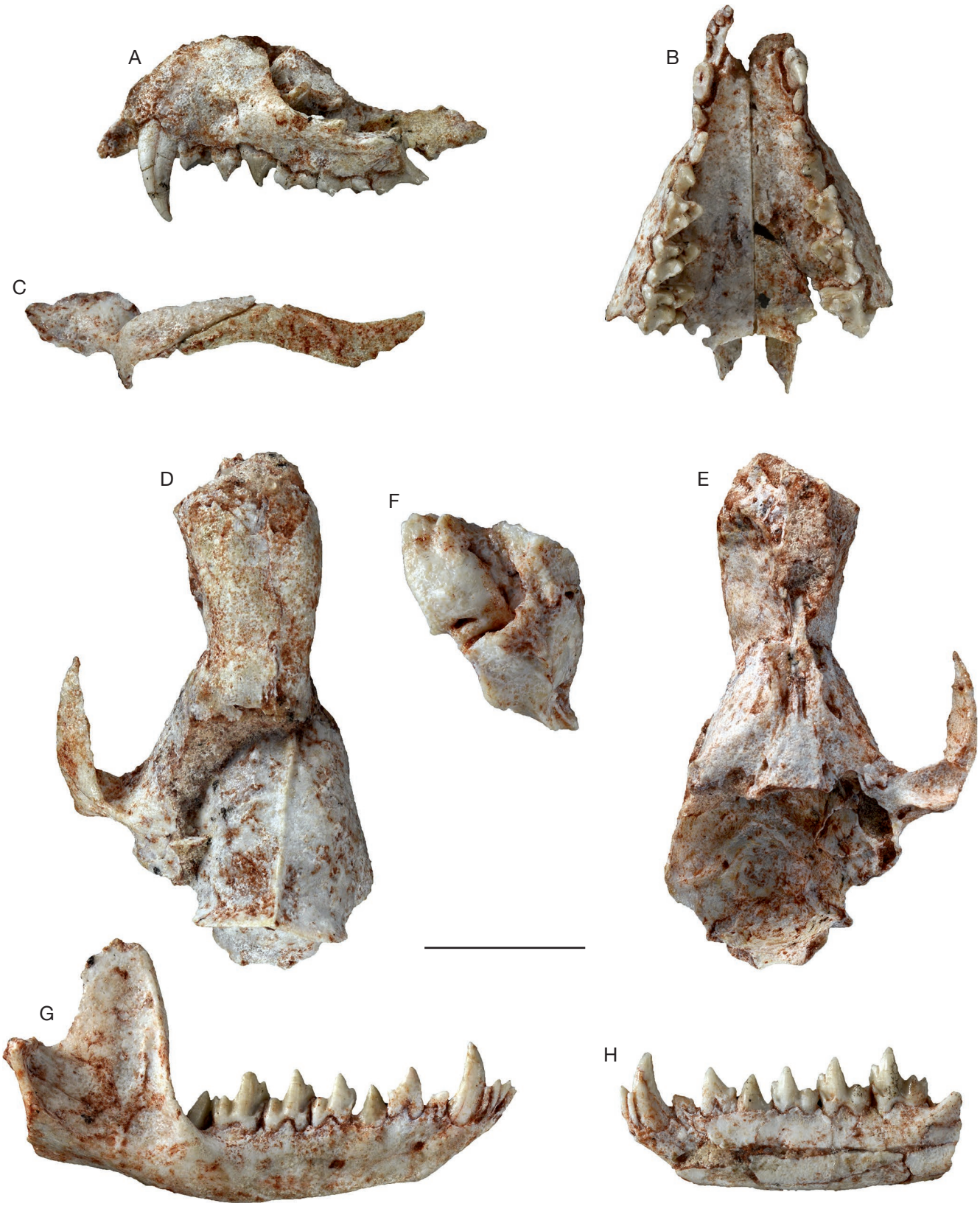


FIG. 1. — *Allqokirus australis*: preserved elements of the cranium and mandible of MHNC 8267: **A**, rostrum in left lateral view; **B**, rostrum in ventral view; **C**, zygomatic arch in lateral view; **D**, braincase and frontals in dorsal view; **E**, braincase and frontals in ventral view; **F** petrosal in ventral view; **G**, right mandible in lateral view; **H**, left mandible in lateral view. Scale bar: A, B, C, D, E, G, H, 1 cm; F, 5 mm.

mandible, anterior vertebrae, and partial left forelimb, and *Asioryctes*, represented by several complete skulls and skeletons, both from the Late Cretaceous of Mongolia (Wible *et al.* 2009; Kielan-Jaworowska 1977, 1981). Ingroup taxa include metatherians that belong to different lineages. To test the phylogenetic affinities of *Mayulestes* and *Allqokirus*, we included 15 post-Palaeocene sparassodonts, mostly represented by well-preserved material, and other well-preserved fossil metatherians (pucadelphyids, stagodontids, peradectids, herpetotheriids, deltatheridiids, *Kokopellia*, and *Asiatherium*). We also included selected Recent marsupials amongst the least derived clades (didelphids, *Dromiciops*, dasyurids, and *Thylacinus*). The complete list of the sampled taxa is given in Appendix 2.

A frequent issue in parsimony analyses concerns the question of the dependency of morphological characters. In the present analysis, we detected some partially dependent characters, most of them being related to the dental morphology. It is obvious that, when a feature is described by many characters, or when a feature responds to the same constraints as another one (for instance, occlusion), some redundancy is inevitable. As a matter of fact, a single cusp may be described by many characters in order to render its presence, its shape, its length, its width, all of its descriptors being closely related but not always redundant (i.e., not scored the same). For some of them, it was inappropriate to merge the different states of the characters because the observed states could not be formalised into a single observation (combining for example length and width, or proportions and localisation) for our sample. If we would have done so, it would have resulted in characters with far too many states, in some cases over 7 states, sometimes with a state being present in only one taxon. We believe that scoring a series of non-redundant (at least not fully redundant) characters, instead of one single multistate character, better reflects the observed morphological diversity. Another example is the relationship between upper and lower cheek teeth. The morphology of the upper molars is obviously tightly related to that of the lower molars, and it is clear that some redundancy exists in the scoring of both structures. However, when comparing the scorings of the characters, an exact similarity between upper and lower molars characters is never observed. This demonstrates that, at least for some of their scorings, these characters provide significant independent information. Therefore, in our analysis, the only characters that were not considered are those having 100% similarity with another character of our list, being therefore fully redundant.

The taxon/character states matrix was analysed using heuristic parsimony searches implemented by PAUP* (Swofford 2002). Each heuristic parsimony search employed 1000 replicates of random taxon addition with TBR branch swapping, saving up to 10 trees. The phylogenetic tree with morphological character state optimisations was generated by PAUP* (Swofford 2002) and Winclada v.1.00.08 (Nixon 2008). Polymorphic taxa were coded with multiple character state entries. Most multistate characters were treated as unordered, but 57 of them were considered as additive (because previous studies have assumed they are morphoclines or because we suspected them to be; see list of characters, Appendix 1). Branch support was assessed by calculating the Bremer index (Bremer 1988) with PAUP* (Swofford 2002) (heuristic searches with 1000 replications, saving up to 10 trees, TBR branch swapping).

The list of generic and specific taxa cited in the text with authorship and date of publication is given on Appendix 3.

INSTITUTIONAL ABBREVIATIONS

| | |
|---|---|
| AMNH | American Museum of Natural History, New York; |
| DGM | Divisão de Geología e Mineralogía do Departamento Nacional da Produção Mineral, Rio de Janeiro; |
| FMNH | Field Museum of Natural History, Chicago; |
| IVPP | Institute of Vertebrate Paleontology and Paleoanthropology, Chinese Academy of Sciences, Beijing; |
| IEEUACG | Instituto de Ecología y Evolución, Universidad Austral de Chile, Valdivia; |
| MACN | Museo Argentino de Ciencias Naturales "Bernardino Rivadavia", Buenos Aires; |
| MB.Ma | Museum für Naturkunde, Berlin, Berlin; |
| MHNC | Museo de Historia Natural "Alcide d'Orbigny", Cochabamba; |
| MLP | Museo de La Plata, La Plata; |
| MNHN | Muséum national d'Histoire naturelle, Paris; |
| MNRJ | Museu Nacional e Universidade Federal do Rio de Janeiro, Rio de Janeiro; |
| NDGS | North Dakota Geological Survey, State Fossil Collection at the North Dakota Heritage Center State Museum, Bismark; |
| OMNH | Oklahoma Museum of Natural History, Norman; |
| PAR | Musée Crozatier du Puy-en-Velay; |
| PIMUZ | Paläontologisches Institute und Museum Zürich; |
| PLV | Paleontología de Vertebrados Lillo, Instituto Miguel Lillo, Tucumán; |
| PSS-MAE | Paleontological and stratigraphy Section (Geological Institute), Mongolian Academy of Sciences, Ulaan Baatar; |
| PVL | Colección de Paleontología de Vertebrados Instituo Miguel Lillo, Universidad Nacional de Tucumán; |
| RH | Robert Hoffstetter collection of Recent vertebrates, in the MNHN; |
| SMF | Senckenberg, Museum of Natural History, Frankfurt; |
| UCMP | Museum of Paleontology, University of California, Berkeley; |
| UMZC | Museum of Zoology Cambridge; |
| UFRJ | Universidad Federal do Estado de Rio de Janeiro, Rio de Janeiro; |
| UM | University of Michigan, Museum of Paleontology, Ann Arbor; |
| USNM | United States National Museum, Smithsonian Institution, Washington DC; |
| UWBM | University of Washington Burke Museum of natural History and Culture, Seattle; |
| YPFB | Yacimientos petrolíferos fiscales de Bolivia; |
| YPM-PU | Princeton University collection housed in the Yale Peabody Museum, Yale University, New Haven; |
| ZPAL | Paleontological Institute of the Polish Academy of Sciences, Warsaw. |

## SUPPLEMENTARY DATA

Supplementary data are available at the following address: http://geodiversitas.com/40/16

PARSIMONY ANALYSIS FILES

– File 1: Nexus file of the data matrix – http://sciencepress.mnhn.fr/sites/default/files/documents/en/file1.nex

3D PDF FILES

– File 2: photogrametric view of the left petrosal of *Allqokirus australis* (MHNC 8267) – http://sciencepress.mnhn.fr/sites/default/files/documents/en/file2.pdf

– File 3: digital rendering of the assemblage of the various preserved elements of the skull of *Allqokirus australis* (MHNC 8267). The parietals and supraoccipital (the dorsal roof of the braincase) which have been displaced during fossilisation, have been virtually placed in their original anatomical position. Furthermore, because the braincase has been slightly distorted during fossilisation, some retrodeformation has been applied to this region of the skull in order to allow a better positioning of the elements – http://sciencepress.mnhn.fr/sites/default/files/documents/en/file3.pdf

– File 4: digital rendering of the reconstruction of the skull of *Allqokirus australis* (MHNC 8267) based on the assemblage presented in File 2. Where possible, the reconstruction has been obtained by mirroring the best-preserved element (e.g. lacrimal, jugal, premaxilla upper canine, dentary). Only the nasals, totally missing on the specimen, have been reconstructed on the basis of these bones in *Mayulestes* – http://sciencepress.mnhn.fr/sites/default/files/documents/en/file4.pdf

– File 5: digital rendering of the right petrosal of *Mayulestes ferox* (holotype, MHNC 1249) – http://sciencepress.mnhn.fr/sites/default/files/documents/en/file5.pdf

– File 6: digital rendering of the left petrosal of *Notogale mitis* (MNHN.F.SAL271) – http://sciencepress.mnhn.fr/sites/default/files/documents/en/file6.pdf

– File 7: digital rendering of the left petrosal of *Sipalocyon gracilis* (AMNH 9254) – http://sciencepress.mnhn.fr/sites/default/files/documents/en/file7.pdf

– File 8: digital rendering of the left petrosal of *Borhyaena tuberata* (YPM PU 15120) – http://sciencepress.mnhn.fr/sites/default/files/documents/en/file8.pdf

## SYSTEMATIC PALAEONTOLOGY

### Superorder PUCADELPHYDA n.

DIAGNOSIS. — Pucadelphydans share three unique synapomorphies, which are absent in other metatherians:
1) a medial process of the squamosal that extends into the middle ear and forms part of the roof of the hypotympanic sinus;
2) a deep groove for the internal carotid artery excavated in medial side of the promontorium apex ventrally;
3) a distinct dorsally projecting tuber on the dorsal edge of the head of the astragalus.
Other synapomorphies of Pucadelphyda are:
4) a fossa for the levator labii muscle in the anterior end of the jugal, present mainly in the maxilla (however, it is equally developed in, both maxilla and jugal in *Thylacosmilus*);
5) a hypotympanic sinus formed by squamosal, alisphenoid, and petrosal (condition absent in *Pucadelphys*);
6) a tensor tympani fossa, which forms a distinct circular pit or elongated fossa (this condition is convergent with *Thylacinus*).

### Order SPARASSODONTA Ameghino, 1894

DIAGNOSIS. — Sparassodonts share the following potential synapomorphies:
1) lower incisors not procumbent (convergent with *Dasyurus*+*Thylacinus*, and *Didelphodon*);
2) Paracone distinctly smaller than metacone in volume and height on M2-3 (convergent with stagodontids and Marsupialia + *Herpetotherium*);
3) Metacone and paracone adjoined at base or for most of their height (convergent with *Deltatheridium* and *Thylacinus*);
4) Postmetacrista on M2-3 distinctly longer than preparacrista (convergent with *Deltatheridium,* stagodontids, *Amphiperatherium*/*Peratherium,* didelphids, dasyurids and thylacinids;
5) Strongly convex labial edge of the protoconid at mid-height, protruding labially and overhanging the base of the crown (convergent with Deltatheridiidae);
6) Paraconid elongated with anterior projection of the paraconid keel mostly in the ventral half of the cusp (convergent with *Thylacinus*);
7) Expanded apex of the rostrum with concave (laterally) tooth rows and lateral edges of the rostrum between canine and infraorbital foramen (convergent with *Thylacinus*);
8) Paracanine fossa extended dorsally: higher dorsoventrally than (or as high as) it is long (i.e., anteroposteriorly) (convergent with *Sminthopsis* and stagodontids);
9) presence of a precanine notch;
10) m4 larger than m3 (convergent with *Thylacinus* and stagodontids);
11) Trigonid basin on m3 wide open lingually;
12) Trigonid basin floor sloping lingually;
13) Trigonid longer than wide (convergent with *Thylacinus*);
14) Metaconid subequal in height to, or much lower than, paraconid (on m3), or absent (convergent with deltatheridiids, stagodontids);
15) Metaconid smaller in volume than paraconid (on m3) (convergent with deltatheridiids, stagodontids, and Dasyuromorphia);
16) anteriorly expanded paraconid ridge;
17) depth/length of the dentary below molars higher than in other metatherian except *Didelphodon*;
18) anteroventral edge of mandibular symphysis forming an angle > 25° (convergent with stagodontids, *Thylacinus*, and deltatheridiids);
19) Nasals do not overhang nasal aperture (convergent with Dasyuromorphia);
20) palatal pits between M2-3-4 (convergent with Deltatheridiidae and Dasyuromorphia);
21) large foramen or groove in lateral edge of postpalatine torus present and large (approximately half the size of the minor palatine foramen or more) (convergent with *Dasyurus*);
22) Sagittal crest extending to frontals (convergent with stagodontids, *Didelphis*, *Dasyurus* + *Thylacinus*);
23) Posterior extension of the neural process of the axis distinctly longer than anterior extension (convergent with *Dasyurus*+*Thylacinus*);
24) Ventral sagittal crest of axis distinctly concave because of the development of a robust ventral process posteriorly (convergent with *Dasyurus*);
25) Scapular notch between 90 and 130° (convergent with *Metachirus* and Dasyuromorphia);
26) Iliac neck short, less than 15% the total pelvis length;
27) Epipubic bones absent (convergent with *Thylacinus*);
28) Astragalar neck narrower than, or as wide as, head;
29) Anteroposterior length of the medial malleolus of the tibia at base subequal to the greatest anteroposterior length of the distal epiphysis (as seen in distal view) (convergent with *Sminthopsis*).

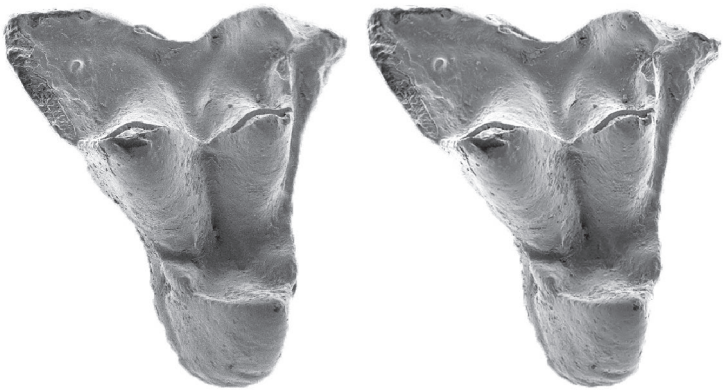

FIG. 2. — *Allqokirus australis* (YPFB Pal 6104), SEM stereophotograph of the holotype: a right maxillary fragment with ?M3. Scale bar: 5 mm.

## Family MAYULESTIDAE Muizon, 1994

INCLUDED GENERA. — *Mayulestes* Muizon, 1994; *Allqokirus* Marshall & Muizon, 1988; *Patene* Simpson, 1935.

DIAGNOSIS. — The three genera of Mayulestidae share the following characters:
1) P1/p1 oblique relative to the tooth row;
2) lack of diastema posterior to p1;
3) metacone present on on M4 but very reduced (less than 50% smaller in occlusal view);
4) protocone anteroposteriorly short on M3;
5) metaconid subequal to slightly smaller than the paraconid;
6) elevated protoconid of m3 and m4, the height of which equals the length of the tooth;
7) talonid basin longer than wide;
8) deep hypoflexid, the depth of which is approximately half the talonid width;
9) subvertical coronoid process of the dentary;
10) mandibular foramen posteriorly placed (posterior to mid-point of coronoid process).

## Genus *Allqokirus* Marshall & Muizon, 1988

TYPE SPECIES. — *Allqokirus australis* Marshall & Muizon, 1988 by original designation.

DIAGNOSIS. — Because the genus is monospecific, the genus diagnosis is that of the species

### *Allqokirus australis* Marshall & Muizon, 1988

HOLOTYPE. — YPFB Pal 6104, fragment of right maxilla with ?M3 (Fig. 2).

HYPODIGM. — The holotype; YPFB Pal 6188, left ?m2 missing the apices of the trigonid cusps; YPFB Pal 6189, left m2 or m3 missing the anterior part of the trigonid; YPFB Pal 6190, left m3; MHNC 8267, disarticulated cranium and mandibles, as described in the material and methods section above (this latter specimen was eroneously referred to *Mayulestes ferox* by Cifelli & Muizon [1998]).

GEOLOGICAL SETTING AND AGE. — The specimen described here was discovered in the site called "The Quarry" at Tiupampa (site 1 in Marshall *et al.* 1995: fig. 1), which has yielded most of the Tiupampa mammal remains. This site occurs in the middle section of the Santa Lucía Formation, which has been referred to the early Palaeocene (Gayet *et al.* 1992; Bonaparte *et al.* 1993; Muizon 1998; Gelfo *et al.* 2009; Woodburne *et al.* 2014a, b). The late Palaeocene age proposed by Marshall *et al.* (1997) and Sempere *et al.* (1997) has been abundantly discussed and rejected by Muizon (1998) and Gelfo *et al.* (2009). The Tiupampa beds are included in a single reversed magnetostratigraphic series (Sempere *et al.* 1997). Taking this datum into account as well as other faunistic data, Gelfo *et al.* (2009) regarded the beds of the "Quarry" as included in the polarity Chrone 28r and suggested that it could represent an equivalent of the late Puercan (Pu3) of North America (see Gelfo *et al.* [2009]) for discussion on the referral of the Tiupampa mammal-bearing beds to Chron 28r rather than to Chron 26r as suggested by Sempere *et al.* [1997]). However, recently, new calibration of the early Palaeocene NALMAs (Sprain *et al.* 2015) modified the age and position of the Chron 28r relative to the NALMAs. According to Sprain *et al.* (2015: fig. 6) the lower limit of Chron 28r is between 65.118 Ma and 65.041 Ma (therefore, *c.* 65 080 Ma) and the upper limit of the chron is at 64.866 Ma. The Torrejonian 1, spans from 65.118 Ma (Sprain *et al.* 2015) to *c.* 63.5 Ma (Vandenberghe *et al.* 2012: fig. 28.10). On the basis of these two calibrations Muizon *et al.* (2015: 410) correlated the mammal-bearing beds of the "Quarry" at Tiupampa, with an equivalent of the base of Torrejonian 1 and evaluated an age of approximately 65 Ma for the Tiupampa mammals. Therefore, the longevity of the Tiupampa mammals probably does not exceed 0.2 Ma (the approximate duration of Chron 28r, according to Sprain *et al.* 2015) and the time span of the Tiupampan in Woodburne *et al.* (2014a and b: fig. 2) and in Goin *et al.* (2016: fig. 7.2) should be, accordingly, significantly shortened.

EMENDED DIAGNOSIS. — Dental formula I5/i4, C/c, P3/p3, M4/m4. Small-sized sparassodont, approximately 20 to 25% smaller than *Mayulestes ferox* in skull length and bizygomatic width, and 40% smaller than *Patene simpsoni* in mandible length.
*Allqokirus australis* differs from *M. ferox* in the following characters: upper canines subvertical (anteriorly projecting on *Mayulestes*); upper molars (M2 and M3) with longer labial edge, shallower ectoflexus, more posteriorly projecting postmetacrista, more massive protocone, and larger stylar cusp B; metaconid of m4 distinctly smaller in volume and height relatively to paraconid; distinct fossula between the anterolabial base of the protoconid and the precingulid; shorter snout, with a ventrally deflected premaxilla bearing a subvertical ascending process; posterior alveolar border of M4 formed by the palatine instead of the maxilla; much narrower glenoid fossa, with a postglenoid process as high as wide; frontals on the roof of the skull approximately 40% narrower; jugal approximately 45% shorter, dentary below embrasure between M2 and M3 approximately 25% lower.

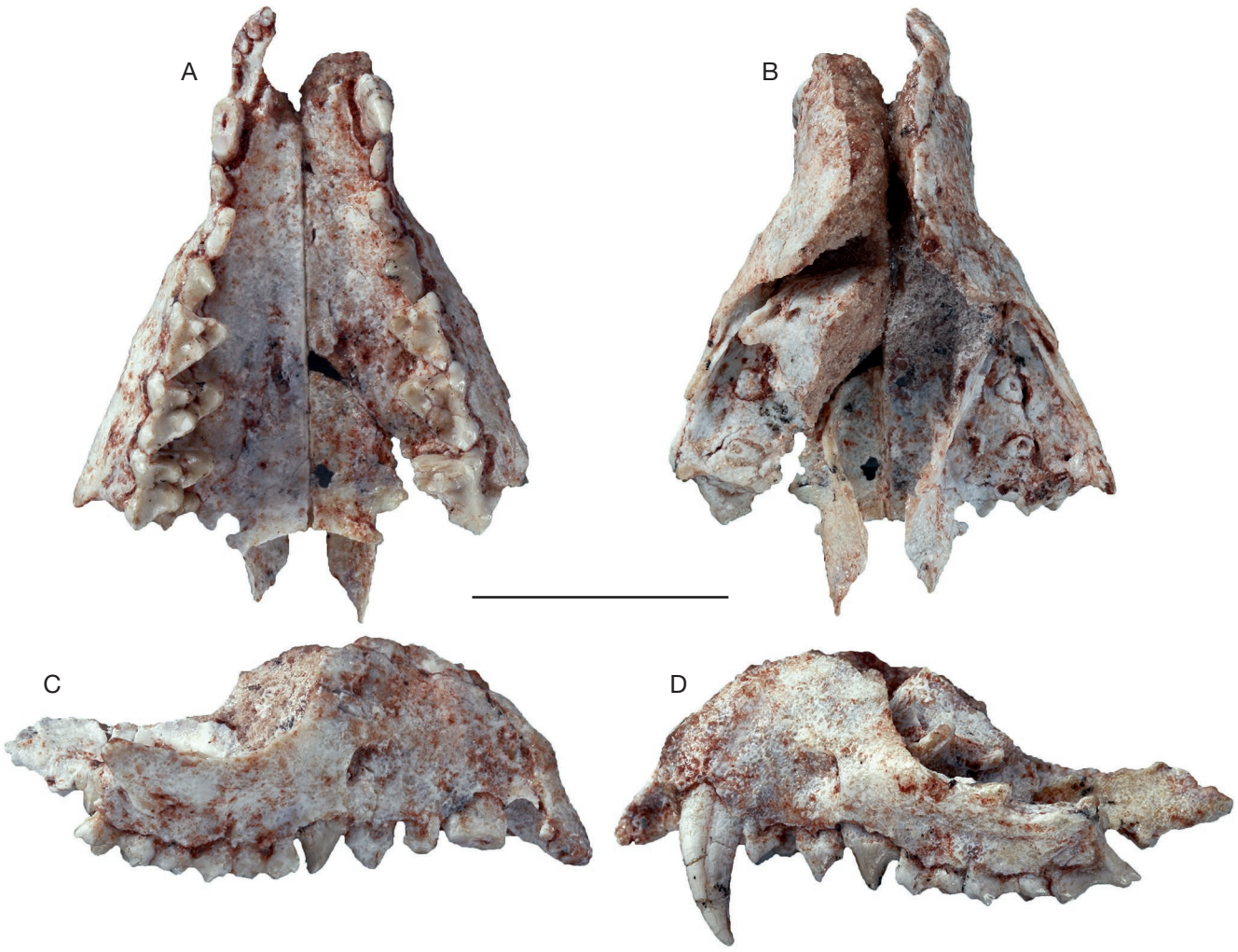


Fig. 3. — *Allqokirus australis* (MHNC 8267): rostrum including both maxillae, the right premaxilla, the left lacrimal, and both palatines, roots of right I2-5; root of right canine, left canine, right and left P1-M3, and right M4: **A**, dorsal view; **B**, ventral view; **C**, right lateral view; **D**, left lateral view. Scale bar: 5 mm.

*Allqokirus australis* differs from all other sparassodonts except *Mayulestes* and *Patene* in the presence of a larger protocone (largest cusp of the molars), larger stylar shelf on molars, which is at least one third the width of the tooth; larger metaconid similar in height to the paraconid on m1-3.

Differs from all other sparassodonts (in which these characters are preserved) except *Mayulestes,* in the following plesiomorphic characters: presence of 5 upper (unknown for *Patene*) and 4 lower incisors; parabolic upper incisor arcade; paracanine fossa bordered laterally by the maxilla; precanine notch (notch, in dorsal view, between the lateral upper incisor and canine) very shallow (incipiently developed); lack of supraorbital process; posterior edge of the palate regularly concave posteriorly without prominent postpalatine spine.

## COMPARATIVE DESCRIPTION

### General features

In ventral view, the rostrum shows concavities on its lateral sides and alveolar borders, anterior and posterior to the canine. The anterior concavity is located at the level of the paracanine fossa, and the posterior is between the infraorbital foramen and the canine. In dorsal view, the posterior concavity is less conspicuous, and the part of the rostrum anterior to the infraorbital foramen presents roughly parallel edges as far as the anterior edge of the canine. Posterior to the infraorbital foramen, the lateral edges of the maxillae diverge posteriorly. Because of this condition, the rostrum of *Allqokirus* present a subtle but distinct anterior flaring (Fig. 3). A similar condition is present in *Mayulestes*. Although the holotype and only known specimen of *Mayulestes ferox* has suffered dorsoventral post-mortem compression, the anterior concavity is observed in dorsal and ventral views and the posterior concavity is observed in ventral view, where the lateral edge of the maxilla is distinctly concave between P1 and P3 (Fig. 4). A well-marked anterior flaring of the rostrum is present in later sparassodonts, a condition which is enhanced by the increase in size of the canines. In most taxa (e.g. *Borhyaena, Prothylacynus, Pharsophorus, Cladosictis, Callistoe*) the lateral edges of the rostrum converge anteriorly from the level of the infraorbital foramen to the canine, and the flaring of the apical snout is characteristic. The condition observed in *Allqokirus* and in the other sparassodonts is absent in *Andinodelphys, Pucadelphys*, and in didelphids, in which the lateral edges of the snout evenly diverge posteriorly and do not present

TABLE 1. — Proportions of the crania of *Allqokirus australis* (MHNC 8267) and *Mayulestes ferox* (MHNC 1249). The first total length of the cranium (40.2 mm) is that measured on the virtual assemblage of the skull (Fig. 5). The second length (42.3 mm) is an estimation of the adult cranium length of the individual. This length has been obtained by addition of an adjustment value (+ 2.28 mm) taking into account the non-eruption of m4 as calculated in the dentary section below. The same adjustment value has been applied to the jugal. It is assumed that the bizygomatic width of the cranium and the rostrum length, as measured, are close to that of the individual if it was adult (although we admit that this is not necessarily true). Because the cranium of *Allqokirus* (MHNC 8267) is lacking the occipital condyles, the total length of the cranium has been taken from the apex of the premaxilla to the dorsal edge of the foramen magnum on both specimens. Abbreviations: **BZW**, bizygomatic width; **JU**, jugal length; **L**, cranium length; **RL**, rostrum length; **e**, estimated values.

| | L | BZW | RL | JU | BZW/L | RL/L | JU/L |
|---|---|---|---|---|---|---|---|
| *Allqokirus* MHNC 8267 | 40.2 | 12.3 × 2 = 24.6e | 12.5 | 16.5 | 0.61 | 0.31 | 0.41 |
| *Allqokirus* full adult estimates | 42.3e | 24.6e | 12.5 | 18.7e | 0.58 | 0.29 | 0.44 |
| *Mayulestes* MHNC 1249 | 51.6 | 33.5 | 20.2 | 24.2 | 0.65 | 0.39 | 0.47 |

a distinct concavity at the level of the infraorbital foramen P3 (Fig. 4). This apical flaring of the snout is also observed on the palate of sparassodonts, which is generally narrowest at the level of P2 and widens at the level of P1. A similar condition to that of the sparassodonts is also present in *Sarcophilus*, thylacinids (e.g. *Thylacinus, Nimbacinus, Badjcinus*) and other carnivorous mammals (e.g. *Crocuta*, *Panthera*) with large canines, although in these taxa the anterior premolars do not diverge as they do in many sparassodonts.

CT scanning of the different elements of the skull of *Allqokirus* (MHNC 8267) has allowed reassembly of the specimen (Fig. 5). Figure 6 provides a digital reconstruction of the skull of *Allqokirus australis* based on the assemblage of the parts in Figure 5. The presence of a complete right jugal, which articulates with the maxilla and with the squamosal, provides a reasonable approximation of the length of the cranium. Furthermore, it has been possible to virtually reposition the parietals (displaced during fossilisation) relative to the frontals and consequently the width of the cranium could be approximated by symmetrising the left side of the cranium on the basis of the right side. From the data provided in Table 1, it appears that the cranium of *Allqokirus* is more gracile than that of *Mayulestes*. Considering the estimated adult cranium length value for MHNC 8267, the cranium of *Allqokirus* is approximately 10% narrower relative to the cranium length than in *Mayulestes*, and its rostrum is approximately (and relatively) 25% shorter (Table 1). Furthermore, the apex of the rostrum of *Allqokirus* is more slender than that of *Mayulestes*.

Comparison of the relative lengths of the jugal in *Allqokirus* and *Mayulestes* is also informative. Because the skull of *Allqokirus* (MHNC 8267) is that of a sub-adult individual in which the M4 are not fully erupted, in order to obtain an estimation of the adult cranium length, an adjustment value corresponding approximately to m4 length (+ 2.28 mm) has been applied to the estimated cranium length of the specimen (see dentary section below). Because, at the growth stage of MHNC 8267, the length increase of the dentary (and therefore of the whole skull) would concern the posterior part of the corpus mandibularis (horizontal ramus), and because this region is located in the orbitotemporal fossa, it is likely that this region would have increased its length more than the other part of the cranium. Therefore, in order to have an estimate of the full adult length of the jugal, we applied the adjustment value calculated for the dentary section to the measurement of the jugal of MHNC 8267. With these values, the length of the jugal (and therefore of the orbitotemporal fossa) relative to the total length of the cranium is approximately 6.4% smaller in *Allqokirus* than in *Mayulestes*. With the measured values of the length of the skull and jugal of MHNC 8267, the jugal and orbitotemporal fossa of *Allqokirus* are *c.* 12.7% smaller than in *Mayulestes*. Therefore, whatever the values of cranium and jugal lengths that are considered, the temporal fossa of *Allqokirus* appears to be relatively smaller than that of *Mayulestes*.

## DENTITION

The dental formula of *Allqokirus australis* is the full ancestral metatherian formula: I5/i4; C1/c1; P3/p3; M4/m4 (Luckett 1993). The specimen described here (MHNC 8267) is that of a sub-adult individual as the P3s, the p3s, the upper (possibly) and lower canines, the right M4 (the only one preserved) and the m4s are not fully erupted. However, because the M4 is half-erupted (only half of the M4 crown is out of its crypt) and the m4 has the trigonid almost fully erupted, the length of the palate and of the dentary are shorter than that of an adult individual. In order to estimate the length of the adult palate, we estimated that it was approaching that of MHNC 8267 plus the anteroposterior length of M4. Similarly, we estimated that the length of the adult dentary was close to that of the dentary of the specimen plus the anteroposterior length of m4 (i.e., that of the non-erupted talonid plus a retromolar space, which is approximately equivalent to the length of the trigonid, as is observed in *Mayulestes* and *Patene*). Based on these assumptions, the adjustment calculated is + 2.28 mm (see dentary section below).

### *Eruption sequence*

As mentioned, the specimen described here is a subadult, with incompletely erupted P3/p3 and M4/m4 (it is noteworthy that this specimen was erroneously referred to *Mayulestes ferox* by Cifelli & Muizon [1998]). On the palate, the P3s are almost fully erupted, as the base of their crown is distinctly below the alveolar border of the maxilla, but remains, however, above the base of the crown of the P2s and M1s. The M4 is not fully erupted either; although the three main cusps and stylar cusps A and B are clearly below the alveolar plane, the base of the crown still remains above it. As a matter of fact, the roots of M4 are incompletely developed yet. On the dentary, the p3s are slightly less erupted than the P3s, and the base of the crown is still in the crypt, below the alveolar border. However, variation exists since the right P3/p3 are slightly less erupted than the left ones. The m4 is partly in its crypt: the two thirds of the protoconid and the tips of

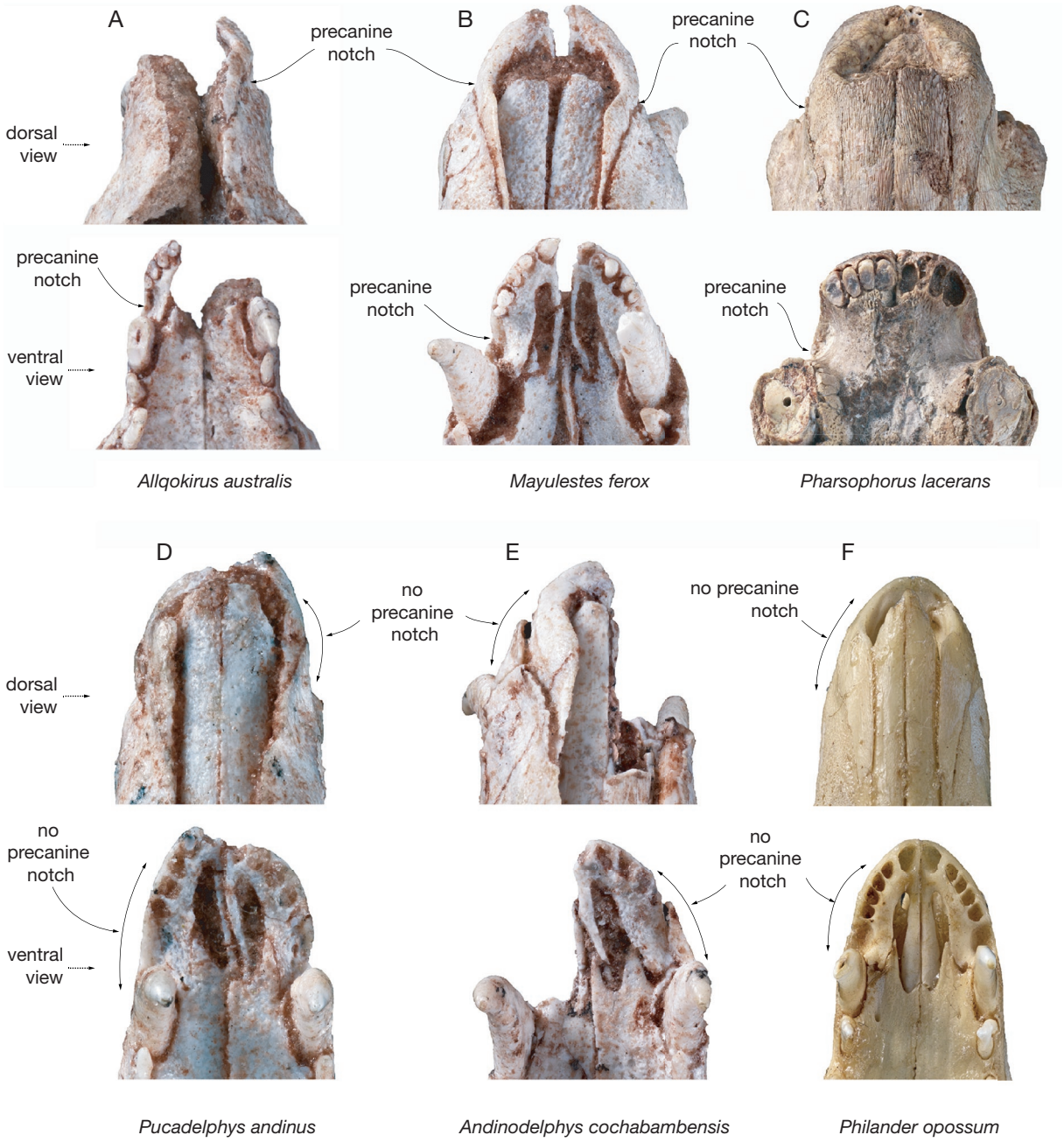


Fig. 4. — Dorsal (**top**) and ventral (**bottom**) views of the rostrum of: **A**, *Allqokirus australis* (MHNC 8267); **B**, *Mayulestes ferox* (MHNC 1249); **C**, *Pharsophorus lacerans* (MNHN.F.SAL96; **D**, *Pucadelphys andinus* (MHNC 8266); **E**, *Andinodelphys cochabambensis* (MHNC 8264); **F**, *Philander opossum* (MNHN 2003-153). Not to scale.

paraconid and metaconid are above the alveolar border of the dentary, but the talonid cusps are barely visible out of the crypt. Therefore, according to observations on MHNC 8267, P3/p3 of *Allqokirus* complete their eruption slightly before M4/m4, and eruption of P3 and M4 occurs slightly before p3 and m4. This condition is regarded as plesiomorphic for Metatheria (Forasiepi & Sánchez-Villagra 2014). It clearly differs from that of Recent didelphids (e.g. *Didelphis, Monodelphis*), in which P3 is fully erupted before p3, and M4 is still mostly in the crypt while m4 is fully erupted. Although considerable variation exists within this family (Astua & Leiner 2008; Forasiepi & Sánchez-Villagra 2014), an obvious heterochrony characterises the eruption of P3 vs p3 vs M4 vs m4. A similar condition is also observed in *Thylacinus* and *Sarcophilus* (Forasiepi & Sánchez-Villagra 2014).

In *Pucadelphys* (observations based on four complete subadult skulls [MHNC 8265, 8384, 8388, 8391]), when P3 is fully erupted, p3 is distinctly less erupted (*c.* half-erupted) and the trigonid of m4 is erupting but its talonid is almost entirely in the crypt. In the upper jaw, the anterior part of the crypt of M4 can be observed on the posterior interalveolar septum of M3, well above the crown of the tooth; however, no bud of M4 has been discovered on the four well-preserved skulls, although the buds may have been lost during fossilization.

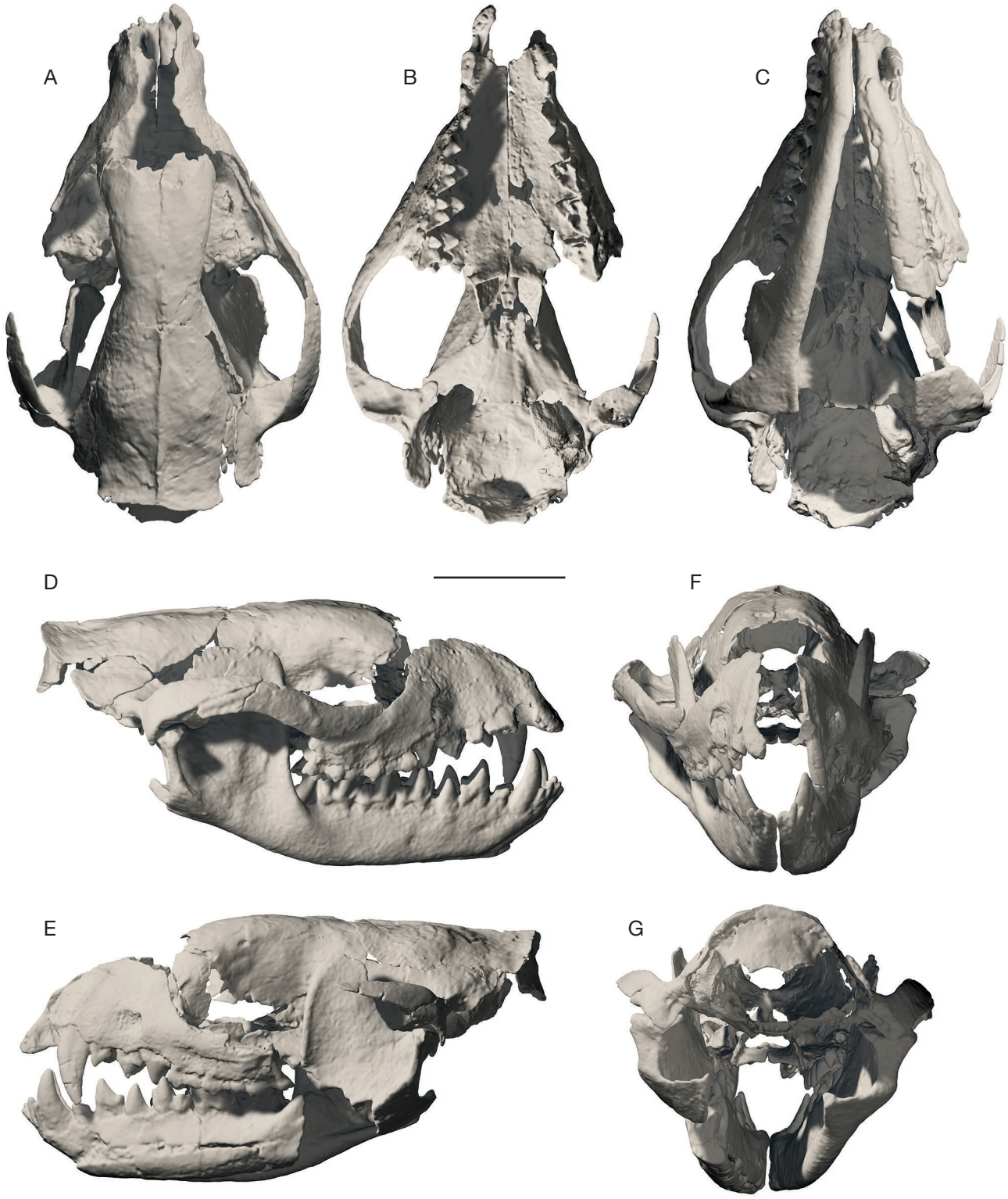


FIG. 5. — *Allqokirus australis*: digital rendering of the assemblage of the various preserved elements of MHNC 8267. The parietals and supraoccipital (the dorsal roof of the braincase), which have been displaced during fossilisation, have been virtually placed in their original anatomical position. Furthermore, because the braincase has been slightly distorted during fossilisation, some retrodeformation has been applied to this region of the skull in order to allow a better positioning of the elements: **A**, dorsal view; **B**, ventral view; **C**, ventral view with dentaries; **D**, right lateral view; **E**, left lateral view; **F**, anterior view; **G**, posterior view; **H**, right anterolateral view; **I**, left anterolateral view. Scale bar: 1 cm.

It is therefore probable that M4 was only barely erupting in these individuals and was far from having reached the stage of eruption of m4. Therefore, *Pucadelphys* is characterised by a moderate but significant heterochrony in the timing of eruption of P3/M4 vs p3/m4. If synchrony is not perfect in *Allqokirus*, considering the individual variation observed in

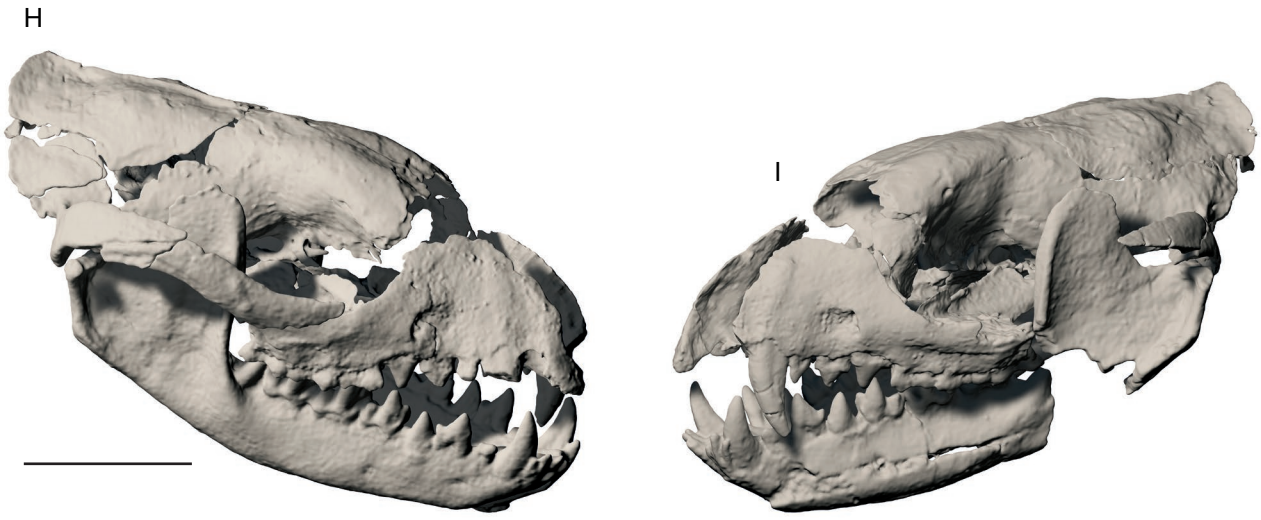


Fig. 5. — Continuation.

the same specimen, it is certainly close to synchronous. In any case, the condition of *Allqokirus* is distinctly closer to synchrony than that of *Pucadelphys*.

Forasiepi & Sánchez-Villagra (2014: 234) observed that sparassodonts are characterised by synchronous eruption of P3/p3 (observed in *Lycopsis* only), and by the fact that "the equivalent upper and lower molar loci erupt in closer synchrony than in the other carnivorous metatherians" (observed in *Arminiheringia*, *Prothylacynus*, and *Lycopsis*). However, synchronous eruption of M4/m4 is not present in all sparassodonts as Engelman *et al.* (2015) observed that M3 and m4 of *Acyon myctoderos* probably erupted simultaneously, therefore m4 erupting well before M4. The only early metatherian (with a comparable eruption stage), to which *Allqokirus* can be compared is *Pucadelphys.* Therefore, the condition of *Allqokirus*, although not identical, more resembles the synchrony observed in three of the four sparassodont taxa in which subadult individuals are known, than that of *Pucadelphys* or Recent marsupials.

*Upper dentition*

**Upper incisors.** Only the four roots of the right lateral upper incisors of MHNC 8267 are known. The medialmost incisor is further distant from the sagittal plane, leaving space for another medial incisor. It is therefore hypothesized that the medial missing incisor is the I1, and the four preserved ones are I2-5. Therefore, the incisor count of *Allqokirus* is similar to that in *Mayulestes, Pucadelphys* and *Andinodelphys*, which represents the plesiomorphic condition for metatherians. In ventral view, the full incisor row can be reconstructed as parabolic, as is observed in *Mayulestes, Pucadelphys*, and *Andinodelphys*. In lateral view, the alveolar border of the incisor row is strongly oblique so that I5 is markedly dorsal to the other incisors, and each incisor is dorsal to the preceding one (Fig. 7). The relatively large space existing between the sagittal plane and the mesial alveolar border of I2 indicates that I1 was probably large and possibly separated from I2 by a small diastema, as is observed in *Mayulestes*. The section of the root of I2 is distinctly smaller than that of I3-4, and slightly larger than that of I5. Considering the size of the sections, I2<< I3<I4>>I5 and I2 >I5. This relative size of the upper I2-5 of *Allqokirus* differs from that of *Mayulestes*, in which I3 is larger than I4, but resembles the condition in *Pucadelphys*, and *Andinodelphys*. The preserved upper incisors (I2-5) of *Allqokirus* are not separated by diastemata, but I5 is separated from the canine by a large paracanine fossa. I5 is located on the anterior edge of the fossa (Fig. 7).

**Upper canines.** The left upper canine only is almost complete, while the right canine is broken at the base of the crown. The canine is long and strongly compressed transversely. The lateral and medial aspects of the canine bear a wide and shallow elongated groove, which extends from tooth apex to the alveolar border. This groove likely extends on the root. Such a condition is absent in *Mayulestes* but present in *Andinodelphys*, although less pronounced in this genus. The tooth is strongly recurved posteriorly, and its apex is slightly posterior to the posterior edge of the alveolus, when the alveolar border of the molars is horizontal. This condition differs from that observed in *Mayulestes,* in which the apex of the canine is well anterior to the posterior alveolar border; therefore, the canine of *Allqokirus* projects ventrally, whereas that of *Mayulestes* distinctly projects anteroventrally. A relatively vertical canine is also observed in *Andinodelphys* and variably in *Pucadelphys*. The canine of MHNC 8267 is smaller (proximodistally) than in *Mayulestes* and *Andinodelphys*, a condition probably related to the lesser degree of eruption in this specimen, due to its younger ontogenetic age.

**Upper premolars.** Three double-rooted premolars are present (Figs 7; 8). They increase in size posteriorly, but P1 is clearly much smaller than P2 and P3. There is no diastema between P1 and the canine, or between premolars. The premolars each bear a single triangular cusp, which is strongly compressed transversely.

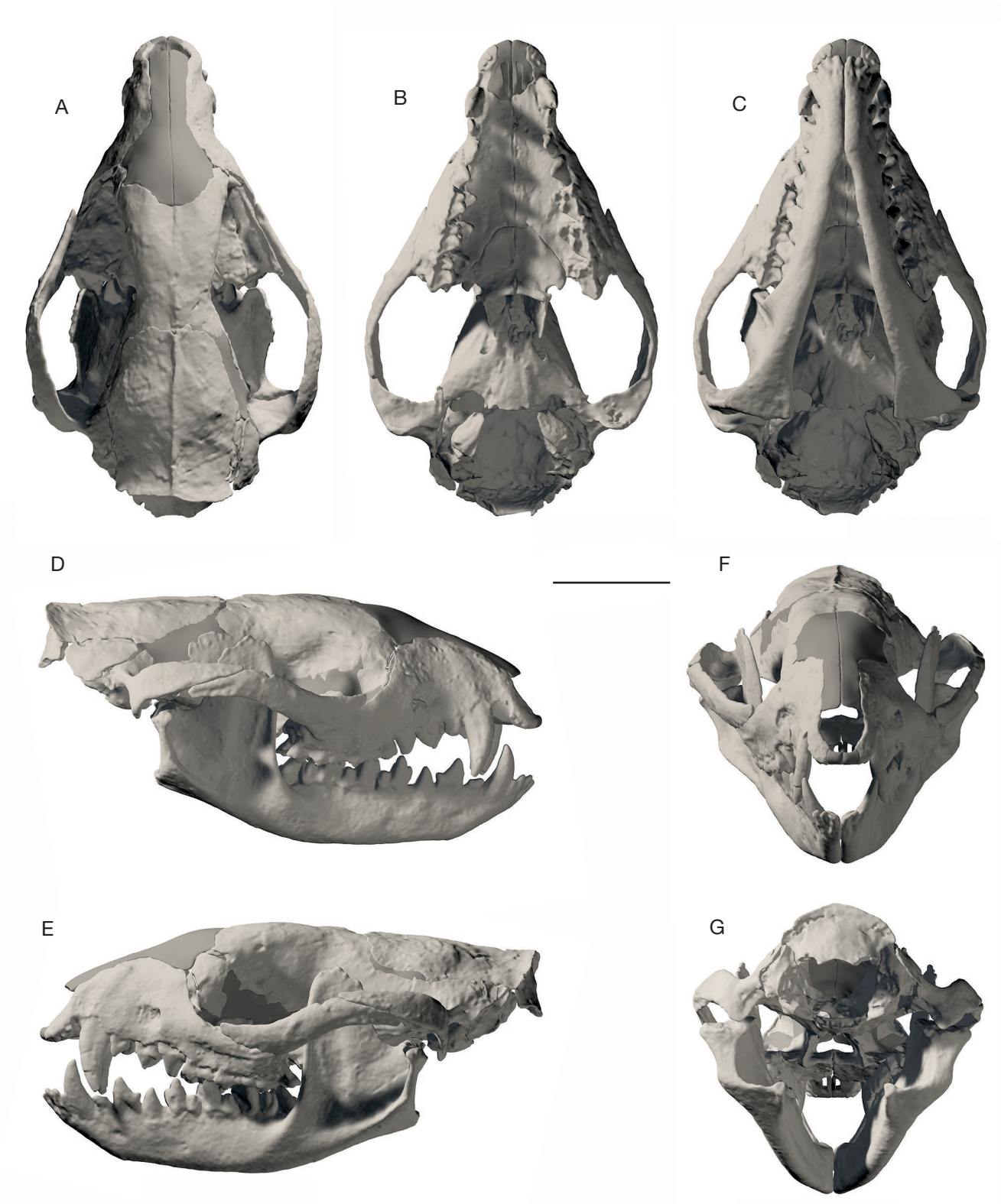


Fig. 6. — *Allqokirus australis*: digital rendering of the reconstruction of the skull based on the assemblage presented in Figure 5. Where possible, the reconstruction has been obtained by mirroring the best-preserved element (e.g. lacrimal, jugal, premaxilla upper canine, dentary). Only the nasals, totally missing on the specimen, have been reconstructed on the basis of these bones in *Mayulestes*: **A**, dorsal view; **B**, ventral view; **C**, ventral view with dentaries; **D**, right lateral view; **E**, left lateral view; **F**, anterior view; **G**, posterior view; **H**, right anterolateral view; **I**, left anterolateral view. Scale bar: 1 cm.

In lateral view, P1 is asymmetrical, its apex being shifted anteriorly and located ventral to the posterior half of the anterior root. In other words, the posterior edge of the main cusp is longer and more oblique than the anterior, which is short and sub-vertical; consequently, the anterior root is smaller than the posterior. The posterior edge of the tooth is straight

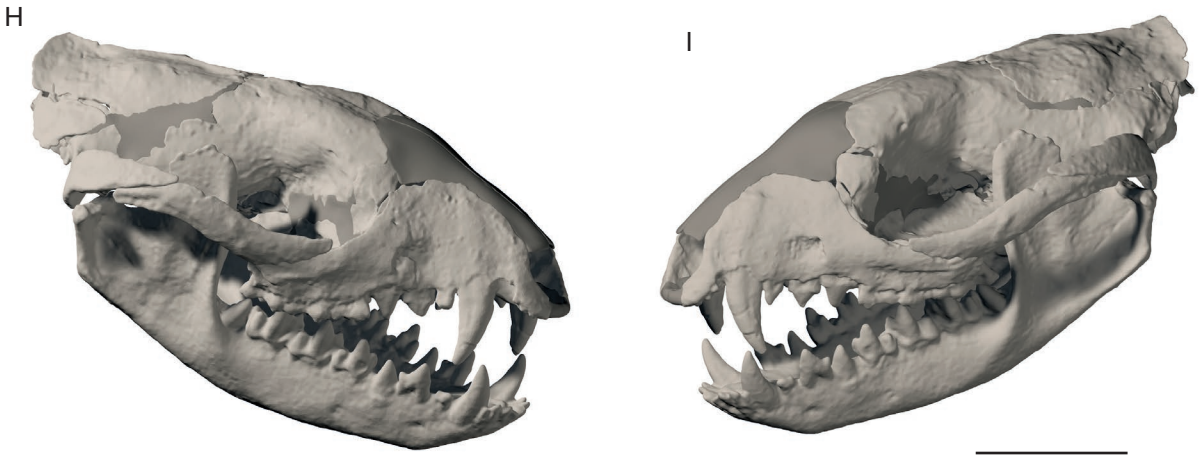


FIG. 6. — Continuation.

in labial view and the anterior border is slightly convex. This condition is present in *Mayulestes, Pucadelphys*, and *Andinodelphys*, but much less pronounced in the latter genus. A tiny cuspule is present on the posterobasal edge of the tooth, posteroventral to the posterior root. In occlusal view, the P1 is obliquely oriented in the maxilla and its anterior root is appressed against the posterolateral edge of the canine. It forms an angle of approximately 30° with the anteroposterior axis of the tooth row. A similar condition is observed in *Mayulestes*, *Pucadelphys,* and *Andinodelphys*.

P2 is much larger than P1 and slightly smaller than P3. It is approximately as high as long. Contrary to the condition in P1, it is oriented parallel to the axis of the tooth row. Its main cusp is elevated and higher than the occlusal plane of the molars. In medial view, the main cusp is roughly symmetrical and its apex is ventral to the interradicular septum. It is compressed transversely, although to a lesser extent than P1. A small cuspule is present at the anterior base of the crown, and a weak cingulum (more a smooth ridge than a cingulum) extends posterolabially. A small posterobasal cusp, larger than the anterior, is present, with a labial cingulum which extends anteriorly from it on the posterolabial quarter of the crown. This cingulum is clearly better developed than the anterolabial one.

P3 is the largest of the three premolars. It is higher than long, and the apex of the main cusp is conspicuously lower than the occlusal plane of the molars, a condition which would be even more pronounced after the tooth is fully erupted. The main cusp is clearly more robust and less transversely compressed than that of the anterior premolars. Its apex is located ventral to the interradicular septum, but, in contrast to the condition of P2, P3 appears asymmetrical in medial view. This condition is due to the convex morphology of the anterior edge of the main cusp, while the posterior edge is straight and strongly concave at its base. A small anterobasal heel (not really a cusp as in P2) is present at the anterior end of the crown. It extends posterolabially as a small cingulum along the base of the crown for approximately half the length of the anterior root. A similar cingulum is observed lingually. Posteriorly, a relatively large, cusp-like heel is observed, which is approximately one quarter of the length of the crown. It is clearly more developed than in P2. Small cingula are present on its labial and lingual sides. The posterior edge of the main cusp forms a sharp crest, while the anterior edge is blunt (Fig. 8).

**Upper molars.** The first three upper molars are more triangular and proportionally longer and narrower than those of *Mayulestes*. From M1 to M3, the length of the alveolar border of the molars is approximately constant, but the teeth widen posteriorly. On M1 and M2, the length of the tooth is greater than the width (measured perpendicular to the alveolar length), while it is slightly shorter on M3. As usual in generalized metatherians (e.g. didelphids, pucadelphyids, dasyurids), the M4 of *Allqokirus* is much shorter anteroposteriorly than transversely wide (Fig. 9).

The general pattern of the upper M1-3 (Figs 7 and 8) is that of dentally plesiomorphic metatherians. They bear a large stylar shelf labially separated from a deep trigon basin by large paracone and metacone. The width of the stylar shelf and that of the trigon basin are respectively approximately one third the total width of the tooth each. The protocone is the most voluminous cusp of the molars, but it is lower than the paracone and metacone. The apex of the protocone approximately reaches mid-height of the paracone and metacone. The protocone is slightly more massive and longer anteroposteriorly than in *Mayulestes*. It is slightly larger than in *Patene*, and conspicuously more slender than in *Pucadelphys* and *Andinodelphys*. It increases in size posteriorly from M1 to M3, and its proportions vary between these teeth. From M1 to M3, it becomes markedly wider transversely and slightly shorter anteroposteriorly. As a result, and in spite of the size increase, the protocone appears more massive on M1 than on M3. On M2-3, as in *Mayulestes* (*contra* Muizon 1998) and *Patene,* the protocone is not inflated basally on its posterior side, in contrast to the condition observed in *Pucadelphys* and *Andinodelphys*. The apex of the protocone is not shifted anteriorly, while this condition is present but weak in *Mayulestes* and *Patene* and


FIG. 7. — Upper dentition of *Allqokirus australis* (MHNC 8267): **A**, lateral view of right tooth row; **B**, stereophotograph of occlusal view of right tooth row. Scale bar: 5 mm.

conspicuous in *Pucadelphys* and *Andinodelphys*. The labial side of the protocone is relatively flat and steep. From the apex of the protocone, the pre- and postprotocristae extend labially as far as the well-developed conules.

The preprotocrista is slightly longer than the postprotocrista on M1 and M2. The para- and metaconules are respectively slightly anterior and slightly posterior to the lingual bases of the para- and metacone. Distinct conular cristae are present. The postparaconular


FIG. 8. — Upper dentition of *Allqokirus australis* (MHNC 8267): **A**, stereophotograph of occlusal view of left tooth row; **B**, lateral view of left tooth row. Scale bar: 5 mm.

and premetaconular cristae are relatively blunt and extend labially to the most medial base of the para- and metacone. The preparaconular crista is sharper, and extends labially from the apex of the paraconule. The preparaconular crista is continous with the well-developed paracingulum, which extends labially along the base of the paracone and reaches stylar cusp A. The postmetaconular crista is also sharp, but it is short and ends labially at the posterolingual base of the metacone and does not reach the labial edge of the tooth. No pre- or post-cingulum is present at the anterior and posterior bases of the protocone, respectively.

The paracone and metacone are large cusps, and the metacone is only slightly smaller in volume than the protocone. In fact, on the holotype (YPFB Pal 6104), the metacone is almost as large as the protocone. This condition differs from that of *Pucadelphys* and *Andinodelphys,* in which the metacone is always distinctly smaller than the protocone. In contrast, it resembles that of *Patene,* which also has a very large metacone. The paracone and metacone are clearly smaller on M1 than on M2-3 and have approximately the same size on M2 and M3. The metacone is larger in height and volume than the

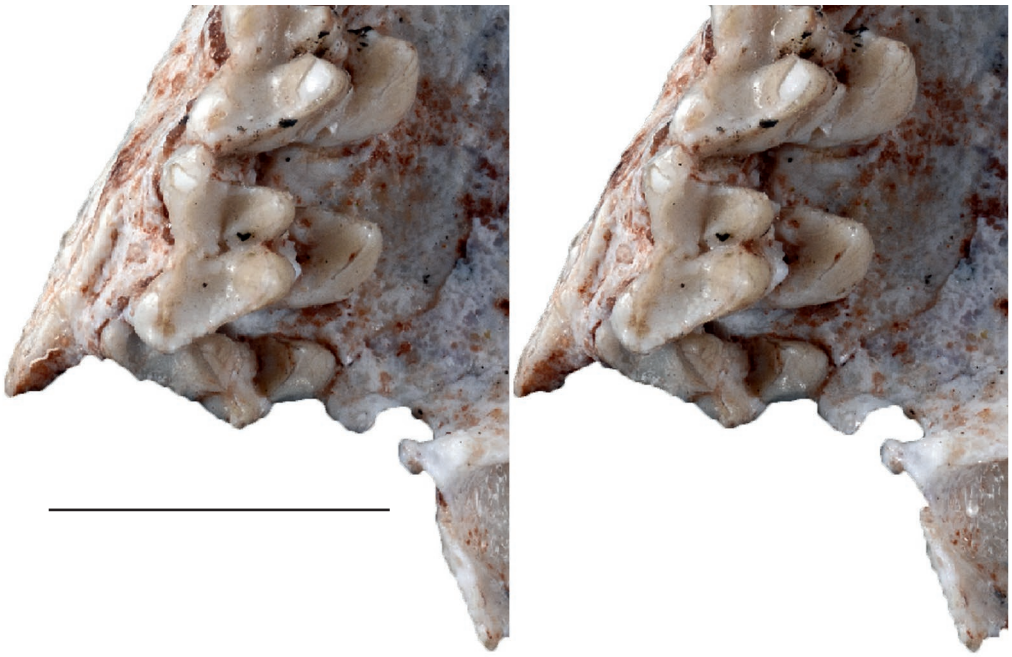

FIG. 9. — *Allqokirus australis* (MHNC 8267): stereophotographs of the right M4 in occlusal view. Scale bar: 5 mm.

paracone on M1-3. This size difference is more pronounced than in *Pucadelphys* and *Andinodelphys*, and resembles that of *Patene*. As matter of fact, a strong size difference between paracone and metacone has been regarded as a synapomorphy of Sparassodonta (Marshall *et al.* 1990; Forasiepi 2009; Forasiepi *et al.* 2015). Both cusps are strongly approximated, and they are fused at their bases on approximately half of their heights (Fig. 10). This condition is similar to that observed in *Mayulestes* (*contra* Goin 2003: 31) and *Patene*, but differs markedly from the fully separated paracone and metacone of *Pucadelphys* and *Andinodelphys*. In dorsal view, the junction point of the postparacrista and premetacrista is not shifted labially, and so the centrocrista is straight as in *Mayulestes* and *Patene*, not V-shaped as in *Pucadelphys* and *Andinodelphys*. As a consequence, the labial surface of the para- and metacone are relatively swollen and convex, as in *Mayulestes* and *Patene*, and differs from the flat surface observed in *Pucadelphys* and *Andinodelphys*. The preparacrista is almost transverse to the axis of the tooth row and contacts the stylar cusp B. It is very short on M1, but increases in length progressively from M1 to M3. The postmetacrista is much longer than the preparacrista and is strongly oblique posteriorly. It is slightly longer on M2-3 than on M1, but the difference in length is less than in the case of the preparacrista. Because of the small size of the preparacrista of M1, the postmetacrista is more than three times longer than the preparacrista on M1, while it is approximately twice longer than the preparacrista on M2-3.

The stylar shelf is large and forms a deep basin between the para- and metacones and the labial edge of the molars. It is smaller and narrower on M1 than on M2-3. On M1, the stylar shelf is strongly asymmetrical, being much narrower anteriorly because of the shortness of the preparacrista. On M2-3, the stylar shelf is roughly rectangular, being much wider in its anterior region than on M1. The stylar shelf condition of *Allqokirus* is very similar to that of *Mayulestes* and *Patene* but also resembles that of *Andinodelphys* and *Pucadelphys*. At the anterolabial angle of the molars, stylar cusp A is small but distinctly separated from the much larger stylar cusp B. The latter is the largest stylar cusp of M1-3 and is only slightly smaller than the paracone. Stylar cusp B is rounded, and forms a marked convex inflation on the anterolabial region of the tooth. Posterior to stylar cusp B, at the level of the junction of the para- and metacones, Stylar cusp C is only represented by a weak thickening of the lateral edge of the stylar shelf on M2, while it is entirely absent on M3. In the posterolabial region of the stylar shelf, there is a large stylar cusp D, although it is smaller than stylar cusp B. It is transversely narrow and distinctly different from that of *Mayulestes*, which is larger and conical. Stylar cusp D is closely approximated to stylar cusp E, which is a small cuspule at the posterior end of the postmetacrista. As a whole, the stylar cusps of *Allqokirus* are well-developed and, in this respect, resemble (with some variations such as the weakness of the stylar cusp C) the condition seen in *Mayulestes*, *Andinodelphys* and *Pucadelphys*. They differ from the clearly reduced stylar cusps observed in *Patene*, although the stylar shelf in this genus is large and approximates in width the condition of *Allqokirus* and *Mayulestes*. The labial edge of the molars is almost straight on M1, but a deep ectoflexus is observed on M2-3. The condition of *Allqokirus* resembles that of *Mayulestes*, but differs from that of *Patene,* in which the ectoflexus is present but shallow on M2-3.

The M4 is, as usual, very different from the other three anterior molars, which justifies a separate description (Fig. 9). The anterior edge of the tooth is as long as the posterior edge of M3. However, the relative sizes of the elements along this edge are quite different. The protocone is smaller than on M3,

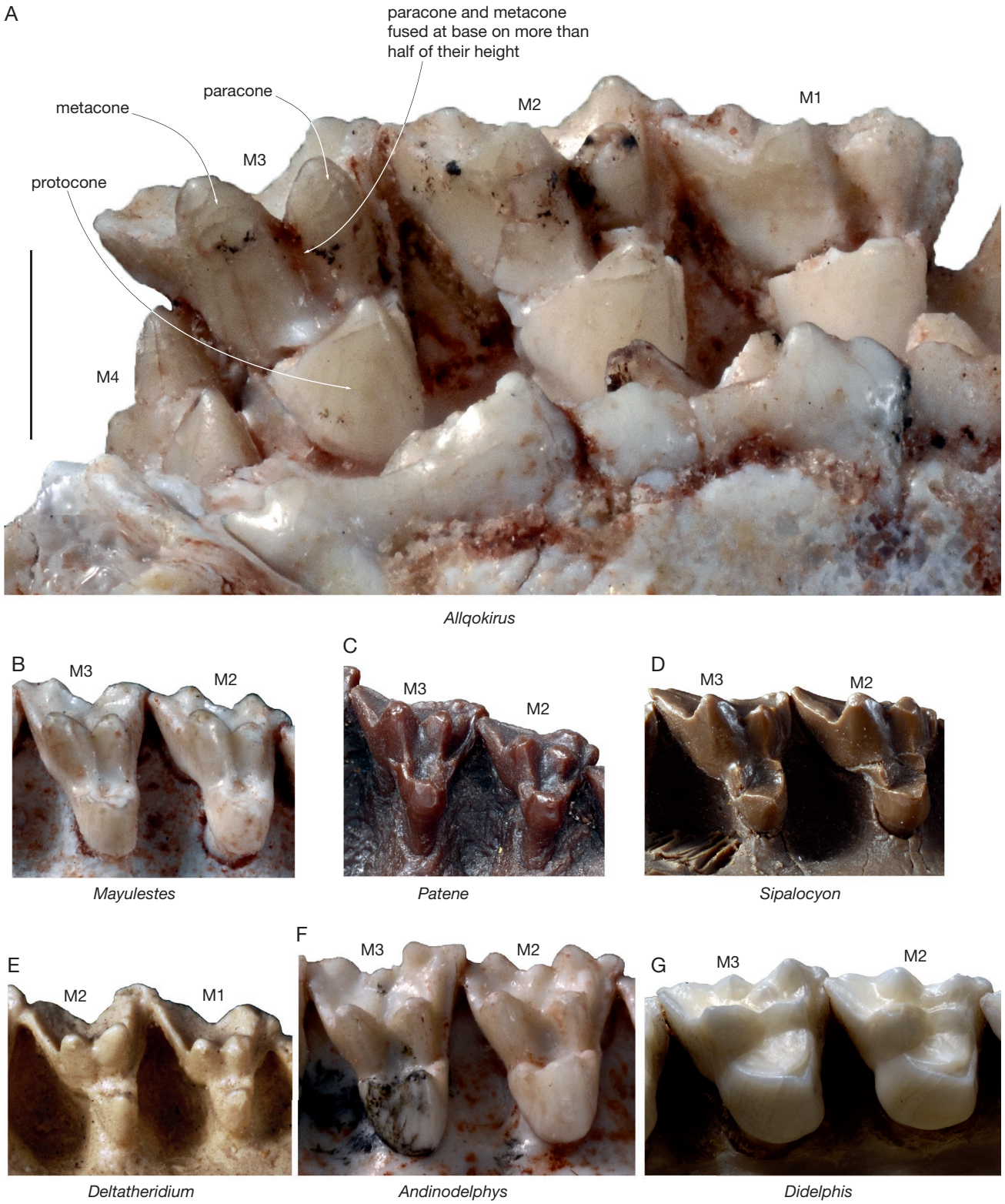


Fig. 10. — Medial view of the right upper molars of several metatherians showing the paracone and metacone adjoined at base on more than half of their height (**A**-**E**) and widely separated at base (**F**, **G**): **A**, *Allqokirus australis* (MHNC 8267); **B**, *Mayulestes ferox* (MHNC 1249); **C**, *Patene simpsoni* (cast of MNRJ 1331-V); **D**, *Sipalocyon gracilis*, (cast of YPM-PU 15373); **E**, *Delathteridium pretrituberculare*, (cast of ZPAL MgM-I/102); **F**, *Andinodelphys cochabambensis* (MHNC 13847); **G**, *Didelphis albiventris* (MNHN RH 120). Scale bar: **A**, 2 mm; **B**-**G**, not to scale.

but the paracone is much larger, being approximately as large as the metacone of M3. The preparacrista and the parastylar area of M4 are distinctly smaller than the corresponding region of M3, but they resemble the postmetacrista and the metastylar area of M3. Posteriorly, the metacone of M4 is very small, much smaller than the paracone and approach-

ing the size of stylar cusps A and B. of the tooth. The apex of the metacone barely overhangs the notch of the centrocrista. Posterior to stylar cusp B, the stylar shelf drastically narrows, and it is totally absent labial to the posterior half of the paracone and to the metacone. A small but distinct paraconule is present, but no metaconule can be observed. As observed on the other molars, M4 is three-rooted. Although structurally similar to that of *Mayulestes,* the M4 of *Allqokirus* is more massive, anteroposteriorly longer, and bears a larger paracone. It is more slender and anteroposteriorly shorter than that of *Patene simpsoni*.

*Lower dentition*

**Lower incisors.** In the description below, we follow the interpretation of Hershkovitz (1982, 1995), that the four lower incisors of metatherians are serially homologous to i2-i5. The four lower incisors are preserved on the right mandible, but i2 is missing most of its crown (Figs 11; 12). The incisor tooth row on the right mandible is roughly straight, and it forms an angle of approximately 60° with the symphyseal plane. It is therefore probable that the complete incisor tooth row was V-shaped or parabolic, with its branches meeting at approximately 120°. This condition differs from that in *Pucadelphys* and *Andinodelphys,* in which the branches of the incisor rows meet at an angle no larger than 90°. The incisors are not procumbent, and in this respect *Allqokirus* resembles *Mayulestes* but differs from *Pucadelphys* and *Andinodelphys.* The roots of the incisors are widely visible in anterior and labial view, and their external portions are three to four times longer than the crown. The i3 is approximately similar in size to i2, and both are larger than the posterior incisors. The i4 is slightly smaller than i3, and i5 is by far the smallest of the four incisors, its diameter being approximately half that of i4. The crown and upper part of the root of i5 is closely appressed against the anterior edge of the canine, as is also observed in *Mayulestes*; this condition is absent in *Pucadelphys* and *Andinodelphys*. The i3 is distinctly staggered; in other words, its root is shifted posteriorly as compared to the roots of i2 and i4. A staggered i3 is also present in *Mayulestes, Pucadelphys* and *Andinodelphys*. A staggered i3 is observed in almost all other metatherians (see Hershkovitz 1982, 1995; Cifelli & Muizon 1997; Voss & Jansa 2009). In many other sparassodonts, such as *Sipalocyon, Cladosictis, Prothylacynus, Borhyaena, Arctodictis, Australohyaena*, *Callistoe*, among others, the staggered condition is very obvious (Hershkovitz 1995; Babot *et al.* 2012; Forasiepi *et al.* 2015). In the sparassodonts with only three lower incisors, the fact that the second incisor is the staggered one indicates that the transition from the plesiomorphic pattern of four incisors to the derived condition of three incisors has been achieved via the loss of i5. The shape of the crowns is peg-like. It has a roughly triangular section on i3 but is slightly compressed labiolingually on i4, being slightly spatulate. The posterior base of the crowns of i3-4 is inflated and expands posteriorly, but no distinct cup is present, thus differing from the condition observed in extant didelphids (Voss & Jansa 2009).

**Lower canine.** The canine is preserved on both mandibles, but is not fully erupted (Figs 11; 12). It is recurved posteriorly, but to a lesser extent than is the upper canine. Its apex is dorsal to approximately the mid-point of the crown at its base. The canine is also slightly curved lingually. The crown is strongly convex labially and flat to concave lingually. The canine bears, on the anterior region of its lingual aspect, a continuous shallow groove, which runs from the alveolar border and extends almost from the apex of the crown to the root.

**Lower premolars.** The three lower premolars are preserved on both mandibles (Figs 11; 12). The p1 is by far the smallest of the three, and p2 is slightly smaller than p3. The difference in size between p1 and p2 is much greater than between p2 and p3. There is no diastema, neither between p1 and the canine, nor between the premolars. The p1 is distinctly procumbent, and its anteriormost edge overhangs the posterior edge of the canine. The tooth is single-cusped. The anterior edge of the cusp is convex and much shorter than the posterior one. It is strongly convex while the posterior edge is straight. The apex of the p1 is shifted anteriorly and overhangs the anterior edge of the anterior root. At the posterior base of the crown is a distinct basal cuspule. The p2 is not procumbent. Its main cusp is triangular, but strongly asymmetrical since the apex of the tooth overhangs the anterior half of the anterior root. The anterior edge of the tooth forms a distinct crest, slightly convex anteriorly. The posterior edge has a sharp and straight crest. At its base is a well-developed heel made of two poorly defined cusps: an anterolabial one and a posterolingual one. These two cusps of the heel form an oblique crest oriented anterolabially-posterolingually. The posterior cusp extends lingually as a conspicuous posterocingulid, which reaches the posterolateral base of the main cusp. No cingulid is present at the anterior base of the tooth. As mentioned above, p3 is not fully erupted. However, its crown is sufficiently visible on the left mandible to provide clear information on its morphology, which is complemented by digital rendering of CT data. The tooth is higher than the m1 that follows it. The main cusp is large and triangular and slightly asymmetrical. However, the asymmetry is less pronounced than on p2 since the apex of the tooth overhangs the interradicular septum. The labial aspect of the main cusp is markedly convex, and its lingual surface is roughly flat. The anterior edge of the main cusp forms a slightly convex crest, which bears at its anterolingual base a small cuspule. A small anterocingulid is present at the anterolabial base of the main cusp. The posterior edge of the main cusp also forms a sharp crest but is very slightly concave posterodorsally. At the posterior end of the tooth is a well-developed heel, larger than on p2. The heel, which is almost a small talonid, bear a labial and a posterior cusp respectively in a hypoconid and hypoconulid position. The anterior edge of the labial cusp contacts the posterior crest of the main cusp on the labial edge of the tooth. At the contact of the two crests a deep notch is visible in labial view. Below this notch, a small posterolabial cingulum is present. From the posterior cusp, a thick ridge extends anterolingually as


FIG. 11. — *Allqokirus australis* (MHNC 8267), left lower dentition: **A**, labial view; **B**, stereophotographs of occlusal view; **C**, lingual view. Scale bar: 5 mm.

far as the posterolingual base of the main cusp. The posterior heel of p3 of *Allqokirus* is clearly better developed than the single cusp observed in *Mayulestes*, which does not have the "proto-talonid" morphology observed in *Allqokirus*. This taxon also differs from *Pucadelphys* and *Andinodelphys*, which resemble *Mayulestes* in this respect.

**Lower Molars.** The first three molars are preserved on both dentaries and are fully erupted (Figs 11; 12; 13). Only the right m4 is fully preserved, and more than half of the tooth is still inside its crypt (the base of the trigonid and most of the talonid). Because the tooth and the bone of the dentary have both the same mineralogy (calcium phosphate) the digital ren-


FIG. 12. — *Allqokirus australis* (MHNC 8267), right lower dentition: **A**, labial view; **B**, stereophotographs of occlusal view; **C**, lingual view. Scale bar: 5 mm.

dering obtained from the CT scanning did not provide enough contrast to discriminate the structures. Therefore, a window has been excavated in the lingual wall of the m4 crypt, which allowed observation of most of the last lower molar morphology.

The molars increase in size posteriorly, but the greatest size increase is between m1 and m2, even if m3 is slightly larger than m2. The m3 and m4 are subequal in size. The trigonid is approximately three times as high as the talonid. The trigonid

and talonid of m1-2 are subequal in width, but on m3-4 the trigonid is distinctly wider. The trigonid is longer than the talonid: measured from the anterior edge to the posterior margin of the protoconid, the trigonid of m3 is 2.20 mm long and the talonid, 1.28 mm. This condition resembles that of *Mayulestes* (2.14 vs 1.22 mm) and markedly departs from that of *Andinodelphys* and *Pucadelphys,* in which trigonid and talonid have approximately the same length. A trigonid much longer than the talonid is also observed in *Patene* (3.04 vs 1.74 mm on MNHN-F-ITB1; 3.64 vs 2.66 mm on DGM 657-M; 3.68 vs 2.03 mm on DGM 654-M). A trigonid longer than the talonid is present in all sparassodonts. The cusps of the trigonid are sharp and elevated. The protoconid is the largest cusp of the trigonid, being at least two times higher than, and more voluminous than, the metaconid and paraconid. The protoconid is triangular in section. It is relatively flat in its lingual aspect, while its labial surface is strongly convex in a horizontal plane but also in vertical plane. In other words, the labial aspect of the protoconid is more salient labially at mid-height than at the apex or at the base of the cusp. This characteristic feature is also present in *Mayulestes*, *Patene*, and in most other sparassodonts. It is absent in *Pucadelphys, Andinodelphys,* didelphids, and dasyurids (Fig. 14). In thylacinids the lateral edge of the protoconid is slightly convex, but never to such an extent as observed in sparassodonts. In occlusal view, the anterolabial aspect of the protoconid is strongly oblique and at an angle of approximately 45° to the anteroposterior axis of the tooth row. The posterior surface of the protoconid is roughly perpendicular to the axis of the tooth row, although less so on m1-2. The preprotocristid is sharp, and it connects to the preparacristid to form a long and robust oblique paracristid. This paracristid forms an angle of approximately 45° with the axis of the tooth row. In occlusal view the preprotocristid is longer than the preparacristid. A deep carnassial notch is present at their junction, which extends slightly onto the anterolabial side of the trigonid. Posteriorly, the postprotocristid connects to the postmetacristid and forms a transversely narrow protocristid. A deep carnassial notch is also observed at the junction of the two crests.

The protoconid of *Allqokirus* is proportionally more elevated than in *Andinodelphys*, *Pucadelphys* and didelphids. A comparison of the height of the protoconid to the length of m3 or m4 (Hpo/Lm) indicates that the protoconid is generally higher in sparassodonts than in other metatherians except *Deltatheridium* and *Dasyurus* (Table 2). However, one sparassodont (*Hondadelphys*) in our sample departs from the other members of the order. Sparassodonts have a Hpo/Lm ratio greater than 0.9. *Allqokirus* and *Mayulestes*, in which the Hpo/Lm ratio varies from 0.95 to 1 clearly resemble the other sparassodonts in this respect. A similar condition is observed in the eutherians selected as outgroups in our analysis (*Prokennalestes, Maelestes*, and *Asioryctes*), in *Deltatheridium*, and in *Dasyurus*. Surprisingly, *Thylacinus* has a Hpo/Lm ratio varying from 0.77 to 0.86, i.e., well below the value obtained in sparassodonts. The ratio in *Pucadelphys* and *Andinodelphys* (0.74-0.79) is close to that observed in extant didelphids (0.68-0.77) and is conspicuously smaller than in sparassodonts.

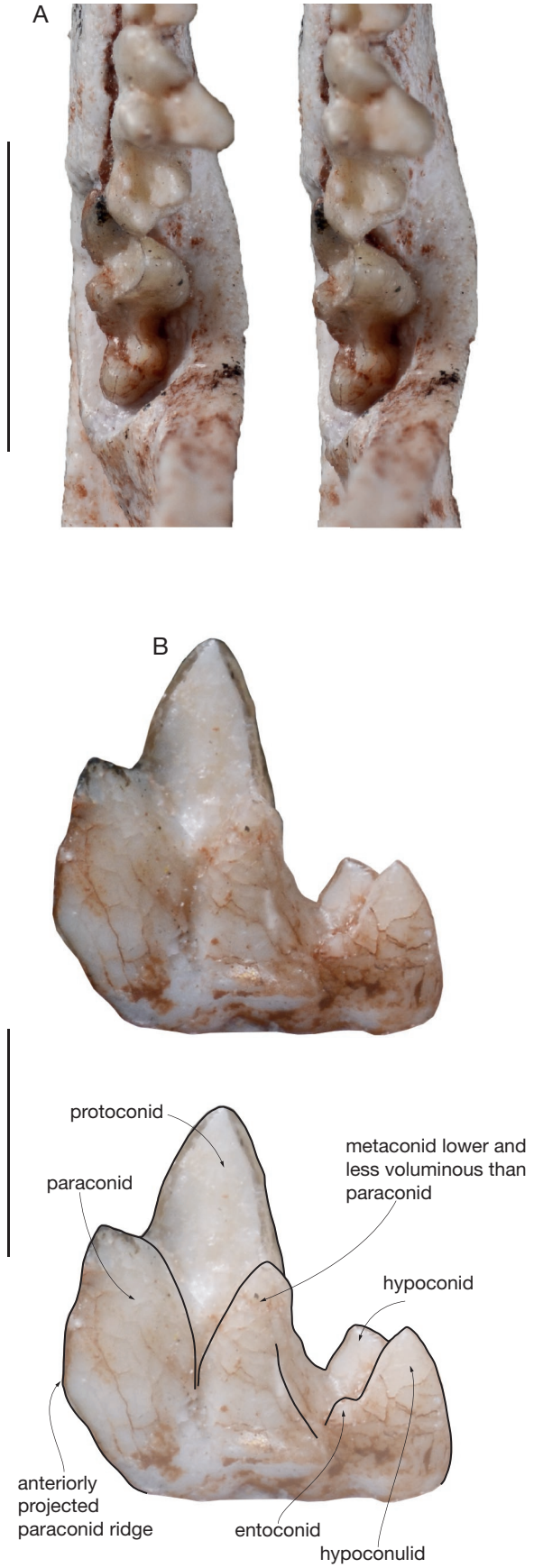


FIG. 13. — *Allqokirus australis* (MHNC 8267): **A**, stereophotographs of the right m3 and m4 in occlusal view; **B**, lingual view of the right m4. Scale bars: A, 5 mm; B, 2 mm.

TABLE 2. — Comparison of the height of the protoconid relative to the length of the penultimate or ultimate lower molar (except that the antepenultimate molar has been used in the case of *Deltatheridium pretrituberculare* and *Herpetotherium valens*). Abbreviations: **P**, indicates that the measurement was obtained from a publication (see taxon list, specimens and related references); **Hpo**, protoconid height; **Lm**, molar length; **pum**, penultimate molar; **um**, ultimate molar.

| Taxon | Specimen number | Tooth | P | L pum or um (if possible) | H po | Hpo/Lm |
|---|---|---|---|---|---|---|
| *Prokennalestes minor* | GI PST 10-6 | m3 | P | 1.86 | 1.72 | 0.92 |
| *P. trofimovi* | GI PST 10-8a | m3 | P | 1.78 | 1.84 | 1.03 |
| *Maelestes gobiensis* | PSS-MAE 607 | m3 | P | 1.72 | 2.00 | 1.16 |
| *Asioryctes nemegetensis* | ZPAL MgM-I/148 | m3 | P | 1.88 | 2.10 | 1.11 |
| | ZPAL MgM-I/56 | m3 | P | 1.63 | 2.04 | 1.25 |
| *Kokopellia juddi* | OMNH 26361 | m4 | – | 2.4 | 1.98 | 0.82 |
| *Deltatheridium pretrituberculare* | PSS-MAE 132 | m2 | – | 3.24 | 3.25 | 1.00 |
| | PSS-MAE 132 | m3 | – | 2.84 | 3.31 | 1.16 |
| *Asiatherium reshetovi* | PI-RAS 3907 | m4 | – | 1.93 | 1.35 | 0.7 |
| *Eodelphis browni* | ROM 701 | m4 | P | 5.6 | 4.33 | 0.77 |
| | UA 7011 | m4 | P | 4.11 | 3.47 | 0.84 |
| | UA 7011 | m3 | – | 3.55 | 2.73 | 0.77 |
| *Didelphodon vorax* | UC52290 | m4 | – | 6.38 | 4.85e | 0.76 |
| *D. vorax* | UCMP 52289 | m2 | – | 5.31 | 4.14 | 0.78 |
| *D. vorax* | UC52288 | m4 | – | 7.76 | 6.04 | 0.78 |
| *Didelphodon coyi* | TMP 84-64-1 | m4 | P | 6.00 | 4.7 | 0.78 |
| *Peradectes chesteri* | UM 71663 | m4 | – | 1.52 | 1.17 | 0.77 |
| *P. chesteri* | USNM 19199 | m3 | P | 1.44 | 1.03 | 0.71 |
| *Peradectes pauli* | USNM 20879 | m4 | – | 1.57 | 1.15 | 0.73 |
| *P. pauli* | USNM 20879 | m3 | – | 1.53 | 1.2 | 0.78 |
| *Herpetotherium fugax* | CM 10424 | m3 | P | 2.07 | 1.49 | 0.73 |
| *Herpetotherium valens* | CM 29416 | m2 | – | 2.17 | 1.70 | 0.78 |
| *Nanodelphys hunti* | AMNH 5266 | m4 | – | 1.43 | 1.11 | 0.77 |
| | AMNH 5267 | m3 | – | 1.42 | 1.12 | 0.79 |
| *Peratherium elegans* | MNHN.F.RZN8 | m4 | – | 2.28 | 1.87 | 0.82 |
| *Peratherium elegans* | MNHN.F.QU8216 | m4 | – | 2.29 | 1.89 | 0.82 |
| *Amphiperatherium minutum* | MNHN.F.GY683 | m4 | – | 1.56 | 1.16 | 0.74 |
| *A. ambiguum* | MNHN.F.QU8215 | m3 | – | 2.35 | 1.94 | 0.82 |
| *Amphiperatherium exile* | MNHN.F.PFR10356 | m4 | – | 1.67 | 1.28 | 0.76 |
| *Peratherium antiquum* | MNHN.F.PFR10363 | m4 | – | 2.44 | 1.81 | 0.74 |
| *Didelphis albiventris* | MNHN RH120 | m4 | – | 6.17 | 4.2 | 0.68 |
| | MNHN RH161 | m4 | – | 5.10 | 3.66 | 0.71 |
| | MNHN RH124 | m3 | – | 6.05 | 4.31 | 0.71 |
| | MNHN RH uncat. | m3 | – | 6.2 | 4.58 | 0.74 |
| *Metachirus nudicaudatus* | MNHN coll. Filhol, uncat. | m4 | – | 3.26 | 2.46 | 0.75 |
| | MNHN RH16 | m3 | – | 4.45 | 3.40 | 0.76 |
| | MNHN RH81 | m4 | – | 3.43 | 2.64 | 0.77 |
| *Monodelphis brevicaudata* | MNHN.AC.258-M | m4 | – | 2.40 | 1.80 | 0.75 |
| | MNHN.AC.2004-317 | m4 | – | 2.41 | 1.81 | 0.75 |
| | MNHN.AC.1995-3216 | m4 | – | 2.64 | 2.03 | 0.77 |
| *Pucadelphys andinus* | MHNC 8280 | m4 | – | 1.89 | 1.44 | 0.76 |
| | MHNC 8266 | m4 | – | 1.92 | 1.51 | 0.78 |
| | MHNC 8351 | m4 | – | 1.99 | 1.56 | 0.78 |
| *Andinodelphys cochabambensis* | MHNC 8308 | m4 | – | 3.14 | 2.47 | 0.78 |
| | MHNC 8264 | m4 | – | 3.21 | 2.38 | 0.74 |
| | MHNC 8370 | m4 | – | 3.06 | 2.41 | 0.79 |
| *Mayulestes ferox* | MHNC 1249 | m4 | – | 3.80 | 3.73 | 0.98 |
| ***Allqokirus australis*** | MHNC 8267 | m3 | – | 3.87 | 3.79 | 0.98 |
| | MHNC 8267 | m4 | – | 3.50 | 3.53 | 1.00 |
| | YPFB Pal 6190 | ?m3 | – | 3.90 | 3.72 | 0.95 |
| | MHNC 13932 | ?m3 | – | 3.53 | 3.63 | 1.02 |
| *Patene simpsoni* | DGM 657-M | m4 | – | 7.27 | 8.34 | 1.14 |
| | DGM 324-M | m3 | – | 5.10 | 5.75 | 1.12 |
| | DGM 654-M | m3 | – | 5.80 | 6.28 | 1.08 |
| *Hondadelphys fieldsi* | UCMP 37960 | m4 | P | 7.81 | 6.63 | 0.84 |
| *Notogale mitis* | MNHN.F.SAL96 | m4 | – | 8.09 | 7.98 | 0.98 |

TABLE 2. — Continuation.

| Taxon | Specimen number | Tooth | P | L pum or um (if possible) | H po | Hpo/Lm |
|---|---|---|---|---|---|---|
| *Sipalocyon gracilis* | MACN 691 | m4 | – | 7.39 | 7.28 | 0.98 |
| | YPM-PU 15373 | m4 | – | 6.29 | 6.27 | 1.00 |
| *Cladosictis patagonica* | MNHN.F.SCZ146 | m4 | – | 9.48 | 9.22 | 0.97 |
| *Cladosictis centralis* | MNHN.F.COL4 | m4 | – | 8.20 | 8.68 | 1.06 |
| *Lycopsis longirostrus* | UCMP 38061 | m3 | P | 15.3 | 15.52 | 1.01 |
| *Prothylacynus patagonicus* | MACN 706 | m4 | – | 14.87 | 13.5e | 0.90 |
| | YPM-PU 15700 | m4 | – | 14.82 | 13.45 | 0.91 |
| *Borhyaena tuberata* | MACN 2074 | m4 | – | 16.63 | 17.04 | 1.02 |
| *Arctodictis sinclairi* | MLP 85-VII-3-1 | m4 | – | 15.5 | 14.4 | 0.93 |
| *Callistoe vincei* | IML PLV 4187 | m4 | P | 14.04 | 13.10e | 0.93 |
| *Thylacosmilus atrox* | FMNH 14407 | M4 | – | 14.17 | 13.06 | 0.92 |
| *Dromiciops gliroides* | IEEUACH 2162 | m4 | – | 1.58 | 1.07 | 0.67 |
| | IEEUACH 2167 | m4 | – | 1.61 | 1.12 | 0.69 |
| *Dasyurus viverrinus* | MNHN.AC.A2627 | m4 | – | 6.66 | 6.03 | 0.93 |
| | MNHN.AC.A12425 | m4 | – | 4.21 | 3.93 | 0.93 |
| | MNHN uncat. | m4 | – | 4.65 | 4.41 | 0.95 |
| *Sminthopsis* sp. | MNHN.AC.1919-30 | m4 | – | 1.83 | 1.57 | 0.86 |
| *Thylacinus cynocephalus* | MNHN.AC.A.3298 | m4 | – | 14.57 | 11.20 | 0.77 |
| | MNHN.AC.1891-327 | m4 | – | 16.16 | 13.27 | 0.82 |
| | MNHN.AC.1891-61 | m4 | – | 15.34 | 12.38 | 0.80 |
| | MNHN.AC.2007-19 | m4 | – | 16.34 | 13.65 | 0.83 |

On the lingual side of the trigonid of m1-2, the paraconid is almost subequal in size to the metaconid: the paraconid is slightly smaller in height than the metaconid but the cusps are subequal in volume. On m3, the paraconid and metaconid are subequal in height but the metaconid is slightly smaller in volume (in occlusal and labial views). On m4, the metaconid is distinctly smaller than the paraconid in terms of both height and volume. A paraconid subequal in height to the metaconid and distinctly smaller in volume is also observed on the lower molar (m2 or m3) referred to *Allqokirus australis* (YPFB Pal 6190) by Marshall & Muizon (1988). as well as on another isolated lower molar referred to this taxon. Therefore, the relative proportions of the paraconid and metaconid observed on MHNC 8267 vary from m1 to m4. The metaconid, which is slightly higher than and subequal in volume to the paraconid on m1, becomes lower and less voluminous than the paraconid on m4. However, the height and volume difference between the two cusps is always moderate whichever of the tooth is considered. The condition in *Allqokirus* resembles that in *Mayulestes* in this respect. The condition in *Patene* approaches that in *Allqokirus*, but in the former genus the metaconid is either subequal in height or lower than the paraconid, and it is always less voluminous. The condition in *Allqokirus* strongly differs from *Pucadelphys*, *Andinodelphys,* and didelphids, in which the metaconid is much higher and more voluminous than the paraconid. In this respect *Allqokirus* (and *Mayulestes*) undoubtedly resemble *Patene* more than the pucadelphyids and didelphids, from which they both clearly depart as far as the relative size of the paraconid and metaconid is concerned. We therefore consider that, relative to the condition of *Pucadelphys, Andinodelphys,* and didelphids, the paraconid and metaconid of *Allqokirus* and *Mayulestes* can be regarded as subequal in size (height and volume).

The paraconid of *Allqokirus* is roughly triangular in section. It bears only one cristid, the preparacristid, (i.e., the labial segment of the paracristid, which joins the preprotocristid posteriorly) and the posterolingual side of the cusp is regularly convex with no trace of postparacristid. At the anterolingual angle of the paraconid is a salient paraconid ridge, which extends on the whole height of the cusp. In lingual view, the paraconid ridge is regularly convex anteriorly and overhangs the anterior root of the molar; it distinctly expands the anteroposterior length of the paraconid, which is the greatest at mid-height of the cusp. The ridge is relatively blunt on m2-3, but it is sharper on m1 and apparently also on m4. The paraconid ridge is weak and does not project anteriorly in *Andinodelphys*, *Pucadelphys* and in didelphids. A well-developed paraconid ridge is present in *Patene* as well, as in all other sparassodonts in which the massiveness of the dentition has not altered this feature (e.g. *Siplaocyon*, *Cladosictis, Sallacyon, Notogale, Lycopsis, Hondadelphys, Acyon*). In other sparassodonts with massive molars (e.g. *Borhyaena, Arctodictis, Prothylacynus*), the paraconid ridge is attenuated but the anteroposterior enlargement of the paraconid in lingual view is still distinct. The paraconid ridge is poorly developed in *Thylacinus* and *Sarcophilus*, but the paraconid of both taxa, in lingual view, is anteroposteriorly expanded at mid-height. Because the condition of fossil thylacinids is similar to that of the Recent species it is uncertain whether an anteriorly expanded paraconid ridge was present in the early evolutionary history of the family. So far, the presence of an anteriorly expanded paraconid ridge appears to be a characteristic of sparassodonts (including *Mayulestes*

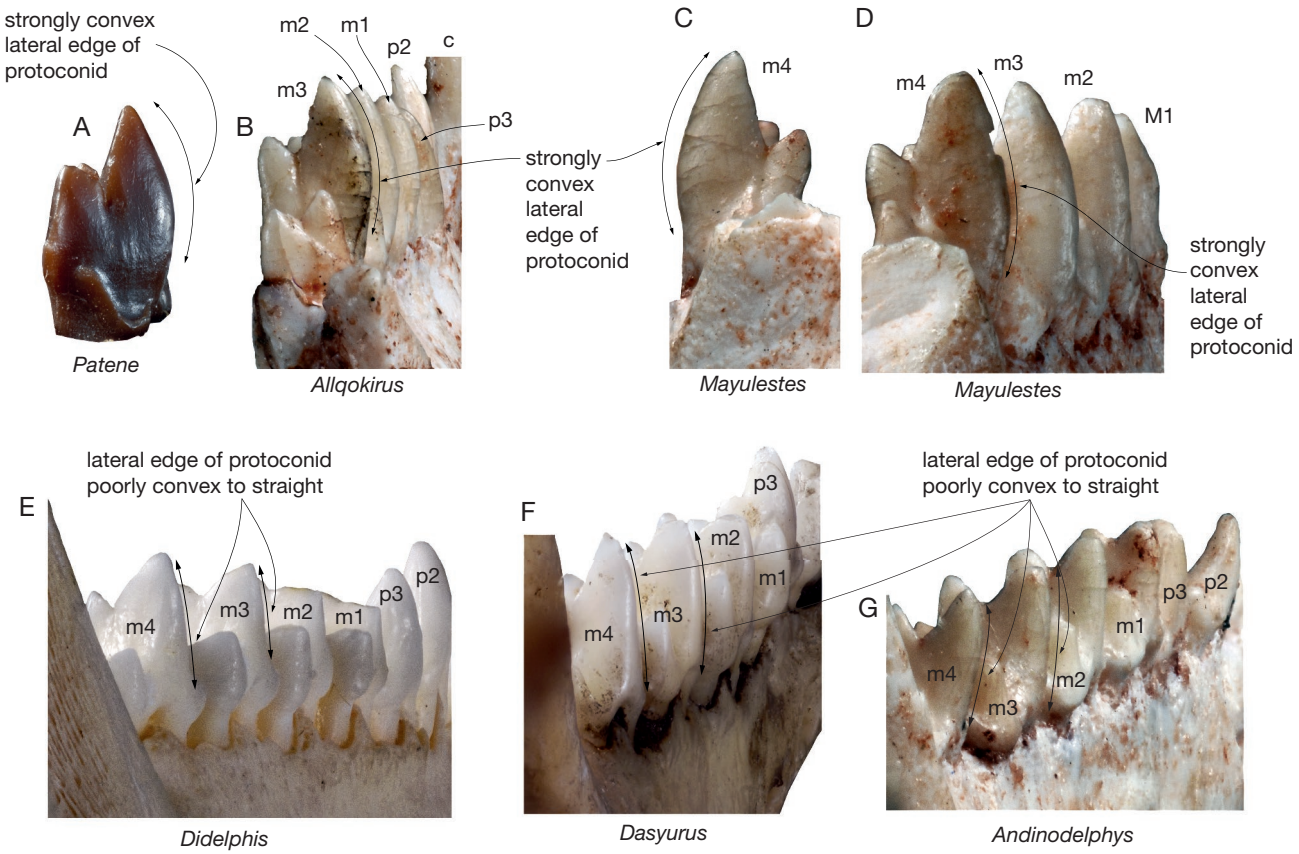


FIG. 14. — Views of the lateral expansion of the protoconid in various metatherians: **A**, *Patene simpsoni* (cast of DGM untalogued specimen), left m4 in anterior view; **B**, *Allqokirus australis* (MHNC 8267), posterolateral view of left mandible (reversed); **C**, *Mayulestes ferox* (MHNC 1249), posterior view of left m4; **D**, *Mayulestes ferox* (MHNC 1249), posterolateral view of right mandible; **E**, *Didelphis viginiana* (SL personal collection), posterolateral view of right mandible; **F**, *Dasyurus hallucatus* (MNHN.ZO-AC-1880-1019), posterolateral view of right mandible; **G**, *Andinodelphys cochabambensis* (MHNC 8264), posterolateral view of left mandible (reversed). Not to scale.

and *Allqokirus*). The presence of a paraconid ridge, which enlarges the length of the paraconid, has been mentioned by Marshall *et al.* (1990) as "paraconid elongated" and included in sparassodont synapomorphies. Labial to the paraconid ridge and at the base of the crown, is a deep vertical notch (the hypoconulid notch), which receives the hypoconulid of the anterior molar.

Labial to the hypoconulid notch is the point of departure of a strong anterolabial cingulid. This cingulid extends from the labial side of the paraconid to the anterolabial edge of the protoconid. At the posterolabial end of the precingulid, the anterolabial surface of the protoconid is excavated by a fossula (especially well-marked on m2 and m3 but not observable on m4 because the labial aspect of the tooth is still partially in its crypt), (Figs 11; 12). It is also present on the m3 referred to *Allqokirus australis* by Marshall & Muizon (1988). This structure is also present but less developed in *Mayulestes*; it is variably present in *Patene* but is distinctly less developed than in *Allqokirus*. An anterolabial fossula of the protoconid is apparently absent in other sparassodonts. It probably received the apex of the large metacone of the upper molars. The metaconid is somewhat conical in section (except for the presence of the small postmetacristid). Its anterolingual surface is regularly convex and blunt and bears no premetacristid. The metaconid is slightly posterolingual to the protoconid in m1 and strictly lingual to this cusp in posterior molars. On the four molars, the metaconid is well separated from the paraconid by a vallid, which extends as far as the base of the crown. This condition is similar to that observd in *Mayulestes* and *Patene*, but differs from that observed on *Pucadelphys* and *Andinodelphys*, in which paraconid and metaconid are fused at their base. As a consequence, the trigonid basin is widely open lingually. In fact, it is more a slope than a basin. This condition is similar to that observed in *Mayulestes* and *Patene*, but differs from that in *Pucadelphys*, *Andinodelphys*, in which the floor of the trigonid basin is subhorizontal or concave. In the other sparassodonts, there is no real trigonid basin since the metaconid is vestigial or lost.

The talonid of *Allqokirus* is distinctly three cusped, but the hypoconid and the hypoconulid are conspicuously larger than the small entoconid. As a consequence of the small size of the entoconid and of its posterolingual position, the talonid basin, although well-developed, is widely open anterolingually. The hypoconid is the largest cusp of the trigonid. On m1 it is approximately two times larger in volume (in occlusal view) than the hypoconulid. This size difference reduces posteriorly: on m3, the hypoconid is only slightly larger than the hypoconulid and on m4 it is distinctly smaller. The

hypoconid is triangular in section, with a flat side facing lingually and forming the labial edge of the talonid basin. The cristid obliqua connects to the posterior edge of the trigonid, slightly labial to the protocristid notch, as is seen in *Mayulestes, Patene, Andinodelphys* and *Pucadelphys*. The hypocristid connects the hypoconid to the hypoconulid and it is formed by two parts: the posthypocristid from the hypoconid, and the hypoconulid cristid from the hypoconulid. On m3, the posthypocristid is roughly as long as the labial hypoconulid cristid. A deep carnassial notch is observed in the middle of the hypocristid, between the apices of the hypoconid and hypoconulid. The hypoconulid is roughly semicircular and has a flat to slightly concave anterior aspect. It is distinctly shifted lingually, being roughly in line with the metaconid. It increases in size from m1 to m4. In terms of both height and volume, the hypoconulid is largest on m4. The entoconid is small. It decreases in size posteriorly and is reduced to a small cuspule on the anterolingual edge of the hypoconulid of m4. On the four molars, the entoconid is closer to the hypoconulid than to the metaconid. From the anterior edge of the entoconid, a weak preentocristid extends anteriorly and reaches the posterolingual base of the metaconid. The hypoflexid is deep. In occlusal view, it is approximately 40% of the talonid width on m1-2, 50% on m3, and 60% on m4. A well-marked postcingulid descends from the labial edge of the hypoconulid and reaches the posterolabial base of the hypoconid (Table 3).

TABLE 3. — Measurements of the teeth of *Allqokirus australis* (MHNC 8267). **e**, estimated values.

| Upper incisors, canine, and premolars | Length | Width | Height |
|---|---|---|---|
| I1 | – | – | – |
| I2 (right) | 0.58 | 0.56 | – |
| I3 (right) | 0.74 | 0.69 | – |
| I4 (right) | 0.82 | 0.73 | – |
| I5 (right) | 0.62 | 0.46 | – |
| C (left) | 2.59 | 1.25 | 4.94 |
| P1 (left) | 1.39 | 0.60 | 0.95 |
| P2 (left) | 2.08 | 0.85 | 1.53 |
| P3 (left) | 2.67 | 1.12 | 2.28 |

| Lower incisors, canine, and premolars | Length | Width | Height |
|---|---|---|---|
| i1 (right) | 0.61 | 0.92 | – |
| i2 (right) | 0.72 | 0.71 | 0.89 |
| i3 (right) | 0.65 | 0.58 | 0.77 |
| i4 (right) | 0.41 | 0.33 | – |
| C (left) | 2.34 | 1.23 | 3.47 |
| p1 (left) | 1.33 | 0.60 | 0.69 |
| p2 (left) | 2.16 | 0.96 | 1.87 |
| p3 (left) | 2.36 | 1.01 | 2.17 |

| Upper molars (right) | M1 | M2 | M3 | M4 |
|---|---|---|---|---|
| Anteroposterior length on labial edge | 3.17 | 3.23 | 3.13 | 2.42 |
| Transverse width on anterior edge | 2.74 | 3.49 | 3.80 | 3.58 |
| Transverse width on posterior edge | 3.64 | 4.45 | 4.45 | 1.83 |
| Anteroposterior width of protocone at conules | 1.38 | 1.43 | 1.42 | 0.84 |
| Distance between apices of para- and metacone | 1.08 | 1.13 | 1.23 | 0.95 |
| Length of postmetacrista | 1.49 | 1.51 | 1.58 | – |

| Lower Molars (m1-3: right; m4: left) | m1 | m2 | m3 | m4 |
|---|---|---|---|---|
| Anteroposterior length | 3.08 | 3.54 | 3.76 | 3.72e |
| Transverse width of trigonid | 1.25 | 1.61 | 1.86 | 1.98e |
| Transverse width of Talonid | 1.08 | 1.43 | 1.51 | 1.12 |
| Anteroposterior length of trigonid on lingual edge | 2.08 | 2.34 | 2.63 | 2.56e |
| Length of trigonid on anterolabial edge | 1.67 | 1.94 | 2.23 | – |
| Length of paraconid on lingual side | 0.92 | 1.01 | 1.12 | 1.28e |
| Length of metaconid on lingual side | 0.87 | 0.94 | 0.97 | 0.99 |
| Height of protoconid on labial side | 2.71 | 3.00 | 3.55 | – |
| Height of paraconid on lingual side | 1.12 | 1.37 | 1.49 | 1.79 |
| Height of metaconid on lingual side | 1.21 | 1.40 | 1.49 | 1.52 |
| Length of talonid | 0.99 | 1.07 | 1.18 | 1.24 |

## BONY SKULL

### *Premaxilla*

Only the incomplete right premaxilla is preserved. As preserved, it bears the roots of I2-5. The bone is incomplete medial to I2, and the posterodorsal process, which inserts between the nasal and the maxilla, is probably missing its posterior apex. The premaxilla is still well-articulated with the maxilla and has suffered no displacement. In lateral view, the major characteristic of the premaxilla is the downward orientation of its alveolar process, the anterior tooth-bearing portion of the bone (Fig. 15). The angle between the alveolar borders of the incisors and a line connecting the posterior edge of I5 and the posterolabial angle of M3 is 133°, while in *Mayulestes* this angle is 163°. A similar angle is measured in *Didelphis, Pucadelphys*, and *Andinodelphys*, in which it varies between 152° and 162°. Therefore, the condition of *Allqokirus* clearly departs from that observed in the other Tiupampa metatherians and extant didelphids. Comparison with the other sparassodonts that preserve the premaxilla is not possible since in these taxa (e.g. *Cladosictis, Prothylacynus, Borhyaena, Australohyaena, Callistoe*) the incisor tooth row is transverse or only slightly curved posteriorly (*Sipalocyon*), and the incisor alveolar border is not visible laterally. Because of this morphology, the alveolar process of the premaxilla of *Allqokirus* strongly dips anteroventrally and does not project anteriorly as much as is observed in *Mayulestes*. Posterior to the last incisor (I5), the premaxilla forms the medial wall of the paracanine fossa, which receives the apex of the lower canine This wall extends form the posterior edge of the I5 to the anterolabial angle of the canine alveolus. The lateral wall of the fossa is formed by the maxilla, as in most generalised metatherians (e.g. *Pucadelphys, Andinodelphys*, didelphids), and differing from the other sparassodonts compared, in which the lateral maxillary wall has disappeared, the fossa being open laterally and completely formed medially by the premaxilla. This wall does not extend much ventrally, and it remains well above the alveolar border of I5. Furthermore, its ventral edge is strongly concave. In contrast, the medial wall of the fossa (formed by the premaxilla) extends ventrally below the alveolar border of the canine and of I5. As a consequence, the paracanine fossa is widely opened laterally and only its dorsal apex is laterally

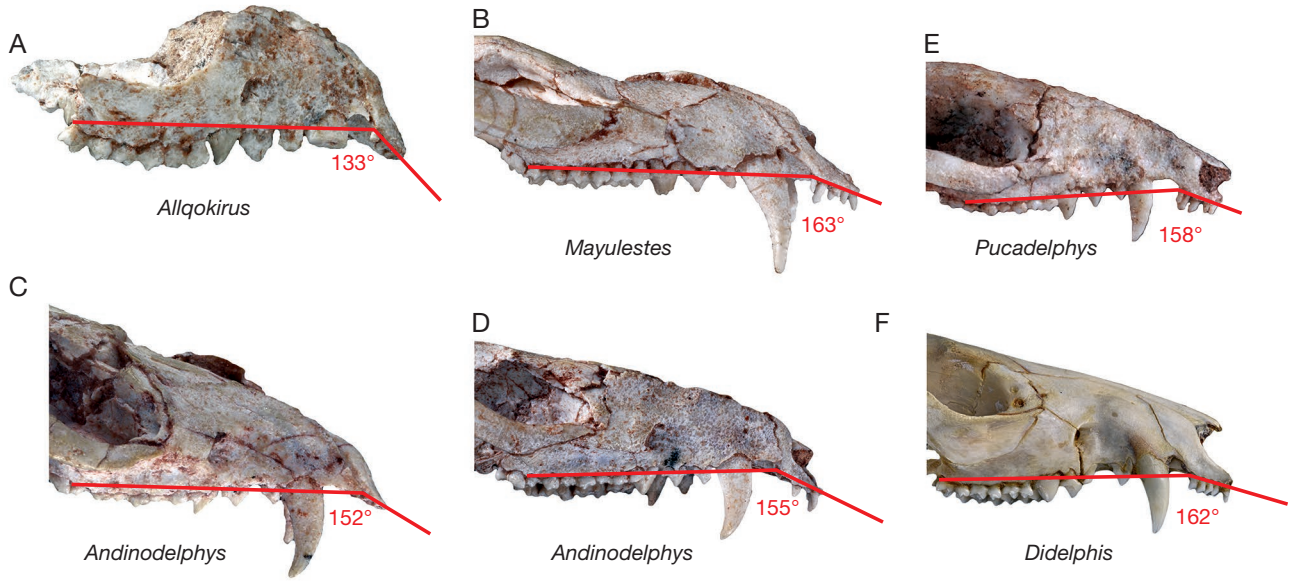


FIG. 15. — Right lateral view of the rostrum showing the ventral orientation of the alveolar process of the premaxilla in: **A**, *Allqokirus australis* (MHNC 8267); **B**, *Mayulestes ferox* (MHNC 1249); **C**, *Pucadelphys andinus*, (MHNC 8378); **D**, *Andinodelphys cochabambensis* (MHNC 8264); **E**, *Andinodelphys cochabambensis* (MHNC 8308); **F**, *Didelphis albiventris* (Coll RH 161). Not to scale.

covered by the maxilla. Furthermore, because of the ventral orientation of the alveolar process of the premaxilla, the paracanine fossa is relatively shorter anteroposteriorly than in *Mayulestes*. The lateral (maxillary) wall of the fossa extends on almost the entire anteroposterior length of the fossa, while in *Mayulestes* (the fossa being longer) the maxillary process is no longer than the posterior third of the fossa, and the anterior two thirds of the fossa are not walled laterally by the maxilla. The paracanine fossa of *Allqokirus* is dorsoventrally higher than anteroposteriorly long. This condition is present in *Mayulestes* as well as in most sparassodonts, where it can be identified. Conversely, in *Pucadelphys*, *Andinodelphys*, and in most didelphids, the fossa is longer than high, except in *Caluromys* in which it is as long as high. The palatal process of the premaxilla of MHNC 8267 is not preserved.

*Maxilla*

Both maxillae are reasonably well preserved, but the right is more complete than the left one (Fig. 3). The facial process forms the dorsolateral wall of the rostrum. It is elevated and steep and is not conspicuously convex as in *Andinodelphys, Pucadelphys* and Recent didelphids. Comparison with *Mayulestes* is not easy since the skull of the holotype and single known specimen is dorsoventrally compressed; it seems however that the facial process of *Mayulestes* was not as steep as in *Allqokirus*. On the lateral aspect of the facial process is a relatively small infraorbital foramen as compared to *Pucadelphys* and *Andinodelphys*. It is similar in size to that of *Mayulestes* and didelphids. It is located above the embrasure between P2 and P3. The foramen has a slightly more posterior position in *Mayulestes*, in which it is dorsal to the posterior root of P3. In *Andinodelphys* and *Pucadelphys*, this foramen is generally above the posterior root of P3, but in some specimens of *Andinodelphys* it clearly overhangs the anterior root of P3. In Recent didelphids the position varies, but it is generally dorsal to the anterior or posterior root of P3. In *Didelphis* and *Caluromys*, however, it overhangs the P2. It is more posterior in dasyuromorphians, being dorsal to M1 in *Dasyurus* and to M2 in *Thylacinus.* In other sparassodonts, the infraorbital foramen varies from a position dorsal to the anterior root of P3 (e.g. *Lycopsis longirostrus*, some specimens of *Sipalocyon gracilis*) to dorsal to M1 (e.g. *Arctodictis munizi*), probably in relation to the length of the infraorbital canal and length of the snout. The infraorbital foramen of *Allqokirus* is oval-shaped, being two to three times higher than wide. The posterior foramen of the infraorbital canal is the maxillary foramen. It opens in the orbit and is formed dorsally by the lacrimal, ventrally and laterally by the maxilla and ventromedially by the palatine. Participation of the palatine in the maxillary foramen is a plesiomorphic feature for metatherians (Rougier *et al.* 1998) also present in *Pucadelphys* and *Andinodelphys* and in all the other sparassodonts. It is absent in didelphids, in which only the lacrimal and maxilla contribute to the maxillary foramen. The maxilla forms most of the floor of the orbit and is pierced by the medial roots of M2-4.

Ventrally, the maxillae form most of the anterior part of the palate. They are poorly preserved anterior to the canines. and the incisive foramina are missing. Only part of the anterolateral palatal process of the maxilla is preserved on the right side of the skull. The intermaxillary suture is straight and extends posteriorly until the embrasure between M1 and M2. From this point the posterior sutures with the palatine diverge posteriorly as far as the posterolateral angle of the palate. The suture between the maxillae and the palatine forms a V that is wide open posteriorly. It ends posterolaterally at the level of the base of the protocone of M4. The anterior aspect of the cusp is bordered by the maxilla, while the posterior one is bordered by the palatine (Fig. 9). This condition is

unusual and has not been observed in any other metatherian. An interpretation could be related to the subadult stage of the specimen described (MHNC 8267), the last molars of which are not fully erupted. However, in several specimens of *Didelphis* of similar ontogenetic stage, or even ontogenetically younger (M3 erupting), the last molar is completely surrounded by the maxilla. This indicates that the condition of MHNC 8267 could be independent of the ontogenetic stage of the individual, and may represent a characteristic of *Allqokirus*. In this respect *Allqokirus* departs from the condition in *Mayulestes*, *Andinodelphys*, and *Pucadelphys,* in which the maxillopalatine suture is always conspicuously medial to the lingual border of the alvaeolus of M4, which is therefore totally surrounded by the maxilla.

In the anteromedial region of the maxillopalatine suture, there is a large major palatine foramen, which notches the palatine posteriorly and grooves the maxilla anteriorly. The condition on the left side is unknown because of the poor preservation of the specimen. The presence of a distinct pair of major palatine foramina in *Allqokirus* is a plesiomorphic character, which is present in *Pucadelphys* and in some specimens of *Andinodelphys* (other specimens of this genus exhibit a small maxillopalatine fenestra, thus indicating that the latter is derived from an enlargement of the major paltine foramen). In most other sparassodonts (e.g. *Callistoe, Borhyaena, Prothylacynus, Arctodictis, Pharsophorus, Sipalocyon*), by contrast, there are several small palatine foramina, which would transmit major palatine artery and nerve (branches of the maxillary artery and nerve respectively) as occurs in some placentals (e.g. Wible & Gaudin 2004). However, this condition varies, since in *Sallacyon* a single large major palatine foramen is present in the maxillopalatine suture, as in *Allqokirus*.

In the embrasure between M1-2 and M2-3 are deep pits, which received the enlarged protoconids of the lower molars (Figs 3; 7; 8). Such pits are present in *Mayulestes*, and a pit is also observed between M3 and M4 in this taxon. Because of the incomplete eruption of the M4 of MHNC 8267, this pit cannot be observed in this specimen and therefore its presence cannot be ascertained in *Allqokirus*. Shallow embrasure pits are also present in *Andinodelphys* but less developed than in *Allqokirus*. They are absent in *Pucadelphys* and didelphids. Deep embrasure pits are also present in most other sparassodonts, but are less developed in dasyurids and thylacinids. Because the palatal pits receive the protoconid of the lower molar their number, width and depth are obviously, at least partly, related to the size of that cusp. Given the values of the Hpo/Lm ratio (High of protoconid/length of ultimate or penultimate molar) obtained in Table 2, it is therefore not surprising to observe deep pits, for example, in deltatheroidans, *Asioryctes*, mayulestids, "hathliacynids". In contrast, *Hondadelphys*, which has relatively low protoconids, has shallow embrasure pits.

On its lateral aspect, dorsal to the molars, the maxilla bears an elongated and relatively smooth surface, which received the articulation of the jugal. This articular surface extends for half of the height of the maxilla and anteriorly reaches the level of the ectoflexus of M1. The posterior end of this surface is a posterodorsally projected process, which imbricates in the

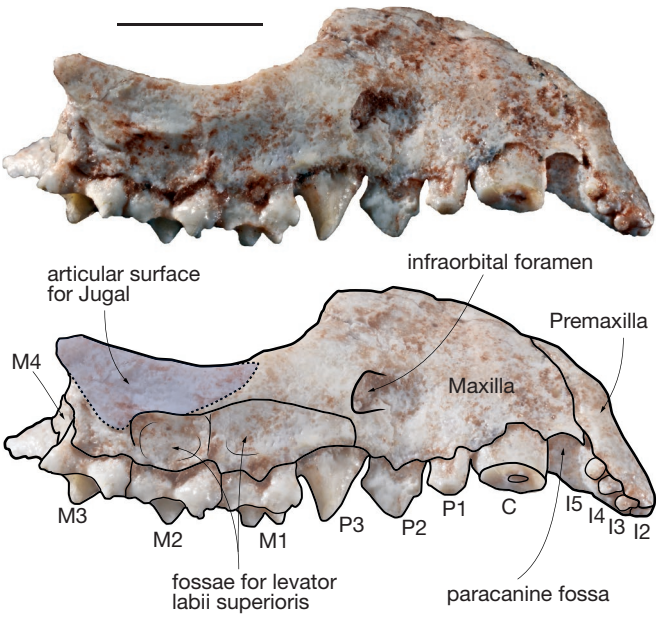


FIG. 16. — *Allqokirus australis* (MHNC 8267), right ventrolateral view of the rostrum showing the jugo-maxillar articulation and possible attachment area of the levator labii muscle. Light blue area is the articular surface for the jugal. Scale bar: 5 mm.

corresponding fossa on the anteromedial aspect of the jugal. In its posteroventral area, the articular surface is bordered by a small ridge against which the anteroventral edge of the jugal abuts. Between the ventral edge of the jugal-maxilla articulation and the alveolar border of M1-2 are two fossae, which probably received the origin of the *levator labii superioris* muscle (Fig. 16). Such a fossa is present in *Mayulestes, Pucadelphys* and *Andinodelphys*. In extant didelphids, the fossa for the *zygomaticus* and *levator labii superioris* is generally deep and well-developed on the anterolateral region of the jugal but does not excavate the maxilla anterior to the jugal-maxilla suture, although the muscles also originate in part on the maxilla (Turnbull 1970). Because the origin of the *levator labii superioris* in *Didelphis* is ventral to that of the *zygomaticus*, it is likely that the fossa observed in *Allqokirus* and the other Tiupampa metatherians corresponds to the origin of the *levator labii superioris*, while the *zygomaticus* probably originated on the jugal.

*Palatine*

Both palatines are preserved. They form the whole posterior region of the palate. They are relatively flat in their anterior region but, because their posterior edge is strongly bent ventrally (in lateral view), their posterior region is markedly concave. The major palatine foramen has been described in the maxilla section above. No accessory palatine foramina can be observed. On the posterolateral angle of the palatine is a large minor palatine foramen. The foramen is not closed in MHNC 8267 but it is open posterolaterally, contrary to the condition generally observed in most South American metatherians. Because the bone did not suffer post mortem damage in this region, we regard this condition as

probably related to the sub-adult ontogenetic age of the individual. It is noteworthy, however, that an incomplete minor palatine foramen is present, but not constant, in dasyurids. The posterior edge of the palate forms a regularly concave single arch, with no post palatine spine in its median region. It is distinctly thickened and constitutes a conspicuous torus. On the lateral edges of the postpalatine torus and posteromedial to the minor palatine foramen is a small groove, which may be the passageway of a branch of the minor palatine artery to the basipharyngeal canal (Fig. 17). A vascular groove, similar to that observed in *Allqokirus*, is present in *Mayulestes*, and in the "hathliacynids" *Sallacyon, Sipalocyon*, and *Cladosictis*. A condition very similar to that of mayulestids and "hathliacynids" is also observed in *Dasyurus* but not in *Thylacinus*. This groove is indistinct in *Prothylacynus, Borhyaena*, and *Arctodictis*. The groove probably corresponds to the small foramen observed by Wible (2003: 144) piercing the postpalatine torus and which is variably open in *Monodelphis*. Such a foramen is present in many other Recent didelphids (e.g. *Didelphis, Marmosa, Metachirus, Caluromys, Philander*). According Wible (2003), it likely transmitted structures from the minor palatine foramen to the the soft palate. A similar small foramen is present in *Andinodelphys*. A tiny foramen or a small groove is variably present in *Pucadelphys*.

Dorsal to this groove and medial to the minor palatine foramen is another small foramen, which pierces the postpalatine torus and exits posteriorly, external to the basipharyngeal canal, on the lateral edge of the lateral wall of the groove mentioned above. Because the foramen observed by Wible (2003) opens within the choanae (i.e., within the basipharyngeal canal), it is likely to be a different structure. Its function has not been elucidated, although it may be also related to the minor palatine artery.

In the orbit, the perpendicular process (ascending process) of the palatine is not preserved. The suture with the maxilla is located on the medial edge of the floor of the orbit. At a level between the medial root of M2 and M3 and in the angle of the floor and the wall of the orbit, is a large sphenopalatine foramen, which enters the nasal cavity (Fig. 18). In life, the sphenopalatine foramen conveys the sphenopalatine artery and vein and the caudal nasal nerve from the orbitotemporal fossa to the nasal cavity (Wible 2008). From the sphenopalatine foramen, a wide groove extends anteriorly towards the maxillary foramen. It probably conveyed the infraorbital artery (a branch of the maxillary artery), which enters the maxillary foramen and supplies the the external region of the snout, and the infraorbital nerve (a branch of the maxillary nerve, CN V2). This anterior groove is variably present in *Pucadelphys* and *Andinodelphys*, and, when present, it is shallower. Its condition is uncertain in *Mayulestes* because of the dorsoventral crushing of the single known specimen. No significant groove is observed in the didelphids examined. Posterior to the sphenopalatine foramen, the palatine forms the walls of the basipharyngeal canal. These walls are thin blades, which form an angle of 45° with the sagittal plane. They do not contact dorsally and were separated by the presphenoid.

*Lacrimal*

The lacrimal has a long anterior suture with the maxilla (Fig. 19). A large triangular wing of the lacrimal extends onto the lateral aspect of the rostrum, anterior to the orbit. A similar condition is observed in *Mayulestes* and *Sallacyon*. A relatively smaller rostral extension of the lacrimal is present in *Pucadelphys* and *Andinodelphys*, in which it is more crescent-like. However, some variation exists as a triangular lacrimal wing is observed in some *Pucadelphys* specimens (e.g. MHNC 8381). The lacrimal bears two oval-shaped lacrimal foramina, which are positioned one above the other. The posteriorly oriented dorsal lacrimal foramen opens in the orbit, and the posterolaterally-oriented ventral foramen opens on the face. This condition resembles that of *Mayulestes, Andinodelphys* and *Pucadelphys*. It differs from that in the Recent didelphids in which both foramina open on the face. *Allqokirus* differs from other sparassodonts, which have a single lacrimal foramen, opening within the orbit (a condition unknown in *Patene*). There is no distinct lacrimal tubercle, thus differing from the condition observed in *Andinodelphys* and *Mayulestes* in which it is weak but present. A distinct lacrimal tubercle is present in other sparassodonts.

*Jugal*

The jugal is preserved on the right side of the specimen only (Fig. 20). It is almost complete but for the anterior tip and the posterior glenoid process. It is a sigmoid bone, more or less symmetrical anteroposteriorly, and roughly as long as the braincase. It articulates anteriorly with the maxilla, and it has a long suture on its ventral edge and especially on its ventromedial side. In this area, the suture is a deep groove, which extends posteriorly on approximately one third of the total length of the bone. At its posterior end, this articular maxillary groove is as wide as half the height of the jugal at this level. The groove slightly widens anteriorly, and, at its anterior extremity, it forms almost the total width of the jugal. At the anterodorsal angle of the jugal, adjacent to the anterodorsal angle of the maxillary groove, is a small triangular fossa for the lacrimal. This fossa opens dorsally and medially. The dorsal edge of the jugal is concave anteriorly at the level of the orbit, and convex posteriorly when reaching the zygomatic process of the squamosal. It bears no postorbital process (frontal process in Wible 2003) departing in this respect from the condition observed in Recent didelphids and dasyurids. In lateral view, the articular suture with the squamosal is rectilinear. In dorsal view, the articular surface is flat, and the morphology of the jugal is an elongated platform, distinctly wider than the sharp ventral edge of the bone. The squamosal-jugal suture extends as far as the glenoid fossa of the squamosal, where it forms a distinct notch. Although the glenoid process of the jugal is missing, its articular surface on the squamosal indicates that it contributed to the articulation with the dentary. The ventral edge of the jugal forms the whole ventral edge of the zygoma. It is conspicuously but moderately concave. The lateral face of the jugal is concave, while its medial surface is strongly convex. Along the ventral edge of the jugal is a faint groove, which is better marked in its posterior region.

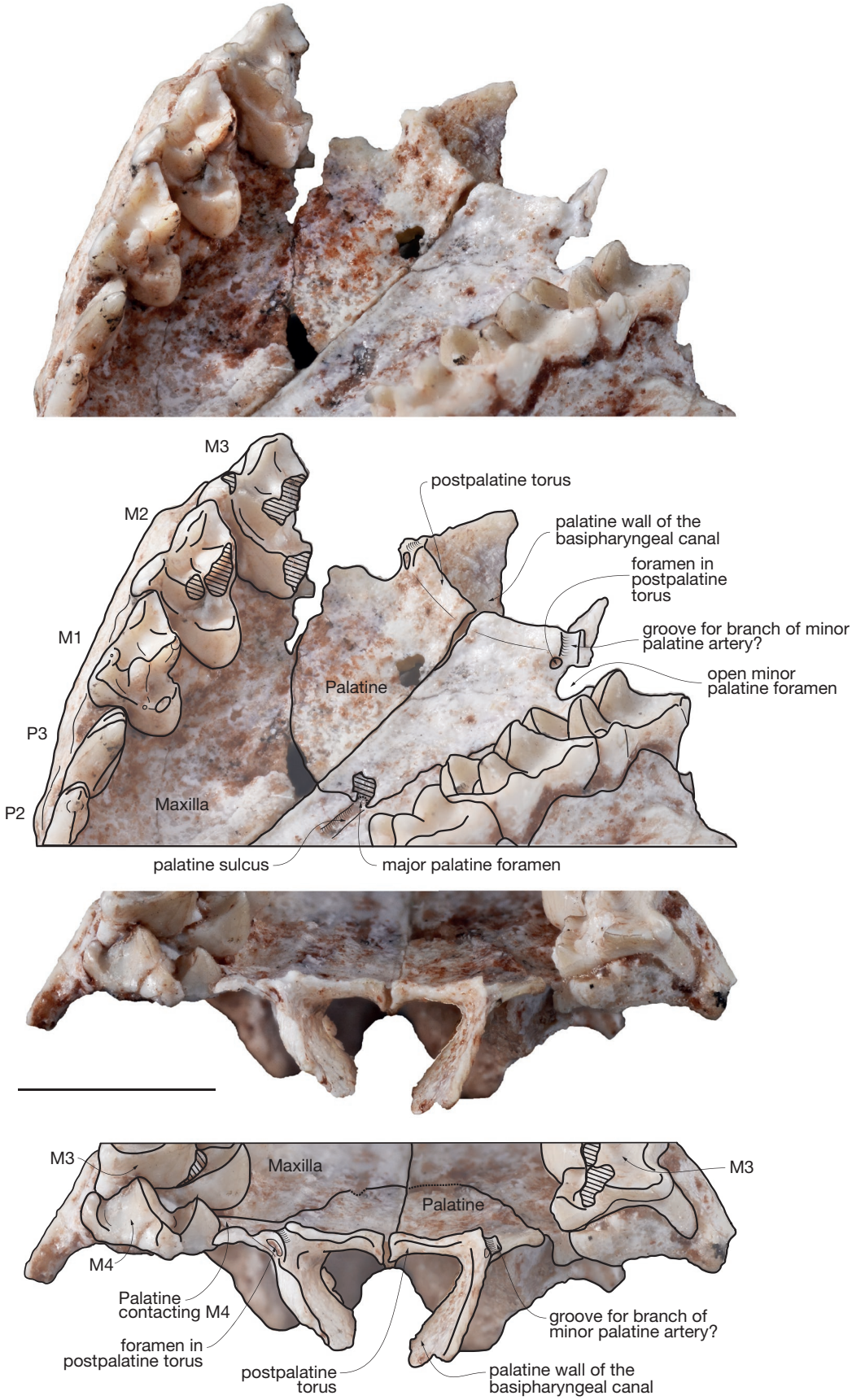


FIG. 17. — *Allqokirus australis* (MHNC 8267), posterior region of the palate: **A**, anteroventrolateral view; **B**, posterior view; **C**, posteroventrolateral view. **Linear hatching** corresponds to breakages. Scale bar: 5 mm.

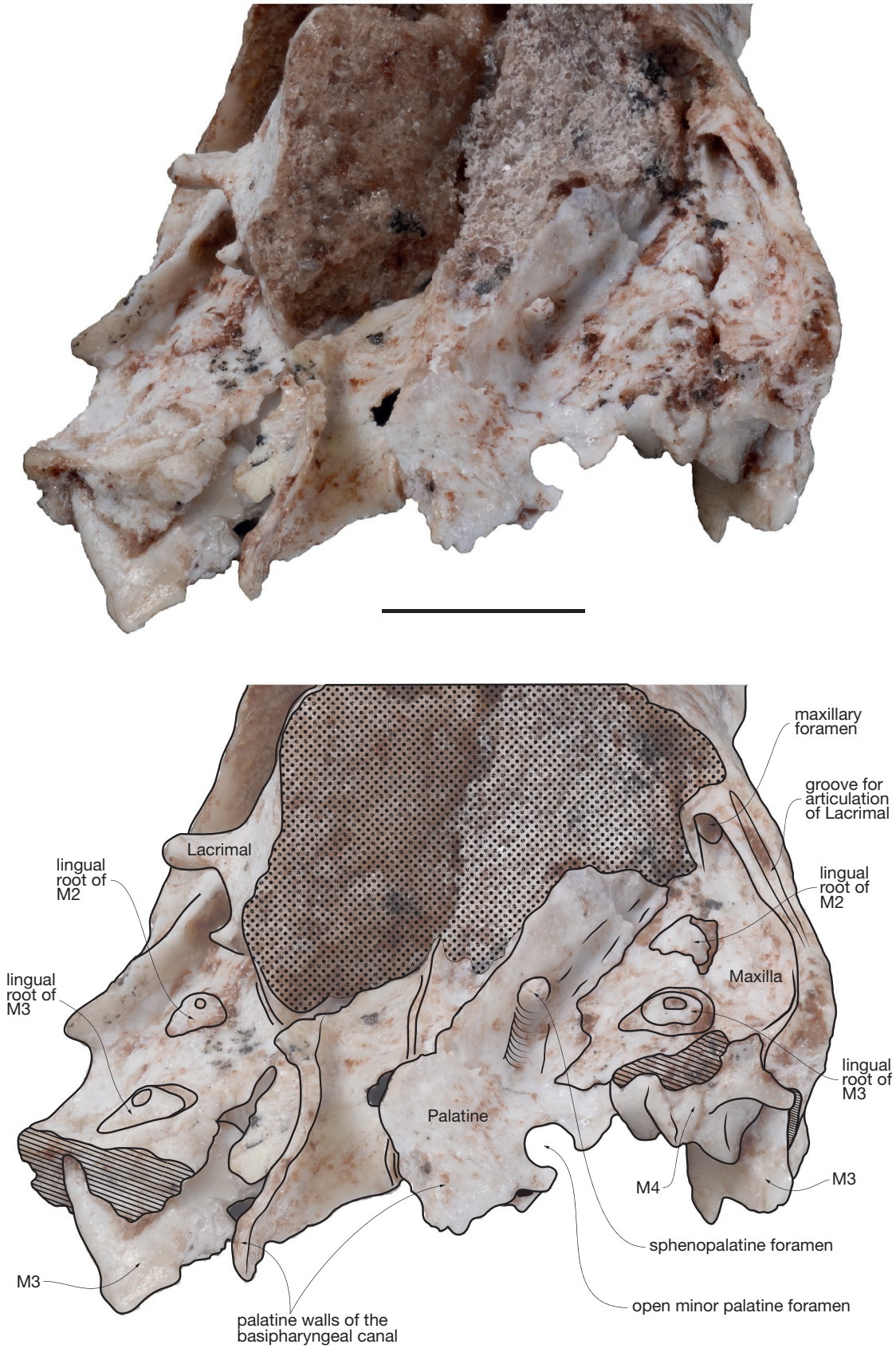


FIG. 18. — *Allqokirus australis* (MHNC 8267), posterodorsolateral view of the right orbit. **Dotted surfaces** indicate sediment and **linear hatching**, corresponds to breakages. Scale bar: 5 mm.

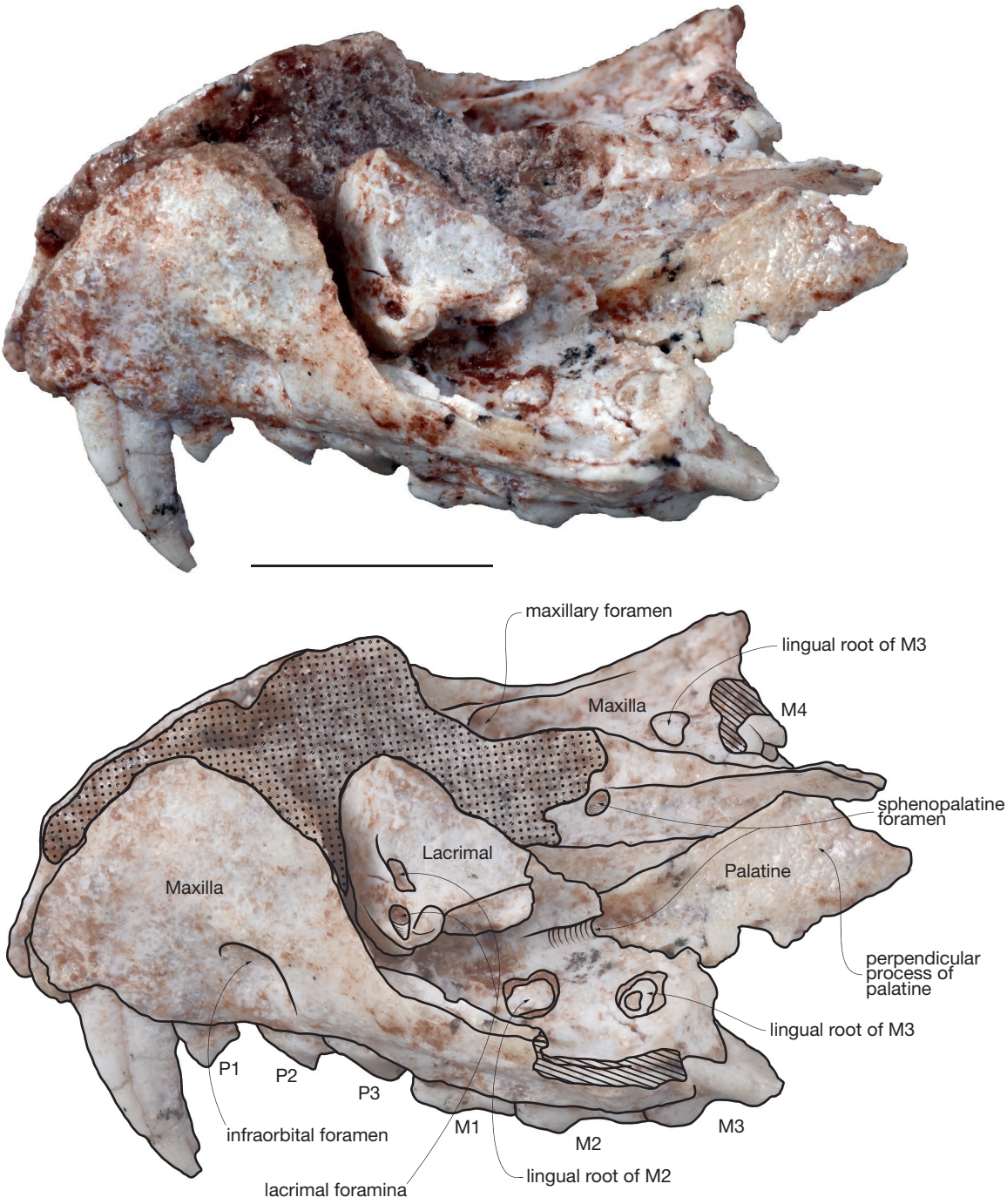


FIG. 19. — *Allqokirus australis* (MHNC 8267), posterodorsolateral view of the left lacrimal. Dotted surfaces indicate sediment and linear hatching corresponds to breakages. Scale bar: 5 mm.

It is present in all Recent didelphids and dasyurids, and corresponds to the origin of the superficial and deep masseter (Hiiemae & Jenkins 1969; Turnbull 1970; Wible 2003). These muscle attachments are much weaker in *Allqokirus* than in *Mayulestes, Pucadelphys*, and most Recent didelphids (e.g. *Didelphis, Caluromys, Metachirus, Monodelphis*). In contrast, *Allqokirus* resembles in this respect the condition observed in *Andinodelphys*. However, the weakness of the masseteric sulcus may also be related to the young age of the specimen MHNC 8267. On the anterior lateral aspect of the jugal of *Allqokirus*, there is no fossa for the origin of the *zygomaticus* and *levator labii superioris* below the infraorbital rim, a condition that contrasts with that observed in Recent didelphids, which bear a large fossa at the anterior end of the jugal (Turnbull 1970; Wible 2003). This fossa is also absent in *Pucadelphys, Andinodelphys,* and *Mayulestes*. As observed above, the origin of the *levator labii superioris* in these taxa was probably on the maxilla. between the alveolar border of the molars and the

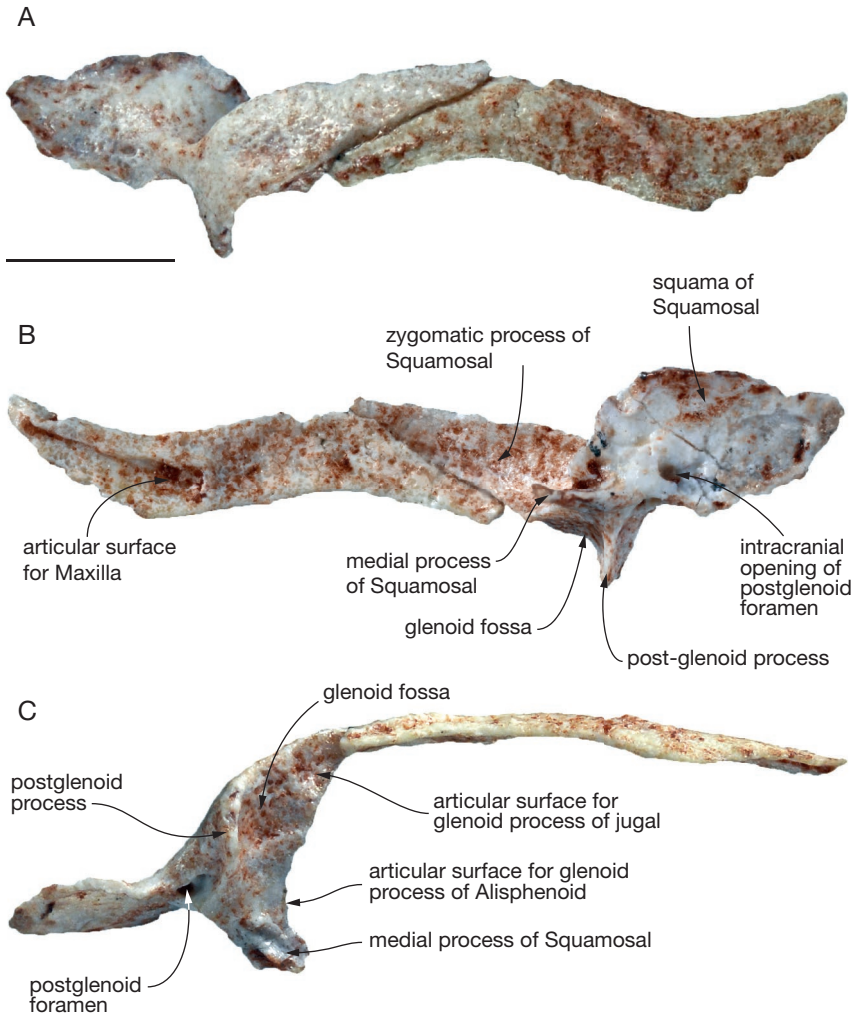


Fig. 20. — *Allqokirus australis* (MHNC 8267), right jugal and squamosal: **A**, lateral view; **B**, medial view; **C**, ventral view. Scale bar: 5 mm.

ventral edge of the jugal-maxilla suture. Although no fossa is observed on the anterior region of the jugal, it is possible that the *zygomaticus* nevertheless originated in this area. As a matter of fact, in MHNC 8267, an oblique ridge extends from the posteroventral end of the maxilla-jugal suture to the anterior end of the squamosal-jugal suture; this ridge could be related to the posterior attachment of the *zygomaticus*.

*Frontal*

The frontals are relatively complete on both sides of the skull (Figs 21; 22). They are not fused medially thus resembling the condition in *Mayulestes, Pucadelphys* and *Andinodelphys*. Dorsally, they bear a relatively acute W-shaped anterior suture for the nasals (not preserved), with a distinct anterior spur-like process wedged between the nasals. The condition in *Allqokirus* resembles that of *Mayulestes* and *Pucadelphys*. It differs from the wide-open W observed in *Sallacyon* and *Sipalocyon*, and from the smoothly concave suture observed in *Borhyaena* and *Arctodictis*. It also differs from the very narrow and acute W-shaped suture observed in most didelphids. Laterally, the anterior suture of the frontal smoothly turns ventrally, with no anterior projection. Such a projection is observed in taxa which have a suture with the maxilla (e.g. *Pucadelphys*, *Andinodelphys*, didelphids). The condition of *Allqokirus* resembles that observed in *Mayulestes*, which suggests that the frontal of *Allqokirus* did not contact the maxilla. As a matter of fact, on the ventrolateral part of the nasal-frontal suture, on both sides, a small anteroposteriorly directed ridge is likely to represent the imprint on the frontal of a nasolacrimal suture (Fig. 22). Ventral to this ridge, the frontolacrimal suture descends posteroventrally on the medial wall of the orbit, along the anterior edge of the frontal process until its ventral edge. Consequently, the morphology of the anterior suture of the frontal indicates that it articulated with both the nasal (dorsomedially) and the lacrimal (ventrolaterally). This condition indicates that a nasolacrimal suture was present in *Allqokirus*, as in all sparassodonts except thylacosmilids. This condition is also present, for example, in *Morganucodon*, *Vincelestes*, and *Deltatheridium*, and represents a plesiomorphic condition for Mammalia.

In dorsal view the inter-orbital bridge is relatively wide but narrows posteriorly as far as the fronto-parietal suture. At this point, the inter-orbital bridge is at its narrowest. The dorsal region of the frontal is relatively flat, but it presents a slightly

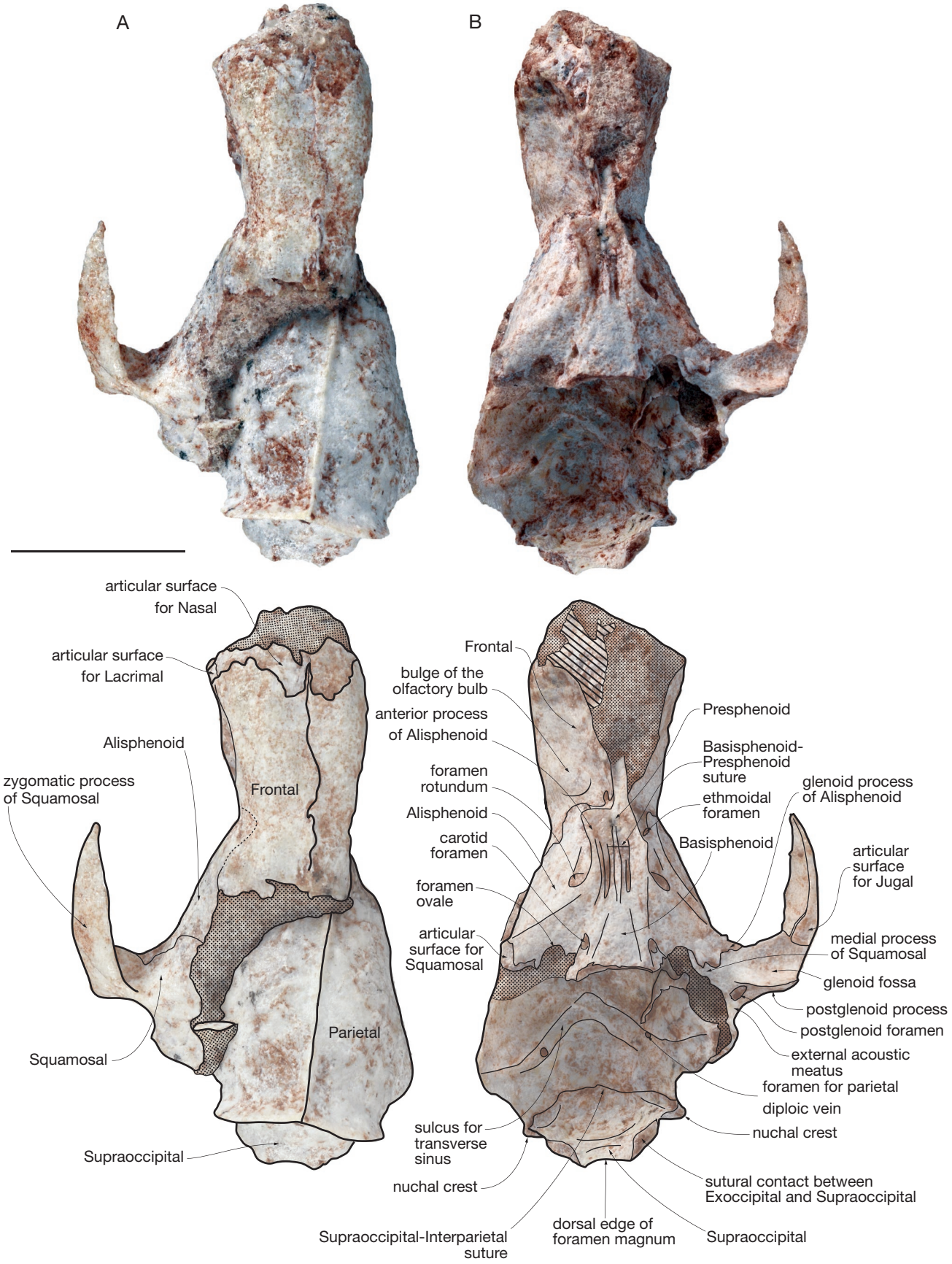


FIG. 21. — *Allqokirus australis* (MHNC 8267), posterior part of the cranium including frontals parietals, supraoccipital, left squamosal, alisphenoid, basisphenoid, presphenoid, and orbitosphenoid: **A**, dorsal view; **B**, ventral view. **Dotted surfaces** indicate sediment and **linear hatching** corresponds to breakages. Scale bar: 1 cm.

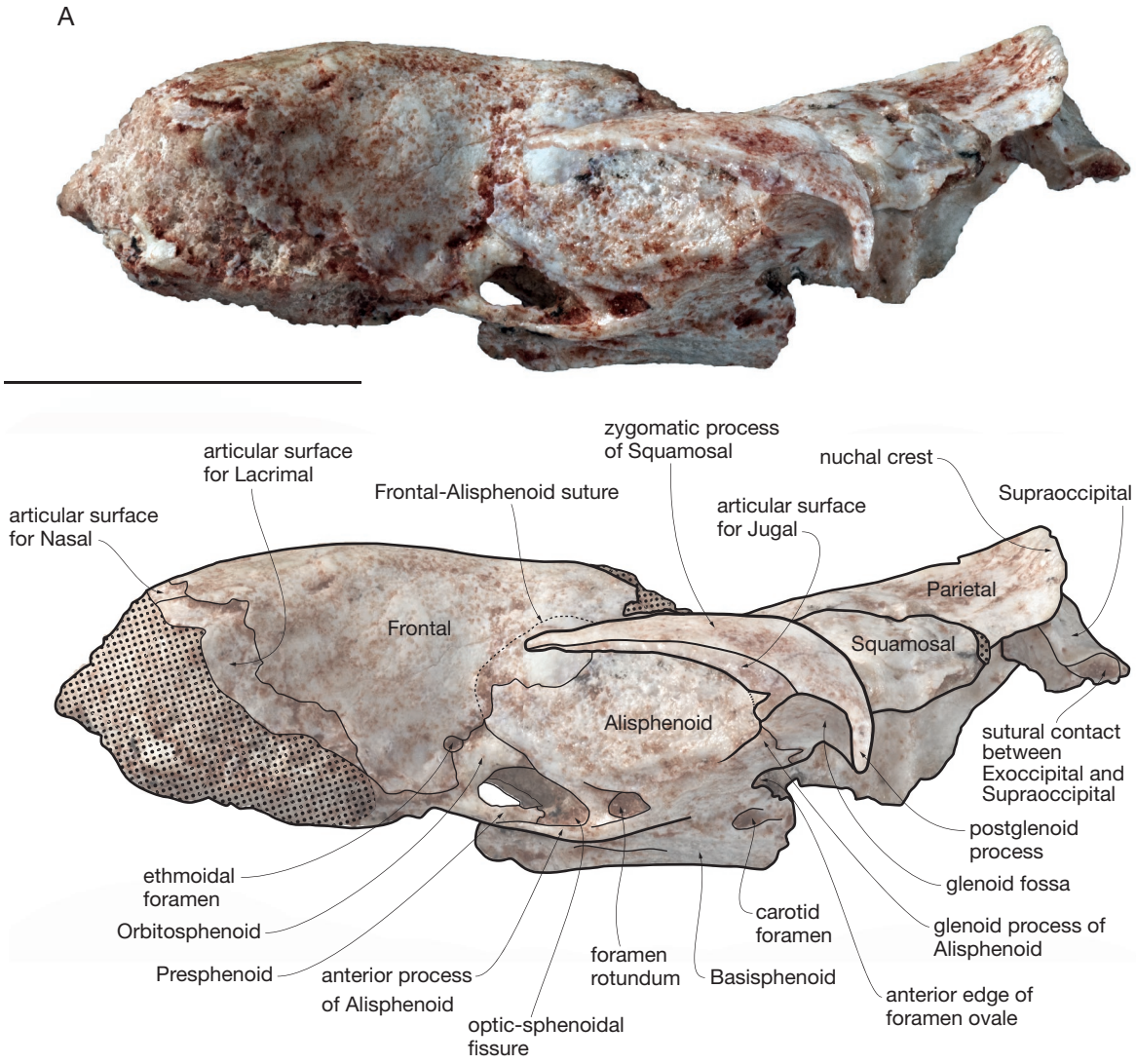


FIG. 22. — *Allqokirus australis* (MHNC 8267). Left lateral view of the posterior part of the cranium: **A**, ventrolateral view; **B**, dorsolateral. **Dotted surfaces** indicate sediment and **linear hatching** corresponds to breakages. Scale bar: 1 cm.

concave median zone just behind the naso-frontal suture. The widest point of the bridge is at the anterior end of the frontals, at the level of the fronto-lacrimal suture. In the region of the frontal dorsal to the orbit, the frontal is smooth and bears neither a supraorbital process or tuberosity. *Allqokirus* differs in this respect from other sparassodonts. In *Mayulestes,* the other sparassodont from Tiupampa, a true supraorbital process is absent but a distinct tuberosity is present. However, because this process is generally more developed in adults than in juveniles (Abdala *et al.* 2001: fig. 2; Flores *et al.* 2010: fig. 3), the condition in *Allqokirus* may be related to the subadult ontogenetic stage of the specimen. On both frontals, at the point where the supraorbital process is usually located, is a large frontal diploic foramen that opens distinctly anteriorly. This foramen likely conveyed the frontal diploic vein, an emissary of the dorsal cerebral vein/dorsal sagittal sinus, or a vein issuing from the frontal diploë (Thewissen 1989; Evans & de Lahunta 2013). Frontal diploic foramina are commonly present in metatherians, for example, in other sparassodonts (e.g. *Mayulestes*, *Sallacyon, Pharsophorus, Arctodictis*), in *Andinodelphys* and *Pucadelphys*, and in Recent didelphids. In the latter, these foramina are generally smaller than in *Allqokirus*. On the dorsal surface of the frontals, the temporal lines are barely identifiable. They join posteriorly at the fronto-parietal suture to form a low sagittal crest.

In the orbitotemporal fossa, a large frontal process forms most of the medial wall of the orbit (Fig. 22A, B). It articulates anteroventrally with the ascending process of the palatine, which almost reaches the dorsal edge of the orbit. The contact of the frontal process with the lacrimal is limited, and restricted to the anterodorsal region of the orbit. The frontal process articulates posteroventrally with the orbitosphenoid and posterodorsally with the alisphenoid. A large ethmoidal foramen is present posteriorly at the contact with the orbitosphenoid. Most of the foramen is bordered anteriorly by the frontal, but its posterior quarter is formed by the orbitosphenoid. The ethmoidal foramen opens posteroventrally. In the orbit, the posterodorsal quarter of the

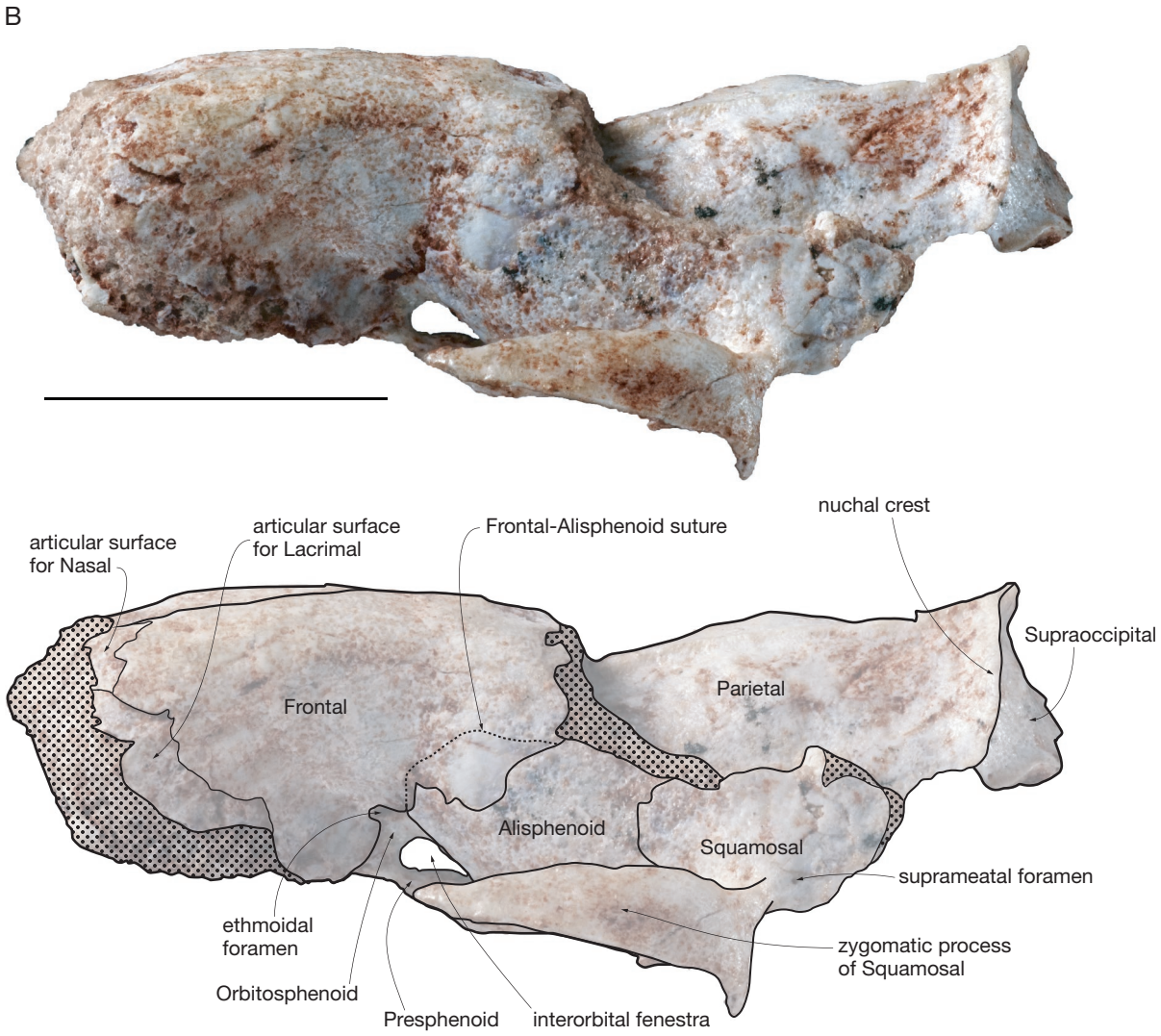


Fig. 22. — Continuation.

frontal process is markedly convex. These inflated areas are located just anterior to the post-orbital constriction, and correspond to the part of the frontals, which, internally, houses the olfactory bulbs. Such inflated frontal processes are observed in *Pucadelphys* and *Andinodelphys* (MHNC 8308). They cannot be observed in *Mayulestes* and in the other specimens of *Andinodelphys* because of the distortion of the specimens. No patent inflation of the frontal process is observed in other sparassodonts.

*Parietal and interparietal*

The parietals form the major part of the roof of the braincase (Figs 21; 22). Because the braincase has been disarticulated, the parietals are not articulated with the frontals, and their anterior suture is not exposed. However, the digital rendering of the reassembled bones of the skull (Fig. 5) provides a good approximation of the morphology of the frontoparietal suture: it is parabolic and anteriorly convex. Both frontoparietal sutures diverge posteriorly until reaching the alisphenoid posteriorly, at the dorsal level of the lateral wall of the braincase. This suture is better observed on the left side of the specimen. The frontal suture of the parietal is oblique posteroventally, and becomes sub-horizontal when the parietal contacts the alisphenoid. There, the parietal has a suture with the alisphenoid along roughly one third of its length. On its posterior third, the lateral edge of the parietal has a dorsally convex suture with the squamosal. In the midline of the braincase, the parietals are tightly fused and no suture is observable, in contrast to the condition observed on the frontals. On the line of junction of the parietals is a small but distinct sagittal crest, which extends from the fronto-parietal suture to the nuchal crest posteriorly. The sagittal crest does not extend anteriorly on the frontals, but terminates at the anterior end of the parietals. Although no suture is visible on the dorsal aspect of the braincase roof in the posterior region of the parietals, an interparietal is assumed to be present in *Allqokirus* since this bone is apparently universal for mammals (Koyabu *et al.* 2012). Therefore, it is probable that the interparietal of MHNC 8267 is fused to the parietals in spite of the young ontogenetical age of the specimen.

However, in intracranial view of the roof of the braincase, a transverse suture is clearly visible (Fig. 21B). In posterior view of the cranium, on the right lateral edge of the occipital shield, this suture extends outside the braincase, on the posterior base of the nuchal crest. Because the bulk of the nuchal crest in *Monodelphis* and *Didelphis* is formed by the interparietal (Toeplitz 1920; Clark & Smith 1993; Wible 2003), we hypothesise that a similar condition is present in *Allqokirus*. Therefore, the suture observed on MHNC 8267 is likely to represent the supraoccipital-interparietal suture. As a consequence, we assume that the nuchal crest of *Allqokirus* is mainly formed by the interparietal since parietals are unlikely to participate significantly in the composition of the nuchal crest. A condition similar to that of *Allqokirus* is present in subadult specimens of *Pucadelphys* (MHNC 8265, 8388), and in two young adult specimens of *Andinodelphys* (MHNC 8370 and 13847). A suture has not been observed in *Mayulestes*, because of the fusion of the interparietal with both the supraoccipital and the parietals as a probable consequence of the full adult (older than young adult) ontogenetic age of the single known specimen of this taxon. With an interparietal fused to the parietals but still partially sutured to the supraoccipital in a subadult individual, *Allqokirus* differs from Recent didelphids, in which the interparietal is generally not fused (or incompletely fused) to the parietals in adults and in which the fusion of interparietal and supraoccipital occurs very early in ontogeny, (Nesslinger 1956; Clark & Smith 1993; Voss & Jansa 2009), much earlier than the ontogenetic stage of MHNC 8267. Among sparassodonts, no distinct suture of the interparietal has been observed in adults and sub-adults on the dorsal surface of the braincase of borhyaenoids. However, a parietal-interparietal suture is clearly present in some adult "hathliacynids" (e.g. *Cladosictis* and *Sipalocyon*), in which it is didelphid-like, being anteroposteriorly elongated and wedged between the parietals.

The nuchal crest is well developed but, in lateral view, with the sagittal crest in horizontal position, it does not extend further posteriorly than the posterior margin of the supraoccipital (Fig. 22).

On the intracranial face of the parietal, wide grooves for the transverse sinuses are observed (Figs 21; 23); they diverge posteriorly from the sagittal plane of the braincase, since they originate from the sagittal sinus at the *confluens sinuum* (Dom *et al.* 1970). The transverse sinus runs posterolaterally toward the lateral edge of the parietal, where it reaches the dorsal region of the petrosal. In its lateral portion, the transverse sinus deeply excavates the parietal on its anterior edge, and its groove forms a sharp, posteroventrally-projecting crest. Proximal to this crest, in the groove, mid-way between the *confluens* and the petrosal, is a relatively large, posteroventrally-opening foramen, which pierces the parietal and penetrates the substance of the bone. The foramen is observed on both sides of the braincase, but the right foramen is distinctly larger than the left one. The diameter of the right foramen is half that of the groove, while that of the left foramen is one third that of the groove. Such foramina are also observed in *Andinodelphys, Didelphis, Dromiciops, Thylacinus, Dasyurus*, among others, and are apparently present in all therians. They are present in the dog and carry the occipital diploic veins (Evans & de Lahunta 2013). The transverse sinus in the dog is located at the level of the parietooccipital suture, which justifies the denomination of the diploic veins emitted by the transverse sinus. Because, in metatherians, this sinus is at the level of the parietal only, the diploic vein it emits penetrates the parietal and is therefore a parietal diploic vein.

*Alisphenoid*

The alisphenoid form most of the ventral region of the lateral wall of the braincase (Figs 21; 22; 23). Anteriorly, it has a long anterodorsally convex suture with the frontal, which ends ventrally where it reaches the orbitosphenoid, slightly dorsal to the ethmoidal foramen. In this region, the alisphenoid is partly squamous and overlaps the frontal anteriorly, a condition observed, for example, in Recent didelphids and in *Pucadelphys* and *Andinodelphys*. Although part of the anterior squama of the alisphenoid has been damaged, the alisphenoid-frontal suture in this region can be easily reconstructed. The ventral suture with the orbitosphenoid is at an angle of approximately 90 to 100° with the alisphenoid-frontal suture. It runs posteroventrally as far as the dorsal edge of the optic-sphenorbital fissure. Dorsally, the alisphenoid-frontal suture ends where it reaches the parietal (Fig. 22B). The alisphenoid-parietal suture is shorter than that with the frontal. It is sub-horizontal and runs posteriorly until reaching the squamosal, approximately at the level of the anterior edge of the glenoid fossa. There, it turns ventrally and runs until the anteromedial angle of the glenoid fossa, where it forms a small glenoid process of the alisphenoid. A small process is also observed in *Mayulestes*, *Andinodelphys* and *Pucadelphys* It is generally absent in other sparassodonts, although a small projection of the alisphenoid toward the glenoid fossa is observed in *Prothylacynus*, *Arctodictis, Borhyaena,* and *Lycopsis* and is interpreted here as a residual (or incipiently developed) glenoid process. From the glenoid process, the squamosal-alisphenoid suture of *Allqokirus* continues medially and borders the foramen ovale, where it ends (Fig. 23). On the ventral side of the skull, no suture is discernible at the limit between the presephenoid and alisphenoid, and the bones are tightly fused.

The alisphenoid participates in the formation of various foramina. The most anterior one is the optic-sphenorbital fissure (the optic-orbital foramen of Marshall & Muizon 1995 and the sphenorbital fissure of Wible 2003). We use this compound term, which acknowledges the passage of the optic nerve in the fissure, in contrast to the sphenorbital fissure of eutherians, which does not. The alisphenoid forms the lateral wall and floor of the fissures, which are confluent dorsomedially. The ventromedial wall of the fissures is formed by the basisphenoid. In metatherians, the optic-sphenorbital fissure transmits the optic (CN II), oculomotor (CN III), trochlear (CN IV), ophthalmic (CN V1), and abducens (CN VI) nerve, and the ophthalmic artery and veins (Kuhn & Zeller 1987; Wible & Rougier 2000; Wible 2003). Therefore, in metatherians, the optic foramen is coa-

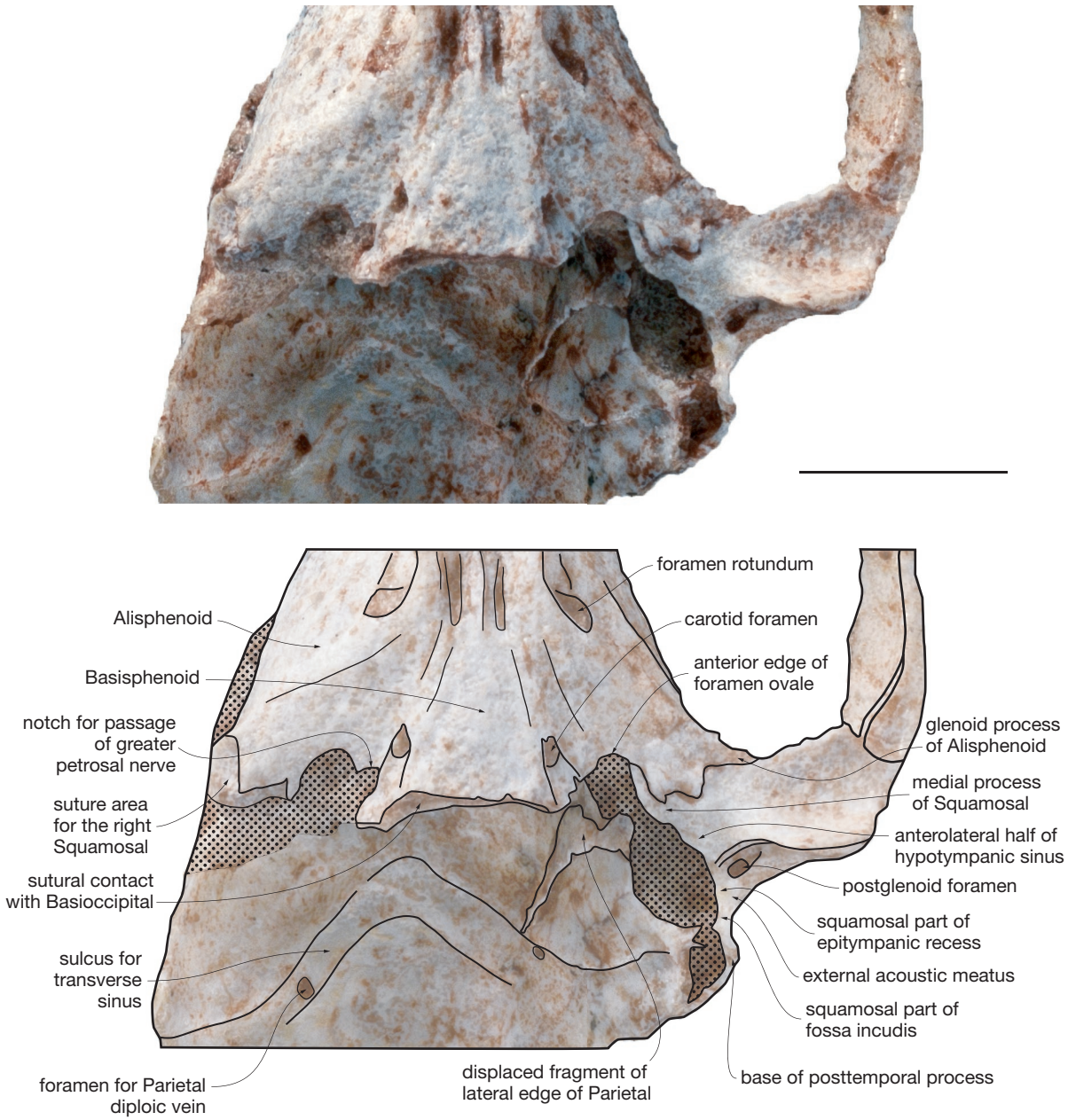


FIG. 23. — *Allqokirus australis* (MHNC 8267), ventral view of the basicranium at the level of the foramen ovale. **Dotted surfaces** indicate sediment. Scale bar: 5 mm.

lescent with the sphenorbital fissure of eutherians. As usually observed in metatherians, the optic-sphenorbital fissures of *Allqokirus* are closely approximated medially. Lateral to the optic-sphenorbital fissure, and distinctly posterior to it, is a large foramen rotundum. It opens anteriorly and is likely to have transmitted the maxillary branch of the trigeminal nerve (CN V2), as is the case in all Recent marsupials. Two wings of bone ventral to the optic-sphenorbital fissures and anteroventral to the foramina rotunda, represent the anterior processes of the alisphenoid, which are tightly fused to the presphenoid anteriorly and the basisphenoid posteriorly. In *Andinodelphys* and *Pucadephys* the pterygoid articulates on the ventral surface of the anterior process but these bones are missing in MHNC 8267.

On the posterior edge of the alisphenoid, just anterior to the petrosal, is a large notch, medial to the glenoid fossa and lateral to the carotid foramen. This notch corresponds to the anterior half of the large foramen ovale (Figs 21; 22; 23). The foramen ovale conveys the mandibular branch of the trigeminal nerve (CN V3) to the dentary. In metatherians, this foramen is primarily formed by the alisphenoid anteriorly and the petrosal posteriorly (primary foramen ovale), as is observed in *Pucadelphys, Andinodelphys*, *Mayulestes,* some sparassodonts that do not have a tympanic process of the alisphenoid (e.g. *Borhyaena, Prothylacynus, Arctodictis, Australohyaena, Callistoe*), and in some didelphids (e.g. *Monodelphis, Caluromys*). In some Recent didelphids (e.g. *Didelphis, Metachirus, Thylamys*), in dasyurids, and in sparassodonts which have a tympanic pro-

cess of the alisphenoid (e.g. *Sipalocyon, Cladosictis, Acyon*), the foramen ovale is totally enclosed in the alisphenoid externally and is therefore a foramen pseudovale (or secondary foramen ovale) but, within the braincase, the mandibular nerve exits the skull between the alisphenoid and the petrosal (Wroe 1997; Voss & Jansa 2003). In the specimen of *Allqokirus* described here, the alisphenoid part of the foramen ovale is completely preserved on the right side. On this side, medial to the large notch of the foramen ovale, is a small notch, located posterolaterally to the carotid foramen, and which appear to be limited medially by the alisphenoid and laterally by the basisphenoid (Fig. 23). This notch is in the same position as the structure described by Wible (2003: fig. 6) in *Monodelphis* and interpreted by him as the foramen for the greater petrosal nerve (the anterior branch of the facial nerve CN VII). This nerve exits the petrosal via the hiatus Fallopii and enters the pterygoid canal anteriorly on the lateral edge of the basipharyngeal groove. Wible (2003) describes this aperture as limited by the basisphenoid and the petrosal. In the specimen of *Allqokirus* described here, the right petrosal is not preserved and, because of the position of the notch for the greater petrosal nerve (on the lateral edge of the groove for the internal carotid), it is not certain if it excavates the basisphenoid only or if part of it (if not all of it) is probably in the alisphenoid. On the left side of the skull, the squamosal is still articulated to the alisphenoid. The alisphenoid-squamosal suture runs along the lateral edge of the foramen ovale, but external to it. As a consequence, the foramen ovale is limited laterally by a narrow strip of the squamosal, which represents the medial part of the medial process of the squamosal, a structure present in *Pucadelphys, Andinodelphys*, and in sparassodonts. The alisphenoid suture with the anterior edge of the medial process of the squamosal forms a short zigzag line between the foramen ovale medially and the glenoid fossa laterally. On the dorsal surface of the posterior root of the zygomatic arch, there is a small contribution of the alisphenoid, which corresponds to the dorsal part of the glenoid process of the alisphenoid.

The alisphenoid has no tympanic process and was apparently not excavated by a hypotympanic sinus. No transverse canal is observed. *Allqokirus* differs in this respect from most extant didelphids, which have a tympanic process of the alisphenoid flooring the hypotympanic sinus, and a transverse canal. In contrast, *Allqokirus* resembles the condition of *Pucadelphys, Andinodelphys* and *Mayulestes,* in which the alisphenoid has neither a tympanic process nor a transverse canal. It is noteworthy that a tympanic process of the alisphenoid is present in the late Cretaceous metatherians *Asiatherium, Didelphodon,* and the deltatheroidan referred to as the "Gurlin Tsav skull" but it is apparently absent in the Late Cretaceous deltatheroidans, *Deltatheridium* and possibly *Lotheridium* (Bi *et al.* 2015). It is also probably absent in *Epidolops* (Beck 2017). Moreover, a typmanic process is also present "herpetotheriids" (Gabbert 1998; Horovitz *et al.* 2008; Selva & Ladevèze 2017) and a small tympanic process is also likely to have been present in *Mimoperadectes* (Horovitz *et al.* 2009) *contra* Beck (2012). A tympanic process of the alisphenoid is present most "hathliacynids", but absent in other sparassodonts.

*Squamosal*

The squamosal has a well-developed squama, which constitutes the posterolateral wall of the braincase. It bears the posterior root of the zygoma, which is composed of the zygomatic process of the squamosal, the glenoid fossa, and the postglenoid process (Figs 20; 21; 22). The zygomatic process of the squamosal is dorsoventrally symmetrical and is not bent ventrally as is observed in some didelphids and especially in *Andinodelphys*. It resembles in this respect that of *Mayulestes*. It is relatively stout, its height at its base being approximately one third its total length, as is observed in *Mayulestes*. It is usually less in *Pucadelphys* and *Andinodelphys* and in most Recent didelphids. It is noteworthy, however, that variation exists, since in some specimens of *Didelphis* the maximum height of the zygomatic process approaches half of its length. The zygomatic process of *Allqokirus* has slightly convex dorsal and ventral edges, and strongly tapers anteriorly. As in *Mayulestes, Andinodelphys,* and *Pucadelphys*, its anterior apex is sharp, while it is generally rounded and does not taper in Recent didelphids. Its dorsal edge is thin and sharp, while its ventral border, which articulates with the jugal, is wide and flat. The jugal-squamosal suture widens posteriorly and extends posteriorly as far as the glenoid fossa, where it distinctly notches the dento-squamosal articulation. This condition clearly suggests that the posterior process of the jugal participated in the articulation. The glenoid fossa is not transversely expanded as is observed in *Mayulestes*. It is approximately 1.5 times as wide as long, while in *Mayulestes* it is more than two times as wide as long. The condition of *Allqokirus* more resembles that of *Pucadelphys* and extant didelphids. *Andinodelphys* is intermediate between *Allqokirus* and *Mayulestes*. The morphology of the glenoid fossa is subcircular to ovoid, rather than cylindrical as in *Mayulestes*. As a consequence, the postglenoid process is almost as wide as high, while it is distinctly wider than high in *Mayulestes* and other sparassodonts. The condition in *Allqokirus* is similar to that observed in *Pucadelphys* and Recent didelphids. On the posteromedial edge of the postglenoid process is a large postglenoid foramen. The foramen extends in a deep groove, which runs ventrally along the medial edge of the postglenoid process and reaches its apex. The postglenoid foramen conveys the sphenoparietal emissary vein (postglenoid vein), a ramification of the transverse sinus, outside the skull. According to Archer (1976: 221), the postglenoid foramen "carries postglenoid vein of transverse sinus system as well as vein from subsquamosal foramen. Also carries postglenoid artery from external carotid to subsquamosal foramen out of which artery passes onto parietal area of cranium". Ventrolateral to the postglenoid foramen is another much smaller foramen, which penetrates laterally into the substance of the squamosal. A similarly placed foramen with a similar orientation has been observed in *Mayulestes, Pucadelphys*, *Andinodelphys*, and *Sallacyon*. One or two (or more, up to five) foramina in a similar position are also present in Recent didelphids. These foramina have been mentioned by Wible (2003) and referred to as postzygomatic foramina (following Gregory 1910), with no identification of the vessels they conduct. According to Archer

(1976: 221) the postzygomatic foramen "carries vein out of the squamosal root of zygomatic arch to postglenoid vein".

Posterior to the posterior root of the zygoma, on the lateral aspect of the squamosal and dorsal to the external acoustic meatus is a small foramen, which we identify as a suprameatal foramen (= subsquamosal foramen of Archer 1976), following Wible (2003). According to Wible (1987, 2003) the suprameatal foramen carries "a temporal branch of the postglenoid artery and accompanying vein to the temporal fossa", which is regarded by Wible (1987) as a ramus temporalis of the stapedial artery system. The suprameatal foramen of *Allqokirus* pierces the squamosal and opens on the medial aspect of the bone, posterior to the medial opening of the postglenoid foramen. Externally, it opens laterally. This condition differs from that mentioned by Wible (2003) in *Monodelphis*. In this genus, the suprameatal foramen is posterolaterally directed and is continuous with the postglenoid foramen. Furthermore, the suprameatal foramen of *Allqokirus* is 5 to 10 times smaller than that of most Recent didelphids (it is absent in *Caluromys*). In contrast, the suprameatal foramen of *Allqokirus* is similar in size to that of *Mayulestes* and *Andinodelphys*. It is distinctly smaller than that of *Pucadelphys*, which approaches the size observed in Recent didelphids.

Medial to the glenoid fossa, the squamosal extends medially between the alisphenoid anteriorly and the petrosal posteriorly, and contributes to the lateral wall of the middle ear cavity. This extension has been termed the medial process of the squamosal by Muizon (1994, 1999). In *Allqokirus* it reaches the foramen ovale medially, and forms part of its lateral edge, as mentioned above. A medial process of the squamosal is present in *Pucadelphys, Andinodelphys, Mayulestes*, and in all other sparassodonts, in which this region is well preserved enough to be observed (e.g. *Notogale, Sipalocyon, Cladosictis, Borhyaena, Prothylacynus, Arctodictis, Paraborhyaena*). It is absent in Recent didelphids and, apparently, in most other metatherians (but see Muizon 1999: 497). The relationships of the medial process of the squamosal with the foramen ovale and alisphenoid vary in the Tiupampa metatherians. However, one feature, apparently constant in the four genera in which this structure is preserved, is the anterior edge of the medial process of the squamosal, which has a characteristic zigzag anterior suture with the alisphenoid. In *Pucadelphys,* based on ten specimens in which this region is well observable, the condition is that described by Marshall & Muizon (1995): the medial process is wedged between the alisphenoid anteriorly and the petrosal posteriorly, and usually its apex has only a small participation to the edge of the foramen ovale, or is very close to its edge. In *Andinodelphys*, in one specimen (MHNC 8308) the condition is the same as that of *Pucadelphys*, but in two specimens (MHNC 8370, 13847) the condition is the same as that of *Allqokirus*, with a small strip of squamosal contributing to the lateral edge of the foramen ovale, and in one specimen (MHNC 8264), the alisphenoid is wedged between the medial process of the squamosal (anteriorly) and the petrosal (posteriorly). In *Mayulestes*, the alisphenoid is also wedged between the medial process of the squamosal and the petrosal (Muizon 1998). Therefore, the condition observed in *Andinodelphys* (Muizon & Ladevèze, in prep.) indicates that an important intraspecific variation may exist in the relationship of the alisphenoid and medial process of the squamosal in the region of the foramen ovale.

The posteromedial edge of the medial process of the squamosal is moderately but distinctly concave, which represents the anterolateral half of a small hypotympanic sinus, as in *Mayulestes*. The posteromedial half of the sinus is described below in the petrosal section.

Posterior to the postglenoid foramen, the ventral edge of the squamosal, ventral to the suprameatal foramen, forms the dorsal edge of the external acoustic meatus. On the medial side of the meatus is a flat elongated surface, which is the lateral, squamosal part of the epitympanic recess. Posterior to it, is the lateral portion of the fossa incudis. Posterior to the external acoustic meatus in *Mayulestes*, *Andinodelphys* and *Pucadelphys* is a blade-like posttympanic process, which is closely appressed against the lateral side of the mastoid process of the petrosal. In *Allqokirus*, the posttympanic process is also blade-like, but it is broken at its base in MHNC 8267, and so it is not possible to evaluate its size.

*Basisphenoid*

The basisphenoid is a trapezoidal bone placed between the alisphenoids and the pterygoids. In MHNC 8267, because the pterygoids are not preserved, we suppose that they had, in *Allqokirus*, a similar position to that observed in *Pucadelphys* and *Andinodelphys*. Posteriorly, the basisphenoid has a straight transverse suture with the basioccipital (Figs 21; 23). Anteriorly, its suture with the presphenoid is slightly anterior to the optic-sphenorbital fissure. Most of the ventral surface of the basisphenoid is relatively flat, but its lateral edges are sloping and form an angle of approximately 45° with the sagittal plane. In its anterior third, between the foramina rotunda, it bears an elevated median carina, which does not extend on the presphenoid. In the posterior region of the basisphenoid, the laterally sloping edges of the bone bear two posteriorly opening carotid foramina. The carotid foramina are approximately in the posterior quarter of the bone. They extend posteriorly as far as the posterior end of the basisphenoid in a conspicuous groove, which was connecting to the carotid groove of the apex of the petrosal (see below in the petrosal description).

*Orbitosphenoid and presphenoid*

The paired orbitosphenoids are tightly fused to the presphenoid. The orbitosphenoid has an oblique posterodorsal suture with the alisphenoid, and a subvertical anterodorsal one with the frontal (Fig. 22A, B). The frontal-orbitosphenoid suture contains the ethmoidal foramen, which opens posterolaterally (see frontal section). Ventrally, the orbitosphenoid likely had a suture with the palatine, as in didelphids (e.g. Wible 2003), *Andinodelphys* and *Pucadelphys*; however, this bone has not been preserved in contact with the orbitosphenoid. The orbitosphenoid wings converge ventrally and are fused to the presphenoid, where they have a saddle-shaped posterior border. At this point is a large vacuity in the base of the

skull, the interorbital fenestra (Asher 2007), which marks the confluence of the left and right optic-sphenorbital fissures (Fig. 22). This vacuity was probably filled by a membrane during life, as is observed in many Recent didelphids (e.g. *Monodelphis, Marmosa, Caluromys, Metachirus*). This condition is also present in *Pucadelphys,* and *Andinodelphys*. As is usual in metatherians, there is no optic foramen and the optic nerve exits the skull through the optic-sphenorbital fissure (Wible 2003).

Ventrally, the presphenoid is a beam-like bone, which has a distinct posterior suture with the basisphenoid (Fig. 21). Because this suture is almost at the level posteriorly of the lateral edge of the optic-sphenorbital foramen, the presphenoid forms most of the floor of the interorbital fenestra. In the Recent didelphids in which this fenestra is observable, it is generally more anterior, so that the floor of the fenestra is formed, half by the basisphenoid posteriorly and half by the presphenoid anteriorly (e.g. *Metachirus, Monodelphis, Thylamys, Caluromys, Marmosa*). In *Didelphis* and *Philander*, we have observed a condition similar to that of *Allqokirus*, but it is noteworthy that, in these genera, the interorbital fenestra is extremely reduced and disappears rapidly during ontogeny.

*Petrosal*

Only the left petrosal of MHNC 8267 is preserved, and it is not articulated to the cranium so that it can be described thoroughly. The bone is almost complete, and is missing only the apex of the promontorium and the anterior edge of the anterior lamina (Figs 24; 25).

**Tympanic view** (Fig. 24A). The petrosal is composed of two major divisions, the pars cochlearis, which consists of the promontorium, and the pars canalicularis consisting of the rest of the petrosal. The pars cochlearis houses the cochlear duct and saccule of the inner ear, and the pars canalicularis houses the semicircular canals and utricle.

The pyriform promontorium is elongated and strongly inflated posteriorly. It is relatively narrow posteriorly, and forms an isosceles triangle whose base is approximately half of its height. It resembles in this respect that of *Mayulestes*, but differs from the more oval-shaped promontorium of *Notogale* and *Sipalocyon*. It is oriented anteromedially-posterolaterally. Although its apex is broken, the posterior part of a deep sulcus for the internal carotid artery is still observable at the anterior region of the promontorium as preserved. This sulcus is roughly parallel to the petrosal-basioccipital suture. It is likely to have conveyed the internal carotid artery to the sulcus posterior to the carotid foramen on the basisphenoid (see above) and to the foramen itself. This sulcus is present in *Pucadelphys, Andinodelphys, Allqokirus,* and *Mayulestes*. It is also present in several other sparassodonts (e.g. *Notogale*, *Sallacyon, Sipalocyon*, *Cladosictis, Pharsophorus, Prothylacynus, Borhyaena, Paraborhyaena, Arctodictis*). In *Arctodictis*, the structure referred by Forasiepi (2009) to a possible fossa for the tensor tympani Muscle is identified here as the carotid groove. Because of the function of the tensor tympani muscle, this fossa is generally located on the lateral edge of the promontorium, anterior to the secondary facial foramen. Given the morphology of the petrosal of *Arctodictis*, a position of the tensor tympani fossa at the anteromedial apex of the promontorium, as is observed on the specimen described by Forasiepi (2009), is unlikely. Furthermore, it is noteworthy that, in many sparassodonts in which the petrosal is sub-vertical (e.g. *Borhyaena, Prothylacinus, Arctodictis, Pharsophorus*), the carotid groove (probably because of the relative position of the groove and carotid foramen) is located at the apex of the promontorium, rather than on its antero-ventral aspect. We have not observed this character in metatherians skulls other than Sparassodonta and Pucadelphyidae. However, it is noteworthy that some isolated petrosals from the early Eocene of Itaboraí (Brazil) exhibit an anterior carotid sulcus. This sulcus is indeed well developed in the types II, III, VI, and VII (Ladevèze 2004, 2007; Ladevèze & Muizon 2010).

On the posteroventral region of the promontorium is a small tubercle, which represents the rostral tympanic process. This process is low and nodular, as is observed in *Mayulestes*. A rostral tympanic process is barely present (or absent) in *Pucadelphys* and *Andinodelphys*. In extant didelphids, the rostral tympanic process is generally more developed and often forms an anterolaterally oriented crest or tubercle, which connects either to the ectotympanic (e.g. *Thylamys, Monodelphis, Marmosa, Didelphis*) or to the tympanic process of the alisphenoid, as is observed in *Caluromys*. In other sparassodonts, a small nodular rostral tympanic process is present, for example in *Notogale, Sipalocyon,* and *Cladosictis*. In these taxa, however, the tubercle extends anteriorly as a thick and low ridge on the medial side of the promontorium.

Posterodorsal to the rostral tympanic process is the external opening of the cochlear fossula. This aperture is crescentic, with an externally convex ventral edge and a concave dorsal one. On the posterolateral angle of the promontorium of MHNC 8267 is a small oval-shaped fenestra vestibuli. Its length is slightly smaller than that of the external opening of the cochlear fossula. However, its stapedial ratio cannot be measured because its width has been reduced by some dorsoventral post-mortem compression of the petrosal. Lateral to the fenestra vestibuli is the facial sulcus, in which opens the secondary facial foramen. It is located anterolaterally to the fenestra vestibuli and opens posteriorly. The secondary facial foramen is the exit of the facial nerve posteriorly. Proximally, the facial nerve exits the petrosal via the primary facial foramen in the cavum supracochleare, which houses the geniculate ganglion. This ganglion is formed by the facial nerve after crossing the petrosal. It produces posteriorly a thick hyomandibular ramus of the facial nerve, which runs in the facial sulcus and exits the middle ear via the stylomastoid notch. Anteriorly, a small branch of the facial nerve, the greater petrosal nerve, exits the petrosal via the hiatus Fallopii. In *Allqokirus*, the hiatus Fallopii is located on the cerebellar surface of the bone, a plesiomorphic condition also present in *Mayulestes* (see supplementary data — http://sciencepress.mnhn.fr/sites/default/files/documents/en/file5.pdf), *Pucadelphys,* and *Andinodelphys* (Ladevèze & Muizon 2007). Anterolateral to the facial canal are two small depressions separated by a short

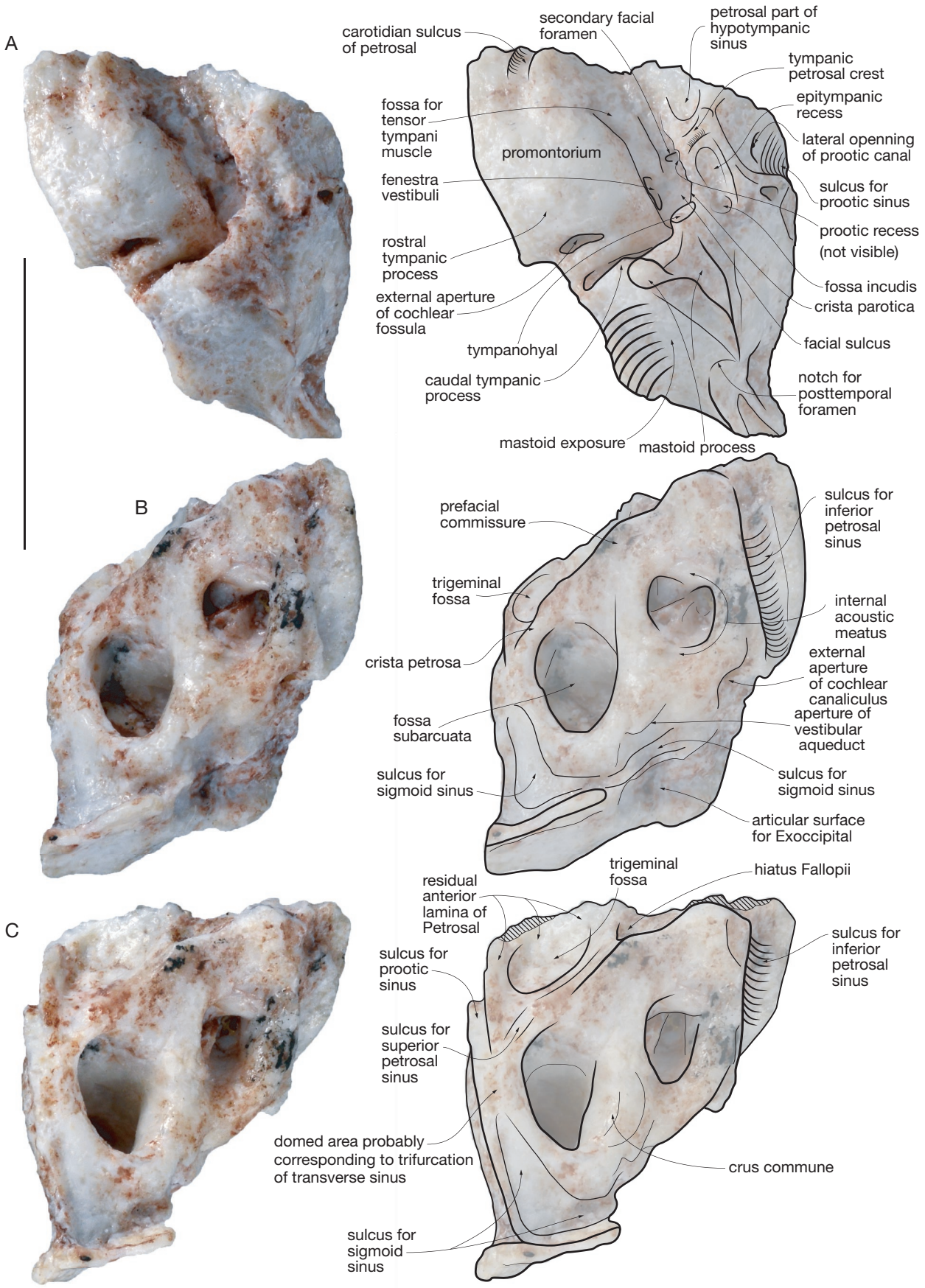


FIG. 24. — Left petrosal of *Allqokirus australis* (MHNC 8267): **A**, tympanic view; **B**, cerebellar (medio-dorsal) view; **C** cerebellar (dorsal) view. Scale bar: 5 mm.

and elevated ridge (Fig. 24A). The anterior depression is the posterior part of the hypotympanic sinus, and the posterior one is the epitympanic recess. The anterior portion of the hypotympanic sinus is excavated in the medial process of the squamosal, which contacts the petrosal anterolaterally (see above, squamosal section and Fig. 23). Therefore, the hypotympanic sinus of *Allqokirus* is composed of the petrosal and the squamosal, in contrast to that of *Mayulestes*, which also includes an alisphenoid contribution. The condition of *Mayulestes* resembles that of *Notogale, Sipalocyon* and *Cladosictis*, although in these taxa the alisphenoid contribution is by far the largest.

Posterior to the hypotympanic sinus is a transverse short ridge, which corresponds to the structure called petrosal crest by Archer (1976), Muizon (1998), Ladevèze & Muizon (2007). However, this term is very similar to term "crista petrosa", a structure on the dorsal aspect of the petrosal, which runs along the lateral border of the subarcuate fossa almost as far as the apex of the bone, and to which is attached the tentorium cerebelli which separates the cerebrum and cerebellum. In order to avoid confusion between the two structures, Ladevèze & Muizon (2010) proposed the term tympanic petrosal crest for the structure in the tympanic cavity, which separates the hypotympanic sinus and the epitympanic recess (see below). Therefore, this term is retained here. The lateral extremity of the tympanic petrosal crest is inflated and forms a small tubercle, which represents an incipiently developed tuberculum tympani (Wible 1990). A tympanic petrosal crest is present in *Pucadelphys, Andinodelphys* and in many sparassodonts (e.g. *Mayulestes, Notogale, Sallacyon, Cladosictis, Sipalocyon*). It is also observed in all Recent didelphids. A tuberculum tympani is absent (or incipiently developed) in *Pucadelphys, Andinodelphys*, and *Mayulestes*. It is large in Recent didelphids and even larger in *Notogale and Sipalocyon,* in which it approaches in length the width of the promontorium. In these taxa, it is conspicuously excavated anteriorly by the hypotympanic sinus and posteriorly by the epitympanic recess, and it is closely appressed against the medial process of the squamosal within the hypotympanic sinus (see Muizon 1999 for the condition in *Notogale*). According to Kuhn & Zeller (1987), the tuberculum tympani is the homologue of the tegmen tympani of eutherians, a statement that can probably be extended to the whole tympanic ventral petrosal crest.

The medial extremity of the tympanic petrosal crest is on the lateral edge of the facial canal, anterolateral to the fenestra vestibuli and just posterolateral to the secondary facial foramen. In *Allqokirus*, dorsal to the medial extremity of the tympanic petrosal crest is a distinct recess, which opens in the facial canal, close to and lateral to the secondary facial foramen. In the bottom of this recess is the medial opening of the prootic canal. This canal conveys the prootic canal vein, which connects the prootic sinus (on the lateral view of the petrosal) to the lateral head vein, which runs in the facial sulcus in metatherians (Wible 1990). Further medially, the lateral head vein joins the inferior petrosal sinus to form the internal jugular vein (Wible & Hopson 1995; Ladevèze & Muizon 2007; Wible *et al.* 2009). This recess on the lateral edge of the facial sulcus, for which we propose the term **prootic recess**, is present in Recent didelphids, but some variation exists in this family since the recess may be somewhat posterior to the medial extremity of the tympanic petrosal crest. A prootic recess is also present in *Pucadelphys, Andinodelphys* and *Mayulestes*. We have observed a prootic recess in *Notogale*, and *Sipalocyon.* It is probably present in *Lycopsis* but apparently absent in *Arctodictis*, and *Borhyaena*. The condition in *Prothylacynus* is unclear on the digitally reconstructed petrosal, which was available during this study and we have not been able to observe the condition of other sparassodonts.

Posterior to the tympanic petrosal crest of MHNC 8267, and lateral to the fenestra vestibuli, is a concave facet dipping anteroventrally. This facet is the petrosal portion of the epitympanic recess. In the posterior region of the facet is a deep pit, which corresponds to the fossa incudis, where the crus breve of the incus would have had a ligamentous attachment with the petrosal. The epitympanic recess is composed of the addition of this petrosal concavity to the medial elongated surface of the squamosal, posterior to the postglenoid foramen mentioned above in the squamosal section. Both structures of the petrosal and the squamosal form the epitympanic recess, the cavity which houses the incudomalleolar articulation (Klaauw 1931). In *Allqokirus*, the petrosal portion of the recess is slightly wider than the squamosal one. A similar condition is observed in *Mayulestes*. In *Andinodelphys* and *Pucadelphys*, both portions are roughly identical in size, whereas in *Notogale* the squamosal portion is distinctly larger than the petrosal one.

The medial edge of the epitympanic recess and fossa incudis is the crista parotica, which is strongly U-shaped ventrally. Medial to the fossa incudis, the crista parotica abuts against a thickened ovale-shaped structure, the tympanohyal. The latter has a truncated and expanded synchondrostic articulation with the stylohyal. Posterior to the tympanohyal, the crista parotica is moderately but distinctly concave and forms the stylomastoid notch through which the facial nerve exits from the middle ear. Posteromedial to the stylomastoid notch is a conspicuous tubercle, which extends in a robust crest on the posterior edge of the petrosal. Both constitute the mastoid process of the petrosal (Fig. 25). The crest of the mastoid process forms the ventrolateral border of the mastoid exposure of the petrosal (in yellow on Fig. 25C). On *Mayulestes*, *Andinodelphys* and *Pucadelphys*, the lateral side of the mastoid process receives the posttympanic process of the squamosal, a thin blade of bone, which also articulates with the lateral surface of the petrosal anterior to the mastoid process. This process is broken on both squamosals of MHNC 8267, but its base is anteroposteriorly oriented as is observed in *Mayulestes*, *Andinodelphys* and *Pucadelphys*. The crest of the mastoid process is approximately one third the total length of the squamosal suture with the mastoid exposure of the petrosal. The condition of *Allqokirus* is similar to that in *Pucadelphys*, *Andinodelphys*, and *Mayulestes*. The mastoid process of *Allqokirus* is small, but conspicuously more developed than in the Recent didelphids, in which it is very

reduced and often absent. On the ventrolateral region of the mastoid exposure, medial to the mastoid crest, is a relatively deep irregular fossa which probably received the insertion of the *sternocephalicus pars mastoidea* muscle (Fig. 25B, C). A relatively deep *sternocephalicus* fossa is present in *Mayulestes*, but it is relatively shallower in *Andinodelphys* and *Pucadelphys*. In didelphids, there is no fossa, and the *sternocephalicus pars mastoidea* inserts on the lateral crest of the mastoid exposure, sometimes extending on the posterior edge of the squamosal that articulates with the pars mastoidea (Coues 1869). When contracted alternately, this muscle flexes the head and neck laterally, and when contracted simultaneously the two muscles flex the head and neck ventrally, two movements that need to be strong in a predaceous mammal.

Medial to the mastoid process, the ventral edge of the mastoid exposure is an anteriorly projecting crest, located posteromedially to the external aperture of the cochlear fossula and which almost reaches the jugular foramen medially. This crest is the caudal tympanic process. It is slightly convex anteriorly and floors the medial region of the stapedius fossa. The latter forms a deep cavity roughly perpendicular to the facial sulcus and excavated in the roof of the middle ear, between the posteromedial angle of the promontorium anteriorly and the continuous wall formed by the tympanohyal-stylomastoid notch-mastoid process-caudal tympanic process series posteriorly. The stapedius fossa is dorsal and posterolateral to the external aperture of the cochlear fossula. It narrows sharply medially and reaches a deep and elongated notch, through which it communicates with the jugular foramen (posterior lacerate foramen). This notch is the passage for the lateral head vein, which joins the inferior petrosal sinus to form the internal jugular vein (Ladevèze & Muizon 2007; Wible *et al.* 2009). The *stapedius* muscle originates in the stapedius fossa, and inserts on the stapes.

**Occipital view** (Fig. 25C). The petrosal has a wide portion of the pars mastoidea exposed on the occiput. This mastoid exposure is wedged between the squamosal laterally, the exoccipital medially, and the supraoccipital dorsally. In posterior view, the squamosal-petrosal suture is the longest of the three. It is markedly convex in its ventral half and concave dorsally. The ventral half of the convex portion is formed by the dorsal crest of the mastoid process. Most of the dorsal concave portion of the suture is notched by a posttemporal notch, through which the arteria and vena diploëtica magna exit the skull. Dorsally, the articular suture with the supraoccipital is sub-horizontal. The articular suture with the exoccipital is sub-vertical, with a small medially convex ridge in its inferior half. The ventral half of the mastoid exposure is wider than the dorsal region, and both planes meet at an angle of approximately 90°. An occipital exposure of the mastoid is present in *Mayulestes* (Muizon 1998) and *Callistoe* (Babot *et al.* 2002: 620, fig. 2). It has not been observed in any post-Eocene sparassodont, in which the pars mastoidea of the petrosal is reduced and totally internal to the skull. However, the condition of *Patene* from the early Eocene of Brazil and Argentina is unknown.

**Cerebellar view** (Fig. 24B, C). The cerebellar view of the petrosal is characterised by four excavations: 1) posterodorsolaterally is the fossa subarcuata, which accommodates the parafloculus of the cerebellum; 2) anterolaterally is a deep basin, which houses at least part of the trigeminal ganglion, and which is formed by the anterior lamina of the petrosal; 3) in the middle of the bone is the internal acoustic meatus; 4) anteromedially is a deep groove for the inferior petrosal sinus.

The subarcuate fossa is bounded by the three semicircular canals, the anterior and the posterior joining at the crus commune. The anterior, lateral and posterior regions of the opening of the fossa subarcuata include the anterior semicircular canal, and the posteromedial region houses the crus commune. The opening of the fossa subarcuata is roughly pear-shaped, being narrower posteriorly than anteriorly. The narrow posterior extremity of the opening is greatly thickened relative to the anterior region. The fossa opens anteromedially.

The anterior edge of the fossa subarcuata is the crista petrosa, which also forms the posteromedial edge of the fossa for the trigeminal ganglion. In *Allqokirus*, the crista petrosa is relatively broad as is observed in *Andinodelphys*, differing from the condition in *Pucadelphys*, where it is sharp and narrow (Ladevèze & Muizon 2007). The subarcuate fossa of *Allqokirus* is deep and large and its aperture is constricted; on other words, its opening is narrower than its greatest diameter. This condition is present in *Pucadelphys, Andinodelphys*, and most Recent didelphids. It is also present in some sparassodonts (e.g. *Mayulestes, Sipalocyon, Cladosictis, Notogale, Sallacyon*); in contrast, it is absent in borhyaenids (*Borhyaena*, *Arctodictis*, *Prothylacynus*), and *Paraborhyaena* (although less shallow in this genus than in the others), which have a shallow subarcuate fossa.

Anterolateral to the fossa subarcuata is a deep anterolaterally facing basin. It is slightly larger than the aperture of the fossa subarcuata and represents the fossa where the trigeminal ganglion (or at least part of it) rests. It corresponds to the posterior floor of the cavum epiptericum, an intracranial space (intracranial in mammals but extracranial primitively), which can also be identified as the trigeminal chamber (separated by the prefacial commissure from the facial chamber, or cavum supracochleare). This fossa is peculiar to the Tiupampa metatherians in which the petrosal is known, and has apparently not be formally named. Therefore, we propose here for this structure the new term "**trigeminal fossa**". It is also present in *Amphiperatherium* and *Peratherium* (Selva & Ladevèze 2017; pers.obs.) and in several isolated petrosals from Itaboraí (Ladevèze 2004, 2007; Ladevèze & Muizon 2010). A small trigeminal fossa is also observed in *Prokennalestes* on the dorsal aspect of the structure identified as an anterior lamina by Wible *et al.* (2001) The trigeminal fossa is excavated in a thin anteriorly projecting blade, which is U-shaped in anterior view. The external aspect of this blade is visible laterally and ventrally. It is present in *Pucadelphys* and *Andinodelphys*, and has been regarded as a residual anterior lamina of the petrosal (Marshall & Muizon 1995; Ladevèze & Muizon 2007).

The anterior lamina of the petrosal is a blade-like intramembranous ossification of the spheno-obturator membrane, located anterolaterally to the petrosal and fused to it, which forms a major part of the posteroventral lateral wall of the braincase posterior to the alisphenoid in non-therian mammals. The ventral portion of the anterior lamina is the lateral flange (Wible & Rougier 2000; Wible *et al.* 2001). In non-therian mammals, the anterior lamina encloses the foramen for the mandibular branch (V3) of the trigeminal nerve, and in some cases the maxillary branch (V2) (see Wible [1990] and Hopson & Rougier [1993] for a review). The anterior lamina and lateral flange reduce and disappear in eutherians and metatherians, and the mandibular branch of the trigeminal nerve exits the skull either between the alisphenoid and the petrosal (metatherians), or the foramen is totally enclosed by the alisphenoid (eutherians). However, in basal metatherian and eutherian taxa a residual anterior lamina is still present, although the pattern of exit of the V3 is that described above. This anterior lamina is: 1) partly ventral (i.e., the posterior rim of the foramen ovale), probably the lateral flange of non-therian mammals; and 2) partly lateral, this portion, a remnant of the anterior lamina, being covered by the squamosal laterally. When the petrosal is viewed dorsally, both ventral and lateral parts of the anterior lamina are clearly visible (Ladevèze & Muizon 2007) and form a deep basin, the trigeminal fossa, which houses the trigeminal ganglion. It is noteworthy that the trigeminal ganglion is also housed in the medial aspect of the anterior lamina of non-therian mammals. A residual anterior lamina has been described in the metatherians *Pucadelphys* (Marshall & Muizon 1995) and *Andinodelphys* (Ladevèze & Muizon 2007), in the eutherians *Alcidedorbignya* (Muizon *et al.* 2015) and *Prokennalestes* (Wible *et al.* 2001), and in isolated "zhelestid" petrosals (Ekdale *et al.* 2004). This interpretation of the occurrence of a residual anterior lamina in metatherians confirms Wible's suggestion that "the anterior lamina […] may not be totally absent in all marsupials" (Wible 1990: 200). This vestigial anterior lamina of *Pucadelphys* and *Andinodelphys* is not exposed on the lateral wall of the braincase, in contrast to the condition, for instance, in *Vincelestes*, in which the anterior lamina separates the alisphenoid anteriorly and the squamosal posteriorly, and is part of the lateral wall of the braincase (Hopson & Rougier 1993). This condition in *Pucadelphys*, led Rougier & Wible (2006: 277) to state that "if that structure – (in *Pucadelphys*) – is the remnant of a primitive morphology lost among later metatherians, it is better considered as part of a lateral flange than an anterior lamina". However, it is noteworthy that the anterior lamina and the lateral flange (the ventral part of the former) are part of the same structure, an intramembranous ossification of the spheno-obturator membrane regarded as homologous to the lamina obturans of monotremes (Wible & Hopson 1993; Hopson & Rougier 1993; Wible & Rougier 2000; Wible *et al.* 2001). In therians, the anterior lamina is reduced and is overlapped by the squamosal, which extends anteriorly and contacts the alisphenoid, therefore excluding the anterior lamina from the lateral wall of the braincase (see Marshall & Muizon [1995: 78-82] for an extensive discussion on the occurrence of an anterior lamina in *Pucadelphys*). Rougier & Wible (2006: 277) discussed and disagreed with the interpretation of the presence of a residual anterior lamina in *Pucadelphys*. However, these authors provided no discussion of the arguments given by Marshall & Muizon (1995), and concluded that an anterior lamina is absent in *Pucadelphys*. Rougier & Wible (2006: 277) partly based their interpretation on the fact that the anterior lamina of *Pucadelphys* (*sensu* Ladevèze & Muizon 2007) has no exposure on the lateral wall of the braincase. They interpret the anterior lamina of *Pucadelphys* as part of the petrosal in origin (rather than an intramembranous ossification of the spheno-obturator membrane; Hopson & Rougier 1993). As explained above, the reduction of the anterior lamina in therians is accompanied by a junction of the squamosal and alisphenoid, which covers the lamina laterally. The lamina therefore loses its exposure on the lateral wall of the braincase. Moreover, because a suture must exist between the anterior lamina and the petrosal (two different ossifications), the other argument of Rougier & Wible (2006) is the absence of a sutural contact in *Pucadelphys*, which would indicate separate ontogenetic origins of the petrosal and anterior lamina (or its ventral border, the lateral flange), which is an intramembranous ossification distinct from the petrosal. They however admitted that a suture is rarely observed in this area. It has been observed only in a juvenile platypus (Wible & Hopson 1993) and in *Vincelestes* (Rougier *et al.* 1992; Hopson & Rougier 1993). However, the absence of a suture on the petrosal of adult metatherians does not necessarily imply that it did not exist in juveniles. Even if a suture is apparently lacking (personal observations) in Recent marsupials (probably because the anterior lamina has totally disappeared), the development of *Pucadelphys* or *Allqokirus* was not necessarily the same as that of recent taxa and, therefore, comparison with development in Recent marsupials should be viewed with caution in this case. Furthermore, although they do not observe a suture between the petrosal and the anterior lamina in *Prokennalestes*, Wible *et al.* (2001) accepted the presence of a rudimentary anterior lamina and lateral flange in this taxon. Rougier & Wible (2006) did not deny either the identification by Ekdale *et al.* (2004) of a lateral flange on a "zhelestid" petrosal although no suture was observed. The same observation could be made concerning *Morganucodon* (Kermack *et al.* 1981), as well as the multituberculate *Kryptobaatar* (Wible & Rougier (2000). No comment on these absences of suture was provided by Wible & Rougier (2000). Therefore, the argument based on the absence of a suture in fossil taxa is irrelevant to the debate regarding the presence or absence of an anterior lamina (and/or lateral flange) as a separate ossification from the petrosal. We therefore refer here to the explanations provided by Marshall & Muizon (1995) and Ladevèze & Muizon (2007) as well as on the comments above, to support the interpretation of a reduced true anterior lamina in *Pucadelphys*. To conclude, we persist in our interpretation of the structure described above, which houses the trigeminal ganglion in *Allqokirus* as a residual anterior lamina, and confirm our interpretation that such a structure is present in *Pucadelphys* and *Andinodelphys* (Ladevèze & Muizon 2007). An anterior lamina and a trigeminal fossa are also present in

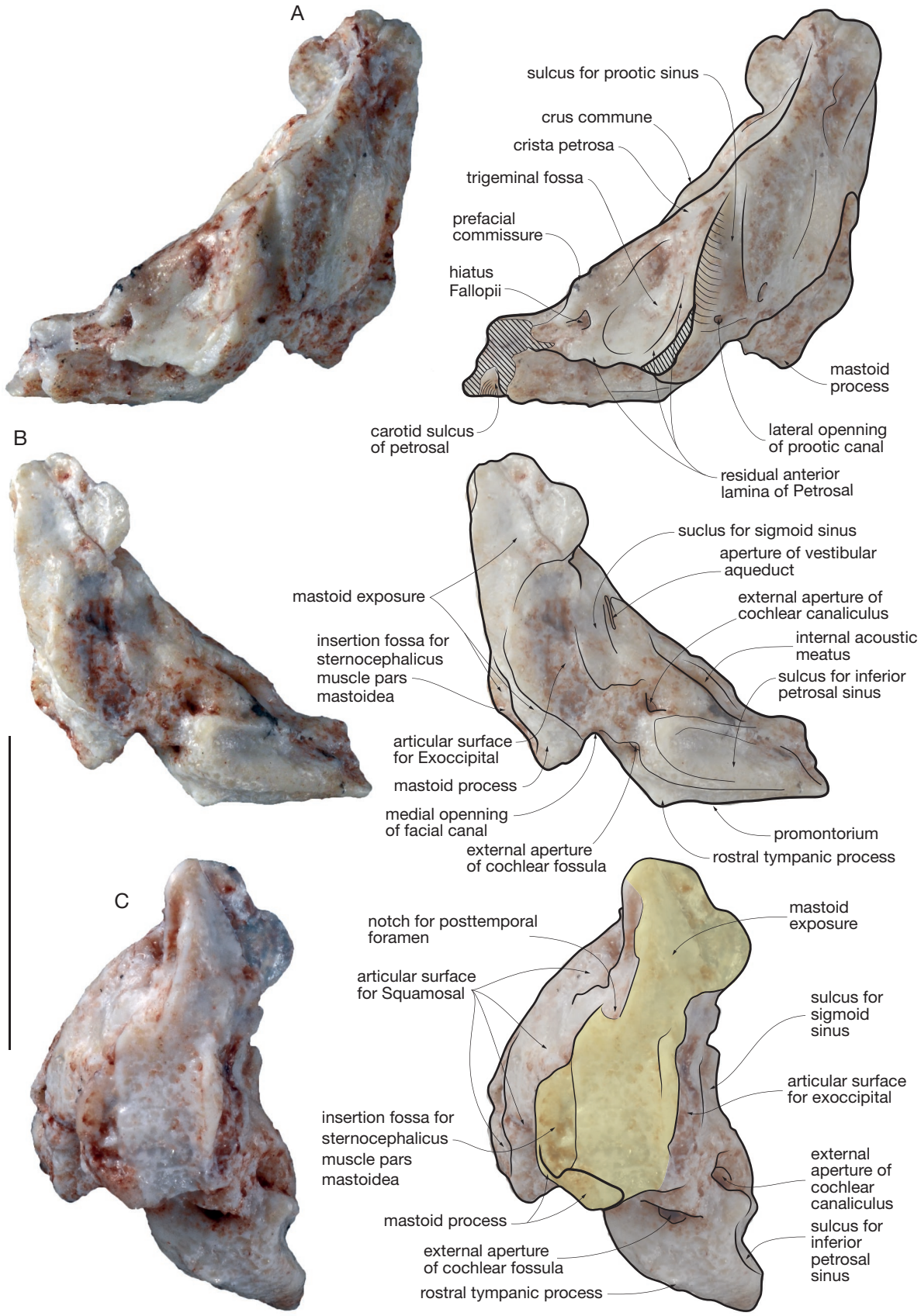


FIG. 25. — Left petrosal of *Allqokirus australis* (MHNC 8267): **A**, squamosal view; **B**, medial view; **C**, occipital view. **Yellow area** indicates mastoid external exposure. Scale bar: 5 mm.

*Mayulestes*, as observed on the digital rendering of CT data of the petrosal of the holotype (see Supplementary data – http://sciencepress.mnhn.fr/sites/default/files/documents/en/file5.pdf). This interpretation confirms the prediction of Wible (1990) that an anterior lamina may be retained in metatherians.

In the anteromedial region of the trigeminal fossa, but external to it, is the opening of the hiatus Fallopii, which is dorsal in *Allqokirus*, as in *Pucadelphys*, *Andinodelphys,* and *Mayulestes*.

The internal acoustic meatus is anteromedial to the fossa subarcuata, and located more ventrally. It is smaller than the subarcuate fossa, as is observed in *Andinodelphys* and *Mayulestes*, some other sparassodonts (e.g. *Sipalocyon, Sallacyon, Notogale*) and Recent didelphids. *Allqokirus* differs from *Pucadelphys,* in which the two structures are subequal in size. The meatus is divided by a thin septum that separates the foramen acousticus superius, dorsally and the foramen acousticus inferius ventrally. The former includes anteriorly, the facial foramen (primary facial foramen), which opens ventrally in the cavum supracochleare (which houses the geniculate ganglion), and the tractus for the passage of the superior branch of the vestibular nerve. The foramen acousticus inferius is slightly damaged, and does not permit the observation of the foramen singulare posteriorly or the tractus spiralis foraminosus anteriorly. The foramen singulare transmits bundles of the inferior vestibular nerve, and the tractus spiralis foraminosus contains a cribriform plate for the passage of the cochlear nerve. Anterolateral to the internal acousticus meatus is a thick and wide prefacial commissure, which is located on the anterior part of the crista petrosa. It overhangs the posteromedial edge of the trigeminal fossa. It is straight, and does not present the conspicuous notch observed in *Andinodelphys* and most Recent didelphids. A wide and un-notched prefacial commissure is observed in *Pucadelphys, Mayulestes, Sipalocyon*, and *Notogale*.

A deep sulcus for the inferior petrosal sinus is present in the anteromedial region of the pars cochlearis. In its posterior part, the sulcus is medial and not visible in dorsal view. Anteriorly, it turns slightly laterally and dorsally and runs on the dorsal surface of the apex of the pars cochlearis. This condition is similar to that observed in *Mayulestes* and *Andinodelphys*. The posterior end of the sulcus is adjacent to the anteromedial angle of the jugular notch, the part of the jugular foramen that excavates the posteromedial angle of the promontorium. At the anterior end of the sulcus, on the dorsal side of the petrosal, is an irregular articular area, which articulates with the anterolateral angle of the basioccipital. In Recent didelphids, the apex of the petrosal bears such an articular fossa, which imbricates, dorsally, with a small wing at the anterolateral angle of the basioccipital. Although the basioccipital of *Allqokirus* is unknown, because of the articular structure observed on the dorsal aspect of the apex of the promontorium, it is likely that the basioccipital also possessed a small articular wing for the apex of the petrosal. A similar condition is observed in *Mayulestes* but apparently not in *Pucadelphys* and *Andinodelphys*. There is no distinct sulcus on the dorsomedial view of the petrosal in *Notogale, Sallacyon,* and *Sipalocyon* for the passageway of the inferior petrosal sinus.

Posterodorsal and lateral to the fossa subarcuata, along its greatest length, is an anteroposteriorly-elongated, triangular fossa. The posterior, narrow edge of this triangle is an elevated wall, roughly rectangular in posterior view and which participates in the most elevated point of the petrosal. The plane of this blade is subvertical and forms approximately a right angle with the plane of the triangular fossa. This posterior blade corresponds to the dorsal part of the occipital mastoid exposure, which articulates with the supraoccipital. This region of the petrosal provides indications regarding the passageways of the three branches issued from the transverse sinus. The paired transverse sinuses derive from the median sagittal sinus and reach the posterodorsal apex of the petrosal. In this region, each transverse sinus divides into three major vessels, the sigmoid sinus, the superior petrosal sinus and the prootic sinus. The sigmoid sinus is medial, and extends ventrally towards the jugular foramen. The prootic sinus is lateral; it extends between the squamosal and the petrosal, and becomes the sphenoparietal emissary vein before it exits the skull through the postglenoid foramen to join the external jugular vein (Wible & Hopson 1995). The superior petrosal sinus extends anteroventrally from the transverse sinus between the sigmoid sinus and the prootic sinus. Indication of the passage of these sinuses is observable on the petrosal of *Allqokirus* (Fig. 24). On the posterolateral edge of the subarcuate fossa is a domed area from which depart the grooves of the three sulci mentioned above. We regard this area as the point at which the transverse sinus divides into its three branches (Fig. 24C). From this dome, we suggest that the sigmoid sinus extended posteriorly along the triangular fossa. Within the fossa, the sinus turned 90° medially and continued its course ventrally and medially in a short but deep groove on the posterior edge of the narrow and thickened posterior border of the fossa subarcuata. This groove passes posterior to the vestibular aqueduct and fades out ventrally at the level of the cochlear aqueduct. From there, the sigmoid sinus continued its course ventrally and exited the skull as the internal jugular vein (merging with the inferior petrosal sinus), through the jugular foramen (Fig. 26). On the anterolateral edge of the fossa subarcuata, lateral to the lateral blade of the anterior lamina, is a deep subvertical sulcus, which almost reaches the tuberculum tympani ventrally. This sulcus is for the prootic sinus, which becomes the sphenoparietal emissary vein more distally, and exits the skull through the postglenoid foramen. On the dorsal extremity of the sulcus for the prootic sinus, on the anterior edge of the elevated area mentioned above, is a small anteromedial bifurcation, from which runs a shallow sulcus on the crista petrosa, along the lateral edge of the fossa subarcuata. This sulcus is for the superior petrosal sinus. The sulcus for the prootic sinus is the largest of the three. Because it is only slightly smaller than the transverse sinus, it appears to be its ventral extension. The other two vessels are smaller diverging rami of the transverse sinus.

On the posteromedial edge of the internal acoustic meatus, just lateral to the posterodorsal edge of the sulcus for the inferior petrosal sinus, is a conical depression for the exit of the cochlear canaliculus. On the posteromedial edge of the subarcuate fossa, anterodorsal to the sulcus for the sigmoid sinus, is the slit-like aperture of the vestibular aqueduct.

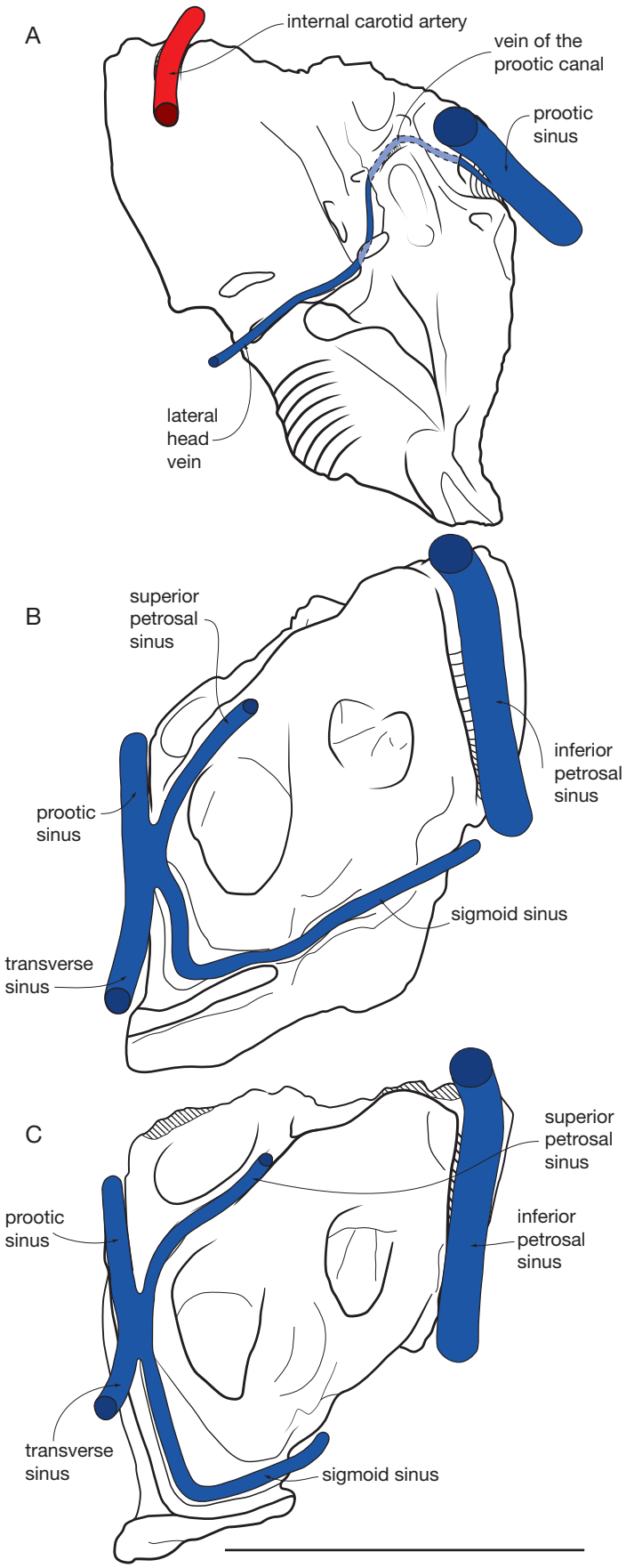


FIG. 26. — *Allqokirus australis*: reconstruction of the major vessels of the auditory region: **A**, tympanic view; **B**, cerebellar (medio-dorsal) view; **C**, cerebellar (dorsal) view. Scale bar: 5 mm.

**Squamosal view** (Fig. 25A). This view is the part of the petrosal covered by the squamosal laterally. The major feature of this view is the wide subvertical sulcus for the prootic sinus. It is wider ventrally than dorsally, and its posterior crest is lower than the anterior one, which is the posterior blade of the anterior lamina. In its ventral region is a small foramen for the prootic canal, which conducts the lateral head vein (which starts in the prootic canal as an offshoot of the prootic sinus) to the facial sulcus. A prootic canal is also present in *Pucadelphys* and *Andinodelphys*. In contrast to earlier assertions (Muizon 1998, 1999; Rougier *et al.* 1998) a prootic canal is not always absent in sparassodonts. It has also been observed in *Mayulestes*, *Notogale* (see Supplementary data – http://sciencepress.mnhn.fr/sites/default/files/documents/en/file6.pdf), and *Sipalocyon* (see Supplementary data — http://sciencepress.mnhn.fr/sites/default/files/documents/en/file7.pdf). Furthermore, we suspect that the deep sulcus observed at the base of the sulcus for the prootic sinus in *Borhyaena* may represent an enlarged prootic canal (see Supplementary data – http://sciencepress.mnhn.fr/sites/default/files/documents/en/file8.pdf). In fact, the specimen, on which we observed this sulcus (YPM-PU 15120), was found detached from the cranial bones, in the endocranium (Archer 1976: 298). It is therefore possible that, because of the detachment process (during fossilisation), the bone suffered some damage and that the prootic canal was partially broken and artificially "transformed" into a sulcus. In *Allqokirus*, on the posterior edge of the posterior crest of the sulcus for the prootic sinus, there is a small foramen at its ventral extremity. Its diameter is much smaller than that of the sulcus for the prootic sinus, but it is much larger than that of the prootic canal. This foramen penetrates the substance of the petrosal, and we have been able to follow it some distance. A similar foramen is present in *Mayulestes* (see Supplementary data – http://sciencepress.mnhn.fr/sites/default/files/documents/en/file5.pdf), but it is absent in *Pucadelphys*, *Andinodelphys*, and we have not observed a similar structure in any other sparassodont. We have no interpretation regarding which vessel may have entered this foramen. On the squamosal aspect of the petrosal, the sulcus for the diploëtic vessels (artery and vein) is not deeply imprinted in contrast to the condition observed in Recent didelphids. On MHNC 8267, a flat elongated surface is observed running posterodorsally from the ventral end of the sulcus for the prootic sinus to the posttemporal notch. There, it turns abruptly dorsally along the lateral edge of the mastoid exposure. During this course, up to the top of the mastoid exposure, it is bordered medially by a sharp crest, the length of which is approximately 40% the total height of the mastoid exposure. A distinct sulcus for the diploëtic vessels has not been observed in *Pucadelphys*, *Andinodelphys, Mayulestes, Notogale, Sipalocyon*. A distinct sulcus is visible on the petrosal type A (FMNH PM53907), described by Wible (1990) and referred to a possible pediomyid, "*Pediomys" hatcheri* or "*P.*" *florencae*, both of which have now been assigned to the genus *Protolambda* (Davis 2007).

**Bony labyrinth of the inner ear** (Fig. 27). The bony labyrinth consists of a set of interconnected spaces within the petrosal bone. It contained in life the perilymph, in which the membranous labyrinth - a series of soft-tissue sacs and ducts - was suspended. The inferior part of the membranous labyrinth includes the cochlear duct, which contains the spiral organ of hearing, and the saccule of the vestibule, which contains receptors sensitive to linear motion. The superior part of the membranous labyrinth is involved in detecting rotational movement of the head; it includes the utricle of the vestibule, the semicircular ducts and ampullae, and the common crus between the anterior and posterior ducts. The bony semicircular and cochlear canals of the bony labyrinth are usually considered as closely following the path and shape of the inner membranous ducts (e.g. Blanks *et al.* 1975; Spoor *et al.* 2007; David *et al.* 2010).

The general aspect of the bony labyrinth of *Allqokirus* is very similar to that reconstructed for the other sparassodonts *Borhyaena*, *Prothylacynus*, and *Sipalocyon* (this study), and also the pucadelphyid *Pucadelphys* (CS, SL, CM in progress).

The complete turns of the cochlea are difficult to approximate because the segmentation of this part was difficult and the resulting 3D rendering is incomplete.

The semicircular canals of the bony labyrinth are thin and relatively circular. The anterior semicircular canal (ASC) is the longest of the three canals. The posterior semicircular canal (PSC) exhibits the widest area (explained by the radius of curvature), as compared to the ASC, which is slightly wider than the lateral semicircular canal (LSC) (Fig. 27; Table 4). The three semicircular canals are wide (expressed as the mean of the radii of curvature compared to the total height of the inner ear) relative to those of other sparassodonts, and their widths are more comparable to that of *Pucadelphys* and the extant marsupials sampled here. The planes of the three canals are almost perpendicular to each other, as observed in other sparassodonts (Table 4). The LSC plane forms an angle of 85° with the planes of both the ASC and PSC. The planes of the PSC and ASC form a similar, near-perpendicular angle (83°). Both these canals meet at the crus commune. There is no secondary crus commune between the LSC and PSC, a condition also observed in *Borhyaena* and *Sipalocyon*. In *Protylacynus* there is an incipient secondary crus commune. The secondary crus commune is usually considered to be a plesiomorphic feature in therians (Ladevèze *et al.* 2008; Ruf *et al.* 2009), and it has been lost in many clades of therians. Here, we found it to be absent in *Pucadelphys*, but present in *Didelphis*.

The vestibule is the central area of the bony labyrinth. It is located between the cochlea (anteriorly) and the semicircular canals (posteriorly). The 3D model of the vestibule of *Allqokirus* is a very small and irregular structure, which exhibits three bulges located at the junction between the vestibule and the canals: the ampullae. The anterior ampulla lies dorsolateral to the vestibule, and connects the ASC to the vestibule. The lateral ampulla lies ventrolateral to the vestibule, and connects the LSC to the vestibule. The posterior ampulla lies ventromedial to the vestibule, and connects the crus commune to

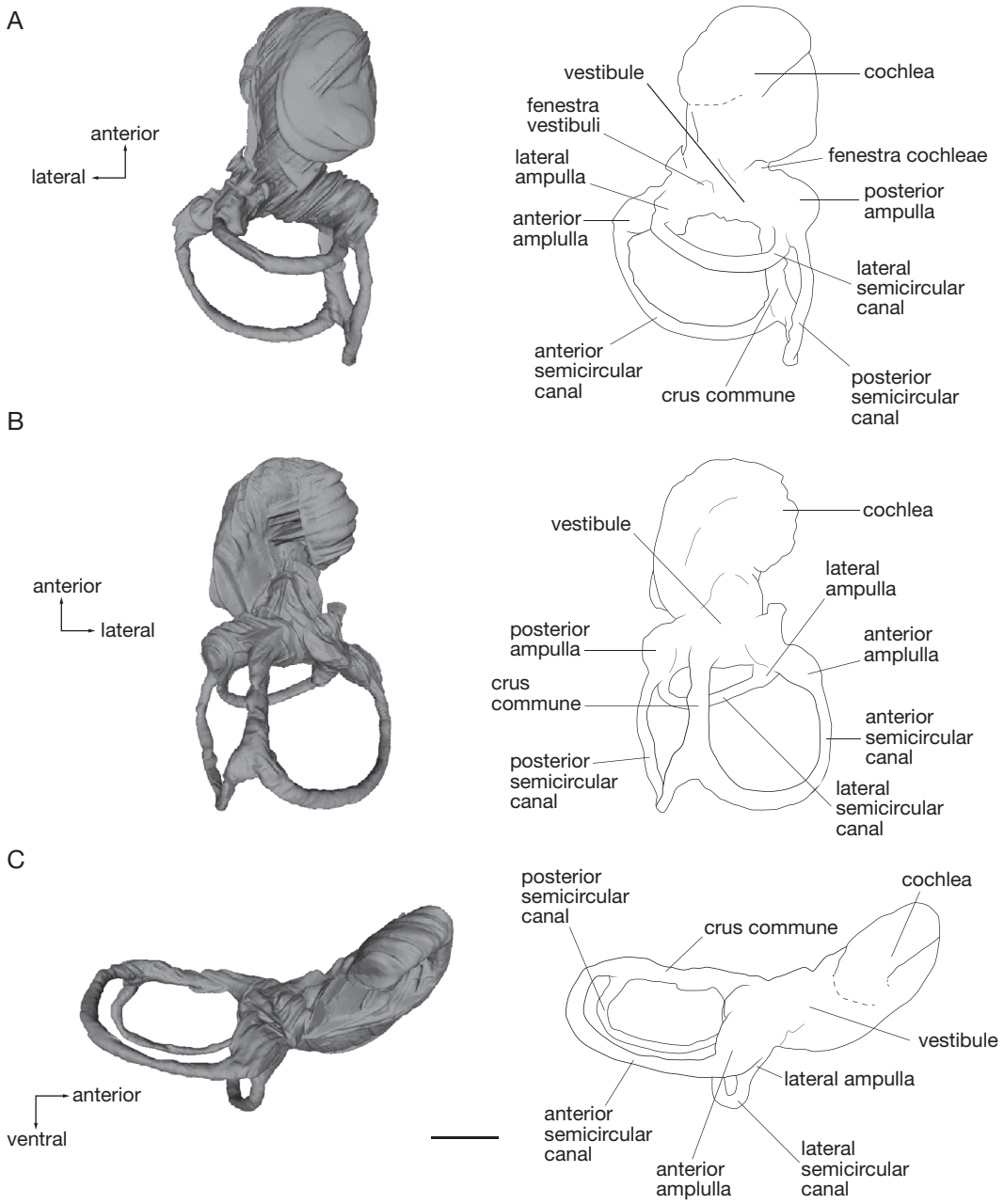


FIG. 27. — Virtual 3D reconstruction of the bony labyrinth of *Allqokirus australis* (MHNC 8267): **A**, tympanic view; **B**; cerebellar view; **C**, lateral view. Scale bar: 1 mm.

the vestibule. Due to the difficult segmentation of the bony labyrinth of *Allqokirus*, neither the spherical nor the elliptical recesses of the vestibule are visible in the 3D model.

*Supraoccipital*

The supraoccipital is the only preserved element of the occipital complex (Figs 21; 22). The basioccipital and the exoccipitals are missing. As exposed in the interparietal section, a distinct transverse suture is visible in intracranial view of the roof of the braincase and is regarded here as the interparietal-supraoccipital suture. It runs at the posterior base of the nuchal crest, which is formed by the interparietal and described in the corresponding section. In posterior view, the ventral margin of the supraoccipital bears five notches. The median is the largest and corresponds the the dorsal edge of the foramen magnum. The two other notches, lateral to the median one, are slightly smaller and correspond to the sutures with the exoccipitals, which, therefore, were not in contact dorsal to the foramen magnum. The lateralmost ones are the sutures with the mastoid exposures of the petrosals; they are similar in size to the sutures for the exoccipitals. In the middle of the supraoccipital is a slightly convex bulge, which corresponds to the underlying vermis of the cerebellum. Above this bulge in the midline, and below the nuchal crest, is a small circular foramen. Such a foramen has been observed by Wible (2003) in *Monodelphis* and interpreted as a probable emissary foramen. A median foramen is

TABLE 4. — Measurements of various semicircular canals aspects, taken in *Allqokirus australis* and a sample of fossil and extant metatherians. For each semicircular canal (**ASC**, **PSC**, **LSC**), height (**H**), width (**W**) and diameter (**D**) were measured, as well as the angles between each other. The inner ear height (**IEH**) was measured after Billet *et al.* (2013). The radius of curvature for each semicircular canal was calculated following Spoor *et al.* (2007).

| Species | Collection number | H ASC | L ASC | R ASC | H PSC | L PSC | R PSC | H LSC | L LSC | R LSC | IEH | Moy. R SC / IEH | H ASC / H PSC | H ASC / H LSC | H PSC / H LSC |
|---|---|---|---|---|---|---|---|---|---|---|---|---|---|---|---|
| *Allqokirus australis* | MHNC 8267 | 2.01 | 2.43 | 0.83 | 1.8 | 1.6 | 1.12 | 1.26 | 1.54 | 0.82 | 4.75 | 0.19 | 1.12 | 1.6 | 1.43 |
| *Pucadelphys andinus* | MHNC 8266 | 1.5 | 1.68 | 0.8 | 1.29 | 1.47 | 0.69 | 1.06 | 1.2 | 0.57 | 3.21 | 0.21 | 1.16 | 1.42 | 1.22 |
| *Borhyaena tuberata* | YPM-PU 15120 | 4.15 | 4.4 | 0.94 | 3.19 | 3.04 | 1.05 | 2.70 | 2.95 | 0.92 | 8.24 | 0.12 | 1.3 | 1.54 | 1.18 |
| *Prothylacynus patagonicus* | YPM-PU 15700 | 3.84 | 3.61 | 1.06 | 3.27 | 2.86 | 1.14 | 2.44 | 2.62 | 0.93 | 7.47 | 0.14 | 1.17 | 1.57 | 1.34 |
| *Sipalocyon gracilis* | AMNH 9254 | 3.09 | 3.18 | 0.97 | 2.79 | 2.79 | 1 | 1.82 | 2.27 | 0.8 | 6.19 | 0.15 | 1.11 | 1.7 | 1.53 |
| *Didelphis marsupialis* | MNHN RH61 | 2.94 | 3.02 | 1.49 | 2.4 | 2.48 | 1.22 | 1.56 | 1.74 | 0.83 | 5.32 | 0.22 | 1.23 | 1.88 | 1.54 |
| *Marmosa murina* | MHNH.ZM.MO.2001.2239 | 1.9 | 1.86 | 0.94 | 1.2 | 1.26 | 0.62 | 0.88 | 1.1 | 0.5 | 3.59 | 0.19 | 1.58 | 2.16 | 1.36 |
| *Caluromys philander* | MNHN.ZM.MO.1987.234 | 2.66 | 2.53 | 1.3 | 1.77 | 1.96 | 0.93 | 1.55 | 1.87 | 0.86 | 5.2 | 0.2 | 1.5 | 1.72 | 1.14 |
| *Dromiciops gliroides* | IEEUACH 2162 | 1.83 | 2 | 0.96 | 1.35 | 1.28 | 0.66 | 0.95 | 1.27 | 0.56 | 4.02 | 0.18 | 1.36 | 1.93 | 1.42 |
| *Caenolestes fuliginosus* | MNHN.ZM.MO.1982.2587 | 1.82 | 1.73 | 0.89 | 1.53 | 1.28 | 0.7 | 0.95 | 1.25 | 0.55 | 3.85 | 0.19 | 1.19 | 1.92 | 1.61 |
| *Perameles nasuta* | MNHN.ZM.AC.A12417 | 3.06 | 2.91 | 1.49 | 2.21 | 2.27 | 1.12 | 1.67 | 2.02 | 0.92 | 6.15 | 0.19 | 1.38 | 1.83 | 1.32 |
| *Phascogale tapoatafa* | MNHN.ZM.MO.2007.18 | 2.18 | 2.3 | 1.12 | 1.85 | 1.73 | 0.9 | 1.65 | 1.92 | 0.89 | 4.78 | 0.2 | 1.18 | 1.32 | 1.12 |

| Species | Collection number | Angle ASC/PSC | Angle ASC/LSC | Angle PSC/LSC | D ASC | D ASC / IEH | D PSC | D PSC / IEH | D LSC | D LSC / IEH |
|---|---|---|---|---|---|---|---|---|---|---|
| *Allqokirus australis* | MHNC 8267 | 82.57 | 84.69 | 85.19 | 0.2 | 0.04 | 0.18 | 0.04 | 0.2 | 0.04 |
| *Pucadelphys andinus* | MHNC 8266 | 101.95 | 97.75 | 83.94 | 0.15 | 0.05 | 0.21 | 0.07 | 0.17 | 0.05 |
| *Borhyaena tuberata* | YPM-PU 15120 | 86.93 | 88.53 | 83.82 | 0.40 | 0.05 | 0.39 | 0.05 | 0.38 | 0.05 |
| *Prothylacinus patagonicus* | YPM-PU 15700 | 89.53 | 89.76 | 86.50 | 0.20 | 0.03 | 0.14 | 0.02 | 0.57 | 0.08 |
| *Sipalocyon gracilis* | AMNH 9254 | 88.23 | 89.57 | 88.15 | 0.26 | 0.04 | 0.42 | 0.07 | 0.26 | 0.04 |
| *Didelphis marsupialis* | MNHN RH61 | 98.96 | 80.29 | 94.41 | 0.19 | 0.04 | 0.21 | 0.04 | 0.24 | 0.05 |
| *Marmosa murina* | MHNH.ZM.MO.2001.2239 | 98.7 | 83.59 | 94.43 | 0.21 | 0.06 | 0.18 | 0.05 | 0.21 | 0.06 |
| *Caluromys philander* | MNHN.ZM.MO. 1987.234 | 93 | 88.28 | 88.74 | 0.11 | 0.02 | 0.2 | 0.04 | 0.15 | 0.03 |
| *Dromiciops gliroides* | IEEUACH 2162 | 113.35 | 81.41 | 94.7 | 0.12 | 0.03 | 0.15 | 0.04 | 0.14 | 0.03 |
| *Caenolestes fuliginosus* | MNHN.ZM.MO.1982.2587 | 93.17 | 86.87 | 99.8 | 0.19 | 0.05 | 0.15 | 0.04 | 0.17 | 0.04 |
| *Perameles nasuta* | MNHN.ZM.AC.A12417 | 93.96 | 84.79 | 90.7 | 0.19 | 0.03 | 0.23 | 0.04 | 0.24 | 0.04 |
| *Phascogale tapoatafa* | MNHN.ZM.MO.2007.18 | 94.86 | 78.45 | 78.55 | 0.15 | 0.03 | 0.13 | 0.03 | 0.14 | 0.03 |

present in *Pucadelphys, Andinodelphys*, *Mayulestes*, and several other Recent didelphids (e.g. *Didelphis, Thylamys, Caluromys*).

### DENTARY

The right dentary of MHNC 8267 is complete (Fig. 28). However, considering the subadult stage of the specimen, because the m4 is not fully erupted, the dentary of the adult would have been longer, even if the other features of the bone are likely to be similar to those of an adult. In order to evaluate the length that the adult dentary of MHNC 8267 would have reached, a reasonable approximation can be obtained by adding to the actual length of the bone, the length of the non-erupted portion of m4 (roughly the talonid) plus a retromolar space equal to the length of the m4 talonid. As observed in *Pucadelphys*, *Andinodelphys*, and *Mayulestes*, the retromolar space is generally as long as the length of the m4 talonid but no longer. This approximation has been made in the parsimony analysis below, in order to score *Allqokirus* for character 104 (depth/length of the dentary below molars). Therefore, the length of the dentary of an adult specimen of *Allqokirus* based on MHNC 8267 is estimated to be: 30.70 (actual length of the dentary as measured) + 2.28 (length of the non-erupted portion of the m4 + m4 talonid length) = 32.98 mm. The length of the dentary is measured from the anterior alveolar border of i1 to the posterior edge of the condylar process. Evaluation of the adult value of the depth of the dentary is more complex. One alternative is to increase the height of the dentary below m3 by the same proportion as that of the length increase (from 30.70 to 32.98 mm), which corresponds to 0.07%. However, in this case, since the relative increase of height and length is the same, the result of the ratio with estimated adult height and length will be the same as the ratio calculated with both subadult measurements. Another alternative is to calculate the ratio with the estimated adult length of the dentary and the actual subadult height (considering that the height change from subadult to

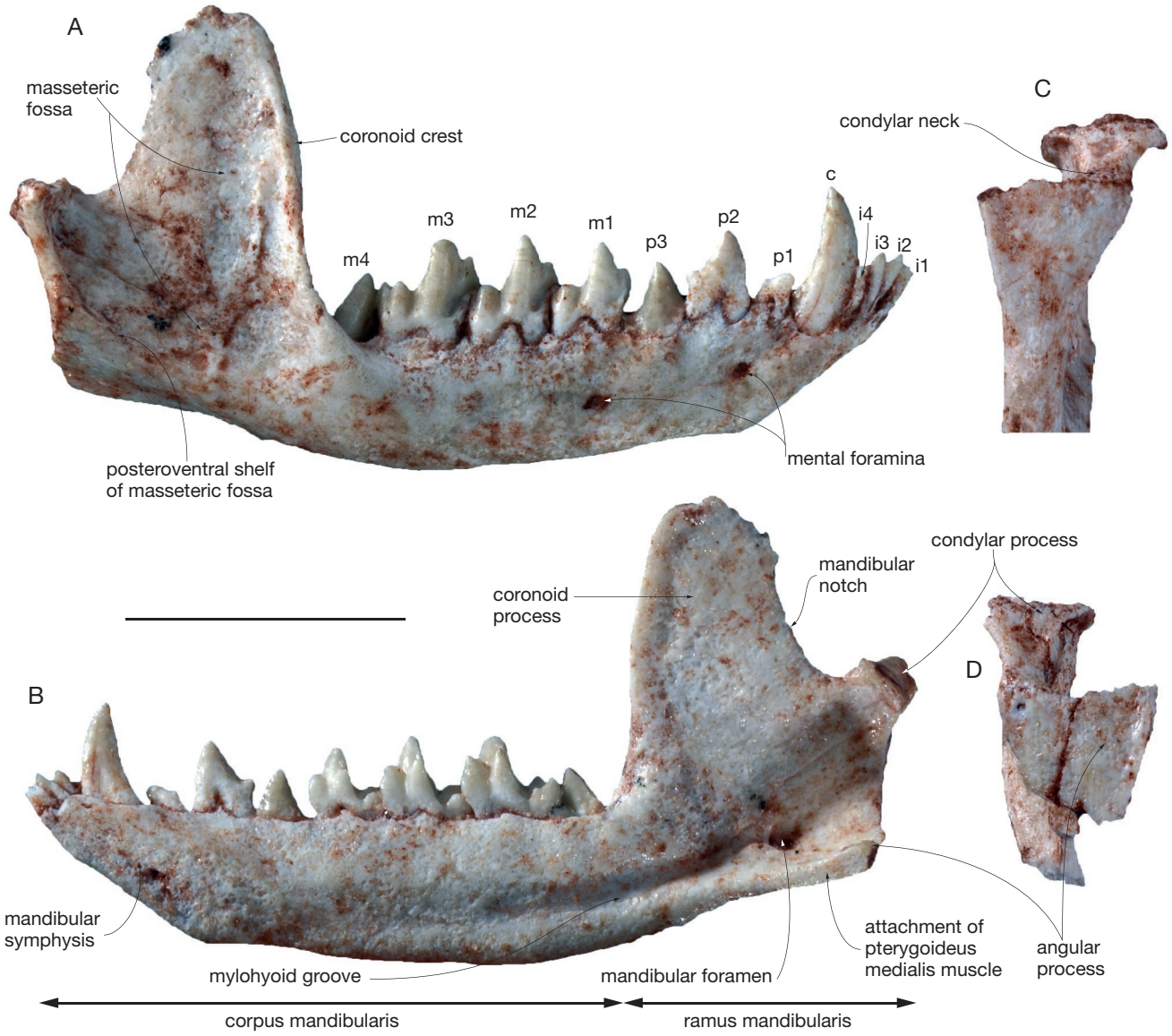


Fig. 28. — Dentary of *Allqokirus australis* (MHNC 8267): **A**, lateral view of right dentary; **B**, medial view of right dentary; **C**, Ventral view of the ramus of the left dentary. Scale bar: 1 cm.

adult is minor). In this case, because the adult height of the dentary is obviously greater than the subadult one, the calculated ratio is a minimum value.

In spite of its shortness related to the subadult age of the specimen, the dentary of *Allqokirus* is relatively stout when compared to that of *Pucadelphys* and *Andinodelphys*. We calculated the two ratios, depth of the dentary below m3/length of the dentary (as mentioned above) as follows: 1) with the actual subadult measured values and 2) with estimated adult length and actual subadult height. Ratio 1 is 4.97/30.70 = 0.162, and ratio 2 is 4.97/32.98 = 0.150 (Table 5). Therefore, the stoutness ratio of *Allqokirus* is bracketed between these values, but we favour a value closer to the higher one. This ratio in *Mayulestes* is slight lower: 6.40/41.96e = 0.152. In the case of *Mayulestes*, because the ramus mandibularis (vertical ramus) is missing on the only known specimen, the length of the dentary has been estimated on the basis of the position of the postglenoid process and articular condyle, when the lower tooth row of the dentary is in occlusion with the upper tooth row. The higher value of the ratio of *Allqokirus* is likely related to the anteroposterior shortness of its premaxillae (because of their downturned position), which determines the length of the dentary.

As indicated in Table 5, this ratio is smaller in *Pucadelphys*, and especially in *Andinodelphys* than in *Allqokirus*. It is also distinctly smaller in most Recent didelphids, but only slightly smaller in *Didelphis*, *Dasyurus,* and *Thylacinus*. In contrast, other sparassodonts have a stout dentary, with a Hm3/LD index either close to that of *Allqokirus* and *Mayulestes* (e.g. *Patene, Sipalocyon, Cladosictis*), or much higher (e.g. *Prothylacynus, Borhyaena, Arctodictis*). The ratio is also very large in other metatherians with obvious crushing feeding habits (e.g. *Didelphodon*, *Sarcophilus*).

TABLE 5. — Proportions of the dentary in pucadelphyids, sparassodonts, didelphids, stagodontids (measurements of *Didelphodon* have been taken from Fox & Naylor [1986: fig. 3]), and dasyuromorphians. Abbreviations: **Hm3**, labial height below m3 between trigonid and talonid; **LD**, length of dentary; **sv**, subadult value; **av**, adult value; **e**, estimated values.

| Taxon | Specimen no. | LD | Hm3 | Hm3/LD |
|---|---|---|---|---|
| *Allqokirus* | MHNC 8267 | 30.70 (sv) | 4.97 (sv) | 0.162 (1) |
| | MHNC 8267 | 32.98e (av) | 4.97 (sv) | 0.150 (2) |
| *Mayulestes* | MHNC 1249 | 41.96e | 6.40 | 0.152 |
| *Andinodelphys* | MHNC 8264 | 38.39 | 4.96 | 0.129 |
| | MHNC 8308 | 38.68 | 4.78 | 0.123 |
| | MHNC 8370 | 34.30 | 4.20 | 0.122 |
| *Pucadelphys* | MHNC 8382 | 26.33 | 3.61 | 0.137 |
| | MHNC 8266 | 25.90 | 3.49 | 0.134 |
| | MHNC 8351 | 25.74 | 3.55 | 0.137 |
| | MHNC 8378 | 22.50 | 2.99 | 0.132 |
| | MHNC 8380 | 21.68 | 2.89 | 0.133 |
| *Didelphis* | MNHN RH 120 | 84.02 | 11.71 | 0.139 |
| *Monodelphis* | MNHN 1967-330 | 28.76 | 3.41 | 0.118 |
| | MNHN 1995-3216 | 27.12 | 3.50 | 0.128 |
| *Marmosa* | MNHN RH 82 | 30.97 | 4.03 | 0.130 |
| *Metachirus* | MNHN RH 81 | 41.76 | 5.33 | 0.127 |
| | coll CM uncat. | 49.81 | 6.51 | 0.130 |
| *Thylamys* | MNHN 2000-658 | 21.41 | 2.58 | 0.120 |
| *Dasyurus* | MNHN A 2627 | 63.69 | 9.45 | 0.148 |
| *Thylacinus* | MNHN A 3298 | 165.10 | 23.01 | 0.139 |
| *Eodelphis* | AMNH 14169 | 63e | 9.2 | 0.146 |
| *Didelphodon* | TMP 84-64-1 | 71.12 | 12.05 | 0.168 |
| *Patene* | PLV 2618 | 56.6 | 8.56 | 0.151 |
| *Cladosictis* | YPM-PU 15170 (right) | 121.71 | 20.80 | 0.170 |
| | YPM-PU 15170 (left) | 119.01 | 18.44 | 0.154 |
| *Sipalocyon* | YPM-PU 15029 | 87.7 | 13.24 | 0.151 |
| *Lycopsis* | UCMP 38061 | 175e | 29.70 | 0.169 |
| *Prothylacynus* | YPM-PU 15700 | 159.10 | 32.00 | 0.201 |
| *Borhyaena* | YPM-PU 15120 | 178.70 | 36.80 | 0.205 |
| *Arctodictis* | MLP 85-VII-3-1 | 175.00 | 41.00 | 0.234 |

In the symphyseal region, the two dentaries of *Allqokirus* are unfused and, on the lingual side of the bone, there is an elongated ovale-shaped area (narrower anteriorly than posteriorly) for the attachment of the symphyseal ligament. The symphysis extends posteriorly as far as the posterior root of p2. Its ventral edge is strongly oblique, and its long axis forms an angle of *c.* 35° with the alveolar border of the molars. A similar angle is observed in *Mayulestes*, while in *Andinodelphys* and *Pucadelphys* this angle is much smaller and the anterior ventral border of the symphysis is strongly slanting. In other sparassodonts, the symphyseal angle is generally either close to the condition observed in *Allqokirus* (e.g. *Cladosictis, Sipalocyon, Lycopsis*) or much larger (*Prothylacynus, Borhyaena, Arctodictis*) (Table 6).

The dentary is formed by two main elements: the corpus mandibularis (horizontal ramus) and the ramus mandibularis (vertical ramus), (Fig. 28). The corpus of *Allqokirus* slightly increases in depth posteriorly and has a straight ventral margin below premolars and anterior molars, but the margin becomes distinctly convex ventrally below m3 and m4. On the lateral side of the dentary are two large mental foramina. The anterior one is below the anterior root of p2, and the posterior one is below the anterior root of m1. The condition of *Allqokirus* is similar to that of *Mayulestes.* Among other sparassodonts, the number and relative positions of the mental foramina varies among species, specimens, and sometimes between the right and left dentary of the same individual (Forasiepi *et al.* 2006)

In contrast, in *Pucadelphys* and *Andinodelphys* the anterior mental foramen is more anteriorly placed, below p1, a condition commonly encountered in Recent didelphids.

On the lower third of the lingual aspect of the corpus mandibularis is a wide and shallow groove, which extends from the anterior root of the angular process posteriorly to the level of the m1 anteriorly. This structure represents the internal groove of Simpson (1928), or mylohyoid groove. Its posterior end is at the ventromedial angle of the mandibular foramen, at the anterior root of the angular process. In this region, and below the m4, the groove is relatively deep, but it becomes shallower anteriorly and almost fades out below m1 posteriorly. The mylohyoid groove marks the course of a neurovascular bundle, which probably included the mylohyoid branch of the inferior alveolar artery and the mylohyoid nerve (Bensley 1902; Meng *et al.* 2003). In *Didelphis*, this groove also receives the mylohyoid muscle, in its posterior part below m3-4 and as far as the anterior root of the angular process, which is involved in mastication and acts as an elevator of the tongue (Hiiemae & Jenkins 1969: fig. 4). It is therefore likely that the posterior part of the mylohyoid groove of *Allqokirus* also received the insertion of the mylohyoid muscle. At the posterior end of the mylohyoid groove is a relatively small mandibular foramen. It is located at the level of the apex of the coronoid process and faces posteromedially. It is oval-shaped, with the main axis dorsomedially-ventrolaterally oriented. The mandibular foramen transmits the inferior alveolar nerve (a branch of the mandibular nerve – CN V3) and accompanying vessels (e.g. Evans & de Lahunta 2013).

The mandibular ramus is composed of three major processes, coronoid, condylar, and angular. The coronoid process is elevated and subvertical. It is almost twice as high as the greatest depth of the corpus mandibularis below the molars. Its anterior edge, the coronoid crest, is slightly convex anteriorly and forms an angle of approximately 90° with the alveolar border of the mandible. It extends anteroventrally on the lateral aspect of the corpus in a blunt and smooth ridge, which vanishes below the talonid of m3. More dorsally, the anterior edge of the coronoid crest is triangular in section and bears sharp medial and lateral crests, the medial crest being slightly anterior to the lateral one. This double crest structure extends as far as the apex of the process. In medial view, the coronoid process is wide, rounded at its apex, and slightly curved posteriorly. The base of the process is narrow anteroposteriorly, and it is approximately one and a half wider than the apex. The lateral surface of the coronoid process bears a shallow masseteric fossa, which is open anteroventrally because of the anterior extension of the anterior coronoid crest. Ventrally the mas-

TABLE 6. — Angle between the ventral edge of the mandibular symphysis and the anteroposterior axis of the tooth row. Abbreviation: **e**, estimated values.

| | | | | | | | | **Mean** |
|---|---|---|---|---|---|---|---|---|
| *Andinodelphys* | | | | | | | | |
| specimen | MHNC 8264 | MHNC 8308 | MHNC 8370 | – | – | – | – | – |
| angle | 21° | 20° | 22° | – | – | – | – | 21° |
| *Pucadelphys* | | | | | | | | |
| specimen | MHNC 8264 | MHNC 8266 | MHNC 8376 | MHNC 8378 | MHNC 8380 | MHNC 8381 | MHNC 8382 | – |
| angle | 27° | 23° | 26° | 25° | 24° | 27° | 22° | 24.8° |
| *Mayulestes* (MHNC 1249) | 33° | – | – | – | – | – | – | 33° |
| *Allqokirus* (MHNC 8267) | 30° | – | – | – | – | – | – | 35° |
| *Patene* (PLV 2618) | 36° | – | – | – | – | – | – | 36° |
| *Sipalocyon* | | | | | | | | |
| specimen | COL 4 | YPM-PU 15373 | – | – | – | – | – | – |
| angle | 39° | 33° | – | – | – | – | – | 35.5° |
| *Cladosictis* | | | | | | | | |
| specimen | SCZ 143 | YPM-PU 15170 | – | – | – | – | – | – |
| angle | 40° | 38° | – | – | – | – | – | 39° |
| *Lycopsis* | 33°e | – | – | – | – | – | – | 36° |
| *Prothylacynus* (YPM-PU 15700) | 46° | – | – | – | – | – | – | 48° |
| *Borhyaena* (YPM-PU 15120) | 51° | – | – | – | – | – | – | 51° |
| *Arctodictis* (MLP 85-VII-3-1) | 59° | – | – | – | – | – | – | 59° |

seteric fossa is limited by the masseteric crest, which expands laterally in its posterior region to form the posteroventral shelf of the masseteric fossa. This shelf is approximately one third the anteroposterior length of the masseteric fossa at its base. In *Didelphis*, the masseteric fossa receives the insertion of the muscle *temporalis pars superficialis* in its dorsal portion and that of the muscle *zygomaticomandibularis* in its ventral portion; the posteroventral shelf is the attachment area for the insertion of the muscle *masseter pars profunda* (Turnbull 1970). The medial aspect of the coronoid process is a flat area, where likely attached the insertion of the *muscle temporalis pars profunda*, as is observed in *Didelphis* (Turnbull 1970). The mandibular notch, which forms the posterior border of the coronoid process, is poorly excavated. Because of the subvertical orientation of the coronoid process, the mandibular notch faces posterodorsally, and its ventral region is located well-above the apices of the molar trigonids.

The subvertical coronoid process of *Allqokirus* markedly differs from those of *Andinodelphys* and *Pucadelphys*, which are strongly inclined posteriorly and with a much deeper masseteric fossa, and in which the posteroventral shelf (the floor of the masseteric fossa) is much wider and longer, extending for more than two thirds of the ventral length of the fossa. Such an upright coronoid process is also absent in Recent didelphids.

The condylar process bears a transversely elongated articular condyle. The condyle is distinctly dorsal to the apex of the trigonid of m2-3, which it overhangs for approximately half the height of their protoconids. It is cylindrical, as its anterior and posterior edges are roughly parallel and its lateral and medial extremities are rounded. In posterior view, the mandibular condyle is shifted laterally relatively to the posterior crest of the coronoid process. The medial extremity of the condyle is almost exactly posterior to the posterior coronoid crest: the part of the condyle medial to the coronoid process is less than 15% the total width of the condyle. Laterally, from the lateral extremity of the condyle, a thick subvertical ridge joins the posteroventral shelf. Anterior to this ridge is a deep fossa, which forms the posteroventral and deepest region of the masseteric fossa. The neck is a triangular area wider dorsally than ventrally, and is posteroventrally oriented. It differs from the condition of *Andinodelphys* and *Pucadelphys,* in which the posterior surface of the neck also faces medially. Furthermore, the condylar neck of *Allqokirus* is subvertical with a small ventral component, while in *Andinodelphys* and *Pucadelphys* the ventral component is significantly higher. Table 7 provides comparison of the angle formed by the posterior plane of the neck in lateral view, and the alveolar border of the lower cheek teeth in several sparassodonts, pucadelphyids, stagodontids, didelphids, and dasyuromorphians. The angle measured in *Allqokirus* is significantly higher than in *Pucadelphys*, *Andinodelphys*, Recent Didelphids, and dasyuromorphians. In contrast, most sparassodonts differ from other metatherians in having a relatively smaller angle, thus indicating that the posterior plane of the neck is less oblique than in other metatherians. However, *Callistoe* and *Thylacosmilus* have a distinctly more inclined posterior surface of the neck than in other sparassodonts. In the dorsomedial region of the neck is a conspicuous sub-triangular fossa that opens medially. Forasiepi (2009) interpreted this fossa in *Arctodictis* as a probable attachment area for the articular capsule, or for the ligament of the temporomandibular joint. However, because of the

TABLE 7. — Angle between the plane of the post-condylar surface and the alveolar border of the lower cheek teeth in several metatherians. Angle values for *Lycopsis, Arctodictis,* and *Callistoe* are approximate because they have been taken from publications (Marshall 1976b; Forasiepi 2009; Babot *et al.* 2002) and from photographs.

| | | | | | | | | | **Mean** |
|---|---|---|---|---|---|---|---|---|---|
| *Allqokirus* (MHNC 8267) | 97° | – | – | – | – | – | – | – | 97° |
| *Cladosictis* (YPM-PU 15170) | 103° | – | – | – | – | – | – | – | 103° |
| *Sipalocyon* | YPM- | YPM- | | | | | | | |
| specimens | PU15373 | PU15029 | – | – | – | – | – | – | – |
| angle | 104° | 104° | – | – | – | – | – | – | 104° |
| *Lycopsis* (UCMP 38061) | 105° | – | – | – | – | – | – | – | – |
| *Prothylacynus* (YPM-PU15700) | 100° | – | – | – | – | – | – | – | 100° |
| *Borhyaena* (YPM-PU15701) | 100° | – | – | – | – | – | – | – | 100° |
| *Arctodictis* (MLP 85-VII-3-1) | 110° | – | – | – | – | – | – | – | 110° |
| *Callistoe* (PLV 4187) | 123° | – | – | – | – | – | – | – | 123° |
| *Thylacosmilus* | 129° | – | – | – | – | – | – | – | 129° |
| *Eodelphis* (AMNH 14169) | 108° | – | – | – | – | – | – | – | 108° |
| *Andinodelphys* | MHNC | MHNC | | MHNC | | | | | |
| specimens | 8264 | 8308 | – | 8370 | – | – | – | – | – |
| angle | 117° | 115° | – | 123° | – | – | – | – | 118.3° |
| *Pucadelphys* | MHNC | MHNC | MHNC | MHNC | MHNC | MHNC | MHNC | MHNC | |
| specimens | 8351 | 8378 | 8376 | 8266 | 8379 | 8380 | 8377 | 8382 | – |
| angle | 110° | 110° | 110° | 112° | 112° | 112° | 118° | 120° | 113° |
| *Didelphis* (RH 120) | 116° | – | – | – | – | – | – | – | 116° |
| *Metachirus* | | Coll CM | | | | | | | |
| specimens | RH 81 | uncat | – | – | – | – | – | – | – |
| angle | 113° | 113° | – | – | – | – | – | – | 113° |
| *Monodelphis* (MNHN 1967-330) | 125° | – | – | – | – | – | – | – | 125° |
| *Thylacinus* (MNHN.ZM.AC. A3298) | 132° | – | – | – | – | – | – | – | 132° |
| *Dasyurus* (MNHN.ZM.AC. A2627) | 135° | – | – | – | – | – | – | – | 135° |

TABLE 8. — Measurements of the dentary of *Allqokirus australis* (MHNC 8267) in mm.

| **Length of the dentary** | **31.38** |
|---|---|
| Depth of dentary below p2 | 4.18 |
| Depth of dentary below m1 | 4.44 |
| Depth of dentary below m2 | 4.55 |
| Depth of dentary below m3 | 4.75 |
| Length of symphysis | 6.50 |
| Height of coronoid process from the alveolar border | 11.90 |
| Height of condyle above ventralmost edge of dentary | 10.51 |
| Transverse width of condyle | 4.75 |
| Anteroposterior length of condyle | 2.02 |
| Length of incisor row at alveolar border | 2.59 |

very large size of this structure in some sparassodonts (e.g. *Cladosictis, Sipalocyon, Prothylacynus*), it more likely represents some muscular attachment. The upper portion of the muscle *pterygoideus medialis*, or, alternatively, the *masseter superficialis*, was probably attached in this fossa, as described by Hiiemae & Jenkins (1969) in *Didelphis*. A similar fossa is present on the posterior edge of the right condyle of *Mayulestes* (unpublished fragment of the holotype). It is absent in *Pucadelphys*, and absent or poorly developed in *Andinodelphys*. It is generally absent in Recent didelphids but it may variably be present and well-developed, as in some specimens of *Didelphis*. It is absent in *Dasyurus* and *Thylacinus*.

In posterior view, the posterior surface of the condylar neck of *Allqokirus* joins the posteromedial angle of the angular process. The contact is angular and marked by a conspicuous transverse oblique ridge. This condition is also observed in *Pucadelphys*, but is poorly marked in *Andinodelphys*. In Recent didelphids and dasyurids, the transition between the posterior aspect of the neck and the angular process is smooth and forms a regularly convex surface. In contrast, in some other sparassodonts (e.g. *Cladosictis, Prothylacynus*) the transition is even more angular and the ridge is much stronger.

The angular process is a large triangular shelf facing mainly ventrally, but with a small lateral component. Its posterior edge is slightly concave posteriorly, and its posteromedial angle does not form a sharp posteriorly projecting spine as is observed in Recent didelphids, dasyurids and thylacinids. It resembles in this respect the condition observed in *Pucadelphys* and *Andinodelphys.* It also resembles the condition observed in *Cladosictis, Sipalocyon* and *Prothylacynus*. The morphology of the posterior region of the angular process of marsupials has been quantified by Sánchez-Villagra & Smith

(1997) in order to evaluate the relative length of the medial spine. With an ASL/AL ratio of 0.87, the angular process of *Allqokirus* is clearly shelf-like (ASL/AL > 0.81), as defined by Sánchez-Villagra & Smith (1997), which is consistent with the weak development of the posteromedial spine. *Pucadelphys, Andinodelphys, Sipalocyon,* and *Prothylacynus* also have a shelf-like angular process. The angular process is intermediate (0.72 < ASL/AL < 0.81) in *Arctodictis, Australohyaena*, and *Borhyaena* (Forasiepi 2009, Forasiepi *et al.* 2015). In contrast, all dasyuromorphians have a rod-like angular process, with an ASL/AL < 0.72.

The medial edge of the angular process of *Allqokirus* is a flat vertical narrow surface, where the muscle *pterygoideus medialis* attached, based on the observations of Hiiemae & Jenkins (1969) and Turnbull (1970) in *Didelphis*. The process narrows anteriorly and merges with the corpus mandibularis at a point located between the mandibular foramen and the anterior edge of the coronoid process.

## PHYLOGENETIC ANALYSIS

### Results

The analysis with PAUP* resulted in four shortest trees (L = 1304, CI = 0.354, RI = 0.677). The phylogenetic relationships within Metatheria (Fig. 29) are relatively well-resolved, with two well-defined sister clades: 1) a clade including the Marsupialia + closely related stem taxa; and 2) a clade including the four Tiupampa metatherians included in the analysis together with the post-Tiupampa sparassodonts. However, in the consensus tree obtained, the positions of Stagodontidae and Peradectidae relative to the more apical metatherians (i.e., which are closer to the crown clade than to any other metatherians) are unresolved. Furthermore, in the apical sparassodonts the positions of: 1) *Australohyaena*; 2) *Borhyaena+Arctodictis sinclairi*; and 3) the Proborhyaenidae + Thylacosmilidae clade are also unresolved.

One of the purposes of this analysis was to adress the question of the phylogenetic relationships of Tiupampa carnivorous metatherians (*Allqokirus* and *Mayulestes*) to other sparassodonts, within Marsupialiformes as defined by Vullo *et al.* (2009). The following description of the resulting consensus tree from the parsimony analysis will therefore only concern the clades that are relevant to this question. For each, we will present a list of unambiguous synapomorphies, which actually gather strictly unambiguous synapomorphies (= the minimal number of synapomorphies, as given in Fig. 29A) and certain ambiguous synapomorphies that are nonetheless optimized at this same exact node by both Acctran and Deltran optimizations.

In the consensus tree we obtained, the two metatherians from the Tiupampa fauna that exhibit carnivorous and predatory adaptations (*Mayulestes* and *Allqokirus*) are sister taxa and together form a clade with the early Eocene sparassodont *Patene* (*P. simpsoni* from Itaboraí, Brazil). *Patene* is the oldest kown post-Tiupampan sparassodont and is included here in the family Mayulestidae, together with *Allqokirus*, *contra* various authors who included the two taxa in the Hathliacynidae (Marshall 1981; Marshall & Muizon 1988; Muizon 1992). As previously argued by Muizon (1999), and contrary to recent studies of sparassodont phylogeny (e.g. Forasiepi 2009; Forasiepi *et al.* 2015; Engelman & Croft 2014; Goin *et al.* 2016), *Mayulestes* is a sparassodont, and, together with its sister taxon *Allqokirus* and *Patene*, is included in the early radiation of sparassodont marsupialiforms from Tiupampa, the Mayulestidae.

If we enforce the exclusion of *Mayulestes* from Sparassodonta, the resulting trees are only four steps longer than the shortest trees of the unconstrained analysis. Excluded from Sparassodonta, *Mayulestes* nonetheless remains sister taxon to other sparassodonts. We also constrained *Mayulestes* to form a clade with Pucadelphyidae, as recovered in previous phylogenies of sparassodonts (see references above). The resulting trees are, in this case, 28 steps longer and, particularly noteworthy, pucadelphyids are shifted into the clade Sparassodonta (pucadelphyids and *Mayulestes* are sister taxa to *Patene* and *Allqokirus*). These analyses therefore provide strong arguments in favour of the monophyly of *Mayulestes* and other sparassodonts.

The high level of homoplasy of dental characters in carnivorous therian mammals has been pointed out by Muizon & Lange-Badré (1997) and Solé & Ladevèze (2017). In order to test the influence of homoplastic characters on our results, we implemented an implied weighting analysis (with downweighted homoplastic characters), with several values of the Goloboff concavity constant k (from 1 to 30). The lower values of the constant have a stronger weighting against homoplastic characters than do higher values. In all the analyses, we obtained one most parsimonious tree (MPT). In the single tree obtained, for all values of k, Peradectidae was the sister-taxon of the Notometatheria, represented by the clade ((*Amphiperatherium-Peratherium*, *Herpetotherium*, Marsupialia), (Pucadelphyidae, Sparassodonta)); the Stagodontidae were sister group of the clade Peradectidae plus Notometatheria. Furthermore, for all values of k, *Australohyaena* was the sister group of the clade comprising *Callistoe*, *Paraborhyaena*, and *Thylacosmilus*. However, the relationships of these latter three taxa varied according to the different k values. With values of k from 1 to 5, *Callistoe* and *Paraborhyaena* are sister-taxa and both are sister-group of *Thylacosmilus*. With values of k from 6 to 30, *Paraborhyaena* and *Thylacosmilus* are sister taxa and form the sister group of *Callistoe*, a condition similar to that obtained in the unweighted consensus tree.

Therefore, under all values of k, Mayulestidae (*Mayulestes, Allqokirus*, and *Patene*) is monophyletic and forms the earliest diverging sparassodont clade.

Interestingly, Pucadelphyidae, a family represented in our sample by the genera *Pucadelphys* and *Andinodelphys*, turns out to be the sister group of the Sparassodonta (under all k values), forming a clade, which we formally designate here as the superorder Pucadelphyda n. superord.: the least inclusive clade containing *Pucadelphys* and *Borhyaena*. However, this result is not surprising given the close relationship between *Mayulestes* and Pucadelphyidae recovered in previous analyses

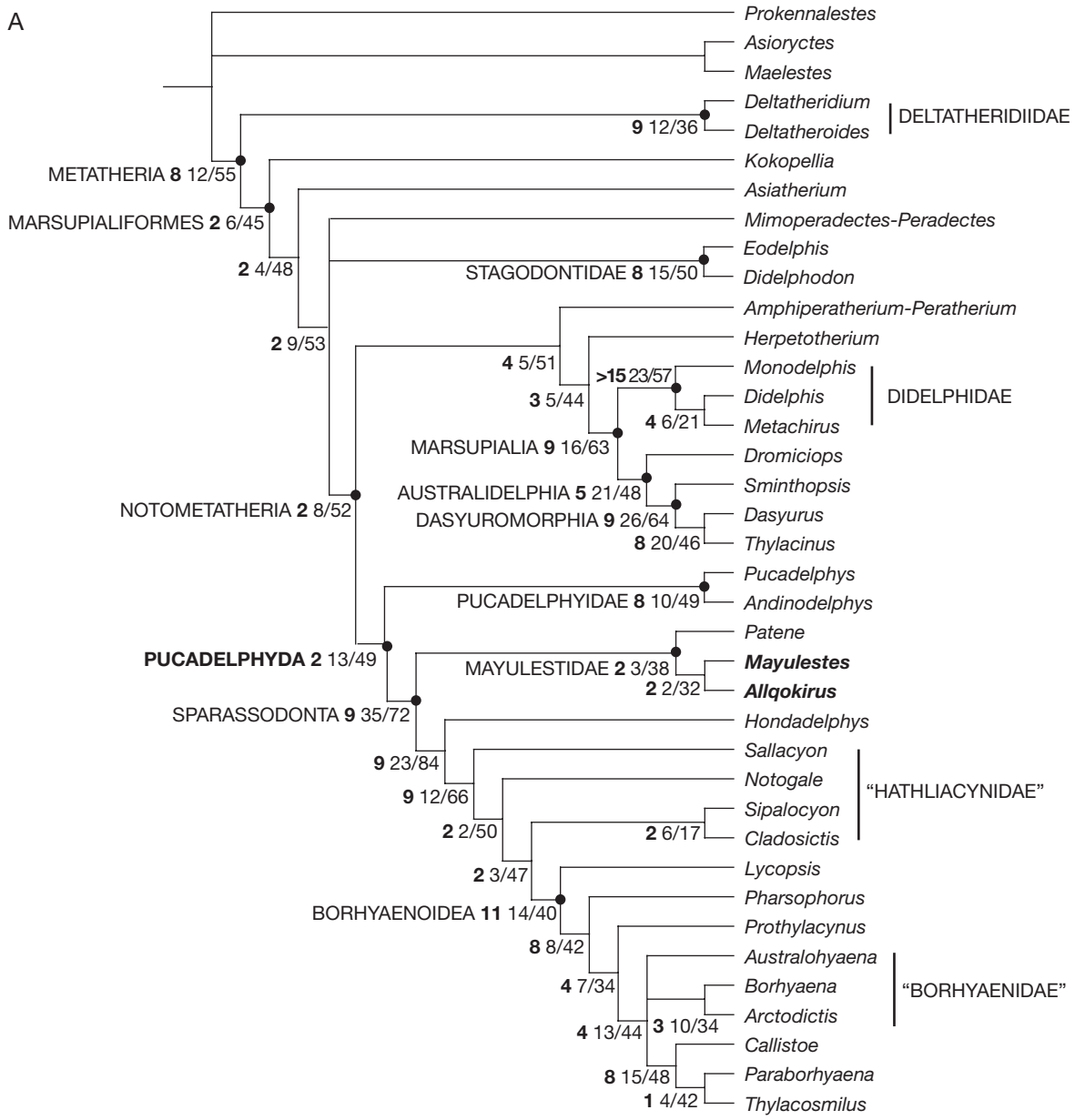


FIG. 29. — Phylogenetic relationships of *Allqokirus* and *Mayulestes*, among other metatherians: **A**, strict consensus tree of four equally parsimonious trees resulting from the analysis of the data matrix of 364 characters and 38 taxa with equally wheighted homoplastic characters (L=1304, CI=0.354, RI=0.677); the Bremer index is given at branches in bold followed by the minimum and maximum numbers of synapomorphies; **B**, single tree resulting from the analysis with down-wheighted homoplastic characters (k=3).

(e.g. Rougier *et al.* 1998; Horovitz & Sánchez-Villagra 2003; Forasiepi 2009; Engleman & Croft 2014; Forasiepi *et al.* 2015; Beck 2017; Wilson *et al.* 2016). The clade, which includes Pucadelphyidae and Sparassodonta, forms the sister-group of a clade (*Amphiperatherium-Peratherium*, *Herpetotherium*, Marsupialia) and the Stagodontidae is the sister group of the clade (Peradectidae (*Amphiperatherium-Peratherium*, *Herpetotherium*, Marsupialia) (Pucadelphyda)).

This topology departs from the results of Forasiepi (2009), in which Stagodontidae (sister-group of *Pediomys*) branches off between Peradectidae basally and a clade ((*Herpetotherium*, Marsupialia) Sparassodonta) apically. The early divergence of Stagodontidae obtained in our analysis is congruent with Forasiepi *et al.* (2015). In this latter work, however, Peradectidae is included in a clade with (*Andinodelphys* (*Pucadelphys*, *Mayulestes*)), which in turn is sister group of the Marsupialia. Our interpretation mainly departs from Forasiepi *et al.* (2015) in the position of these Tiupampa marsupialiforms: on the one hand, the Pucadelphyidae (*Pucadelphys* and *Andinodelphys*) are sister group of the Sparassodonta and, on the other hand, the Tiupampa Mayulestidae (*Mayulestes* and *Allqokirus*) are included in this order. The sister group relationship between Stagodontidae and Sparassodonta retrieved by Engelman & Croft (2014) is likely due to convergent adaptations to carnivory. As a matter of fact, some dental characters associated with a carnivorous diet (see Muizon & Lange-Badré 1997;

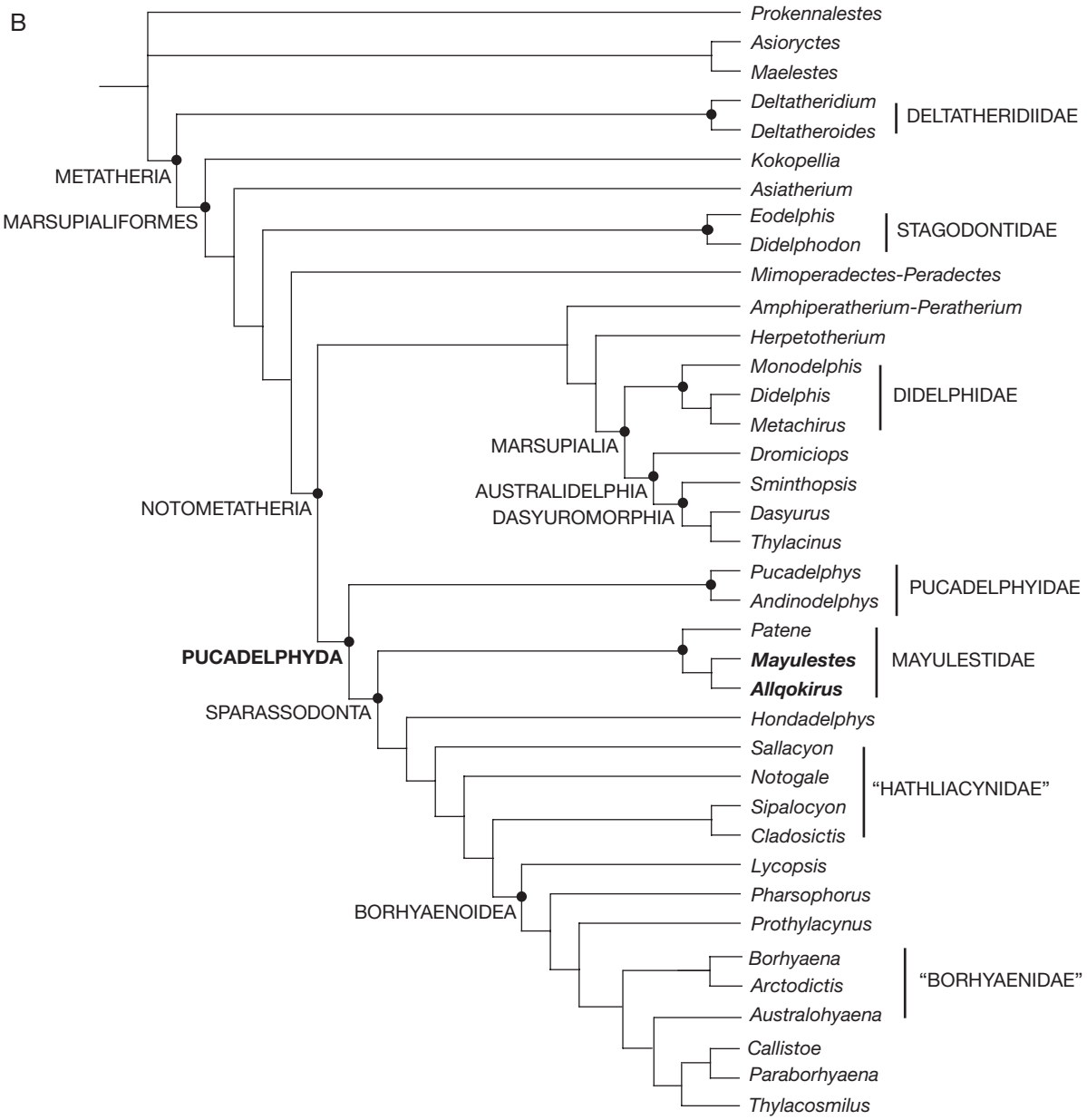


FIG. 29. — Continuation.

Solé & Ladevèze 2017) support this relationship. It is noteworthy that the inclusion of new codings of cranial characters of stagodontids permitted by the recent description of the skull of *Didelphodon* (Wilson *et al.* 2016), probably minimised the influence of dental characters in our analysis.

1) PUCADELPHYDA

The Pucadelphyda represent the Tiupampian radiation of carnivorous marsupialiaformes. This clade comprises the two extinct South American lineages Pucadelphyidae and Sparassodonta. Seventeen unambiguous synapomorphies and a Bremer index of 2 (relative to a mean of 5) support this clade. One out of the seventeen unambiguous synapomorphies is a dental character, eight are cranial characters (with five from the basicranial area), and eight are postcranial characters.

In our analysis, Pucadelphyda is defined by, among others, two unique synapomorphies among metatherians: the presence of a medial process of the squamosal (Char. 185), and a deep curved groove for the internal carotid artery at the apex of the promontorium (Char. 210). It is noteworthy that the latter character is not present in all the Tiupampa metatherians, since it is absent in an isolated metatherian petrosal, referable to a different taxon from the two pucadelphyids considered here.

Such a deep groove for the carotid on the promontorium is also present in some iolated petrosals from Itaboraí, this condition being especially conspicuous on the Type II petrosals as defined by Ladevèze (2004) and Ladevèze & Muizon (2010). As a matter of fact, the parsimony analysis of Ladevèze & Muizon (2010) concluded in a sister-group relationship between Type II petrosals and *Pucadelphys* +

TABLE 9. — Measurments (in mm) of upper and lower molar lengths in *Andinodelphys cochabambensis* and *Itaboraidelphys camposi*. Abbreviations: **LM**, length of upper molars series; **Lm**, length of lower molars series; **l**, left; **r**, right.

| Taxon | LM2-3l | LM2-3r | Lm1-4l | Lm1-4r |
|---|---|---|---|---|
| *Andinodelphys cochabambensis* | | | | |
| MHNC 8308 | 5.85 | 5.69 | 11.32 | 11.18 |
| MHNC 8264 | 5.84 | – | 11.38 | 11.21 |
| mean | 5.79 | | 11.27 | |
| *Itaboraidelphys camposi* | | | | |
| DGM 817-M | – | – | – | 14.88 |
| DGM 814-M | – | – | – | 14.04 |
| mean of DGM 814-M and 817-M | – | – | – | 14.46 |
| DGM 926-M | 7.93 | – | – | – |

*Andinodelphys*, therefore, implicitely including these petrosals within the Pucadelphyda as defined here. Recently, Beck (2017) referred the Type II petrosals of Itaboraí to *Epidolops ameghinoi*, a taxon represented by a partial skull in the Itaboraí fauna, on the basis of two lines of evidence: the skull length and the relative abundance of the taxa as compared to that of the isolated petrosals. This result would therefore include *E. ameghinoi* within the Pucadelphyda. We question this hypothesis and phylogenetic results (Beck 2017: fig 14b) for the following reasons. First, consideration of the skull length is a very poor critertion in the case of the Itaboraí fauna since, except *E. ameghinoi*, no metatherian taxon of this locality is known by complete enough cranial remains, allowing measurement of the cranial length. Therefore, the use of the skull length, alone, as a discriminant character, *de facto,* eliminates all the other metatherian taxa from the comparison, since their cranium is unknown. The fact that the expected value of the promontorium area obtained by Beck (2017: 391) for *E. ameghinoi* is "almost identical to that of the Type II petrosals" is certainly not an evidence that other taxa of Itaboraí could not fit the promontorium area of Type II petrosals as well. Besides the size (the sole morphological character used, but certainly not the most adequate to assign isolated petrosals to taxa known by other osteological and dental features), Beck (2017) also used the relative abundance to refer the Type II petrosals to *E. ameghinoi* because this species is by far the most abundant at Itaboraí. However, if Type II petrosals are actually referable to *E. ameghinoi*, the abundance of dental and cranial remains of this taxon should also be observed in the record of Type II petrosals, which is not the case as this type is relatively rare, being represented by two specimens only. Therefore, we consider that the two lines of evidence advocated by Beck (2017) do not firmly support referral of Type II petrosals to *E. ameghinoi*.

Ladevèze & Muizon (2010: fig. 5 and table 3) referred the Type II petrosals of Itaboraí to *Bobbschaefferia fluminensis* or *Procaroloameghinia pricei* on the basis of a comparison of the promontorium area to molars area (M2-3, m3-2). We agree that this referral is not supported either by the relative abundance of these taxa as compared to that of the petrosals in question. However, it is noteworthy that on table 3 of Ladevèze & Muizon (2010), two taxa, *Epidolops* and *Itaboraidelphys*, are immediately outside the confidence interval of the estimated molars areas expected for the promontorium area of Type II. *Epidolops* is just below the lower value and *Itaboraidelphys* is just above the higher value, and both taxa are clearly more abundant than *Bobbschaefferia* and *Procaroloameghinia*. Furthermore, on the basis of morphological characters other than size, Ladevèze (2007) and Ladevèze & Muizon (2010) performed a parsimony analysis including the isolated metatherian petrosals from Itaboraí, which resulted in a sister group relationship of Type II petrosals and pucadelphyids (*Pucadelphys*, *Andinodelphys*). The two major synapomorphies of this clade are the presence of a deep groove for the internal carotid artery on the ventral apex of the promontorium and the presence of a "tympanic sinus in the lateral trough of the petrosal" (sic). The latter structure is the prootic recess as formally designated above in *Allqokirus*. In other respects, Marshall & Muizon (1988: 35) and Muizon (1992), when describing *Andinodelphys*, noted strong dental similarities between this Tiupampan taxon and *Itaboraidelphys,* stating that "of known early Tertiary didelphids, *Andinodelphys* compares best with *Itaboraidelphys camposi* Marshall & Muizon 1984 from the middle Paleocene (Itaboraian) fauna at Itaboraí, Brazil" (sic). As mentioned by these authors *Andinodelphys* averages 25% smaller than *Itaboraidelphys*. Both taxa share large, elevated, and transversely compressed stylar cusps B and D, a much smaller, often twinned, stylar cusp C, very large posteriorly bulging metaconule, well-individualised (although approximated) entoconid and hypoconulid with diverging apices and which are separated by a deep valley, anteroposteriorly elongated and transversely compressed entoconid. These comparisons in mind, we have measured the labial length of M2-M3 (the best upper molar series available for *Itaboraidelphys*) and the length of m1-m4 (two specimens available for *Itaboraidelphys*) of *Andinodelphys* and have compared the values to the promontorium area of *Andinodelphys* in order to determine a correlative evaluation of the promontorium area of *Itaboraidelphys* to be compared with the actual value measured on the two specimens. In order to better include the two specimens of Type II petrosals (the apex of MNRJ 6729-V is slightly broken) we have slightly modified the measurements on the promontorium used by Ladevèze & Muizon (2010). Length is the distance between the anterolateral angle of the carotid sulcus and the posterior edge of the promontorium at the anteromedial angle of the stapedial fossa. Width is the distance between the posteromedial angle of the secondary facial foramen and the medial edge of the promontorium. These values are significantly smaller than those of Ladevèze (2007) and Ladevèze & Muizon (2010) (Tables 9 and 10).

Assuming that the promontorium area relative to the length of the molars was similar in *Andinodelphys* and *Itaboraidelphys*, we calculated an estimation of the promontorium dimensions in *Itaboraidelphys*, for which we have

TABLE 10. — Measurements (in mm for lengths, mm² for areas) of the promontorium in *Andinodelphys cochbambensis* and Type II petrosals of Itaboraí. Abbreviations: Lproml, length of left promontorium; Lpromr, length of right promontorium; Pr.ar/l, area of the left promontorium; Pr.ar/r, area of the right promontorium; Pr.ar X, mean area of the promontorium; $\overline{X}$, mean.

| Taxon | Lproml | Wproml | Pr.ar/l | Lpromr | Wpromr | Pr.ar/r | Pr.ar $\overline{X}$ |
|---|---|---|---|---|---|---|---|
| *Andinodelphys cochabambensis* | | | | | | | |
| MHNC 8308 | 3.93 | 2.34e | 9.20 | 4.02 | 2.47 | 9.93 | 9.56 |
| MHNC 8264 | 3.89 | 2.42 | 9.41 | 3.83 | 2.39 | 9.15 | 9.28 |
| mean of MHNC 8308 and 8264 | – | – | – | – | – | – | 9.42 |
| Type II petrosal | | | | | | | |
| MNRJ 6728-V | 3.77 | 2.95 | 11.1 | – | – | – | – |
| MNRJ 6729-V | – | – | – | 4.18 | 3.34 | 13.96 | – |
| mean of MNRJ 6728-V and 6729-V | – | – | – | – | – | – | 12.53 |

the molar measurements given in Table 9. Calculation of the promontorium area of *Itaboraidelphys* on the basis of the length of m1-m4 as compared to the mean of the two areas measured on *Andinodelphys* (MHNC 8308 and 8267) gives an expected value for the promontorium area of *Itaboraidelphys* of 12.1 mm². A similar calculation based on the length of M2-M3 gives an expected value for the promontorium area of *Itaboraidelphys* of 12.9 mm². These two calculated estimated values fall within the range measured on the two Type II petrosals (11.1 mm² – 13.96 mm²) and confirm a size congruence between Type II petrosals and dental remains of *Itaboraidelphys*. As expected, the mean promontorium area of *Andinodelphys* (9.42 mm²) is 24.8% smaller than the mean area of *Itaboraidelphys* (12.53 mm²) according to the size difference evaluated by Marshall & Muizon (1988) between the teeth of *Andinodelphys* and *Itaboraidelphys*, the former being approximately 25% smaller than the latter.

Furthermore, it is noteworthy that, although not as abundant as *Epidolops ameghinoi*, *Itaboraidelphys camposi* is clearly more abundant than *Bobbschaefferia fluminensis* and *Procaroloameghinia pricei* and, in this respect also, referral of Type II petrosals to *Itaboraidelphys* is plausible.

We therefore conclude that, on the basis of dental and petrosal morphological characters (other than size), size, and relative abundance, Type II petrosals of Itaboraí are more plausibly referred to *Itaboraidelphys* than to *Epidolops* and regard Beck's hypothesis as less supported than the one advocated here. On the basis of our hypothesis, we consider that the phylogenetic affinities of *Epidolops ameghinoi* are more satisfactorily represented in fig 14a of Beck (2017), in which the petrosal characters are unscored for *Epidolops*, than in fig 14b in which these characters are scored. Furthermore, fig. 14b's hypothesis (Beck 2017) is conflicting with the referral of polydolopimorphians to australidelphians supported by Goin *et al.* (2009), Sigé *et al.* (2009), and Goin *et al.* (2016), whereas fig. 14a does not. We, therefore, regard that close relationships of *Epidolops* with pucadelphydans are unlikely; in contrast, we favor a possible inclusion of *Itaboraidelphys* in this superorder, a hypothesis which will be discussed in a work in progress on the cranial anatomy of *Andinodelphys cochabambensis* by two of us (CM and SL).

*Unambiguous synapomorphies supporting the clade Pucadelphyda*

**93 (1).** Hypoconulid of ultimate molar taller than the other talonid cusps (= reversion from node Metatheria; absent in Borhyaenoidea; convergent with *Sminthopsis*, *Kokopellia*);

**104 (2).** Ventral margin of the dentary behind last molar continuous to condyle is angled (reversion at node Borhyaenoidea excluding *Lycospis*, then reacquisition in *Thylacosmilus*; convergent with *Didelphodon*, and Australidelphia);

**145 (0).** Flaring of maxillary cheek posterior to infraorbital foramen (= reversion from node [peradectids stagodontids Notometatheria]; reversion in *Lycopsis*, *Hondadelphys*);

**147 (2).** Fossa for the levator labii muscle in the anterior end of the jugal present mainly in the maxilla (equally developed in both maxilla and jugal in *Thylacosmilus*);

**183 (1).** Hypotympanic sinus formed by squamosal, alisphenoid, and petrosal (absent in *Pucadelphys*);

**185 (1).** Medial process of the squamosal extends into the middle ear and forms part of the roof of the hypotympanic sinus;

**210 (1).** Deep groove for the internal carotid artery excavated in medial side of the promontorium apex ventrally;

**213 (0).** Rostral tympanic process of the petrosal absent, or low ridge or small tubercle (= reversion from node Marsupialiformes);

**214 (1).** Tensor tympani fossa forms a distinct circular pit or elongated fossa (convergent with *Thylacinus*);

**260 (1).** Foramen on dorsal arch of last lumbar vertebrae present (convergent with Dasyuromorphia; absent in *Arctodictis*);

**262 (1).** Ventral median keel on anterior lumbar vertebrae (convergent with *Metachirus*, *Dromiciops*, *Thylacinus*; absent in *Prothylacinus*);

**272 (1).** Supraspinous fossa narrower than infraspinous fossa at the level of the neck (convergent with *Dromiciops*, reversion in *Sipalocyon* and Borhyaenidae + (*Callistoe* (*Paraboryhaena*, *Thylacosmilus*)));

**282 (1).** Extension of the deltoid crest reaches distal half of the humerus (convergent with Didelphidae);

**287 (1).** Lateral extension of capitulum straight with a flat shelf and/or a salient crest [convergent with (*Didelphis*, *Metachirus*), and *Thylacinus*];
**331 (1).** Dorso-distal tuber of the astragalar head present;
**353 (0).** Entocuneiform distal to navicular (convergent with Dasyuromorphia);
**360 (1).** Mt III thinner than Mt I (convergent with Dasyuromorphia).

*Fourteen ambiguous synapomorphies (Acctran, fast) may also support Pucadelphyda*
**20 (1).** Oblique first upper and lower premolars relative to tooth row (parallel to sub-parallel in Sparassodonta except Mayulestidae, and oblique again in Borhyaenoidea except *Lycopsis*, transverse in *Arctodictis* and *Paraborhyaena*) (= Deltran synapomorphy of Mayulestidae);
**21 (1).** First upper premolar strongly asymmetrical in lateral view (reversion in Sparassodonta except Mayulestidae; reacquired in (*Callistoe* (*Paraborhyaena*, *Thylacosmilus*) and peradectids);
**45 (0).** Stylar cusp E present and distinct [= reversion from node (peradectids, stagodontids, Notometatheria); reversion in Sparassodonta except Mayulestidae];
**70 (0).** Trigonid wider than talonid (on penultimate or antepenultimate molar) (= reversion from Marsupialiformes; subequal in width in *Pucadelphys*) (=Deltran synapomorphy of Sparassodonta);
**100 (0).** Deep hypoflexid (*c.* 40-50% of talonid width) (= reversion from node [peradectids, stagodontids, Notometatheria]; shallow or absent in Sparassodonta except Mayulestidae) (= Deltran synapomorphy of Mayulestidae);
**150 (0).** Palatal vacuities absent (= reversion from Marsupialiformes);
**156 (1).** Postpalatine torus foramen wide open groove (the section is approximately half a circle or less) (convergent with Dasyuromorphia, enclosed in palatine in *Andinodelphys*) (= Deltran synapomorphy of Sparassodonta);
**181 (0).** Absence of transverse canal (= reversion from Metatheria; present in *Andinodelphys* and node (*Notogale* ((*Sipalocyon*, *Cladosictis*) Borhyaenoidea)) but absent again in borhyaenoids+(*Callistoe* (*Paraborhyaena*, *Thylacosmilus*)) (= Deltran synapomorphy of Sparassodonta);
**182 (0).** Absence of tympanic process of the alisphenoid (= reversion from node Metatheria; present in Sparassodonta except Mayulestidae but absent again in Borhyaenoidea);
**283 (1).** Distal end of deltoid crest forming a distinct angle or process [convergent with (*Didelphis*, *Metachirus*), *Dromiciops*, *Dasyurus*; reversion in Sparassodonta except Mayulestidae, then distinct angle or process (1) again in Borhyaenoidea except *Lycospis*, then reversion again – merging with diaphysis in *Borhyaena* and *Callistoe*];
**303 (2).** Gluteous fossa larger than iliac fossa (convergent with *Metachirus* and Dasyuromorphia);
**315 (1).** Straight tibia [reversion in Mayulestidae and (*Paraborhyaena*, *Thylacosmilus*); convergent with *Thylacinus*];
**323 (0).** Astragalonavicular facet does not extend onto ventromedial side of head (reversion in Sparassodonta except Mayulestidae; but does not extend onto ventromedial side of head again (0) in *Paraborhyaena* and *Thylacosmilus*);
**354 (1).** Navicularmetatarsal facet parallel to the distal metatarsal facet of ectocuneiform [reversion in borhyaenids + (*Callistoe* (*Paraborhyaena*, *Thylacosmilus*); convergent with Dasyuromorphia].

*Nine ambiguous synapomorphies (Deltran, slow) may also support the Pucadelphyda*
**97 (1).** Entoconid (on antepenultimate or penultimate molar) located between posterior edge of trigonid and posterior margin of tooth (mid-way or in anterior half of the distance between the posterior base of trigonid and posterior margin of tooth) (convergent with peradectids, *Amphiperatherium*/*Peratherium*, reversion in *Hondadelphys*);
**198 (1).** Jugular foramen at least three times larger than fenestra cochleae (convergent with *Herpetotherium*, *Didelphis*, and Dasyuromorphia);
**223 (0).** Hiatus Fallopii on dorsal (cerebellar) face of petrosal (intermediate in *Salacyon*, ventral in (*Notogale* ((*Sipalocyon*, *Cladosictis*) Borhyaenoidea)), reversion to dorsal in (*Prothylacinus* (Borhyaenidae + (*Callistoe* (*Paraborhyaena*, *Thylacosmilus*)))); convergent with *Herpetotherium*);
**248 (1).** Dorsal third of the cranial facet of atlas much more concave than the ventral two thirds and strongly inflected medially (reversion in *Prothylacinus* and (*Borhyaena*, *Arctodictis*); convergent with didelphids and (*Dasyurus*, *Thylacinus*));
**257 (2).** C7 transverse foramen complete (convergent with *Thylacinus* and didelphids);
**326 (0).** No angle between lateral tibial and fibular facets of astragalus (convergent with *Herpetotherium* and *Dromiciops*);
**330 (1).** Malleolar shelf of the astragalus (convergent with *Eodelphis*);
**337 (0).** Peroneal process of calcaneus at the level of the edge of the cuboid facet (reversion in *Sipalocyon* and *Thylacosmilus*; convergent with *Herpetotherium*, *Dasyurus*, and *Sminthopsis*);
**340 (1).** Outline of sustentacular process of calcaneus rectangular (convergent with *Herpetotherium*).

2) Sparassodonta

The relatively high Bremer index of the node Sparassodonta (9, relative to a mean of 5) in the equally weighted analysis indicates a strong support of our analysis to the inclusion of *Mayulestes* and *Allqokirus* in the Sparassodonta. It also demonstrates that this characteristic lineage of South American

marsupialiforms had started to diversify as early as the basal Palaeocene.

In our analysis, Sparassodonta is supported by 35 unambiguous synapomorphies, twelve of which are dental characters, two are mandibular, thirteen are cranial, and eight are postcranial.

One out of the five synapomorphies of the clade Sparassodonta from the analysis of Forasiepi *et al.* (2015) is maintained here [i.e., characters 70(0) with a delayed optimization]. The four other synapomorphies from Forasiepi *et al.* (2015) are not present in basal sparassodonts (i.e., *Patene*, *Mayulestes*, *Allqokirus*), or even in every sparassodont [characters 31(1), 52(1), 79(1), and 118(0)].

*Unambiguous synapomorphies*

**12 (1).** Lower incisor not procumbent (convergent with *Dasyurus*+*Thylacinus*, and *Didelphodon*);

**38 (1).** Postmetacrista on antepenultimate or penultimate molar distinctly longer than preparacrista [convergent with stagodontids, didelphids, (*Dasyurus*, *Thylacinus*), *Amphiperatherium*/*Peratherium*, and *Deltatheridium*];

**46 (2).** Paracone distinctly smaller than metacone in volume and height (*c.* 30% smaller) on penultimate or antepenultimate molar (much smaller in Borhyaenoidea excluding *Lycospis*, absent or simple bulge in *Australohyaena* and *Thylacosmilus*; convergent with stagodontids, Marsupialia + *Herpetotherium*);

**48 (1).** Metacone and paracone adjoined at base (adjoined on most of their height in Borhyaenoidea excluding *Lycospis;* convergent with Deltatheridium and *Thylacinus*);

**64 (1).** Ultimate lower molar larger than penultimate molar (convergent with *Thylacinus* and stagodontids);

**66 (0).** Trigonid basin on penultimate molar (where known) wide open lingually: angle between protocristid (or postprotocristid when metaconid is lost) and paracristid more than 45° (convergent with *Thylacinus* and *Deltatheroides*);

**67 (1).** Trigonid basin floor sloping lingually;

**68 (2).** Trigonid longer than wide (convergent with *Thylacinus*);

**71 (0).** Strongly convex labial edge of the protoconid at mid-height, protruding labially and overhanging the base of the crown (apex and base of the trigonid are more lingual than the mid-height region of the cusp and the trigonid is therefore wider at mid-height than at its base) (convergent with Deltatheridiidae);

**80 (1).** Paraconid elongated with anterior projection of the paraconid keel mostly in the ventral half of the cusp (reversion in *Callistoe*, convergent with *Thylacinus*);

**84 (1).** Metaconid subequal in height to paraconid (on m3) (=reversion from Marsupialiformes without *Kokopellia*; lower in Sparassodonta excluding Mayulestidae);

**85 (2).** Metaconid smaller in volume than paraconid (on m3) [convergent with deltatheridiids, stagodontids, and (*Dasyurus*, *Thylacinus*)];

**103 (1).** Depth/length of the dentary below molars between 1,5 and 2 (intermediate) (elevated in Borhyaenoidea excluding *Lycopsis*, and then again intermediate in *Borhyaena* and *Thylacosmilus*; convergent with *Didelphodon*);

**106 (1).** Anteroventral edge of mandibular symphysis forming an angle > 25° (convergent with stagodontids, *Thylacinus*, and deltatheridiids);

**121 (1).** Expanded apex of the rostrum with concave tooth rows and lateral edges of the rostrum between canine and infraorbital foramen (convergent with *Thylacinus*);

**126 (1).** Paracanine fossa extended dorsally: higher dorsoventrally than (or as high as) long (anteroposteriorly) (convergent with *Sminthopsis* and stagodontids);

**127 (1).** Precanine notch present (reversal in *Sipalocyon*);

**133 (1).** Nasals do not overhang nasal aperture [reversal in (*Callistoe (Paraborhyaena, Thylacosmilus*)), convergent with Dasyuromorphia];

**134 (1).** Nasals lacking anterior parabolic protrusion, which overhangs nasal aperture [reversal in (*Callistoe (Paraborhyaena, Thylacosmilus*))];

**138 (1).** Orbital crests present (convergent with didelphids, *Dasyurus*, and *Thylacinus*);

**139 (0).** Naso-lacrimal contact present (reversal in *Thylacosmilus*, convergent with *Deltatheridium*);

**140 (0).** Facial process of the lacrimal large, triangular, and pointed anteriorly [reversal in (borhyaenids (*Callistoe (Paraborhyaena, Thylacosmilus*))) but 0 again in *Callistoe*; convergent with peradectids, *Herpetotherium*, *Thylacinus*];

**149 (2).** Two palatal pits between ultimate, penultimate and antepenultimate molars (independent of their size) [one in *Borhyaena*+*Arctodictis*; convergent with Deltatheridiidae and (*Dasyurus*, *Thylacinus*)];

**155 (2).** Foramen or groove in lateral edge of postpalatine torus present and large (approximately half the size of the minor palatine foramen or more) [reversion in Borhyaenidae+(*Callistoe* (*Paraborhyaena*, *Thylacosmilus*)), convergent with *Dasyurus*];

**159 (0).** Anteroposterior position of the sphenopalatine foramen relative to the molars above penultimate or antepenultimate molar [reversion in Borhyaenidae+(*Callistoe* (*Paraborhyaena*, *Thylacosmilus*)), convergent with *Monodelphis*, and (*Dasyurus*, *Thylacinus*)];

**170 (0).** Sagittal crest extending to frontals (convergent with stagodontids, *Didelphis*, *Dasyurus*+*Thylacinus*);

**177 (1).** Postglenoid foramen medial to postglenoid process [reversion in *Thylacosmilus*; convergent with (*Didelphis*, *Metachirus*) and *Thylacinus*];

**251 (1).** Posterior extension of the neural process of the axis distinctly longer than anterior extension (convergent with *Dasyurus*+*Thylacinus*);

**252 (1).** Ventral sagittal crest of axis distinctly concave because of the development of a robust ventral process posteriorly (convergent with *Dasyurus*);
**273 (1).** Scapular notch between 90 and 130° (convergent with *Metachirus* and Dasyuromorphia);
**301 (1).** Iliac neck short, less than 15% the total pelvis length;
**304 (1).** Epipubic bones absent (convergent with *Thylacinus*);
**306 (1).** No torsion between proximal and distal epiphyses of femur [reversion in *Lycopsis*, and (*Callistoe* (*Paraborhyaena*, *Thylacosmilus*)); convergent with didelphids];
**320 (0).** Anteroposterior length of the of the medial malleolus of the tibia at base subequal to the greatest anteroposterior length of the distal epiphysis (as seen in distal view) (convergent with *Sminthopsis*);
**329 (1).** Astragalar neck narrower or as wide as head.

Many of the unambiguous synapomorphies from the molar morphology are likely linked to a carnivorous diet For example: the elongated postmetacrista (38[1]) (convergent with stagodontids, didelphids, *Dasyurus*, *Thylacinus*, *Amphiperatherium*/*Peratherium*, and *Deltatheridium*); the reduction of the paracone relative to the metacone (46[2]) (convergent with stagodontids, Marsupialia + *Herpetotherium*); the fusion of the metacone and paracone at their base (48[1]) (convergent with *Thylacinus*); the large ultimate lower molar (64[1]) (convergent with *Thylacinus* and stagodontids), the elongation of the trigonid (68[2]) (convergent with *Thylacinus*). Finally, the enlargement of the paraconid with anterior projection of the paraconid keel (80[1]) (reversion in *Callistoe*, convergent with *Thylacinus*) was previously regarded as a sparassodont synapomorphy by Marshall *et al.* (1990) as "paraconid elongated".

Two cranial unambigous synapomorphies may also be correlated with carnivory because they indicate powerful and extensisve temporalis muscle: the presence of orbital crests [138(1) convergent with didelphids, *Dasyurus*, and *Thylacinus*]; and the sagittal crest extending to frontals (170[0]) (convergent with stagodontids, *Didelphis*, *Dasyurus*, and *Thylacinus*). Concerning the postcranial features of Sparassodonta, many are convergent with other carnivorous marsupialiforms, for example: posterior extension of the neural process of the axis distinctly longer than anterior extension (251[1]) (convergent with *Dasyurus*+*Thylacinus*); ventral sagittal crest of axis distinctly concave because of the development of a robust ventral process posteriorly (252[1]) (convergent with *Dasyurus*); scapular notch between 90 and 130° (273[1]) (convergent with *Metachirus* and Dasyuromorphia); epipubic bones absent (304[1]) (convergent with *Thylacinus*); anteroposterior length of the medial malleolus of the tibia at base subequal to the greatest anteroposterior length of the distal epiphysis (as seen in distal view) (320[0]) (convergent with *Sminthopsis*). The fist two character states are clearly related to carnivory and indicate a strong neck musculature related to prey capture (Muizon 1998; Argot 2004a)

*Ambiguous synapomorphies (Acctran, fast) of the Sparassodonta*

**24 (0).** Diastema posterior to first lower premolar absent (= reversion from Notometatheria; reversion in node (*Sallacyon*, *Notogale* ((*Sipalocyon*, *Cladosictis*) Borhyaenoidea)) then absent again in (*Pharsophorus*, *Prothylacynus* (borhyaenoids, (*Callistoe* (*Paraborhyaena*, *Thylacosmilus*))))) (= Deltran synapomorphy of Mayulestidae);
**43 (0).** Stylar cusp C absent or tiny (= reversion from Notometatheria; convergent with Australidelphia);
**44 (2).** Stylar cusp D absent (reversion in *Mayulestes*+*Allqokirus*; convergent with *Dromiciops*);
**47 (0).** Paracone and metacone conical (= reversion from Notometatheria; convergent with *Thylacinus*);
**49 (1).** Metacone extremely reduced on last molar [reversion in *Hondadelphys*, absent in clade (*Notogale* (*Sipalocyon*, *Cladosictis*) (Borhyaenoidea)), convergent with Marsupialia] (=Deltran synapomorphy of Mayulestidae);
**50 (0).** Straight centrocrista (= reversion from Notometatheria; convergent with *Dromiciops* and *Thylacinus*);
**54 (0).** Conules with wing-like cristae present (= reversion from Notometatheria; convergent with *Dasyurus* and *Thylacinus*);
**57 (1).** Protocone (on penultimate or antepenultimate molar) small and anteroposteriorly narrow (= reversion from Marsupialiformes; reversion in *Hondadelphys*, absent or very small in Borhyaenoidea except *Lycopsis*; convergent with *Thylacinus*);
**72 (1).** Trigonid (on penultimate or antepenultimate molar) longer than talonid (convergent with *Thylacinus* and *Dasyurus*);
**82 (1).** Protoconid height/length of ultimate or penultimate lower molar (Hp/Lm) > 0.9 (reversion in *Hondadelphys*; convergent with *Dasyurus*) (Deltran synapomorphy of Mayulestidae);
**95 (1).** Entoconid transversely compressed (= reversion from Notometatheria; vestigial or absent in Borhyaenoidea except *Lycopsis*; convergent with didelphids);
**124 (1).** Palate and basicranium at the same level [reversal in (*Callistoe* (*Paraborhyaena*, *Thylacosmilus*)); convergent with Dasyuromorphia];
**141 (0).** Lacrimal tubercle present (= reversion from Marsupialiformes; reversion in *Allqokirus*; convergent with *Herpetotherium*);
**160 (1).** Pterygoids well-developed and expanded on medial side but no midline contact (reversion in *Mayulestes* and *Arctodictis*; convergent with *Dromiciops* and *Thylacinus*);
**228 (1).** Large tuberculum tympani (reversion in *Mayulestes*, convergent with Marsupialia+*Herpetotherium*);
**256 (1).** C6 spinous process laminar (convergent with (*Didelphis*, *Metachirus*) and (*Dasyurus*, *Thylacinus*));
**258 (2).** First thoracic vertebra with a tall spinous process (relative to other vertebrae) is T3 (convergent with *Sminthopsis*);

**274 (1).** Clavicle absent;
**293 (0).** Articular facet for the humerus on the radius anteroposteriorly compressed (= reversion from node [peradectids, stagodontids, Notometatheria], convergent with *Sminthopsis*);
**310 (1).** Ossified patella present (convergent with *Amphiperatherium*/*Peratherium* (SL and CS personal observation);
**327 (1).** Medial extent of sustentacular facet of astragalus reaches the medial edge of the neck (reversion in Borhyaenoidea, and 1 again in *Callistoe*);
**334 (1).** Longest dimension of ectal facet of calcaneus: anteroposterior (transverse in Sparassodonta except Mayulestidae).

*Ambiguous synapomorphies (Deltran, slow) of the Sparassodonta*
**70 (0).** Trigonid wider than talonid (on penultimate or antepenultimate molar) (= reversion from Marsupialiformes, convergent with *Andinodelphys*) (= Acctran synapomorphy of Pucadelphyda);
**89 (1).** Paracristid longer than protocristid (convergent with clade Marsupialia + Herpetotheriidae, and deltatheridiids);
**102 (1).** Postcingulid absent on last molar (reversion in *Australohyaena*; convergent with clade Marsupialia + Herpetotheriidae and clade Deltatheridiidae);
**156 (1).** Postpalatine torus foramen forms a wide-open groove (the section is approximately half a circle or less) (convergent with *Pucadelphys* and Dasyuromorphia) (= Acctran synapomorphy of Pucadelphyda);
**181 (0).** Transverse canal absent [= reversion from node Marsupialiformes without *Kokopellia*; convergent with *Pucadelphys*; reversion in clade (*Notogale* (*Sipalocyon*, *Cladosictis*) (Borhyaenoidea)), then absent again in borhyaenids+*Callistoe* (*Paraborhyaena*, *Thylacosmilus*))] (= Acctran synapomorphy of Pucadelphyda);
**221 (1).** Stapedius fossa diameter distinctly less than twice the size of that of the fenestra vestibuli (=small and shallow) (convergent with *Didelphodon* and *Herpetotherium* + Marsupialia).

*Clade Mayulestidae (*Patene *(*Mayulestes*,* Allqokirus*))*
The parsimony analysis places *Mayulestes* and its sister taxon *Allqokirus* in a clade of early diverging sparassodonts that also includes *Patene*. This clade is here recognized as the family Mayulestidae and is supported by three unambiguous synapomorphies from the dental and mandibular morphology, and a Bremer index of 2 (relative to a mean of 5).

Because *Patene* is known by teeth, maxillaries and dentaries only, the synapomorphies of the Mayulestidae (see below among unambiguous and delayed transformations) are essentially dental.

*Unambiguous synapomorphies*
**74 (0).** Proportions of talonid basin: longer than wide (= reversion from node Marsupialiformes except *Kokopellia*);
**112 (0).** Angle between coronoid process and tooth row subvertical (between 95° and 105°) [= reversion from Notometatheria; convergent with didelphids and (*Paraborhyaena*, *Thylacosmilus*)];
**116 (0).** Anteroposterior position of mandibular foramen-posterior to mid-point of coronoid process [convergent with didelphids, and *Sipalocyon*).

*Ambiguous synapomorphies (Acctran, fast)*
Most of the ambiguous synapomorphies that are optimized as accelerated transformations (Acctran, fast) are strongly homoplastic (CI ≤ 0.250). Two of these are alternatively optimised as synapomorphies of the clade (*Mayulestes*, *Allqokirus*) (Deltran, slow) (i.e., 23[0, 154(0)]).

**4 (1).** First upper incisors well separated from I2 and protruding anteriorly (convergent with didelphids, *Sminthopsis*, and *Andinodelphys*);
**23 (0).** No diastema posterior to first upper premolar (= reversion from Notometatheria; convergent with Borhyaenoidea without *Lycopsis*);
**137 (1).** Postorbital process is a weak tuberosity (= reversion from node (stagodontids, peradectids, Notometatheria); absent in *Allqokirus*; convergent with node (*Prothylacinus* (borhyaenids, (*Callistoe* (*Paraborhyaena*, *Thylacosmilus*)))) and node Marsupialia + herpetotheriids);
**154 (0).** Posterior palatine spine weak or absent and posterior edge of the palate concave posteriorly (= reversion from Notometatheria);
**266 (1).** Angle between scapular spine and dorsal border of infraspinatus fossa: obtuse;
**269 (1).** Anterior extension of the acromion process: anterior or just lateral to anterior edge of glenoid fossa (convergent with Australidelphia);
**290 (1).** Medial development of ulnar coronoid process: medially protruding (convergent with *Herpetotherium*, *Metachirus*, (*Dasyurus*, *Thylacinus*), *Prothylacinus*, *Arctodictis*);
**299 (0).** Ilium deflected dorsally relative to ischium in lateral view (convergent with *Pucadelphys*, (*Didelphis*, *Metachirus*), (*Dasyurus*, *Thylacinus*));
**307 (1).** Greater trochanter, higher than femoral head (convergent with didelphids, *Sminthopsis*, Borhyaenoidea without *Lycopsis*);
**315 (0).** Sigmoid shaped tibia (= reversion from node Pucadelphyda; convergent with (*Paraborhyaena*, *Thylacosmilus*));
**316 (0).** Torsion between proximal and distal epiphyses of tibia (convergent with didelphids, *Sminthopsis*, *Lycopsis,* (*Borhyaena, Arctodictis*));
**318 (0).** Posterior shelf of the tibia does not extend posteriorly beyond the medial astragalotibial articulation;
**335 (0).** Mostly medial orientation of the calcaneoastragalar (ectal) facet of calcaneus (convergent with *Sminthopsis* and *Lycopsis*, (*Borhyaena, Arctodictis*));

**347 (1).** Lateral orientation of the calcaneal facet for the fibula (convergent with *Dasyurus*, *Andinodelphys*, and (*Callistoe* (*Paraborhyaena*, *Thylacosmilus*)));
**348 (0).** Tuber calcis of the calcaneus longer than the body (= reversion from Notometatheria; convergent with (*Dasyurus*, *Thylacinus*), *Cladosictis*, and *(Borhyaena, Arctodictis*));
**349 (1).** No medial curvature of the tuber calci (convergent with Marsupialia and Borhyaenoidea without *Lycopsis*) (convergent with Marsupialia and (*Callistoe* (*Paraborhyaena*, *Thylacosmilus*)));
**361 (0).** Sharp median keel on palmar/plantar surface of metapodials (convergent with Dasyuromorphia, (borhyaenids (*Callistoe* (*Paraborhyaena*, *Thylacosmilus*)))].

*Ambiguous synapomorphies (Deltran, slow)*
All the ambiguous synapomorphies optimized as delayed transformations are strongly homoplastic, none of which displaying a CI > 0.5.

It is noteworthy that each of these ambiguous synapomorphies may alternatively be optimized at the Pucadelphyda node or at the Sparassodonta node.

**20 (1).** Oblique first upper and lower premolars relative to tooth row (convergent with *Andinodelphys* and Borhyaenoidea without *Lycopsis*) (=Acctran synapomorphy of Pucadelphyda);
**24 (0).** Diastema posterior to first lower premolar absent (convergent with stagodontids, peradectids, *Hondadelphys*, and Borhyaenoidea without *Lycopsis*) (=Acctran synapomorphy of Sparassodonta);
**49 (1).** Metacone extremely reduced on last molar [convergent with Marsupialia, and (*Sallacyon* (*Notogale* ((*Sipalocyon*, *Cladosictis*) Borhyaenoidea)))] (=Acctran synapomorphy of Sparassodonta);
**57 (1).** Protocone small and anteroposteriorly narrow (on penultimate or antepenultimate molar) [convergent with *Thylacinus* and (*Sallacyon* (*Notogale* ((*Sipalocyon*, *Cladosictis*) Borhyaenoidea)))] (=Acctran synapomorphy of Sparassodonta);
**82 (1).** Height of protoconid / length of ultimate or penultimate lower molar (Hp/Lm) > 0.9 [= reversion from node Marsupialiformes without *Kokopellia*; convergent with *Dasyurus*, and (*Notogale* ((*Sipalocyon*, *Cladosictis*) Borhyaenoidea))] (=Acctran synapomorphy of Sparassodonta);
**100 (0).** Deep hypoflexid (*c.* 40-50% of talonid width) [= reversion from node (peradectids, stagodontids, Notometatheria); convergent with Pucadelphyidae] (=Acctran synapomorphy of Pucadelphyda).

**Clade (*Mayulestes*, *Allqokirus*)**
The sister taxon relationship of *Mayulestes* and *Allqokirus* is supported by two unambiguous synapomorphy and a Bremer index of 2.

*Unambiguous synapomorphies*
**91 (1).** Carnassial notch in cristid obliqua present (convergent with *Andinodelphys* and (*Dasyurus*, *Thylacinus*));
**96 (0).** Entoconid lower than hypoconid (= reversion from node Marsupialiformes; convergent with *Herpetotherium*, *Thylacinus*, and (*Sallacyon* (*Notogale* ((*Sipalocyon*, *Cladosictis*) Borhyaenoidea)))).

*Ambiguous synapomorphies (Acctran, fast)*
**44 (1).** Stylar cusp B larger than D (= reversion from Sparassodonta).

*Ambiguous synapomorphies (Deltran, slow):*
**21 (1).** First upper premolar strongly asymmetrical in lateral view (convergent with pucadelphyids, *Callistoe*, and peradectids) (= Acctran synapomorphy of Pucadelphyda);
**23 (0).** No diastema posterior to first upper premolar [= reversion from Notometatheria; convergent with *Pharsophorus* and (borhyaenids (*Callistoe* (*Paraborhyaena*, *Thylacosmilus*)))] (=Acctran synapomorphy of Mayulestidae);
**45 (0).** Stylar cusp E present and distinct [= reversion from (peradectids, stagodontids, Notometatheria; convergent with Pucadelphyidae] (= Acctran synapomorphy of Pucadelphyda);
**154 (0).** Posterior palatine spine weak or absent and posterior edge of the palate concave posteriorly (= reversion from Notometatheria) (= Acctran synapomorphy of Mayulestidae);
**182 (0).** Tympanic process of the alisphenoid absent (= reversion from Marsupialiformes without *Kokopellia*; convergent with Pucadelphyidae, and Borhyaenoidea) (= Acctran synapomorphy of Pucadelphyda).

## DISCUSSION

It is commonly accepted that marsupialiforms from South America had their origin in a Holarctic stock most probably derived from North America as early as the Late Cretaceous (e.g. Luo *et al.* 2003; Horovitz *et al.* 2009; Ladevèze & Muizon 2010; Forasiepi *et al.* 2015). Previous recent analyses (e.g. Forasiepi 2009; Forasiepi *et al.* 2015) suggest several dispersal events favouring an independent origin of a Tiupampan clade (*Mayulestes*, *Pucadelphys*, *Andinodelphys*) and a group formed by the common ancestor of marsupials, sparassodonts and all its descendants. The strict consensus obtained by Forasiepi (2009: fig. 2) requires at least four events: 1) the clade (*Mayulestes*, (*Pucadelphys*, *Andinodelphys*)); 2) Peradectidae; 3) Marsupialia; and 4) Sparassodonta. The result of Forasiepi *et al.* (2015: fig. 7B) is more parsimonious and only requires two dispersal events to South America: 1) a clade formed by the Peradectidae [(present at Tiupampa (Muizon 1992)], the Tiupampan taxa *Mayulestes-Andinodelphys-Pucadelphys*, and the Marsupialia; and 2) Sparassodonta. This scenario therefore advocates for separate episodes of vicariance (or migration)

for the three Tiupampa taxa (*Mayulestes-Andinodelphys and Pucadelphys*) and the sparassodonts, since the former are part of the sister clade of the Marsupialia. The present analysis also suggests several dispersal events (three): 1) Peradectidae; 2) Marsupialia; 3) Pucadelphyda. The major difference with the previous hypotheses is the fact that the four Tiupampan taxa (*Pucadelphys, Andinodelphys, Mayulestes,* and *Andinodelphys*) are part of the same event with the other sparassodontans, since they are included in the same pucadelphydan clade.

The fact that "herpetotheriids" are unknown, so far, in South America, suggests that it is a Marsupialia ancestor that migrated to South America and gave rise, on this sub-continent, to the radiation, which persists today. Similarly, because, so far, no pucadelphydan is known in North America (*contra* Carneiro 2018), the radiation of this clade may have taken place exclusively in South America. In contrast, if herpetotheriids are convincingly demonstrated to have been present in the early Cenozoic of South America, then, according to our results, only one single dispersal event may have been necessary to give rise to the radiation including the clade Peradectidae + Notometatheria (Fig. 29B). However, this scenario would imply a northward migration of "herpetotheriids", probably during the Maastrichtian or Palaeocene. This migration could have taken place earlier in the Late Cretaceous if the Campanian taxon *Ectocentrocristus* is actually a herpetotheriid as advocated by Williamson *et al.* (2014: fig. 6), a result, however, not accepted by Carneiro (2018: fig. 4) and questioned by Goin *et al.* (2016: 215). Such a scenario would also imply a northward migration of peradectids, which would have been part of this southern radiation.

However, it is noteworthy that the three parsimony analyses mentioned above (Forasiepi 2009; Forasiepi *et al.* 2015; this paper) do not include polydolpimorphian; the latter are present at Tiupampa and, in fact, represent the earliest known mammals in the Cenozoic of South America (Goin *et al.* 2006). Moreover, several other South American taxa known almost exclusively by dental remains (e.g. paucituberculates, carolomaeghiniids protodidelphids, jaskhadelphids) have not been included either in these analyses. Consequently, the palebiogeographic history the South American metatherians may be more complex than the few dispersal events suggested by the phylogenetic results of the analyses mentioned above and which mainly focus on sparassodonts affinities. Current metatherian phylogenies including numerous fossil taxa are greatly unstable because they are mostly based on dental characters, which are well known to be highly homoplastic. Much more stable phylogenetic results, also based on more complete cranial material (other than dental), are necessary to approach a better understanding of metatherian phylogeny and, therefore, of their dispersal and radiation respectively to and in South America.

Be that as it may, the result of this analysis, which retrieved a clade including the Marsupialia (+ stem-Marsupialia, i.e., "herpetotheriids") and the Pucadelphyda (= Pucadelphyidae + Sparassodonta), suggests the occurrence of, at least, two main metatherian radiations in South America: one extant lineage (the common ancestor of marsupials, "herpetotheriids" and all its descendants) and one extinct carnivorous lineage. The latter is here described as a new superorder, Pucadelphyda, because it is consistent, both phylogenetically (two unique synapomorphies among metatherians) and biogeographically (all the taxa are South American, *contra* Carneiro 2018). Its systematic delimitation follows the node-based definition from the Phylocode: the clade originating with the most recent common ancestor of *Borhyaena* and *Pucadelphys* or the least inclusive clade containing *Borhyaena* and *Pucadelphys.*

The ages of origin and diversification of Sparassodonta have been a matter of discussion, because they depend on the specific phylogenetic hypothesis being assumed. Most recent analyses place this clade either as part of stem Metatheria (Notometatheria being paraphyletic; e.g. Ladevèze & Muizon 2007), or as a sister-group to a mixed clade comprising Marsupialia, herpetotheriids, peradectids, and pucadelphyids (e.g. Forasiepi *et al.* 2015). Moreover, the question whether or not include *Mayulestes*, a crucial taxon for time-calibrating phylogenies, within Sparassodonta has been a subject of debate. Most recent phylogenies advocate a close relationship of *Mayulestes* and pucadelphyids (e.g. Forasiepi 2009; Engelman & Croft 2014; Forasiepi *et al.* 2015; Suarez *et al.* 2015), the former being excluded from sparassodont. These phylogenies, are based on the same data matrix [Forasiepi (2009), which is based on indirect codings of the Tiupampan taxa] adapted to the new specimens described and consequently obtained almost identical results. Moreover, and contrary to what stated Goin *et al.* (2016), the analysis of Ladevèze & Muizon (2007) does not show any close relationships of *Mayulestes* with pucadelphyids, but instead a close relationship of *Mayulestes* with borhyaenoids (only represented by *Notogale* and *Sallacyon*) as a clade or a paraphyletic association. Furthermore, Goin *et al.* (2016) overstated that, in the analyses of Horovitz & Sánchez-Villagra (2003) and Horovitz *et al.* (2009), *Mayulestes* has been related to pucadelphyids (rather than to sparassodonts), whereas these analyses did not include any other sparassodonts.

Furhtermore, Goin (2003), on the basis of dental characters, regarded *Mayulestes* as closely related to Peradectidae, possibly representing a carnivorous specialisation of the family. However, we find that *Mayulestes* differs from peradectids in numerous dental characters:

1) *Mayulestes*: paracone and protocone are joined at base on more than half of their height (*contra* Goin 2003); peradectids: they are widely separated;

2) *Mayulestes*: paracone is distinctly smaller than metacone; peradectids: they are subequal;

3) *Mayulestes*: protocone of M2-4 anteroposteriorly compressed and wider than long; peradectids: protocone as long as wide;

4) *Mayulestes*: metacrista (on M3) distinctly enlarged (*contra* Goin 2003) and, at least, twice as long as paracrista; peradectids: metacrista subequal to paracrista or slightly longer only;

5) *Mayulestes*: protoconid widened labially at mid-height with markedly convex labial edge; peradectids: labial edge of protoconid not salient labially but oblique and roughly straight from apex to base;

6) *Mayulestes*: metaconid of m1 lingual to protoconid; peradectids: metaconid distinctly posterolingual to protoconid;

7) *Mayulestes*: posterior aspect of metaconid on m3-4 in lingual view, subvertical; peradectids: sloping;

8) *Mayulestes*: metaconid subequal in height to paraconid and smaller in volume (*contra* Goin 2003); peradectids: metaconid always higher and more voluminous than paraconid, even on m4;

9) *Mayulestes*: entoconid on m1-3, reduced and distinctly smaller than hypoconulid; peradectids: entoconid not reduced and generally subequal to hypoconulid;

10) *Mayulestes*: paraconid anteroposteriorly enlarged, strongly convex mesially and distinctly longer than metaconid in lingual view; peradectids: paraconid more or less as long as metaconid or shorter.

Consequently, we consider that the peradectid affinities of *Mayulestes* suggested by Goin (2003) are not supported by the dental anatomy, and regard them as unlikely.

Interestingly, the recent analysis of Wilson *et al.* (2016) resulted in a clade including (borhyaenids (*Mayulestes* (*Jaskhadelphys* (*Andinodelphys, Pucadelphys*)))), in other words, Pucadelphyda as defined here. However, in our analysis we did not include *Jaskhadelphys*, because we regard this taxon as too incompletely known (the holotype only, a maxillary fragment with M2-3). Nevertheless, our result is very close to that of Wilson *et al.* (2016), with the difference that our analysis places *Mayulestes* within Sparassodonta [a taxon, which Wilson *et al.* (2016) have restricted to the borhyaenids)]. The reason for the slight divergence between our results is probably explained by the fact that we included 17 sparassodont taxa in our analysis, while the imprecise designation "borhyaenids" of Wilson *et al.* (2016) is likely to be only partially representative of the taxon Sparassodonta. In fact, the analysis of Wilson *et al.* (2016) used the data matrix of Rougier *et al.* (1998, 2004, 2015) and therefore their "borhyaenoids" is clearly derived from the taxon Borhyaenidae employed by Rougier *et al.* (1998, 2004, 2015) to represent the Sparassodonta and for which they did not specify either the taxa they included in this family. In our analysis (as well as in that of Forasiepi *et al.* 2015), the taxon Borhyaenidae is represented by three genera (*Borhyaena, Arctodictis* and *Australohyaena*), and which resulted here as paraphyletic. Our results confirm the interpretation of Muizon (1998) and include *Mayulestes* (as well as *Allqokirus*) within Sparassodonta, which implies for the clade a minimal age of earliest Palaeocene. Furthermore, it is noteworthy that the analysis of Wilson *et al.* (2016) based on dental, cranial and post-cranial characters, resulted in a nesting of the peradectids within the Marsupialia, whereas *Mayulestes* is included in the first diverging clade of Marsupialiformes, and therefore, is not closely related to peradectids. In this respect, the results of Wilson *et al.* (2016) analysis strongly resembles ours and contradicts the suggestion of Goin (2003) discussed above.

Furthermore, the results of the analysis performed by Bi *et al.* (2015: fig. 5) based on the data matrix of Rougier *et al.* (1998, 2004, 2015), retrieved a clade including the Marsupialia and the Pucadelphyda (the latter as a paraphyletic group) as follows: (Gurlin Tsav Skull (Borhyaenids (*Mayulestes* (*Jaskhadelphys* (*Pucadelphys* (*Andinodelphys* (Marsupialia)))))). This topology, although not identical to ours, clearly supports close relationships of *Mayulestes* with the borhyaenoids (*sensu* Rougier *et al.* 1998, 2004, 2015) and with the pucadelphyids. The results of Rougier *et al.* (1998, 2004, 2015) and Bi *et al.* (2015) also support the inclusion of the Pucadelphyda and the Marsupialia in the same clade and, in this respect, is clearly reminiscent of the results presented here.

In a recent analysis Carneiro (2018) suggested that a new species of *Varalphadon* (*V. janetae*) from the early Late Cretaceous of North America could be referred to the Sparassodonta, thus representing the earliest member of the order and the first outside South America. However, the holotype and referred specimens of *V. janetae* do not present clear similarities with the oldest sparassodonts, the Mayulestidae. On the basis of Carneiro (2018)'s figures 2 and 3, we find that *V. janetae* differs from the sparassodonts in the following dental characters:

1) *V. janetae*: postmetacrista not significantly enlarged and metastylar area does not extend posterolabially; sparassodonts: postmetacrista distinctly enlarged and posterolabially extended;

2) *V. janetae*: paracone and metacone widely separated at base; sparassodonts: paracone and metacone are adjoined at base at least on half of their height (see Fig. 10) and fused in derived taxa;

3) *V. janetae*: paracone subequal in height and volume to metacone; sparassodonts: paracone is always markedly smaller in height and volume than metacone;

4) *V. janetae*: protocone is larger and more extended anteroposteriorly than in sparassodonts; sparassodonts: protocone relatively small (lost is derived taxa) and compressed anteroposteriorly.

5) *V. janetae*: protoconid small in height (height on m3 is *c.* 80% the length of the tooth) and volume; sparassodonts: protoconid high subequal to length of m3/m4 or greater (between 90 and 114%), except in the case of *Hondadelphis* (84%) (see table2);

6) *V. janetae*: labial edge of protoconid slightly convex with maximum width of protoconid at base of cusp; sparassodonts: labial edge of protoconid conspicuously inflated at mid-height and overhanging base of cusp, with maximum width of protoconid at mid-height (see Fig. 14);

7) *V. janetae*: metaconid conspicuously higher and more voluminous than paraconid, sparassodonts: metaconid either subequal in size and volume to paraconid, or distinctly smaller.

Because *V. janetae* does not exhibit any of the sparassodont dental features, we do not support Carneiro (2018)'s hypothesis and consider that, so far, sparassodont are absent in North America.

Within Sparassodonta, the first diverging clade is the family Mayulestidae, composed of the Tiupampan (early Palaeocene) *Mayulestes* and *Allqokirus*, and the Itaboraian (early Eocene) *Patene*. Sparassodonta are here included in the Pucadelphyda, which constitutes a local radiation at Tiupampa of carnivorous notometatherians. This clade displays the early radiation of the sparassodont lineage, which very probably originated earlier than the Tiupampian and possibly as early as the Late Cretaceous. Further-

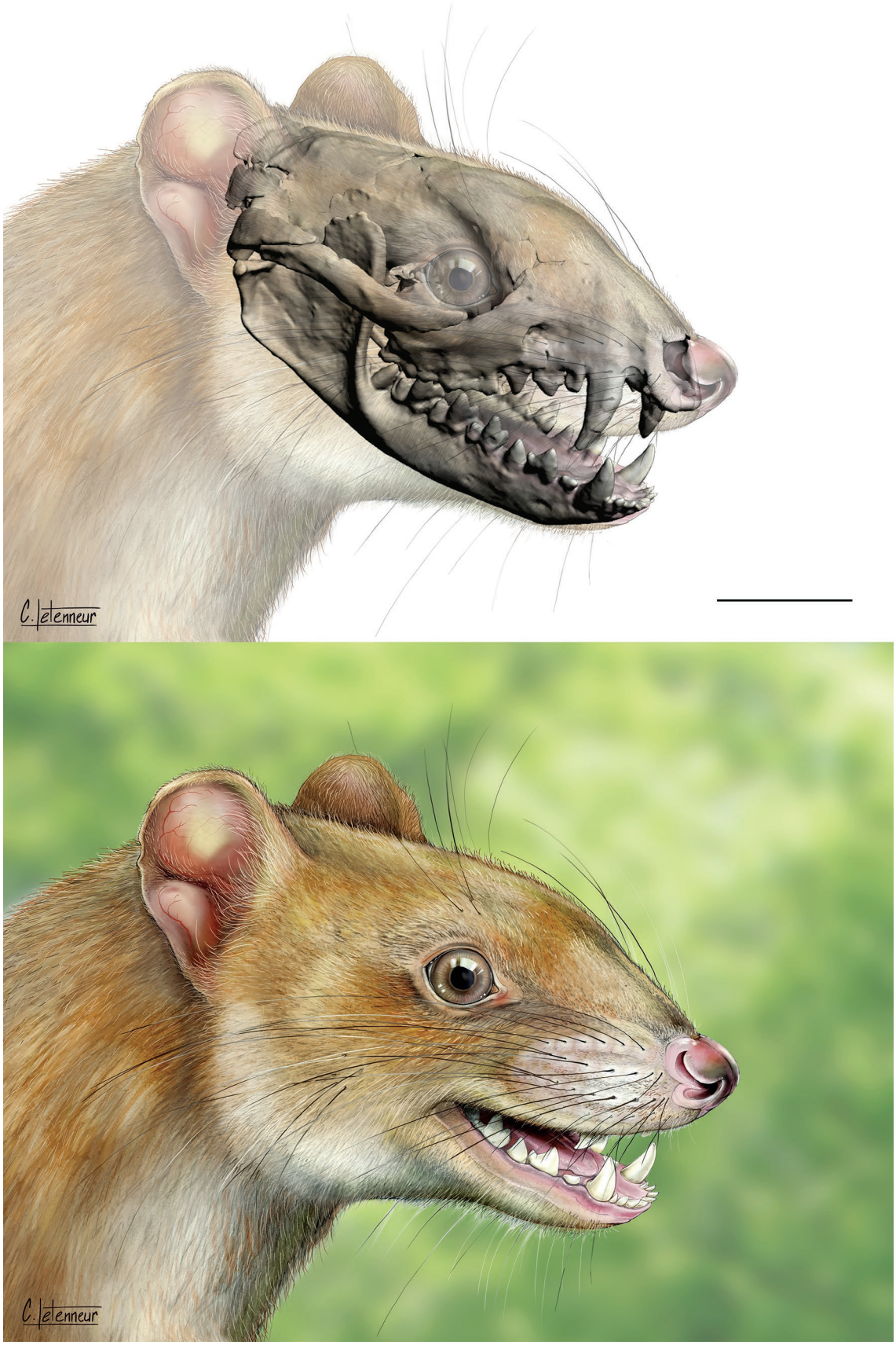


Fig. 30. — Reconstruction of the head of *Allqokirus australis* in anterolateral view (Charlène Letenneur); **top**, positioning of the silhouette of 3D digital rendering of the skull on which the life reconstruction has been based; **bottom**, life reconstruction. Scale bar: 1 cm.

more, our analysis points out that the sparassodonts stem from a "didelphimorphian"-like South American radiation represented, in the Tiupampan, by a pucadelphyid morphotype. The clade Pucadelphyda is well separated from the Marsupialia and, apparently, no representative of the Pucadelphyda have been discovered so far in North America (*contra* Carneiro 2018; see above). The North American taxa that could potentially share affinities with the Pucadelphyda are *Herpetotherium* and *Peratherium*, but they appear to be more closely related to Marsupialia (Selva & Ladevèze 2017).

## GENERAL CONCLUSIONS

The early Palaeocene mammal fauna of Tiupampa (Bolivia) has yielded an exceptional amount of metatherian taxa, given its age (65 Ma), and, even more exceptional, some of them being represented by sub-complete skulls and skeletons. Among them, *Allqokirus australis* was originally described on the basis of a few isolated molars (Marshall & Muizon 1988) and was assigned to the family Mayulestidae, together with *Mayulestes* (Muizon 1998). A disarticulated cranium and mandibles have since then completed the hypodigm of *Allqokirus*, and are here thoroughly described, almost twenty years after the description of *Pucadelphys andinus* (Marshall *et al.* 1995) and *Mayulestes ferox* (Muizon 1998).

*Allqokirus australis* is a small-sized sparassodont, the cranium of which is smaller and more gracile than that of *Mayulestes*. Body masses for both taxa have been calculated by Beck (2015) on the basis of the size of upper molars. Values for *Mayulestes* (based on M2 and M3) span from 181.3 g (equation of Gordon 2003) to 355.5 g (equation of Myers 2001). Surprizingly, the body mass estimate for *Allqokirus* based on the single upper molar known at that time (?M3) is higher than that of *Mayulestes* and spans from 247.7 g (equation of Gordon 2003) to 445.9 g (equation of Myers 2001). In fact, this difference probably simply indicates that the teeth of *Mayulestes* are proportionally smaller as compared to the cranium than in *Allqokirus*.

Some of the traits observed in *Allqokirus* interestingly indicate incipient adaptations to carnivory. For instance, the apical flaring of the snout is probably linked to the increase in size of the canines, as in other highly carnivorous metatherians. The molars still retain a typical tribosphenic pattern but exhibit early signs of a specialised dentition for carnivory. In hypercarnivorous mammals, dental adaptations are characterised by a reduction of prevallum-postvallid shear (occlusion of the distal facet of the metaconid and the mesial facet of the parastyle) together with an increase in postvallum-prevallid shear (paraconid/protoconid and postmetacrista). In *Allqokirus*, the metaconid is not obviously reduced as compared to the paraconid, except on m4 where it is slightly smaller than paraconid. This is the condition observed in *Mayulestes* and *Patene*, which differs from that of pucadelphyids, in which the metaconid is much more voluminous. The protoconid is very large, very high, and its labial aspect is more salient labially at mid-height than at the apex or at the base of the cusp. This feature is also present in *Mayulestes* and *Patene*, but it is absent in pucadelphyids. The talonid is not reduced when compared to non-carnivorous metatherians, except on m3-4. The entoconid is very small. On the upper molars, the protocone is not obviously reduced (it is even slightly more massive than in *Mayulestes*) as compared to later sparassodont. It is however anteroposteriorly compressed on M3, and not inflated basally as it is in pucadelphyids. The postmetacrista is very long, and more so on the M3. The paracone and metacone are fused at their base, while they are distinctly separated in pucadelphyids.

Scrutinised in a phylogenetic analysis, the morphological characters of *Allqokirus* confirm its assignation to the family Mayulestidae, which also includes (according to our analysis) *Patene simpsoni* from the early Eocene of Itaboraí (Brazil). As suggested by Muizon (1998), Mayulestidae belongs to the South American radiation of carnivorous marsupialiforms, Sparassodonta, which makes *Allqokirus* and *Mayulestes* the oldest representatives of the clade.

As early as the earliest Palaeocene, or most probably even earlier, there occurred in South America a major diversification event, with the rapid radiation of the Pucadelphyda clade, leading to the emergence of carnivorous forms. The marsupialiforms from Tiupampa are crucial in the understanding of the earliest steps of the evolution and radiation of Sparassodonta. Both Pucadelphyidae (the sister group of Sparassodonta) and Mayulestidae – the first diverging sparassodont clade - allow reconstruction of an ancestral morphotype for Sparassodonta, which exhibits the first steps of a specialisation to hypercarnivory and some arboreal abilities.

Both *Mayulestes* and *Allqokirus* remains were found in "the Quarry" (or "site 1"), in which most of the Tiupampa mammal remains were discovered. The latter have clear trophic relationships, with the eutherians being mostly herbivorous and partly omnivorous, and the marsupialiforms insectivorous-frugivorous, omnivorous, and carnivorous (Muizon 1992, 1998; Argot 2004a). The two carnivorous taxa were similar in size, although *Allqokirus* was slightly smaller, and more slender. They were approximately as large as a small opossum such as *Philander opossum*, however, they probably represent the largest metatherian taxa in the Tiupampa fauna. *Mayulestes* had obvious arboreal abilities (as demonstrated by the postcranial elements of *Mayulestes*; Muizon 1998; Argot 2001, 2002, 2003a, 2004a), but the postcranial skeleton of *Allqokirus* is unknown. Climbing abilities may have permitted escape from terrestrial predators (especially the cursorial sebecid crocodiles) and provided access to the large source of food represented by arboreal insects. The diet of *Allqokirus* and *Mayulestes* probably comprised an abundant fauna of small insectivorous marsupials (see Argot 2004a for a list of potential preys for *Mayulestes*), small mioclaenid condylarths, small amphibians, and perhaps eggs of crocodiles, turtles or birds, and large insects (Fig. 30).

**Acknowledgements**
The specimen described in this paper was discovered in 1996 during a field season at Tiupampa funded by the Institut Français d'Etudes Andines and the CNRS. Fossil collecting was carried out under the auspices of research agreements between the Fundacion para las ciencias (Bolivia) and the Muséum national d'Histoire naturelle (France). The specimen MHNC 8267 is the property of the MHNC and has been provided on loan to the MNHN for curation and publication. Field expedition has benefited of logistical support from the IRD (Institut de Recherche pour le Dévelopement) in Bolivia. We thank our Bolivian colleagues (Ricardo Céspedes-Paz, Ramiro Suarez-Sorruco, Mario Suarez-Riglos) for their collaboration and logistic assistance during the field season. Special thanks are due to Michael Novacek, Jin Meng, Ruth O'Leary, Judith Galkin, and Suzanne Goldberg (American Museum of Natural History), Sara Lyons (National Museum of Natural History, Smithsonian Institution), Daniel Brinkman and Christopher Norris (Yale Peabody Museum) Philip Gingerich (Museum of Paleontology, University of Michigan), Richard Cifelli (Oklahoma Museum of Natural History), for access to the specimens under their care and for loans of specimens. Céline Bens, Géraldine Véron, Jacques Cuisin, Christine Lefèvre, Luc Vives (MNHN) provided access to MNHN specimens under their care. Warm thanks to William Clemens who provided excellent photographs (taken by David Strauss) of the holotypes of *Lycopsis longirostrus* and *Hondadelphys fieldsi*, to Steve Wroe for providing stl files of the skulls of *Thylacinus cynocephalus* and *Nimbacinus dicksoni*, and to Judith Babot for the photographs of the mandibles of *Patene simpsoni* (PLV 2618). Special thanks also to Gregory Wilson for providing access to the CT data of the skulls of *Didelphodon vorax* NDGS 431 and UW BM 94084. Our warmest and most grateful thanks are due to Analia Forasiepi who revised an earlier version of the manuscript and had us benefit of her wide experience on carnivorous metatherians; her extremely careful revision of the text, of the character list and definition, and of the taxa scorings allowed considerable improvement of our work. Special thanks are due to the reviewers, R. M. Beck and M. O. Woodburne, who provided unvaluable comments, which significantly improved the manuscript. Photographs were made by Philippe Loubry and Lilian Cazes, the photogrammetric pdf File2 of the supplementary data is by Lilian Cazes and the gorgeous reconstruction of Fig. 30 is by Charlène Letenneur. CT scanning of the specimens was performed by Miguel Garcia at the AST-RX technical platform of scientific access to RX tomography (UMS 2700 "outils et méthodes de la systématique intégrative", CNRS-MNHN, Paris) Data processing was undertaken at the 3D imaging facilities Lab of the UMR 7207 CR2P (MNHN CNRS UPMC-Paris6).

## REFERENCES

ABDALA F., FLORES D. A. & GIANNINI N. P. 2001. — Postweaning ontogeny of the skull of *Didelphis albiventris*. *Journal of Mammalogy* 82: 190-200. https://doi.org/10.1644/1545-1542(2001)082<0190:POOTSO>2.0.CO;2

ARCHER M. 1976. — The basicranial region of marsupicarnivores (marsupialia), interrelationships of carnivorous marsupials, and affinities of the insectivorous marsupial peramelids. *Zoological Journal of the Linnean Society* 59: 217-322. https://doi.org/10.1111/j.1096-3642.1976.tb01016.x

ARGOT C. 2001. — Functional-adaptive anatomy of the forelimb in the Didelphidae and the paleobiology of the Paleocene marsupials *Mayulestes ferox* and *Pucadelphys andinus*. *Journal of Morphology* 247: 51-79.

ARGOT C. 2002. — Functional-adaptive analysis of the hind limb anatomy of extant marsupials and the paleobiology of the Paleocene marsupials *Mayulestes ferox* and *Pucadelphys andinus*. *Journal of Morphology* 253: 76-108. https://doi.org/10.1002/jmor.1114

ARGOT C. 2003a. — Functional-adaptive anatomy of the axial skeleton of some extant marsupials and the paleobiology of the Paleocene marsupials *Mayulestes ferox* and *Pucadelphysandinus*. *Journal of Morphology* 255: 279-300. https://doi.org/10.1002/jmor.10062

ARGOT C. 2003b. — Postcranial functional adaptations in the South American Miocene borhyaenoids (Mammalia, Metatheria): *Cladosictis, Pseudonotictis*, and *Sipalocyon*. *Alcheringa* 27: 303-356. https://doi.org/10.1080/03115510308619110

ARGOT C. 2003c. — Functional adaptations of the postcranial skeleton of two borhyaenoids (Mammalia, Metatheria), *Borhyaena* and *Prothylacynus*, from South America. *Palaeontology* 46 (6): 1213-1267. https://doi.org/10.1046/j.0031-0239.2003.00339.x

ARGOT C. 2004a. — Evolution of South American mammalian predators (Borhyaenoidea): anatomical and palaeobiological implications. *Zoological Journal of the Linnean Society* 140: 487-521. https://doi.org/10.1111/j.1096-3642.2004.00110.x

ARGOT C. 2004b. — Functional adaptive analysis of the postcranial skeleton of a Laventan borhyaenoids, *Lycopsis longirostris* (Marsupialia, Metatheria). *Journal of Vertebrate Paleontology* 24 (3): 689-708. https://doi.org/10.1671/0272-4634(2004)024[0689:FAOTPS]2.0.CO;2

ARGOT C. 2004c. — Functional-adaptative features and palaeobiologic implications of the postcranial skeleton of the late Miocene sabretooth borhyaenoids *Thylacosmilus atrox* (Metatheria). *Alcheringa* 28: 229-266. https://doi.org/10.1080/03115510408619283

ARGOT C. & BABOT J. 2011. — Postcranial morphology, functional adaptations and palaeobiology of *Callistoe vincei*, a predaceous metatherian from the Eocene of Salta, Northwestern Argentina. *Palaeontology* 54 (2): 447-480. https://doi.org/10.1111/j.1475-4983.2011.01036.x

ASHER R. J. 2007. — A web-database of mammalian morphology and a reanalysis of placental phylogeny. *BMC Evolutionary Biology* 2007 (7): 108. https://doi.org/10.1186/1471-2148-7-108

ASTUA D. & LEINER N. O. 2008. — Tooth eruption sequence and replacement pattern in woolly opossums, genus *Caluromys* (Didelphimorphia, Didelphidae). *Journal of Mammalogy* 89 (1): 244-251. https://doi.org/10.1644/06-MAMM-A-434.1

BABOT M. J. 2005. — *Los Borhyaenoidea (Mammalia, Metatheria) del Terciario inferior del noroeste argentino. Aspectos filogenéticos, paleobiolólogicos y bioestratigráficos.* Unpublished PhD thesis, Universidad Nacional de Tucumán.

BABOT M. J., POWELL J. E. & MUIZON C. DE 2002. — *Callistoe vincei*, a new Proborhyaenidae (Borhyaenoidea, Metatheria, Mammalia) from the early Eocene of Argentina. *Geobios* 35: 615-629. https://doi.org/10.1016/S0016-6995(02)00073-6

BABOT M. J., GARCÍA LÓPEZ D. A. & GAUDIN T. J. 2012. — The most ancient xenarthran petrosal: morphology and evolutionary significance. *Journal of Vertebrate Paleontology* 32 (5): 1186-1197. https://doi.org/10.1080/02724634.2012.686466

BI S., JIN X., LI S. & DU T. 2015. — A new Cretaceous metatherian mammal from Henan, China. *PeerJ* 3: e896. https://doi.org/10.7717/peerj.896

Beck R. M. 2012. — An 'ameridelphian' marsupial from the early Eocene of Australia supports a complex model of Southern Hemispere marsupial biogeography. *Naturwissenschaften* 99: 715-729. https://doi.org/10.1007/s00114-012-0953-x

Beck R. M. 2015. — A peculiar faunivorous metatherian from the early Eocene of Australia. *Acta Palaeontologica Polonica* 60 (1): 123-129. https://doi.org/10.4202/app.2013.0011

Beck R. M. 2017. — The skull of *Epidolops ameghinoi* from the early Eocene Itaboraí fauna, Southern Brazil, and the affinities of the extinct marsupialiform order Polydolopimorphia. *Journal of Mammalian Evolution* 24 (4): 373-414. https://doi.org/10.1007/s10914-016-9357-6

Beck R. M., Travouillon K. J., Aplin K. P., Godthelp H. & Archer M. 2014. — The osteology and systematics of the enigmatic Australian Oligo-Miocene metatherian *Yalkaparidon* (Yalkaparidontidae; Yalkaparidontia; ?Australidelphia; Marsupialia). *Journal of Mammalian Evolution* 21 (2): 127-172. https://doi.org/10.1007/s10914-013-9236-3

Bensley B. A. 1902. — On the identification of the Meckelian and mylohyoid grooves in the jaws of Mesozoic and Recent mammals. *University of Toronto Studies, Biological Series* 3: 75-82. https://doi.org/10.5962/bhl.title.66541

Billet G., Germain D., Ruf I., Muizon C. de & Hautier L. 2013. — The inner ear of *Megatherium* and the evolution of the vestibular system in sloths. *Journal of Anatomy* 223: 557-567. https://doi.org/10.1111/joa.12114

Blanks R. H. I., Curthoys I. S. & Markham C. H. 1975. — Planar relationships of the semicircular canals in man. *Acta Oto-Laryngologica* 80: 185-196. https://doi.org/10.3109/00016487509121318

Bonaparte J. F., Van Valen L. M. & Kramartz A. 1993. — La fauna local de Punta Peligro, Paleoceno inferior, de la Provincia del Chubut, Patagonia, Argentina. *Evolutionary Monographs* 14: 1-61.

Bremer K. 1988. — The limits of amino acid sequence data in angiosperm phylogenetic reconstruction. *Evolution* 42 (4): 795-803. https://doi.org/10.1111/j.1558-5646.1988.tb02497.x

Cabrera A. 1927. — Datos para el conocimiento de los dasyuroideos fósiles Argentinos. *Revista del Museo de la Plata* 30: 271-315.

Carneiro L. M. 2018. — A new species of *Varalphadon* (Mammalia, Metatheria, Sparassodonta) from the upper Cenomanian of southern Utah, North America: Phylogenetic and biogeographic insights. *Cretaceous Research* 84: 88-96. https://doi.org/10.1016/j.cretres.2017.11.004

Cifelli R. L. 1993. — Early Cretaceous mammal from North America, and the evolution of marsupial dental characters. *Proceedings of the National Academy of Sciences of the United States* 90 (20): 9413-9416. https://www.ncbi.nlm.nih.gov/pmc/articles/PMC47578/

Cifelli R. L. & Muizon C. de 1997. — Dentition and jaw of *Kokopellia juddi*, a primitive marsupial or near-marsupial from the Medial Cretaceous of Utah. *Journal of Mammalian Evolution* 4 (4): 241-258. https://doi.org/10.1023/A:1027394430433

Cifelli R. L. & Muizon C. de 1998. — Tooth eruption and replacement pattern in early marsupials. *Comptes Rendus de l'Académie des Sciences, Série 2, Sciences de la Terre et des Planètes* 326 (3): 215-220. https://doi.org/10.1016/S1251-8050(00)89038-2

Clark C. T. & Smith K. K. 1993. — Cranial osteogenesis in *Monodelphis domestica* (Didelphidae) and *Macropus eugenii* (Macropodidae). *Journal of Morphology* 215: 119-149. https://doi.org/10.1002/jmor.1052150203

Clemens W. A. 1966. — Fossil mammals from the type Lance Formation, Wyoming. Part II. Marsupialia. *University of California Publications in Geological Sciences* 62: 1-122.

Clemens W. A. 1968. — A mandible of *Didelphodon vorax* (Marsupialia, mammalia). *Contribution in Science* 133: 1-11. https://biodiversitylibrary.org/page/52117669

Coues E. 1869. — The osteology and myology of *Didelphis virginiana*. *Memoirs of the Boston Society of Natural History* 2: 41-154. https://doi.org/10.5962/bhl.title.61012

Crochet J. Y. 1980. — *Les marsupiaux du Tertiaire d'Europe*. Éditions de la Fondation Singer Polignac, Paris. 279 p. https://gallica.bnf.fr/ark:/12148/bpt6k3326526p/f9.image

Crompton A. W. 1971. — The origin of the tribosphenic molar, *in* Kermack D. M. & Kermack K. A. (eds), Early Mammals. *Zoological Journal of the Linnean Society* 50: 65-87.

David R., Droulez J., Allain R., Berthoz A., Janvier P. & Bennequin D. 2010. — Motion from the past. A new method to infer vestibular capacities of extinct species. *Comptes Rendus Palevol* 9: 397-410. https://doi.org/10.1016/j.crpv.2010.07.012

Davis B. M. 2007. — A revision of "pediomyid" marsupials from the Late Cretaceous of North America. *Acta Palaeontologica Polonica* 52 (2): 217-256.

Dom R., Fisher B. L. & Martin G. F. 1970. — The venous system of the head and neck of the opossum (*Didelphis virginiana*). *Journal of Morphology* 132: 487-496. https://doi.org/10.1002/jmor.1051320408

Echarri S. & Prevosti F. J. 2015. — Differences in mandibular disparity between extant and extinct species of metatherian and placental carnivore clades. *Lethaia* 48: 196-204. https://doi.org/10.1111/let.12099

Echarri S., Ercoli M. D., Chemisquy M. A., Turazzini G. & Prevosti F. J. 2017. — Mandible morphology and diet of the South American extinct metatherian predators (Mammalia, Metatheria, Sparassodonta). *Earth and Environmental Science Transactions of the Royal Society of Edinburgh* 106: 277-288. https://doi.org/10.1017/S1755691016000190

Ekdale E. G., Archibald D. J. & Averianov A. O. 2004. — Petrosal bones of placental mammals from the Late Cretaceous of Uzbekistan. *Acta Palaeontologica Polonica* 49 (1): 161-176.

Engelman R. K. & Croft D. A. 2014. — A new species of small-bodied sparassodont (Mammalia: Metatheria) from the Middle Miocene locality of Quebrada Honda, Bolivia. *Journal of Vertebrate Paleontology* 34: 672-688. https://doi.org/10.1080/02724634.2013.827118

Engelman R. K., Anaya F. & Croft D. A. 2015. — New specimens of *Acyon myctoderos* (Metatheria, Sparassodonta) from Quebrada Honda, Bolivia. *Ameghiniana* 52 (2): 204-225. https://doi.org/10.5710/AMGH.19.11.2014.2803

Evans H. E. & de Lahunta A. 2013. — *Miller's Anatomy of the Dog*. Saunders, St Louis, 850 p.

Flores D. A., Abdala F. & Giannini N. 2010. — Cranial ontogeny of *Caluromys philander* (Didelphidae: Caluromyinae): a qualitative and quantitative approach. *Journal of Mammal*ogy 91 (3): 539-550. https://doi.org/10.1644/09-MAMM-A-291.1

Forasiepi A. M. 2009. — Osteology of *Arctodictis sinclairi* (Mammalia, Metatheria, Sparassodonta) and phylogeny of Cenozoic metatherian carnivores from South America. *Monografías del Museo Argentino de Ciencias Naturales* 6: 1-174.

Forasiepi A. M. & Sánchez-Villagra M. R. 2014. — Heterochrony, dental diversity, and the circumvention of constraints in marsupial mammals and extinct relatives. *Paleobiology* 40 (2): 222-237. https://doi.org/10.1666/13034

Forasiepi A. M., Babot M. J. & Zimicz N. 2015. — *Australohyaena antiqua* (Mammalia, Metatheria, Sparassodonta), a large predator from the late Oligocene of Patagonia. *Journal of Systematic Palaeontology* 13(6): 503-525. https://doi.org/10.1080/14772019.2014.926403

Forasiepi A. M., Sánchez-Villagra M. R., Goin F. J., Takai M., Shigehara N. & Kay R. F. 2006. — A new species of Hathliacynidae (Metatheria, Saprassodonta) from the middle Miocene of Quebrada Honda, Bolivia. *Journal of Vertebrate Paleontology* 26 (3): 670-684. https://doi.org/10.1671/0272-4634(2006)26[670:ANSOHM]2.0.CO;2

Fox R. C. & Naylor B. G. 1986. — A new species of *Didelphodon* Marsh (Marsupialia) from the Upper Cretaceous of Alberta, Canada: paleobiology and phylogeny. *Neues Jahrbuch für Geologie und Paläontologie* 172 (3): 357-380.

FOX R. C. 1981. — Mammals from the Upper Cretaceous Oldman Formation, Alberta. V *Eodelphis* Matthew, and the evolution of the Stagodontidae. *Canadian Journal of Earth Sciences* 18 (2): 350-365. https://doi.org/10.1139/e81-027

FOX R. C. 1983. — Notes on the North American Tertiary marsupials *Herpetotherium* and *Peradectes*. *Canadian Journal of Earth Sciences* 20 (10): 1565-1578. https://doi.org/10.1139/e83-146

GABBERT S. L. 1998. — Basicranial anatomy of *Herpetotherium* (Marsupialia: Didelphimorphia) from the Eocene of Wyoming. *American Museum Novitates* 3235: 1-13. http://hdl.handle.net/2246/3244

GAYET M., MARSHALL L. G. & SEMPERE T. 1992. — The Mesozoic and Palaeocene vertebrates of Bolivia and their stratigraphic context: a review. *Revista Técnica de YPFB* 12 (3-4): 393-433.

GEISLER J. H. 2001. — New morphological evidence for the phylogeny of Artiodactyla, Cetacea, and Mesonychidae. *American Museum Novitates* 3344: 1-53. https://doi.org/10.1206/0003-0082(2001)344<0001:NMEFTP>2.0.CO;2

GELFO J. N., GOIN F. J., WOODBURNE M. O. & MUIZON C. DE 2009. — Biochronological relationships of the earliest South American Paleogene mammalian faunas. *Palaeontology* 52 (1): 251-269. https://doi.org/10.1111/j.1475-4983.2008.00835.x

GOIN F. J. 2003. — Early marsupial radiations in South America, *in* JONES M., DICKMAN C., ARCHER M. (eds), *Predators with Pouches. The Biology of Carnivorous Marsupials*. CSIRO Publishing, Victoria: 30-42.

GOIN F. J. & PASCUAL R. 1987. — News on the biology and taxonomy of the marsupials Thylacosmilidae (late Tertiary of Argentina). *Anales de la Academia nacional de Ciencias exactas y naturales* 39: 219-246.

GOIN F. J., PALMA R. M., PASCUAL R. & POWELL J. E. 1986. — Persistencia de un primitivo Borhyaenidae (Mammalia, Marsupialia) en el Eoceno temprano de Salta (FM. Lumbrera, Argentina). Aspectos geologicos y paleoambientales relacionados. *Ameghiniana* 23 (1-2): 47-56.

GOIN F. J., CANDELA A. M., ABELLO M. A. & OLIVEIRA E. V. 2009. — Earliest South American paucituberculatans and their significance in the understanding of 'pseudodiprotodont' marsupial radiations. *Zoological Journal of the Linnean Society* 155: 867-884. https://doi.org/10.1111/j.1096-3642.2008.00471.x

GOIN F. J., PASCUAL R., TEJEDOR M., GELFO J. N., WOODBURNE M., CASE J., REGUERO M., BOND M., CIONE A., UDRIZAR SAUTHIER D., BALARINO L., SCASSO R., MEDINA F. A. & UBALDÓN M. C. 2006. — The earliest Tertiary therian mammal from South America. *Journal of Vertebrate Paleontology* 26 (2): 505-510. https://doi.org/10.1671/0272-4634(2006)26[505:TETTMF]2.0.CO;2

GOIN F. J., WOODBURNE M. O., ZIMICZ A. N., MARTIN G. M. & CHRONOGUBSKY L. 2016. — *A Brief History of South American Metatherians. Evolutionary Contexts and Intercontinental Dispersals*. Springer, Dordrecht, 237 p. https://doi.org/10.1007/978-94-017-7420-8

GORDON C. L. 2003. — A first look at estimating body size in dentally conservative marsupials. *Journal of Mammalian Evolution* 10: 1-21. https://doi.org/10.1023/A:1025545023221

GREGORY W. K. 1910. — The orders of mammals. *Bulletin of the American Museum of Natural History* 27: 1-524. http://hdl.handle.net/2246/313

GREGORY W. K. & SIMPSON G. G. 1926a. — Cretaceous mammal skulls from Mongolia. *American Museum Novitates* 225: 1-20. http://hdl.handle.net/2246/3193

GREGORY W. K. & SIMPSON G. G. 1926b. — Cretaceous mammal skulls from Mongolia. *Nature* 118: 698-699. https://doi.org/10.1038/118698a0

HERSHKOVITZ P. 1982. — The staggered marsupial lower third incisor (i3). *Geobios*, Mémoire spécial 6: 191-200. https://doi.org/10.1016/S0016-6995(82)80113-7

HERSHKOVITZ P. 1995. — The staggered marsupial third lower incisor: hallmark of Cohort Didelphimorphia, and description of a new genus and species with staggered i3 from the Albian (Lower Cretaceous) of Texas. *Bonner Zoologische Beiträge* 45: 153-169. https://biodiversitylibrary.org/page/44799597

HIIEMAE K. & JENKINS F. A. 1969. — The anatomy and internal architecture of the muscles of mastication in *Didelphis marsupialis*. *Postilla* 140: 1-49. https://biodiversitylibrary.org/page/10598730

HOPSON J. A. & ROUGIER G. W. 1993. — Braincase structure in the oldest skull of a therian mammal: implications for mammalian systematic and cranial evolution. *American Journal of Science* 293: 268-299. https://doi.org/10.2475/ajs.293.A.268

HOROVITZ I. & SÁNCHEZ-VILLAGRA M. R. 2003. — A morphological analysis of marsupial mammal higher-level phylogenetic relationships. *Cladistics* 19: 181-212. https://doi.org/10.1111/j.1096-0031.2003.tb00363.x

HOROVITZ I. 2000. — The tarsus of *Ukhaatherium nessovi* (Eutheria, Mammalia) from the Late Cretaceous of Mongolia: an appraisal of the evolution of the ankle in basal therians. *Journal of Vertebrate Paleontology* 20: 547-560. https://doi.org/10.1671/0272-4634(2000)020[0547:TTOUNE]2.0.CO;2

HOROVITZ I., LADEVÈZE S., ARGOT C., MACRINI T. E., MARTIN T., HOOKER J. J., KURZ C., MUIZON C. DE & SÁNCHEZ-VILLAGRA M. R. 2008. — The anatomy of *Herpetotherium* cf. *fugax* Cope 1873, a metatherian from the Oligocene of North America. *Palaeontographica* 284 (4-6): 109-141. https://doi.org/10.1127/pala/284/2008/109

HOROVITZ I., MARTIN T., BLOCH J., LADEVÈZE S., KURZ C. & SÁNCHEZ-VILLAGRA M. R. 2009. — Cranial anatomy of the earliest marsupials and the origin of opossums. *PlosOne* 4 (12): 1-9. https://doi.org/10.1371/journal.pone.0008278

KERMACK K. A., MUSSETT F. & RIGNEY H. W. 1981. — The skull of *Morganucodon*. *Zoological Journal of the Linnean Society* 71: 1-158. https://doi.org/10.1111/j.1096-3642.1981.tb01127.x

KIELAN-JAWOROWSKA Z. 1975a. — Preliminary description of two new eutherian genera from the Late Cretaceous of Mongolia. *Palaeontologia Polonica* 33: 5-16.

KIELAN-JAWOROWSKA Z. 1975b. — Evolution of the therian mammals in the Late Cretaceous of Asia. Part I. Deltatheridiidae. *Palaeontologia Polonica* 33: 103-132.

KIELAN-JAWOROWSKA Z. 1977. — Evolution of the therian mammals in the Late Cretaceous of Asia. Part II. Postcranial skeleton in *Kennalestes* and *Asioryctes*. *Palaeontologia Polonica* 37: 65-83.

KIELAN-JAWOROWSKA Z. 1981. — Evolution of the therian mammals in the Late Cretaceous of Asia. Part IV. Skull structure of *Kennalestes* and *Asioryctes*. Results of the Polish-Mongolian Paleontological Expeditions. Part IX. *Palaeontologia Polonica* 42: 25-78.

KIELAN-JAWOROWSKA Z. & DASHZEVEG D. 1989. — Eutherian mammals from the Early Cretaceous of Mongolia. *Zoologica Scripta* 18: 347-355. https://doi.org/10.1111/j.1463-6409.1989.tb00460.x

KIRSCH J. A. W., LAPOINTE F.-J. & SPRINGER, M. S. 1997. — DNA-hybridisation studies of marsupials and their implications for metatherian classification. *Australian Journal of Zoology* 45: 211-280. https://doi.org/10.1071/ZO96030

KLAAUW J. C. VAN DER 1931. — The auditory bulla in some fossil mammals with a general introduction to this region of the skull. *Bulletin of the American Museum of Natural History* 62: 1-352. http://hdl.handle.net/2246/353

KORTH W. W. 1994. — Middle Tertiary marsupials (Mammalia) from North America. *Journal of Paleontology* 68 (2): 376-397. https://doi.org/10.1017/S0022336000022952

KOYABU D., MAIER W. & SÁNCHEZ-VILLAGRA M. R. 2012. — Paleontological and developmental evidence resolve the homology and dual embryonic origin of a mammalian skull bone, the interparietal. *Proceedings of the National Academy of Sciences* 109: 14075-14080. https://doi.org/10.1073/pnas.1208693109

KRISHTALKA L. & STUCKY R. K. 1984. — Middle Eocene marsupials (Mammalia) from Norhteastern Utah and the mammalian fauna from Powder Wash. *Annals of the Carnegie Museum* 53 (2): 31-45. https://biodiversitylibrary.org/page/52373392

KRISHTALKA L. & STUCKY R. K. 1983a. — Revision of the Wind River Faunas, early Eocene of central Wyoming. Part 3. Marsupialia. *Annals of the Carnegie Museum* 52 (9): 205-227. https://biodiversitylibrary.org/page/52426228

KRISHTALKA L. & STUCKY R. K. 1983b. — Paleocene and Eocene marsupials of North America. *Annals of the Carnegie Museum* 52 (10): 229-263. https://biodiversitylibrary.org/page/52426252

KUHN H.-J. & ZELLER U. 1987. — The cavum epiptericum in monotremes and therian mammals, *in* KUHN H.-J. & ZELLER U. (eds), *Morphogenesis of the Mammalian Skull*. Verlag Paul Parey, Hamburg: 51-70.

KURZ C. & HABERSETZER J. 2004. — Untersuchungen der Zahnmorphologie von Beutelratten aus Messel mit der Mikroröntgenmethode CORR. *Courier Forschungsinstitut Senckenberg* 252: 13-21.

KURZ C. 2005. — Ecomorphology of opossum-like marsupials from the Tertiary of Europe and a comparison with selected taxa. *Kaupia* 14: 21-26.

LADEVÈZE S. 2004. — Metatherian petrosals from the late Paleocene of Itaboraí, Brazil, and their phylogenetic implications. *Journal of Vertebrate Paleontology* 24 (1): 202-213. https://doi.org/10.1671/16

LADEVÈZE S. 2007. — Petrosal bones of metatherian mammals from the Late Palaeocene of Itaboraí (Brazil), and a cladistic analysis of petrosal features in metatherians. *Zoological Journal of the Linnean Society* 150 (1): 85-115. https://doi.org/10.1111/j.1096-3642.2007.00282.x

LADEVÈZE S. & MUIZON C. DE 2007. — The auditory region of early Palaeocene Pucadelphydae (Mammalia, Metatheria) from Tiupampa with phylogenetic implications. *Palaeontology* 50 (5): 1123-1154. https://doi.org/10.1111/j.1475-4983.2007.00703.x

LADEVÈZE S. & MUIZON C. DE 2010. — Evidence of early evolution of Australidelphia (Metatheria Mammalia) in South America: phylogenetic relationships of the metatherians from the Late Palaeocene of Itaboraí (Brazil) based on teeth and petrosal bones. *Zoological Journal of the Linnean Society* 159 (2): 746-784. https://doi.org/10.1111/j.1096-3642.2009.00577.x

LADEVÈZE S., SMITH R. & SMITH T. 2012. — Reassessment of the morphology and taxonomic status of the earliest herpetotheriid marsupials of Europe. *Journal of Mammalian Evolution* 19: 249-261. https://doi.org/10.1007/s10914-012-9195-0

LADEVÈZE S., ASHER R. J., & SÁNCHEZ-VILLAGRA M. R 2008. — Petrosal anatomy in the fossil mammal *Necrolestes*: evidence for metatherian affinities and comparisons with the extant marsupial mole. *Journal of Anatomy* 213: 686-697. https://doi.org/10.1111/j.1469-7580.2008.00985.x

LADEVÈZE S., MUIZON C. DE, BECK R., GERMAIN D. & CÉSPEDES-PAZ R. 2011. — Earliest evidence of mammalian social behaviour in the basal Tertiary of Bolivia. *Nature* 474: 83-86. https://doi.org/10.1038/nature09987

LUCKETT W. P. 1993. — Ontogenetic staging of the mammalian dentition, and its value for assessment of homology and heterochrony. *Journal of Mammalian Evolution* 1 (4): 269-282. https://doi.org/10.1007/BF01041667

LUO Z.-X., JI Q., WIBLE J. R., & YUAN C.-X. 2003. — A new tribosphenic mammal and metatherian evolution. *Science* 302: 1934-1940. https://doi.org/10.1126/science.1090718

MACPHEE R. D. 1981. — Auditory regions of primates and eutherian insectivores: Morphology, ontogeny, and character analysis. *Contribution in Primatology* 18: 1-282.

MARSHALL L. G. 1976a. — Evolution of the Thylacosmilidae, extinct saber-tooth marsupials of South America. *PaleoBios* 23: 1-30.

MARSHALL L. G. 1976b. — New didelphine marsupials from the La Venta fauna (Miocene) of Colombia, South America. *Journal of Paleontology* 50 (3): 402-418.

MARSHALL L. G. 1977. — A new species of *Lycopsis* (Borhyaenidae: Marsupialia) from the La Venta fauna (late Miocene) of Colombia, South America. *Journal of Paleontology* 51 (3): 633-642.

MARSHALL L. G. 1978. — Evolution of the Borhyaenidae, extinct South American predaceous marsupials. *University of California Publications in Geological Sciences* 117: 1-89.

MARSHALL L. G. 1979. — Review of the Prothylacininae, an extinct subfamily of South American "dog-like" marsupials. *Fieldiana Geology,* new series, 3: 1-50. https://biodiversitylibrary.org/page/2842762

MARSHALL L. G. 1981. — Review of the Hathlyacyninae, an extinct subfamily of South American "dog-like" marsupials. *Fieldiana Geology,* new series, 7: 1-120. https://biodiversitylibrary.org/page/2865302

MARSHALL L. G. & MUIZON C. DE 1984. — Un nouveau Marsupial didelphidé (*Itaboraidelphys camposi* nov. gen. nov. sp.) du Paléocène moyen (Itaboraïen) de Sao José de Itaboraí (Brésil). *Comptes Rendus hebdomadaires des Séances de l'Académie des Sciences*, Paris, sér. II, 299 (18): 1297-1300.

MARSHALL L. G. & MUIZON C. DE 1988. — The dawn of the age of mammals in South America. *National Geographic Research* 4 (1): 23-55.

MARSHALL L. G. & MUIZON C. DE 1995. — Part II: The skull, *in* MUIZON C. DE (ed.), *Pucadelphys andinus* (Marsupialia, Mammalia) from the early Palaeocene of Bolivia. Muséum national d'Histoire naturelle, Paris: 21-90 (Mémoires du Muséum national d'Histoire naturelle ; 165).

MARSHALL L. G. & SIGOGNEAU-RUSSELL D. 1995. — Part III: Postcranial skeleton, *in* MUIZON C. DE (ed.), *Pucadelphys andinus* (Marsupialia, Mammalia) from the Early Paleocene of Bolivia. Muséum national d'Histoire naturelle, Paris: 91-164 (Mémoires du Muséum national d'Histoire naturelle ; 165).

MARSHALL L. G., MUIZON C. DE & SIGE B. 1983. — Late Cretaceous mammals (Marsupialia) from Bolivia. *Geobios* 16 (6): 739-745. https://doi.org/10.1016/S0016-6995(83)80090-4

MARSHALL L. G., CASE J. A. & WOODBURNE M. O. 1990. — Phylogenetic relationships of the families of marsupials, *in* GENOWAYS H. H. (ed.), *Current Mammalogy*. New York, Plenum Press: 433-505.

MARSHALL L. G., MUIZON C. DE & SIGOGNEAU-RUSSELL D. 1995. — Part I: The locality of Tiupampa: age, taphonomy and mammalian fauna, *in* MUIZON C. DE (ed.), *Pucadelphys andinus* (Marsupialia, Mammalia) from the Early Paleocene of Bolivia. Muséum national d'Histoire naturelle, Paris: 11-20 (Mémoires du Muséum national d'Histoire naturelle ; 165).

MARSHALL L. G., SEMPERE T. & BUTLER R. F. 1997. — Chronostratigraphy of the mammal-bearing Palaeocene of South America. *Journal of South American Earth Sciences* 10: 49-70. https://doi.org/10.1016/S0895-9811(97)00005-9

MATTHEW W. D. 1916. — A marsupial from the Belly River Cretaceous. *Bulletin of the American Museum of Natural History* 35: 477-500.

MENG J., HU Y., WANG Y. & LI C. 2003. — The ossified Meckel's cartilage and internal groove in Mesozoic mammaliaforms: implications to origin of the definitive mammalian middle ear. *Zoological Journal of the Linnean Society* 138: 431-448. https://doi.org/10.1046/j.1096-3642.2003.00064.x

MENG J., HU Y. & LI C. 2003. — The osteology of *Rhombomylus* (Mammalia, Glires): implications for phylogeny and evolution of Glires. *Bulletin of the American Museum of Natural History* 275: 1-247. https://doi.org/10.1206/0003-0090(2003)275<0001:TOORMG>2.0.CO;2

MONES A. 1986. — Paleovertebrata Sudamericana. Catálogo sistemático de los vertebrados fósiles de América del Sur. Parte 1. Lista preliminar y bibliográfica. *Courier Forschungsinstitut Senckenberg* 82 (3): 1-625.

MUIZON C. DE 1992. — La fauna de mamíferos de Tiupampa (Paleoceno inferior, Formación Santa Lucía), Bolivia, *in* SUAREZ R. S. (ed.), Fósiles y facies de Bolivia. Vol. I Vertebrados. *Revista Técnica de Yacimientos Petrolíferos y Fiscales de Bolivia* 12 (3-4): 575-624.

MUIZON C. DE 1994. — A new carnivorous marsupial from the Palaeocene of Bolivia and the problem of marsupial monophyly. *Nature* 370: 208-211. https://doi.org/10.1038/370208a0

MUIZON C. DE 1998. — *Mayulestes ferox*, a borhyaenoid (Metatheria, Mammalia) from the early Palaeocene of Bolivia. Phylogenetic and palaeobiologic implications. *Geodiversitas* 20 (1): 19-142.
MUIZON C. DE 1999. — Marsupial skulls from the Deseadan (late Oligocene) of Bolivia and phylogenetic analysis of the Borhyaenoidea (Marsupialia, Mammalia). *Geobios* 32 (3): 483-509. https://doi.org/10.1016/S0016-6995(99)80022-9
MUIZON C. DE & ARGOT C. 2003. — Comparative anatomy of the didelphimorph marsupials from the early Palaeocene of Bolivia (*Pucadelphys*, *Andinodelphys*, and *Mayulestes*). Palaeobiologic implications, *in* JONES M. DICKMAN C. & ARCHER M. (eds), *Predators with Pouches. The Biology of Carnivorous Marsupials*. CSIRO Publishing, Sydney: 42-63.
MUIZON C. DE & LANGE-BADRÉ B. 1997. — Carnivorous dental adaptations in marsupials and placentals and phylogenetical reconstruction. *Lethaia* 30 (4): 351-366. https://doi.org/10.1111/j.1502-3931.1997.tb00481.x
MUIZON C. DE, CIFELLI R. L. & CÉSPEDES-PAZ R. 1997. — The origin of the dog-like borhyaenoid marsupials of South America. *Nature* 389: 486-489. https://doi.org/10.1038/39029
MUIZON C. DE, GAYET M., LAVENU A., MARSHALL L. G., SIGE B. & VILLARROEL C. 1983. — Late Cretaceous vertebrates including mammals from Bolivia. *Geobios* 16 (6): 747-753. https://doi.org/10.1016/S0016-6995(83)80091-6
MUIZON C. DE, BILLET G., ARGOT C., LADEVÈZE S. & GOUSSARD F. 2015. — *Alcidedorbignya inopinata,* a basal pantodont (Eutheria, Mammalia) from the early Palaeocene of Bolivia: anatomy, phylogeny, and palaeobiology. *Geodiversitas* 37 (4): 397-634. https://doi.org/10.5252/g2015n4a1
MUIZON C. DE, LADEVÈZE S. & CESPEDES R. 2018 (in press). — The beginning of the age of therian mammals in South America: Tiupampa, a transition between Northern and Southern worlds in the basal Paleocene, *in* ROSENBERGER A. & TEJEDOR M. (eds), *Origins and Evolution of Cenozoic South American Mammals*. Springer Verlag, New York (in press).
MYERS T. J. 2001. — Marsupial body mass prediction. *Australian Journal of Zoology* 49: 99-118. https://doi.org/10.1071/ZO01009
NESSLINGER C. L. 1956. — Ossification centers and skeletal development in the postnatal Virginia opossum. *Journal of Mammalogy* 37: 382-394. https://doi.org/10.2307/1376739
NIXON K. 2008. — WinClada, version 1.00.08. Computer program published by the author, Ithaca, New York, USA.
PATTERSON B. & MARSHALL L. G. 1976. — The Deseadan, Early Oligocene Marsupialia of South America. *Fieldiana Geology* 41 (2): 37-100. https://biodiversitylibrary.org/page/2853620
PATTERSON B. 1965. — The auditory region of the borhyaenid marsupial *Cladosictis*. *Breviora* 217: 1-9. https://biodiversitylibrary.org/page/4312642
PAULA COUTO C. DE 1952. — Fossil mammals from the beginning of the Cenozoic in Brazil: Condylarthra, Litopterna, Xenungulata, and Astrapotheria. *Bulletin of the American Museum of Natural History* 99: 355-394. http://hdl.handle.net/2246/417
PETTER G. & HOFFSTETTER R. 1983. — Les marsupiaux du Déséadien (Oligocène supérieur) de Salla (Bolivie). *Annales de Paléontologie* 69 (3): 175-234.
RIGGS E. S. 1934. — A new marsupial saber-tooth from the Pliocene of Argentina and its relationships to other South American predacious marsupials. *Transactions of the American Philosophical Society*, n.s., 24 (1): 1-32. https://doi.org/10.2307/3231954
ROUGIER G. W. & WIBLE J. R. 2006. — Major changes in the mammalian ear region and basicranium, *in* CARRANO M. T., GAUDIN T. J., BLOB R. W. & WIBLE J. R. (eds), *Amniote Paleobiology: Perspective on the Evolution of Mammals, Birds, and Reptiles*. University of Chicago Press, Chicago: 269-311.
ROUGIER G. W., DAVIS B. M. & NOVACEK M. J. 2015. — A deltatheroidan mammal from the upper Cretaceous Baynshiree Formation, eastern Mongolia. *Cretaceous Research* 52:167-177. https://doi.org/10.1016/j.cretres.2014.09.009
ROUGIER G. W., WIBLE J. R. & HOPSON J. A. 1992. — Reconstruction of the cranial vessels in the Early Cretaceous mammal *Vincelestes neuquenianus*: implications for the evolution of the mammalian cranial vascular system. *Journal of Vertebrate Paleontology* 12: 188-216. https://doi.org/10.1080/02724634.1992.10011449
ROUGIER G. W., WIBLE J. R. & NOVACEK M. J. 1998. — Implications of *Deltatheridium* specimens for early marsupial history. *Nature* 396: 459-463. https://doi.org/10.1038/24856
ROUGIER G. W., WIBLE J. R. & NOVACEK M. J. 2004. — New specimen of *Deltatheroides cretacicus* (Metatheria, Deltatheroidea) from the Late Cretaceous of Mongolia. *Bulletin of the Carnegie Museum of Natural History* 36: 245-266. https://doi.org/10.2992/0145-9058(2004)36[245:NSODCM]2.0.CO;2
RUF I., LUO Z.-X., WIBLE J. R. & MARTIN T. 2009. — Petrosal anatomy and inner ear structures of the Late Jurassic *Henkelotherium* (Mammalia, Cladotheria, Dryolestoidea): insight into the early evolution of the ear region in cladotherian mammals. *Journal of Anatomy* 214: 679-693. https://doi.org/10.1111/j.1469-7580.2009.01059.x
SÁNCHEZ-VILLAGRA M. R. & SMITH K. K. 1997. — Diversity and evolution of the marsupial mandibular angular process. *Journal of Mammalian Evolution* 4: 119-144. https://doi.org/10.1023/A:1027318213347
SELVA C. & LADEVÈZE S. 2017. — Computed microtomography investigation of the skull of Cuvier's famous 'opossum' (Marsupialiformes, Herpetotheriidae) from the Eocene of Montmartre. *Zoological Journal of the Linnean Society* 180 (3): 672-693. https://doi.org/10.1111/zoj.12495
SEMPERE T., BUTLER R. L., & MARSHALL L. G. 1997. — Stratigraphy and chronology of the Upper Cretaceous-Lower Paleogene strata in Bolivia and northwest Argentina. *Geological Society of America Bulletin* 109 (6): 709-727. https://doi.org/10.1130/0016-7606(1997)109<0709:SACOUC>2.3.CO;2
SIGÉ B., ARCHER M., CROCHET J.-Y., GODTHELP H., HAND S. & BECK R. 2009. — *Chulpasia* and *Thylacotinga*, late Paleocene-earliest Eocene trans-Antarctic Gondwanan bunodont marsupials: new data from Australia. *Geobios* 42: 813-823. https://doi.org/10.1016/j.geobios.2009.08.001
SIGOGNEAU-RUSSELL D., DASHZEVEG D. & RUSSELL D. E. 1992. — Further data on *Prokennalestes* (Mammalia, Eutheria *inc. sed.*) from the Early Cretaceous of Mongolia. *Zoologica Scripta* 21: 205-209. https://doi.org/10.1111/j.1463-6409.1992.tb00322.x
SIMPSON G. G. 1928 — Mesozoic Mammalia. XII. The internal mandibular groove of Jurassic mammals. *American Journal of Science* 15 (90): 461-470. https://doi.org/10.2475/ajs.s5-15.90.461
SIMPSON G. G. 1935. — Descriptions of the oldest known South American mammals from the Rio Chico Formation. *American Museum Novitates* 793: 1-25. http://hdl.handle.net/2246/2125
SINCLAIR W. J. 1906. — Mammalia of the Santa Cruz Beds: Marsupialia. *Reports of the Princeton University Expeditions to Patagonia* 4 (3): 333-460. https://biodiversitylibrary.org/page/51838575
SOLÉ F. & LADEVÈZE S. 2017. — Evolution of the hypercarnivorous dentition in mammals (Metatheria, Eutheria) and its bearing on the development of tribosphenic molars. *Evolution & Development* 19 (2): 56-68. https://doi.org/10.1111/ede.12219
SPOOR F., GARLAND T., KROVITZ G., RYAN T. M., SILCOX M. T. & WALKER A. 2007. — The primate semicircular canal system and locomotion. *Proceedings of the National Academy of Sciences* 104 (26): 10808-10812. https://doi.org/10.1073/pnas.0704250104
SPRAIN C. J., RENNE P. R., WILSON G. P. & CLEMENS W. A. 2015. — High-resolution chronostratigraphy of the terrestrial Cretaceous-Paleogene transition and recovery interval in the Hell Creek region, Montana. *Geological Society of America Bulletin* 127: 393-409. https://doi.org/10.1130/B31076.1
SUAREZ C., FORASIEPI A. M., GOIN F. J. & JARAMILLO C. 2015. — Insights into the Neotropics prior to the Great American Biotic Interchange: new evidence of mammalian predators from the Miocene of Northern Colombia. *Journal of Vertebrate Paleontology* 36 (1): e1029581. https://doi.org/10.1080/02724634.2015.1029581

SZALAY F. S. & TROFIMOV B. A. 1996. — The Mongolian Late Cretaceous *Asiatherium*, and the early phylogeny and paleobiogeography of Metatheria. *Journal of Vertebrate Paleontology* 16 (3): 474-509. https://doi.org/10.1080/02724634.1996.10011335

SWOFFORD D. L. 2002. — *PAUP*: Phylogenetic analysis using parsimony (and other methods), version 4.0b1.0*. Sunderland, Massachusetts: Sinauer.

THEWISSEN J. G. M. 1989. — Mammalian frontal diploic vein and the human foramen caecum. *The Anatomical Record* 223: 242-244. https://doi.org/10.1002/ar.1092230217

TOEPLITZ C. 1920. — Bau und Entwicklung des Knorpelschädels von *Didelphis marsupialis*. *Zoologica* 27 (3): 1-84. https://biodiversitylibrary.org/page/10072646

TURNBULL W. D. & SEGALL W. 1984. — The ear region of the marsupial sabretooth, *Thylacosmilus*: influence of the sabretooth lifestyle upon it, and convergence with placental sabertooths. *Journal of Morphology* 181: 239-270. https://doi.org/10.1002/jmor.1051810302

TURNBULL W. D. 1970. — Mammalian masticatory apparatus. *Fieldiana Geology* 18 (2): 149-356. https://biodiversitylibrary.org/page/4357533

URBAN D. J., ANTHWAL N., LUO Z.-X., MAIER J. A., SADIER A., TUCKER A. S. & SEARS K. E. 2017. — A new developmental mechanism for the separation of the mammalian middle ear ossicles from the jaw. *Proceedings of the Royal Society of London, B* 284: 20162416. https://doi.org/10.1098/rspb.2016.2416

VANDENBERGHE N., HILGEN F. J., SPEIJER R. P., WITH CONTRIBUTION BY OGG J. G., GRADSTEIN F. M., & HAMMER O. ON THE MAGNETOCHRONOLOGY, BIOCHRONOLOGY AND THE TIME SCALE, AND BY HOLLIS C. J. & HOOKER J. J. ON THE BIOSTRATIGRAPHY. 2012. — The Paleogene period, *in* GRADSTEIN F. M., OGG J. G. SCHMITZ M. D. & OGG G. M. (eds), *The Geological Time Scale 2012*. Vol. 2 Chapter 28, Oxford: 855-921.

VILLARROEL C. & MARSHALL L. G. 1982. — Geology of the Deseadan (Early Oligocene) age estratos Salla in the Salla-Luribay Basin, Bolivia, with description of new Marsupialia, *in* BUFFETAUT E., JANVIER P., RAGE J.-C., & TASSY P. (eds), *Phylogénie et paléogéographie*. *Geobios*, Mémoire spécial 6: 201-212. https://doi.org/10.1016/S0016-6995(82)80114-9

VOSS R. S. & JANSA S. A. 2003. — Phylogenetic studies on didelphid marsupials II. Nonmolecular data and new IRBP sequences: separate and combined analyses of didelphine relationships with denser taxon sampling. *Bulletin of the American Museum of Natural History* 276: 1-82. https://doi.org/10.1206/0003-0090(2003)276<0001:PSODMI>2.0.CO;2

VOSS R. S. & JANSA S. A. 2009. — Phylogenetic relationships and classification of didelphid marsupials, an extant radiation of New World metatherian mammals. *Bulletin of the American Museum of Natural History* 322: 1-177. https://doi.org/10.1206/322.1

VULLO R., GHEERBRANT E., MUIZON C. DE, & NÉRAUDEAU D. 2009. — The oldest modern therian mammal from Europe and its bearing on stem marsupial paleobiogeography. *Proceedings of the National Academy of Sciences of the United States of America* 106 (47): 19910-19915. https://doi.org/10.1073/pnas.0902940106

WIBLE J. R. 1987. — The eutherian stapedial artery: character analysis and implications for superordinal relationships. *Zoological Journal of the Linnean Society* 91:107-135. https://doi.org/10.1111/j.1096-3642.1987.tb01725.x

WIBLE J. R. 1990. — Petrosals of Late Cretaceous marsupials from North America, and a cladistic analysis of the petrosal in therian mammals. *Journal of Vertebrate Paleontology* 10 (2): 183-205. https://doi.org/10.1080/02724634.1990.10011807

WIBLE J. R. 2003. — On the cranial osteology of the short-tailed opossum *Monodelphis brevicaudata* (Marsupialia, Didelphidae). *Annals of the Carnegie Museum* 72 (3): 137-202. https://biodiversitylibrary.org/page/52469617

WIBLE J. R. 2008. — On the cranial osteology of the Hispaniolan solenodon, *Solenodon paradoxus*, Brandt, 1833 (Mammalia, Lipotyphla, Solenodontidae). *Annals of the Carnegie Museum* 77 (3): 321-402. https://doi.org/10.2992/0097-4463-77.3.321

WIBLE J. R. & HOPSON J. A. 1993. — Basicranial evidence for early mammal phylogeny, *in* SZALAY F. S., NOVACEK M. J. & MCKENNA M. C. (eds), *Mammal Phylogeny: Mesozoic Differentiation, Multituberculates, Monotremes, Early Therians, and Marsupials*. Springer-Verlag, New York: 45-62. https://doi.org/10.1007/978-1-4613-9249-1_5

WIBLE J. R. & HOPSON J. A. 1995. — Homologies of the prootic canal in mammals and nonmammalian cynodonts. *Journal of Vertebrate Paleontology* 15: 331-356. https://doi.org/10.1080/02724634.1995.10011233

WIBLE J. R. & GAUDIN T. J. 2004. — On the cranial osteology of the yellow armadillo *Euphractus sexcinctus* (Dasypodidae, Xenarthra, Placentalia). *Annals of Carnegie Museum* 73: 117-196. https://biodiversitylibrary.org/page/52457342

WIBLE J. R. & ROUGIER G. W. 2000. — Cranial anatomy of *Kryptobaatar dashzevegi* (Mammalia, Multituberculata), and its bearing on the evolution of mammalian characters. *Bulletin of the American Museum of Natural History* 247: 1-124. https://doi.org/10.1206/0003-0090(2000)247<0001:CAOKDM>2.0.CO;2

WIBLE J. R., ROUGIER G. W., NOVACEK M. J. & ASHER R. J. 2009. — The eutherian mammal *Maelestes gobiensis* from the Late Cretaceous of Mongolia and the phylogeny of Cretaceous Eutheria. *Bulletin of the American Museum of Natural History* 327: 1-123. https://doi.org/10.1206/623.1

WIBLE J. R., ROUGIER G. W., NOVACEK M. J. & MCKENNA M. C. 2001. — Earliest eutherian ear region: a petrosal of *Prokennalestes* from the Early Cretaceous of Mongolia. *American Museum Novitates* 3322: 1-44. http://hdl.handle.net/2246/2939

WILLIAMSON T. E., BRUSATTE S. L. & WILSON G. P. 2014. — The origin and early evolution of the metatherian mammals: the Cretaceous record. *Zookeys* 465: 1-76. https://doi.org/10.3897/zookeys.465.8178

WILSON G. P., EKDALE E. G., HOGANSON J. W., CALEDE J. J. & VANDER LINDEN A. 2016. — A large carnivorous mammal from the Late Cretaceous and the North American origin of marsupials. *Nature Communications* 7: 13734. https://doi.org/10.1038/ncomms13734 https://doi.org/10.1038/ncomms13734

WOODBURNE M. O., GOIN F. J., BOND M., CARLINI A. A., GELFO J. N., LOPEZ G. M., IGLESIAS A. & ZIMICZ A. N. 2014a. — Paleogene land mammal faunas of South America; a response to global climatic changes and indigenous floral diversity. *Journal of Mammalian Evolution* 21: 1-73. https://doi.org/10.1007/s10914-012-9222-1 https://doi.org/10.1007/s10914-012-9222-1

WOODBURNE M. O., GOIN F. J., RAIGEMBORN M. S., HEIZLER M., GELFO J. N. & OLIVEIRA E. V. 2014b. — Revised timing of the South American Early Paleogene land mammal ages. *Journal of South American Earth Sciences* 54: 109-119. https://doi.org/10.1016/j.jsames.2014.05.003

WROE S. 1997 — A reexamination of proposed morphology-based synapomorphies for the families of Dasyuromorphia (Marsupialia). 1. Dasyuridae. *Journal of Mammalian Evolution* 4 (1): 19-52. https://doi.org/10.1023/A:1027379610196

WROE S., EBACH M., SHANE A., MUIZON C. DE & MUIRHEAD J. 2000. — Cladistic analysis of dasyuromorphian (Marsupialia) phylogeny using cranial and dental characters. *Journal of Mammalogy* 81: 1008-1024. https://doi.org/10.1644/1545-1542(2000)081<1008:CAODMP>2.0.CO;2

*Submitted on 15 January 2018;*
*accepted on 2 April 2018;*
*published on 23 August 2018.*

# APPENDICES

APPENDIX 1. — Character list, established mainly on the basis of that of Forasiepi *et al.* (2015). However, several charactrers have been re-defined and when necessary, comments have been added to explain our concept. As mentioned in the Materials and Methods section, 82 characters are new. Therefore, this character list is significantly different from that of Forasiepi *et al.* (2015) that was used as a starting point. When the characters are identical to those of Forasiepi *et al.* (2015), it bears the number of Forasiepi et al.'s list as follows: (F000). When the character states have been modified or when some rewording has been necessary, it is indicated as follows: (F000 modified). We refer to Forasiepi *et al.* (2015) and to Forasiepi (2009) for the credit on the original mention of these characters. Characters: **1**-**103**, dental characters; **103**-**118**, mandibular characters; **119**-**242**, cranial characters; **243**-**364**, post-cranial characters.

## DENTAL CHARACTERS

1. — **Number of upper incisors (F108)**: five (0); four (1); three (2); two or less (3). **Ordered**.

*Comment: in the sparassodonts and Dasyuromorphia with four incisors, it is probable that the I5 has been lost (Forasiepi 2009; Hershkovitz 1995). The sparassodonts with three upper incisors probably also lost the I1 (see Forasiepi 2009: 149, 150 and references therein for a discussion on the homologies of metatherian upper incisors).*

2. — **Size of extra-alveolar portion of root of I1 (F109, modified)**: longer than on others incisors and longer than crown; (the length of the extra-alveolar root is greater than that of the crown) (0); as long as on other incisors and as long as crown (1).

*Comment: This character corresponds in part to the character formulated by several authors as "size (or shape) of first upper incisor" (Muizon* et al. *1997; Rougier* et al. *1998; Wroe* et al. *2000; Luo* et al. *2003.). However, we consider that this formulation is imprecise and often erroneous in stating that the I1 is enlarged. In fact, in most cases the crown of I1 is not significantly larger than that of the other incisors, but in some cases, it is only slightly longer. The most characteristic feature is the length of the extra-alveolar portion of the root which is notably long. The sparassodonts with three incisors are scored inapplicable because the I1 is assumed to be missing (see character 1).*

3. — **Implantation of the first upper incisors in anterior view**: incisors parallel (0); roots diverging dorsally (1).

4. — **Diastema between 11 and I2**: Absent (0); Present (1).

5. — **Size of I4 vs I3 (F110)**: I4 subequal to I3 (0); I4 larger (1). Changes in scorings of Forasiepi *et al.* (2015): *Andinodelphys* ? > 0.

6. — **Size of I3 vs I2**: I3 > I2 (0); I3 = I2 (1); I3 < I2 (2). **Ordered**.

7. — **Size of I5 vs I4 (F111)**: I5 subequal to or larger than I4 (0); I5 smaller than I4 (1); I5 lost (2). Changes in scorings of Forasiepi *et al.* (2015): *Andinodelphys* ? > 1. **Ordered**.

8. — **Shape of upper incisors**: peg-shaped (0); spatulate (1).

9. — **Upper incisor arcade (F112 modified)**: parabolic (0); slightly convex anteriorly (1); transverse (2); not an arcade, compressed transversely with incisors telescoped (3). **Ordered**.

10. — **Number of lower incisors (F113)**: four (0); three (1); less than three (2). **Ordered**.

11. — **Staggered i3 (F114)**: absent (0); present (1).

12. — **Lower incisors procumbent**: present (0); absent (1).

13. — **Lower canine procumbent**: absent (0); present (1).

14. — **Shape of canines (F115)**: small: same height or lower than apex of molars protoconid (0); large: taller than apex of molars protoconid (1); saber-like upper canines (2). **Ordered**.

15. — **Pulp cavity of canines (F116)**: closed in adults (0); open in upper canines only (1); open in upper and lower canines (2). **Ordered**.

16. — **Roots of canine (F117)**: smooth (0); corrugated (1).

17. — **Number of roots of upper canine**: two (0); one (1) (Rougier *et al.* 1998).

18. — **Number of postcanine tooth family**: eight or more (0); seven or fewer (1) (Rougier *et al.* 1998, modified).

19. — **Number of premolars (F118)**: five (0); four (1); three (2), two or fewer (3) (Rougier *et al.* 1998). **Ordered**.

20. — **Orientation of first upper and lower premolars relative to tooth row (F119 modified)**: parallel (0); oblique (1); transverse (2). **Ordered**.

21. — **First upper premolar strongly asymmetrical in lateral view**: absent or weak (0); distinctly present (1).

*Comment: in state (0), the apex of the tooth is roughly above the space between the two roots, or the middle of the crown when the tooth is single-rooted. In state (1), the apex of the tooth is above the anterior root, or above anterior edge of the crown when the tooth is single-rooted.*

22. — **Diastema anterior to first upper premolar (F120)**: absent (0); present (1).

23. — **Diastema posterior to first upper premolar (F121)**: absent (0); present (1).

24. — **Diastema posterior to first lower premolar (F122)**: absent (0); present (1).

APPENDIX 1. — Continuation.

25. — **Shape of premolars (F123):** transversely compressed and uninflated (0); bulbous (1)

26. — **Ultimate premolar protocone**: absent (0); small posterolingual bulge or cusp (1); distinct protocone with basin (2). **Ordered**.

27. — **Size of penultimate lower premolar (F125 modified)**: smaller than ultimate premolar (0); subequal to ultimate premolar (1); larger than ultimate premolar (2). **Ordered**.

28. — **Change in height of the lower premolars (F126)**: abrupt change in size between antepenultimate premolar and penultimate-ultimate premolar (0); abrupt change in size between antepenultimate-penultimate premolar and ultimate premolar (1).

29. — **Roots of lower premolars (F127)**: not inflated, as wide as crown (0); bulbous on only one premolar (1); bulbous on all premolars and some molars (2). **Ordered**.

30. — **Anterobasal cusp or cingulid on penultimate premolar (F128 modified)**: absent (0); present (1).

31. — **Ultimate lower premolar symmetry of main cusp (F129)**: absent: anterior edge of cusp more convex than posterior edge (0); present: both edges similar in curvature (1).

32. — **Timing of eruption of ultimate upper and lower premolars relative to ultimate or penultimate upper and lower molars (F130)**: ultimate upper and lower premolars with penultimate or antepenultimate upper and lower molars (0); ultimate upper and lower premolars with ultimate upper and lower molars (1). Changes in scorings of Forasiepi *et al.* (2015): *Mayulestes*: 1 > ?.

33. — **Size of molars (upper and lower) increases posteriorly (F132)**: moderate (0); marked (1). Changes in scorings of Forasiepi *et al.* (2015): *Sallacyon* ? > 1.

*Comment: concerning the upper molars, the ultimate molar is not considered in the size increase.*

34. — **Width (labiolingual) of ultimate relative to penultimate upper molar (F133 modified)**: narrower (0); subequal or wider (1).

35. — **Width of stylar shelf (on penultimate molar) (F151 modified)**: uniform in width (0); slightly reduced labial to paracone (1); strongly reduced labial to paracone (2); vestigial to absent (3). **Ordered**.

36. — **Stylar shelf vs tooth width (on penultimate or antepenultimate molar) (F151 modified)**: 50% of transverse width or more (0); less than 50% of transverse width (1).

37. — **Deep ectoflexus (F152 modified)**: present on one or more teeth (0); absent on any tooth (1). See Ladevèze & Muizon (2007: ch. 20) for comments on the definition of this character as defined here vs that of Rougier *et al.* (1998) and Forasiepi *et al.* (2015).

*Comment: the depth of the ectoflexus has been shown to be highly variable for the same dental locus in some fossil and extant metatherians (e.g.* Pucadelphys andinus, Peratherium elegans, Marmosa murina; *see Ladevèze* et al. *2011, 2012).*

38. — **Postmetacrista (on antepenultimate or penultimate molar) (F148 modified)**: subequal or shorter than preparacrista (0); distinctly longer than preparacrista (1).

39. — **Carnassial notch in postmetacrista at posterolabial base of metacone**: absent (0); present (1).

40. — **Stylar cusp A (F153)**: distinct but smaller than B (0); subequal to larger than B (1). Changes in scorings of Forasiepi *et al.* (2015): *Sipalocyon*, *Borhyaena*, *Arctodictis*, *Australohyaena* – > 1; *Sallacyon*, *Callistoe* 0 > 1; *Thylacosmilus* 0 > –; *Thylacinus* 0 > 1.

41. — **Stylar cusp B (F154 modified)**: present but smaller than paracone (0); subequal to or approaching the size of the paracone (1); vestigial to absent (2).

42. — **Anterolabial cingulum on upper molars**: absent (0); present (1).

*Comment: stylar cusps A and B are present but poorly individualized and integrated in a variably developed anterolabial cingulum.*

43. — **Stylar cusp C (F155)**: absent or tiny (0); present (1). Changes in scorings of Forasiepi *et al.* (2015). *Patene* 1 > 0.

*Comment: this feature has been evidenced as highly variable in some fossil and extant metatherians (e.g.* Pucadelphys andinus, Peratherium elegans, Marmosa murina*; see Ladevèze* et al. *2011, 2012).*

44. — **Relative size of Stylar cusp B and D**: B smaller or subequal to D (0); B larger than D (1).

45. — **Stylar cusp E (F157)**: present and distinct (0); indistinct or tiny (1).

46. — **Relative size of paracone vs metacone (on penultimate or antepenultimate molar) (F134 modified)**: subequal or slightly larger (0); slightly smaller in volume and height (*c.* 10%) (1); distinctly smaller in volume and height (*c.* 30% smaller) (2); much smaller (*c.* 50% or less) (3); absent or simple bulge on the anterior edge of metacone (4). **Ordered**.

47. — **Shape of paracone and metacone (F136)**: conical (0); triangular (flat labial face) (1).

Appendix 1. — Continuation.

48. — **Metacone and paracone contact (F137 modified)**: separated – i.e., point of junction of premetacrista and postparacrista approximately at the level of the floor of trigon and/or stylar shelf basin (0); adjoined at base (on, at least, half of their height) – i.e., point of junction of premetacrista and postparacrista well below the level of the floor of the trigon and stylar shelf basin (1); adjoined on most of their height, apices of cusps only are separated (2). **Ordered**.

*Comment: see Fig. 10 for the condition in* Allqokirus.

49. — **Metacone on last molar (F139)**: present and distinct (0); extremely reduced (1); absent (2). Changes in scorings of Forasiepi *et al.* (2015): *Prothylacinus* 1 > 2. **Ordered**.

50. — **Centrocrista (F138)**: straight (0); V-shaped (1). Changes in scorings of Forasiepi *et al.* (2015): *Thylacinus* – > 0.

51. — **Relative lengths of preparacristae of penultimate and ultimate molars (F147)**: preparacrista of ultimate molar shorter than that of penultimate molar (0); preparacrista of ultimate molar subequal to longer than that of penultimate molar (1). Changes in scorings of Forasiepi *et al.* (2015): *Cladosictis* 0 > 1.

52. — **Orientation of preparacrista (on penultimate or antepenultimate molar) (F146 modified)**: transverse (0); anterolabial (1).

53. — **Conules (F143)**: present (0); absent (1).

54. — **Conules wing-like cristae (F144)**: present (0); absent (1).

55. — **Conules labiolingual position (on penultimate or antepenultimate molar) (F145)**: at or lingual to mid-point between protocone and para/metacone (0); closer to para/metacone (1).

56. — **Trigon basin**: absent (0); present (1).

57. — **Protocone size (on penultimate or antepenultimate molar) (F141, modified)**: absent or very small (0); small and anteroposteriorly narrow (1); anteroposteriorly expanded (2); with posterolingual projection (3). **Ordered**.

58. — **Protocone height (F142 modified)**: approximately half the height of metacone or less (0); only slightly lower than metacone (1); almost the size of metacone or higher (2). **Ordered**.

59. — **Roots on ultimate molar (F140)**: 3 (0); 2 or 1 (1).

60. — **Paracingulum (on penultimate or antepenultimate molar) (F149)**: continuous between stylar margin and paraconule (0); interrupted between stylar margin and paraconule (1); absent (2). **Ordered**.

61. — **Postprotocrista labial extension**: does not extend labially past the base of the metacone (0); extends labially past the base of metacone (1).

62. — **Precingulum (on penultimate or antepenultimate molar)**: absent or weak (0); present (1).

63. — **Postcingulum (on penultimate or antepenultimate molar) (F150)**: absent or weak (0); present (1).

64. — **Size of ultimate lower molar (F158)**: subequal or smaller in height and/or length than penultimate molar (0); larger in height and/or length than penultimate molar (1). Changes in scorings of Forasiepi *et al.* (2015): *Pucadelphys, Andinodelphys* 1 > 0.

65. — **Ventral extent of the enamel above posterior root lower than above anterior root on labial side of the crown of lower molars (F159)**: absent (0); present only on first and second molars and weakly developed (1); on the first three molars and strongly developed (2).

66. — **Lingual opening of trigonid basin on penultimate molar when possible (F162 modified)**: wide open: angle between protocristid (or postprotocristid when metaconid is lost) and paracristid more than 45°; (0); less open: angle proto-paracristid between *c.* 45 and 15° (1); anteroposteriorly compressed: cristids subparallel (2). **Ordered**.

67. — **Trigonid basin floor**: sub-horizontal (0); sloping lingually (1); lost (2).

68. — **Trigonid proportions**: wider than long (0); as wide as long (1); longer than wide (2). **Ordered**.

69. — **Trigonid height (on penultimate or antepenultimate molar) (F167 modified)**: much higher than talonid (more than twice) (0); moderately higher than talonid (twice or less) (1).

*Comment: when the talonid is extremely reduced or lost this character is coded as inapplicable.*

70. — **Trigonid vs talonid width (on penultimate or antepenultimate molar) (F166)**: wider than talonid (0); as wide as talonid (1); narrower than talonid (2). Changes in scorings of Forasiepi *et al.* (2015): *Pucadelphys* 2 > 1; *Andinodelphys* 2 > 0; *Mayulestes* 1 > 0.

*Comment: taxa with incomplete trigonid (lack of metaconid) are scored as inapplicable.*

71. — **Protoconid labial expansion**: the labial edge of the protoconid at mid-height is strongly convex, protruding labially and overhangs the base of the crown; as a consequence, the apex and base of the trigonid are more lingual than the mid-height region of the cusp and the trigonid is therefore wider at mid-height than at its base (see Fig. 14); present (0); absent (1).

Appendix 1. — Continuation.

*Comment: state (1) corresponds to a protoconid regularly widening towards the base of the cusp, which is therefore wider at its base than at mid-height.*

72. — **Trigonid vs talonid length (on penultimate or antepenultimate molar) (F165)**: subequal in length to talonid (0); longer than talonid (1); shorter than talonid (2). Changes in scorings of Forasiepi *et al.* (2015): *Mayulestes* 0 > 1. **Ordered**.

73. — **Talonid**: small heel (0); multicusped basin (1).

74. — **Proportions of talonid basin (F175)**: longer than wide (0); as long as wide (1); wider than long (2). Changes in scorings of Forasiepi *et al.* (2015): *Pucadelphys* ? > 1. **Ordered**.

75. — **Relative size and shape of talonid of ultimate vs penultimate molar (F160)**: talonid of ultimate molar similar to anterior tooth (0); talonid of ultimate molar reduced and narrower than on anterior tooth (1). Changes in scorings of Forasiepi *et al.* (2015): *Andinodelphys* 0 > 1.

76. — **Paraconid position (on penultimate or antepenultimate molar) (F163 modified)**: at anterior edge of the trigonid (0); at anterolingual angle of trigonid (1).

*Comment: the wording of this character considers the position of the paraconid on the trigonid rather than the metaconid as in Character 163 of Forasiepi* et al. *(2015). Because, implicitly, it is the relative position of the two cusps, which is considered, this formulation gives identical results in term of scoring. We prefer to refer to the paraconid because the transverse position of this cusp varies considerably in therian lower molar morphology evolution, while that of the metaconid is less variable. Furthermore, the position of the lingual edge of the metaconid is displaced labially when the metaconid is reduced, a bias which is avoided if considering the paraconid.*

77. — **Number of cusps on last molar talonid**: three (0); two (1); one (2). **Ordered**.

78. — **Vertical keel (ridge) at anterolingual angle of paraconid labially bordered by hypoconulid notch (vertical sulcus at lingual end of precingulid) (F172)**: absent (0); present (1). Changes in scorings of Forasiepi *et al.* (2015): *Deltatheridium* 0 > 1.

79. — **Orientation of protocristid (or postprotocristid) vs anteroposterior axis of the molar (on penultimate or antepenultimate molar) (F164 modified)**: transverse or slightly oblique (i.e., less than 45°) (0); strongly oblique (i.e., more than 45°) or parallel (1).

80. — **Paraconid elongated with anterior projection of the paraconid keel (ridge) mostly in the ventral half of the cusp**: absent (0); present (1). (Marshall *et al.* 1990, modified).

*Comment: as a consequence of the anterior projection of the paraconid keel the anterior edge of the cusp is markedly convex.*

81. — **Precingulid (F173)**: on protoconid and paraconid (0); on paraconid (1); absent (2). **Ordered**.

82. — **Height of protoconid (Hpo) relative to length of ultimate or penultimate lower molar (Lm)**: Hpo/Lm < 0.9 (0); Hp/Lm > 0.9 (1).

83. — **Protoconid height in trigonid (F171)**: tallest cusp of trigonid (0); sub-equal to para- and/or metaconid (1).

84. — **Height of metaconid vs paraconid (on penultimate molar) (F170 modified)**: higher (0); subequal (1); lower (2). **Ordered**.

*Comment: taxa in which metaconid is lost are scored inapplicable.*

85. — **Volume of the metaconid vs paraconid (on penultimate molar), in occlusal and lingual views**: larger (0); subequal (1); smaller (2).

*Comment: taxa in which metaconid is lost are scored inapplicable.*

86. — **Metaconid on first molar (F168)**: present (0); absent (1).

87. — **Metaconid on molars between the first and last molar (F169 modified)**: present (0); present, but extremely reduced as a tiny cuspule at the posterior base of the protoconid (1); absent (2).

88. — **Metaconid on ultimate lower molar**: present (0); vestigial or absent (1)

89. — **Relative lengths of para- and protocristid**: subequal (0); paracristid > protocristid (1); protocristid > paracristid (2).

90. — **Anterior end of cristid obliqua (F184)**: beneath carnassial notch (0); lingual to carnassial notch (1); labial to carnassial notch (2).

*Comment: taxa which lack a metaconid also lack a carnassial notch and are scored as unapplicable.*

91. — **Carnassial notch in cristid obliqua (F186)**: absent (0); present (1). Changes in scorings of Forasiepi *et al.* (2015): *Mayulestes* 0 > 1.

92. — **Hypoconulid position (F180 modified)**: in median position (0); shifted lingually, close to entoconid (1); absent (2).

93. — **Hypoconulid of last molar (F181 modified)**: as tall as or lower than other talonid cusps (0); taller than other talonid cusps (1); absent (2).

94. — **Hypoconid position (F176)**: middle of labial margin of tooth (0); posterolabial angle of tooth (1); absent (2).

Appendix 1. — Continuation.

95. — **Shape of entoconid (F177)**: conical (0); transversely compressed (1); vestigial to absent (2). Changes in scorings of Forasiepi *et al.* (2015): *Mayulestes* 0 > 0,1; *Patene* 1 > 0,1; *Sminthopsis* 0 > 2.

96. — **Relative height of entoconid (F178)**: lower than hypoconid (0); subequal to taller than hypoconid (1); absent (2). Changes in scorings of Forasiepi *et al.* (2015): *Andinodelphys* 0 > 1.

97. — **Position of entoconid relative to trigonid (on antepenultimate or penultimate molar) (F179 modified)**: at posterolingual corner of tooth (in posterior half of the distance between the posterior base of trigonid and posterior margin of tooth) (0); between posterior edge of trigonid and posterior margin of tooth (mid-way or in anterior half of the distance between the posterior base of trigonid and posterior margin of tooth) (1).

98. — **Entocristid (F182 modified)**: absent or weakly developed (0); well-developed and sharp (1). Changes in scorings of Forasiepi *et al.* (2015): *Patene* 0 > 1.

99. — **Posthypocristid**: oblique relatively to long axis of tooth (0); transverse relative to long axis of tooth (1).

100. — **Hypoflexid (F185)**: deep (*c.* 40-50% of talonid width) (0); shallow or absent (less than 40% of talonid width) (1).

101. — **Labial postcingulid (F187)**: absent (0); present (1).

102. — **Postcingulid on last molar**: present (0); absent (1).

Mandibular characters

103. — **Depth/length of the dentary below molars (F97)**: shallow (less than 0.15) (0); intermediate (between 1.5 and 2) (1); elevated (more than 2) (2). Changes in scorings of Forasiepi *et al.* (2015): *Mayulestes*: ? > 1. **Ordered**.

*Comment: in the case of* Mayulestes*, because the ramus mandibularis (vertical ramus) is missing on the only specimen known, the length of the dentary has been estimated on the basis of the position of the postglenoid process and articular condyle, when the lower tooth row of the dentary is in occlusion with the upper tooth row*.

104. — **Ventral margin of the dentary behind last molar continuous to condyle (F98)**: straight (0) or gently curved (1); angled (2).

105. — **Mandibular symphysis (F99)**: unfused (0); fused (1).

106. — **Anteroventral edge of mandibular symphysis**: slanting and forming a small angle with tooth row (< 25°) (0); less slanting, forming an angle > 25° (1).

107. — **Posteriormost mental foramen (F100)**: below last premolar or anterior (0); at last premolar/m1 embrasure (1); below first molar (2); posterior to first molar (3). Changes in scorings of Forasiepi *et al.* (2015): *Didelphis* 2,3 > 3; *Monodelphis* 1,2 > 2,3; *Sallacyon* 2,3 > 3; *Sipalocyon* 2 > 3. **Ordered**.

108. — **Masseteric fossa**: restricted dorsally by crest reaching condyle (0); extended ventral to lower margin of dentary (1), (Rougier *et al.* 1998: ch. 67).

109. — **Posterior shelf of masseteric fossa**: absent (0); present (1), (Rougier *et al.* 1998: ch. 68).

110. — **Labial mandibular foramen (F102)**: present (0); absent (1).

111. — **"Coronoid" facet**: present (0); absent (1), (Rougier *et al.* 1998: ch. 76).

112. — **Angle between coronoid process and tooth row (F104)**: subvertical between 95 and 105° (0); between 106 and 125° (1); more than 125° (2). Changes in scorings of Forasiepi *et al.* (2015): *Pucadelphys* 0 > 0,1; *Andinodelphys* 0 > 1; *Sipalocyon*, *Cladosictis* 0 > 1. **Ordered**.

*Comment: the condition in* Patene *has been measured on the left mandible of IML-PV 2618, in which the ramus mandibularis is in correct position relative to the corpus mandibularis. On the right dentary, the ramus is not in anatomical position and, in medial view, it is slightly turned clockwise. Because of this incorrect position of the ramus, the angle of the coronoid process of the right dentary is distinctly greater than on the left dentary.*

113. — **Retromolar space (F101)**: absent (0); present (1). Changes in scorings of Forasiepi *et al.* (2015): *Andinodelphys*, *Mayulestes* ? > 1.

114. — **Angular process medially inflected**: absent (0); present (1), (Rougier *et al.* 1998: ch. 73, modified).

115. — **Morphology of medially inflected angular process (F103)**: shelf-like (ASL/AL > 0.81) (0); intermediate (0.72 < ASL/AL < 0.81) (1); rod-like (ASL/AL < 0.72) (2). **ASL**, angular process shelf length; **AL**, angular process length. Changes in scorings of Forasiepi *et al.* (2015): *Pucadelphys* 0,1 > 0; *Andinodelphys* ? > 0; *Patene* ? > 0; *Lycopsis* 0,1 > ? **Ordered**.

116. — **Anteroposterior position of mandibular foramen (F105)**: posterior to mid-point of coronoid process (0); at mid-point of coronoid process (1); anterior to mid-point of coronoid process (2). Changes in scorings of Forasiepi *et al.* (2015): *Andinodelphys* ? > 1. **Ordered**.

APPENDIX 1. — Continuation.

117. — **Morphology of mandibular condyle (F106)**: subspherical (0); cylindrical (1). Changes in scorings of Forasiepi *et al.* (2015): *Andinodelphys* ? > 1; *Mayulestes* ? > 1; *Patene* ? > 1.

118. — **Condyle vertical position vs tooth row (F107)**: approximately at the same level or slightly below (0); above (1). Changes in scorings of Forasiepi *et al.* (2015): *Patene*, *Sipalocyon*, *Lycopsis* 0 > 1.

*Comment: the condition in* Patene *has been scored on the left mandible of IML-PV 2618, in which the ramus mandibularis is in correct position relative to the corpus mandibularis. On the right dentary, the ramus is not in anatomical position and, in medial view, it is slightly turned clockwise. Because of this incorrect position of the ramus, the condyle appears to be almost at the level of the tooth row, as stated by Goin* et al. *(1986). On the left dentary, in which the position of the ramus is correct, the condyle is located well above the tooth row.*

CRANIAL CHARACTERS

119. — **Length of the skull (F1)**: short (less than twice width at the level of zygomatic arch) (0); long (more than twice width at level of zygomatic arch) (1). Changes in scorings of Forasiepi *et al.* (2015): *Mimoperadectes* 1 > 0.

120. — **Length of the rostrum (F2)**: less than (or equal to) ⅓ total length of the skull (0); between ⅓ and ½ total length of the skull (1); more than ½ total length of the skull (2). Changes in scorings of Forasiepi *et al.* (2015): *Pucadelphys* 0 > 0,1; *Andinodelphys*, *Mayulestes* 0 > 1; *Sipalocyon* 1 > 0.

*Comment: the length of the rostrum of* Allqokirus *has been estimated because the only skull known (MHNC 8267) is that of a subadult individual in which the M4 and m 4 are not fully erupted. The correction applied is the length of the m4 (*c. *3.5 mm). With this correction,* Allqokirus *is scored 1 for this character.*

121. — **Expanded apex of the rostrum with concave tooth rows and lateral edges of the rostrum between canine and infraorbital foramen**: absent (0); present (1).

122. — **Width of the braincase versus maximum postorbital width (F3)**: braincase at base of zygomatic arches wider than maximum postorbital width (0); braincase narrower than maximum postorbital width (1). Changes in scorings of Forasiepi *et al.* (2015): *Didelphis* 1 > 0.

123. — **Proportions of the braincase (F4 modified)**: almost as wide as long (0); distinctly wider than long (1); longer than wide (2).

124. — **Level of the palate relative to basicranium (F5)**: palate lower than basicranium (0); palate and basicranium at the same level (1). Changes in scorings of Forasiepi *et al.* (2015): *Mayulestes* 0 > ?; *Thylacinus* 0 > 1.

125. — **Anterolateral process of the maxilla in the paracanine fossa (F6 modified)**: present: the anterolateral process of the maxilla closes the fossa laterally; the paracanine fossa is composed of the maxilla and premaxilla (0); absent: the fossa is opened laterally; the paracanine fossa is composed of the premaxilla only (1).

126. — **Paracanine fossa morphology: not extended dorsally**: longer (anteroposteriorly) than high (dorsoventrally) (0); extended dorsally: higher dorsoventrally than (or as high as) long (anteroposteriorly) (1).

127. — **Precanine notch (F7)**: absent (0); present (1).

*Comment: in dorsal or ventral view, the presence of a precanine notch results in a transverse constriction of the rostrum just anterior to the canine. The precanine notch is scored present in* Allqokirus *and* Mayulestes *because the weak but distinct concavity observed anterior to the canine is regarded as an incipient development of this character (see Figs 3 and 4).*

128. — **Lateral palatal process of the premaxilla (F8 modified)**: anterior to anterior border of canine alveolus (0); just reaches anterior border of canine alveolus (1); posterior to anterior border of canine alveolus (2). **Ordered**.

129. — **Posterior border of incisive foramen (F9)**: anterior to or just reaches anterior border of canine alveolus (0); posterior to anterior border of canine alveolus (1).

130. — **Dorsoventral position of the medial palatal process of the premaxilla (F10)**: horizontal (0); with posterior end shifted dorsally, forming an incisive fossa (1). Changes in scorings of Forasiepi *et a*l. (2015): *Mayulestes* 0 > 1.

131. — **Distinct narial tubercle or process at the anterodorsomedial angle of the premaxilla (F11)**: absent (0); present (1). Changes in scorings of Forasiepi *et al.* (2015): *Andinodelphys* ? > 1; *Herpetotherium* ? > 0.

132. — **Posterior end of the facial (posterodorsal) process of the premaxilla (F12 modified)**: above canine or anterior (0); above P1 or P2 (1); posterior to P2 (2). Changes in scorings of Forasiepi *et al.* (2015): *Sminthopsis* 2 > 1,2. **Ordered**.

133. — **Anterior parabolic protrusion of nasals, which overhangs nasal aperture (F13)**: present (anterior protrusion is approximately as long as width of the nasal at the level of anteriormost point of the nasal-premaxilla suture) (0); absent (1). Changes in scorings of Forasiepi *et al.* (2015): *Mayulestes* 0 > 1.

*Comment:* Mayulestes *has been scored 1 for this character in spite of statement by Muizon (1998: 34) that these "bones extend anteriorly beyond the anteriormost point of the nasal-premaxilla suture". In fact, this statement is biased by the distortion (dors-*

Appendix 1. — Continuation.

*oventral compression) of the specimen. The distortion has pushed the nasal ventrally and the maxillae dorsally. More important, the distortion also shows a slight anteroposterior component, which has pushed the maxillae and premaxillae posteriorly. This condition is evidenced on the posterior part of the Na-Mx suture, where the maxillae clearly overlap the nasals (in the anterolateral portion of the posterior expanded region of the nasals). In this respect, the reconstruction of Muizon (1998: fig. 6A) is clearly inaccurate. Given that, although the anterior edge of the nasals of* Mayulestes *is slightly convex anteriorly, their condition is clearly more similar to those of* Thylacinus *and* Arctodictis *than to those of* Didelphis *and* Pucadelphys*. In these taxa, the anterior extension of the nasal is at least as large as the width of the nasal at the level of the anterior end of the Nasal-Premaxilla suture. This is certainly not the case in* Mayulestes*. In contrast,* Callistoe*, in which the nasals distinctly protrude anteriorly, has been scored 0.*

134. — **Anterior end of the nasals**: V-shaped (or parabolic) (0); transverse or slightly convex anteriorly (1); notched (V-shaped posteriorly) (2). **Ordered**.

135. — **Shape of naso-frontal suture (F14 modified)**: acute W- or V-shaped (0); wide open W or posteriorly convex (1).

136. — **Nasofrontal suture with medial process of the frontals wedged between the nasals**: present (0); absent (1), (Rougier *et al.* 1998: ch. 84).

137. — **Postorbital process (F15 modified)**: absent (0); weak tuberosity (1); conspicuous protruding process (2). **Ordered**.

138. — **Orbital crests (F35)**: absent (0); present (1).

139. — **Naso-lacrimal contact (F16)**: present (0); absent (1).

140. — **Facial process of the lacrimal (F30 modified)**: large triangular and pointed anteriorly (0); small crescentic and rounded anteriorly (1).

141. — **Lacrimal tubercle (F31 modified)**: present, knob-like (0); present, crest-like (1); absent (2).

142. — **Lateral wall of ventral or lateral lacrimal foramen (F32 modified)**: distinctly anterior to medial wall (foramen exposed on face and faces laterally or posterolaterally) (0); at the same anteroposterior level as the medial wall (foramen not exposed on face and faces posteriorly) (1); intermediate (one foramen on face, the other in the orbit) (2).

143. — **Number of lacrimal foramina (F33)**: two (0); one (1).

144. — **Infraorbital foramen position (F18 modified)**: above penultimate premolar (0); above ultimate premolar (1); above M1 or posterior (2). **Ordered**.

145. — Flaring of maxillary cheek posterior to infraorbital foramen (F19): present (0); absent (1). Changes in scorings of Forasiepi *et al.* (2015): Callistoe 1 > 0.

*Comment:* Callistoe *has been scored 0 contra Forasiepi* et al. *(2015), because the holotype in ventral view present a small but distinct flaring of the maxillae behind the infraorbital foramina. Furthermore, it is noteworthy that the skull has suffered some transverse (mediolateral) compression, which suggests that the flaring was even more pronounced than the condition actually observed on the holotype.*

146. — **Angle (posterior angle) between maxilla-jugal suture and plane of the tooth row in lateral view (F17)**: more than 140° (0); between 140 and 95° (1).

147. — **Fossa for the levator labii muscle in the anterior end of the jugal**: absent (0); present mainly in the jugal (1); present mainly in the maxilla (2).

148. — **Anterior medial and lateral palatal processes of the maxilla**: both processes approximately of the same size (0); medial process much smaller than the lateral or absent (1).

149. — **Number of palatal pits independently of their size**: none (0); one (between ultimate and penultimate molar) (1); two between ultimate, penultimate and antepenultimate molars (2); two pits between first, antepenultimate, and penultimate molars (3).

150. — **Palatal vacuities (F22)**: absent (0); present (1).

151. — **Major palatine foramen (F23)**: well individualized, within maxilla and/or palatine (0); multiple small foramina in palatine and/or maxilla (1). Changes in scorings of Forasiepi *et al.* (2015): *Sallacyon* ? > 0;

152. — **Minor palatine foramen (F24 modified)**: present and complete (closed posteriorly) (0); incomplete (open posteriorly) or absent (1).

153. — **Palatal expansion with regard to ultimate molar (F25 modified)**: posterior (0); even with (1); anterior (2). **Ordered**.

154. — **Posterior palatine spine (F26 modified)**: weak or absent and posterior edge of the palate concave posteriorly (0); absent and posterior edge of the palate straight (1); prominent and posterior edge of the palate double-arched (2), (see Wible *et al.* 2009: ch. 192).

155. — **Size of foramen or groove in lateral edge of postpalatine torus**: absent (0); present and small (less than half the diameter of the minor palatine foramen or groove) (1); present and large (approximately half the diameter of the minor palatine foramen or more (2). **Ordered**.

APPENDIX 1. — Continuation.

*Comment: state (1) present in didelphids corresponds to the postpalatine torus foramen of Wible (2003: 144, fig. 9).*

156. — **Morphology of the postpalatine torus foramen**: totally or almost totally enclosed in the palatine (0); wide-open groove (the section is approximately half a circle or less) (1).

157. — **Palatine enters the posterior opening of the infraorbital canal (maxillary foramen) (F27)**: present (0); absent (1).

158. — **Position of sphenopalatine foramen (F28)**: posterior to the level of the posterior border of lacrimal (0); anterior to the level of the posterior border of lacrimal (1). Changes in scorings of Forasiepi *et al.* (2015): *Pucadelphys, Andinodelphys, Mayulestes*, *Sallacyon* ? > 0.

159. — **Anteroposterior position of the sphenopalatine foramen relatively to the molars**: above penultimate or antepenultimate molar (0); above ultimate molar or posterior (1).

160. — **Development of pterygoids (F29)**: well-developed and expanded on medial side with midline contact (0); well developed and expanded on medial side but no midline contact (1); reduced, not expanded on medial side (2). Changes in scorings of Forasiepi *et al.* (2015): *Pucadelphys* ? > 0; *Andinodelphys* 1,2 > 0; *Mayulestes* 0 > 1. **Ordered**.

161. — **Posterior process of pterygoids, which covers the alisphenoid-basisphenoid suture**: present (0); absent (1).

162. — **Orbitotemporal canal**: present (0); absent (1), (Rougier *et al.* 1998: ch. 103).

163. — **Optic foramen (F48)**: well separated from sphenorbital fissure (0); confluent with sphenorbital fissure (1).

164. — **Interparietal (F36)**: present (0); absent (or fused to parietals) (1). Changes in scorings of Forasiepi *et al.* (2015): *Notogale* ? > 0.

165. — **Frontoparietal suture (F37)**: with posterior wedge of the frontals (0); with anterior wedge of the parietals (1); no wedge, roughly straight (2). Changes in scorings of Forasiepi *et al.* (2015): *Andinodelphys*, *Sallacyon* ? > 0.

166. — **Parietal-alisphenoid or fronto-squamosal contact (F38)**: parietal-alisphenoid (0); fronto-squamosal (1).

167. — **Foramina for temporal rami (F95 modified)**: present (0); absent (1).

168. — **Anterior lamina of the petrosal**: present but rudimentary (0); absent (1) (Marshall & Muizon 1995; Ladevèze & Muizon 2007: ch. 123). **Ordered**.

169. — **Nuchal crest (F73)**: at or posterior to the level of the condyles (0); anterior to condyles (1).

170. — **Sagittal crest (F72)**: extending to frontals (0); restricted to parietals (1); absent (2). Changes in scorings of Forasiepi *et al.* (2015): *Mayulestes* 1 > 0. **Ordered**.

171. — **Glenoid process of the jugal (F34)**: with articular facet (0); without articular facet (1).

172. — **Postorbital (frontal) process of the jugal**: absent (0); present (1).

173. — **Width of the glenoid fossa (F39)**: less than twice anteroposterior length (0); more than twice anteroposterior length (1), (Rougier *et al.* 1998: ch. 115, modified).

174. — **Preglenoid process of the squamosal (F40)**: absent (0); present (1). Changes in scorings of Forasiepi *et al.* (2015): *Andinodelphys* ? > 0.

175. — **Proportions of the postglenoid process (F41, modified)**: higher than wide and roughly parabolic (0); as wide as high (1); very low and wider than high (2). **Ordered**.

176. — **Width of the postglenoid process**: as wide as glenoid fossa (0); narrower than glenoid fossa (1).

177. — **Location of postglenoid foramen (F42)**: posterior to postglenoid process (0); medial to postglenoid process (1). Changes in scorings of Forasiepi *et al.* (2015): *Didelphodon*, *Mayulestes*, *Pucadelphys*, *Didelphis*, *Dasyurus*, *Thylacinus*, *Sipalocyon*, *Cladosictis*, *Hondadelphys*, *Borhyaena*, *Arctodictis*, *Australohyaena*, *Thylacosmilus*, 1 > 0; *Sallacyon*, *Lycopsis* ? > 0.

178. — **Suprameatal foramen (F43 modified)**: absent (0); below postzygomatic crest (1); at the same level or above postzygomatic crest (2).

*Comment: Domiciops is scored as "non-applicable" because the postzygomatic crest does not reach the level of the suprameatal foramen posteriorly.*

179. — **Paroccipital process of exoccipital**: low tubercle or absent (0); long process with diameter at apex smaller than proximodistal length (1).

180. — **Glenoid process of alisphenoid (F47)**: absent (0); present, does not contribute to glenoid fossa (1); present, contributes to glenoid fossa. Changes in scorings of Forasiepi *et al.* (2015): *Lycopsis*, *Arctodictis* 0 > 1.

*Comment: a conspicuous glenoid process is generally absent in sparassodonts other than* Mayulestes *and* Allqokirus*, although a small projection of the alisphenoid toward the glenoid fossa is observed in* Prothylacynus, Arctodictis, Borhyaena*, and* Lycop-

APPENDIX 1. — Continuation.

sis. *This condition is interpreted here as a residual (or incipiently developed) glenoid process of the alisphenoid.*

181. — **Transverse canal (F49)**: absent (0); present (1).

182. — **Tympanic process of the alisphenoid (F50)**: absent (0); present (1).

183. — **Hypotympanic sinus (F51)**: absent (0); formed by squamosal, alisphenoid and petrosal (1); formed by alisphenoid alone or alisphenoid and petrosal (2). Changes in scorings of Forasiepi *et al.* (2015): *Eodelphis* 1,2 > ?.

184. — **Dorsal epitympanic expansion of the hypotympanic sinus above the glenoid fossa**: absent (0); present (1).

185. — **Medial process of the squamosal, which extends into the middle ear and forms part of the roof of the tympanic cavity (F52)**: absent (0); present (1). Changes in scorings of Forasiepi *et al.* (2015): *Prothylacinus, Arctodictis, Australohyaena* 0 > 1.

*Comments:*

*1) When a hypotympanic sinus is present, the medial process of the squamosal is part of the cavity (generally with the alisphenoid and the petrosal);*

*2) In the data matrix we have changed the scoring of Forasiepi* et al. *(2015) for* Prothylacinus, Arctodictis, *and* Australohyaena, *because in these three taxa the squamosal-petrosal suture distinctly enters the hypotympanic sinus. Therefore, the squamosal is part of the sinus (with the petrosal and alisphenoid) and consequently projects medially within the middle ear cavity. As a matter of fact, this condition is clearly mentioned by Forasiepi* et al. *(2015: 510) in* Australohyaena, *although the authors scored the medial process of the squamosal absent in this genus;*

*3) We also observed a medial process of the squamosal in* Borhyaena *(YPM-PU 15120). However, because we have not observed all the available skulls of this genus, we cautiously follow Forasiepi* et al. *(2015), who scored this character as polymorphic for this taxon.*

186. — **Intratympanic sinus excavated in the exoccipital**: absent (0); present (1).

187. — **Intratympanic sinus in the pars mastoidea**: absent (0); present (1).

188. — **Anterior expansion of the middle ear sinus within the lateral wall of the braincase**: absent (0); present (1), (Muizon 1999: ch. 14; Babot *et al.* 2002: ch. 13).

*Comment: in* Paraborhyaena, Thylacosmilus *and* Callistoe, *in addition to the spherical dorsal expansion, the hypotympanic sinus has a narrow and pointed anterior extension (not dorsal as stated by Muizon 1999), which inserts in the lateral wall of the braincase, affecting the squamosal and alisphenoid.*

189. — **Squamosal extratympanic sinus excavated in the roof of the external acoustic meatus**: absent (0); present (1).

190. — **Pneumatization of the squamosal with air cells present at the posterior base of the zygomatic process (F55)**: absent (0); present (1).

191. — **Notch or foramen in alisphenoid for greater petrosal nerve (F59)**: present (0); absent (1). Changes in scorings of Forasiepi *et al.* (2015): *Andinodelphys, Mayulestes* 1 > 0.

192. — **Primary foramen ovale (F57 modified)**: between petrosal and alisphenoid (0); in alisphenoid or between alisphenoid and squamosal (1). **Ordered**.

*Comment:* Didelphodon *is coded (?)* contra *Wilson (2016) because the foramen ovale coded by Wilson is in fact a secondary foramen ovale, which is bordered ventrally by the tympanic process of the alisphenoid. The primary foramen ovale is hidden by the tympanic process of alisphenoid and is not observable on Wilson's digital renderings.*

193. — **Secondary foramen ovale totally enclosed in the alisphenoid (F58)**: absent (0); present (1). Changes in scorings of Forasiepi *et al.* (2015): *Lycopsis*, *Prothylacinus* 0 > 1.

*Comment: Didelphodon is here coded present.*

194. — **Carotid foramen position (F60)**: well anterior to basioccipital-basisphenoid suture (0); in basisphenoid at the level of basioccipital-basisphenoid suture (1).

195. — **Hypoglossal foramen number (F61 modified)**: confluent with jugular foramen (0); two or more (1); one (2). **Ordered**.

196. — **Groove between hypoglossal foramina and foramen for inferior petrosal sinus (F62)**: absent or faint (0); present and deep (1). Changes in scorings of Forasiepi *et al.* (2015): *Hondadelphis*, *Lycopsis* 0 > 1; *Paraborhyaena* ? > 1.

197. — **Jugular foramen vs inferior petrosal sinus**: separated from foramen for inferior petrosal sinus (0); confluent with foramen for inferior petrosal sinus, (Rougier *et al.* 1995: ch. 150).

198. — **Size of jugular foramen relative to fenestra cochleae**: subequal or slightly larger (0); much larger, at least three times larger (1), (Ladevèze & Muizon 2007).

199. — **Median keel on basioccipital (F65)**: absent (0); present (1). Changes in scorings of Forasiepi *et al.* (2015): *Pucadelphys*, *Andinodelphys*, *Mayulestes* 0 > 1.

200. — **Midline rod-shaped eminence on basisphenoid (F66 modified)**: absent (0); present (1), (Wible *et al.* 2009: ch. 240).

APPENDIX 1. — Continuation.

201. — **Dorsoventral position of petrosal (F76)**: at the level of the basioccipital (0); distinctly dorsal to the basioccipital (1).

202. — **Orientation of the pars cochlearis of the petrosal**: plane defined by the apex of the promontorium-fenestra vestibuli-fenestra cochleae: sub-horizontal or slightly oblique (0); sub-vertical (1), (Muizon 1999: ch. 20, modified; Babot *et al.* 2002: ch. 18, modified).

*Comment: In this character, the axis of rotation of the pars cochlearis is oriented anteromedially-posterolaterally but remains in a roughly horizontal plane. The rotation is clockwise on the left side.*

203. — **Orientation of the major axis of the petrosal (axis subarcuate fossa- internal acoustic meatus)**: subhorizontal to slightly oblique (0); oblique to subvertical (1); vertical (2), (Muizon 1999: ch. 20, modified; Babot *et al.* 2002: ch. 18, modified). **Ordered**.

*Comment: in this character, the axis of rotation is oriented anterolaterally-posteromedially, approximately horizontal, i.e., at 90° to the axis of rotation of character 202.*

204. — **Anteromedial flange (F83)**: present (0); absent (1).

*Comment: the epitympanic wing, or anteromedial flange of Wible (2003), is a medially expanded crest which borders the anterior and anteromedial edge of the promontorium and which contacts the basioccipital medially. It forms the floor of the groove for the inferior petrosal sinus.*

205. — **Cavum epiptericum (F79 modified)**: floored by petrosal alone (0); floored by petrosal and alisphenoid (1); floored primarily or exclusively by alisphenoid (2); open as a pyriform fenestra (3). **Ordered**.

*Comment:* Didelphodon *is coded (1) taking into account that that the petrosal contributes to the floor of the cavum epiptericum, as indicated in Wilson (2016: supplementary figures 8a, b).*

206. — **Medial expansion of the crista petrosa that forms a thin and straight lamina covering the anterolateral part of the fossa subarcuata**: absent (0); present (1), (Muizon & Ladevèze 2007: ch. 122).

207. — **Internal acoustic meatus (F80)**: deep with thick prefacial commissure (0); shallow with thin prefacial commissure (1).

208. — **Internal acoustic meatus (IAM) and subarcuate fossa**: subequal and separated by sharp wall (0); IAM narrower than the opening of the subarcuate fossa and separated by a thick wall (1) (Muizon & Ladevèze 2007: ch. 125).

209. — **Fossa subarcuata (F81 modified)**: deep: greatest diameter larger than aperture (spherical) (0); intermediate: greatest diameter subequal to aperture (cylindrical) (1); wide open: greatest diameter is the aperture (conical) (2); very shallow or absent: just a depression (3). **Ordered**.

210. — **Deep groove for internal carotid artery excavated in medial side of promontorium apex ventrally (F82)**: absent (0); present (1). Changes in scorings of Forasiepi *et al.* (2015): *Sallacyon, Notogale, Cladosictis, Sipalocyon, Borhyaena, Pharsophorus, Arctodictis, Callistoe, Paraborhyaena, Lycopsis* 0 > 1.

*Comment: in some taxa with a subvertical promontorium, the groove is located at the anterior end of the apex of the promontorium (i.e.,* Borhyaena, Pharsophorus, Arctodictis*) rather than on the ventral aspect of the apex as in taxa in which the promontorium is not subvertical (i.e.,* Notogale, Cladosictis, Sipalocyon*). In* Arctodictis*, the structure referred by Forasiepi (2009) as a possible fossa for the tensor tympani Muscle is identified here as the carotid groove. Because of the function of the tensor tympani muscle, this fossa is generally located on the lateral edge of the promontorium, anterior to the secondary facial foramen. Given the morphology of the petrosal of* Arctodictis*, a position of the tensor tympani fossa at the anteromedial apex of the promontorium is unlikely.*

211. — **Prootic canal (F84)**: present (0); absent (1). Changes in scorings of Forasiepi *et al.* (2015): *Mayulestes*, *Notogale*, *Sipalocyon*, *Borhyaena* 1 > 0; *Sminthopsis*, *Thylacinus* 0 > 1.

*Comment: the prootic canal of* Mayulestes, Notogale, Siplaocyon *and* Borhyaena *has been observed on CT data (see Supplementary data –* http://geodiversitas.com/40/16*, Files 5-8). The scoring of* Thylacinus *and* Sminthopsis *follows Archer (1976) and Wroe* et al. *(2000: 1024, see comment on character 77).*

212. — **Prootic canal morphology**: large with endocranial opening (0); reduced with intramural opening (1), (Muizon & Ladevèze 2007: ch. 148).

213. — **Rostral tympanic process of petrosal (F85, modified)**: absent or smooth tubercle (0); distinct crest and/or erected process (1).

214. — **Tensor tympani fossa**: smooth and shallow area (0); distinct elongated fossa at anterolateral edge of promontorium (1); long and narrow groove bordering the anterolateral edge of promontorium (2) (Geisler 2001: ch. 14; Ladevèze & Muizon 2007: ch. 128).

215. — **Eustachian foramen in posteroventromedial petrosal sinus (F56, modified)**: absent (0); present (1).

*Comment: This foramen is observed at the junction of the rostral tympanic process and the tympanic process of the alisphenoid. The rostral tympanic process greatly develops, ventrally and laterally and floors the whole promontorium (e.g. in* Dasyurus*) anteroventrally and forms a ventromedial sinus, closed ventrally by its contact with the alisphenoid process. The exit of the Eustachian tube from the middle ear is through a foramen anteriorly at the junction of the alisphenoid and rostral tympanic processes.*

APPENDIX 1. — Continuation.

216. — **Rostral tympanic process anterolaterally directed wing**: absent (0); wing restricted to posterior region of promontorium (1); wing extend over the whole length of promontorium and contacts the alisphenoid tympanic process anteriorly (2), (Ladevèze & Muizon 2007: ch. 134). **Ordered**.

217. — **Petrosal plate**: absent (0); present (1), (MacPhee 1981; Ladevèze & Muizon 2007: ch. 142).

*Comment: The petrosal plate is formed by the ventral junction of the rostral and caudal tympanic processes of the petrosal.*

218. — **Caudal tympanic process anterior extension**: absent (0); present (1), (Ladevèze & Muizon 2007: ch. 141).

*Comment: In state 1 the caudal tympanic process extends anteriorly and totally floors the postpromontorial sinus.*

219. — **Relative size of posttympanic and paroccipital processes (F45)**: paroccipital process longer (0); both processes are similar in size (1). Changes in scorings of Forasiepi *et al.* (2015): *Asiatherium*, – > 1; *Andinodelphys*, *Pucadelphys* – > 0,1; *Herpetotherium* – > ?; *Mayulestes* – > ?; *Dromiciops* – > 0.

220. — **Orientation of the posttympanic and/or paroccipital processes (F46)**: ventrally projected (0); anteroventrally projected (1).

*Comment: when the processes are anteroventrally projected, they tend either to contact the tympanic process of the alisphenoid when present (*Notogale, Cladosictis*, and* Sipalocyon*) or to contact the medial region of the posterior wall of the postglenoid process or the anterior wall of the external auditory meatus (*Lycopsis, Paraborhyaena*). An extreme condition is found in* Thylacosmilus*, in which the postmeatal and paroccipital processes contact the alisphenoid and squamosal anteriorly, medial to the glenoid fossa. Since* Thylacosmilus *has no tympanic process of the alisphenoid, the tympanic cavity is floored ventrally by the postmeatal and paroccipital processes only.*

221. — **Diameter of stapedius fossa (F94)**: approximately twice the size of that of fenestra vestibuli (0); distinctly less than twice the size of that of the fenestra vestibuli (= small and shallow) (1). Changes in scorings of Forasiepi *et al.* (2015): *Pucadelphys*, *Andinodelphys* 1 > 0; *Sallacyon*, *Paraborhyaena* ? > 1.

222. — **Mastoid process (= paroccipital process of Rougier *et al.* 1998) (F86 modified)**: proximodistally long and vertical (0); small nodular tubercle on posterolateral border of stylomastoid notch (1); indistinct or absent (2), (Ladevèze & Muizon 2007: ch. 139).

223. — **Hiatus Fallopii (F87 modified)**: on dorsal (cerebellar) face of petrosal (0); intermediary (i.e., neither visible in dorsal nor in ventral views) (1); ventral (tympanic) face of petrosal (2). **Ordered**.

224. — **Exit of facial nerve (F88)**: stylomastoid notch (0); stylomastoid foramen (1).

225. — **Floor of cavum supracochleare (F89)**: absent (0); present (1).

226. — **Roof of cavum supracochleare**: open dorsally in cavum epiptericum (0); closed (1), (Rougier *et al.* 1998: ch. 128).

227. — **Tympanic petrosal crest (= petrosal crest of Archer 1976 and Muizon 1999) (F93)**: absent (0); present (1). Changes in scorings of Forasiepi *et al.* (2015): *Pucadelphys*, *Andinodelphys*, *Mayulestes*, *Sallacyon*, 0 > 1.

228. — **Tuberculum tympani**: weakly developed (0); large (1).

229. — **Epitympanic recess (F91 modified)**: squamosal part as large as petrosal one (0); squamosal part distinctly smaller than petrosal one (1); squamosal part distinctly larger than petrosal one (2). **Ordered**.

230. — **Fossa incudis and epitympanic recess (F92)**: continuous (0); separated by distinct ridge (1). Changes in scorings of Forasiepi *et al.* (2015): *Dasyurus*, *Thylacinus* 1> 0.

231. — **Stapedial ratio (F90)**: subcircular (less than 1.8) (0); elliptical (more than 1.8) (1). Changes in scorings of Forasiepi *et al.* (2015): *Pucadelphys* 0 > 0,1; *Andinodelphys* 0 > ?; *Mayulestes* 0 > ?; *Didelphis, Monodelphis* 0 > 1,0; *Thylacinus* 1 > 0.

*Comment: Measurements taken in extant marsupials (Segall 1970; Horovitz* et al. *2008) show very variable values within a genus or even a species. For instance,* Monodelphis *exhibits values of stapedial ratio from 1.25 to 2.00 and* Philander *from 1.23 to 1.88 (Horovitz* et al. *2008). Stapedial ratio in* Andinodelphys *and* Mayulestes *are scored "?" because the fenestra vestibuli has suffered* post-mortem *distortion, being generally dorsoventrally compressed.*

232. — **Mastoid exposure (F77, modified)**: large on occiput (0); narrow (1); mastoid internal, wedged between the squamosal and exoccipital (2). **Ordered**.

233. — **Posttemporal notch or foramen (F96)**: present (0); absent (1).

234. — **Posttemporal sulcus on squamosal surface of petrosal**: present (0); absent (1), (Ladevèze & Muizon 2007: ch. 152).

235. — **Stapes (F74)**: collumelliform (not perforated) (0); bicrurate (perforated) (1).

236. — **Ectotympanic shape (F75)**: ring-shaped (0); transversely expanded (1).

Appendix 1. — Continuation.

237. — **Ectotympanic attachment to the skull**: loose connection (no marked ridges and grooves on the skull) (0); tight attachment with marked ridges and grooves (1); fused to rostral tympanic process of petrosal (2), (Muizon 1999: ch. 4; Babot *et al.* 2002: ch. 3). **Ordered**.

238. — **Squamosal at external acoustic meatus**: squamosal not thickened at meatus (0); squamosal thickened at meatus with mediolateral width mediolateral width shorter than anteroposterior length (1); squamosal thickened at meatus with mediolateral width mediolateral width longer than anteroposterior length (2), (Muizon 1999: ch. 16; Babot *et al.* 2002: ch. 15). **Ordered**.

239. — **Ascending canal**: present (0); absent (1), (Rougier *et al.* 1998: ch. 152).

240. — **Contribution of squamosal to occiput**: absent or small (0); large (1), (Muizon 1999: ch. 21; Babot *et al.* 2002: ch. 19).

241. — **Dorsal margin of the foramen magnum (F67)**: formed by exoccipitals, which contact medially (0); formed by the supraoccipital medially and exoccipitals, which do not contact medially (1). Changes in scorings of Forasiepi *et al.* (2015): Notogale ? > 1.

242. — **Connection between condylar articular facets on ventral edge of foramen magnum (F69)**: absent (0); present (1). Changes in scorings of Forasiepi *et al.* (2015): Dromiciops 1 > 0.

Post-cranial characters:

243. — **Atlantal foramen (F188)**: absent (0); present (1).

244. — **Atlas transverse foramen (F189)**: absent (0); present (1).

245. — **Ventral foramen at the base of the transverse process of the atlas (F190)**: absent (0); present (1).

246. — **Posterior extent of transverse processes of the atlas (F191)**: anterior or just reach caudal facets for axis (0); extend caudally beyond level of caudal facet for axis (1). Changes in scorings of Forasiepi *et al.* (2015): *Mayulestes* 0 > ?

247. — **Shape of the transverse processes of the atlas**: proximodistaly short and roughly circular or quadrate (0); distinctly elongated (proximodistal length longer than transverse width) (1).

248. — **Shape of the cranial facets of atlas (F193)**: concavity is roughly constant along the whole height of the facet (0); dorsal third of the facet much more concave than the ventral two thirds and strongly inflected medially (1).

249. — **Atlas and intercentrum (F194)**: unfused (0); fused (1). Changes in scorings of Forasiepi *et al.* (2015): *Pucadelphys* 1 > 0; *Andinodelphys* ? > 0.

250. — **Axis transverse foramen (F195)**: absent represented by a notch (0); present, enclosed (1).

251. — **Axis, posterior extension of the neural process (F196)**: shorter or subequal than anterior extension (0); distinctly longer than anterior extension (1). Changes in scorings of Forasiepi *et al.* (2015): *Mayulestes* 0 > 1.

*Comment: in state (1) the spinous process bears a sharp finger-like posterior process, which overhangs the C3 posteriorly and in some cases almost reaches the posterior edge of the centrum of C3.*

252. — **Ventral sagittal crest of axis**: roughly straight (0); distinctly concave because of the development of a robust ventral process posteriorly (1).

253. — **C3-C4 ventral sagittal process (F197)**: absent (0); present (1). Changes in scorings of Forasiepi *et al.* (2015): *Andinodelphys* ? > 0; *Mayulestes* 0 > ?

254. — **C5 transverse process heads in lateral view (F198 modified)**: ventral head enlarged in a ventral lamina with the dorsal head as a tubercle, dorsal to the posterior part of the ventral lamina (0); ventral (anteroventral) head triangular to rod-like and anteriorly projected with the dorsal (posterodorsal), head rod-like, posteriorly elongated, and widely separated from the anterior head; the posterodorsal head is either almost at the same level as the anteroventral one or slightly dorsal (in lateral view) and never overhangs the ventral head (1). Changes in scorings of Forasiepi *et al.* (2015): *Andinodelphys* ? > 0.

*Comment: both states of this character, as reformulated, more clearly describe the states originally defined by Horovitz & Sánchez-Villagra (2003). Note that state 0 is state 1 of Horovitz & Sánchez-Villagra (2003) and* vice versa.

255. — **C5 and T1 body length (F199)**: C5 subequal or longer than T1 (0); C5 shorter than T1. Changes in scorings of Forasiepi *et al.* (2015): *Andinodelphys* ? > 0.

256. — **C6 spinous process (F200)**: absent or protuberance (0); lamina (1).

257. — **C7 transverse foramen (F201)**: absent (0); represented by a notch (1); complete foramen (2). Changes in scorings of Forasiepi *et al.* (2015): *Pucadelphys* 0 > 2; *Andinodelphys* ? > 0. **Ordered**.

258. — **First thoracic vertebra with a (relative to other vertebrae) tall spinous process (F203)**: T1 (0); T2 (1); T3 (2).

APPENDIX 1. — Continuation.

259. — **Anticlinal vertebra (F204)**: on lumbar (0); on thoracic (1); no anticlinal vertebra (2).

260. — **Foramen on dorsal arch of last lumbar vertebra (F205)**: absent (0); present (1).

261. — **Mammillary processes (metapophyses) in third lumbar vertebra anterior to the last lumbar (F206)**: absent or weak (0); present (1). Changes in scorings of Forasiepi *et al.* (2015): *Mayulestes* 0 > 1; *Andinodelphys* ? > 0.

262. — **Ventral median keel on anterior lumbar vertebrae (F207 modified)**: absent (0); present (1). Changes in scorings of Forasiepi *et al.* (2015): *Mayulestes* 0 > 1; *Andinodelphys* ? > 1.

263. — **Auricular process of the sacrum (F208)**: developed on two sacral vertebrae (0); developed on one sacral vertebra (1). Changes in scorings of Forasiepi *et al.* (2015): *Andinodelphys* ? > 1.

264. — **Size of sacral spinous process (F209)**: shorter than last lumbar (0); taller than last lumbar (1). Changes in scorings of Forasiepi *et al.* (2015): *Andinodelphys* ? > 0.

265. — **Length of the tail (F210)**: shorter than twice the length of the precaudal vertebral column (0); longer than twice the length of the precaudal vertebral column (1). Changes in scorings of Forasiepi *et al.* (2015): *Andinodelphys* 0 > 1.

266. — **Angle between scapular spine and dorsal border of infraspinatus fossa (F211)**: acute or almost right (between 80 and 95°) (0); obtuse (more than 95°) (1).

267. — **Coracoid process (F212)**: large (extends beyond medial border of glenoid fossa) (0); small (just reaches medial border of glenoid fossa) (1). Changes in scorings of Forasiepi *et al.* (2015): *Pucadelphys*, *Andinodelphys* ? > 0; *Dromiciops* 1 > 0,1.

268. — **Distal extension of acromion process (F213)**: extends distally beyond glenoid fossa (0); does not extend distally beyond glenoid fossa (1).

269. — **Anterior extension of the acromion process**: posterior to anterior edge of glenoid fossa (0); anterior or just lateral to anterior edge of glenoid fossa (1).

270. — **Width of infraspinatus fossa (F214)**: less than ¼ its length (0); more than ¼ its length (1).

271. — **Width of the acromion process at the level of the neck (F215)**: wider than infraspinatus fossa (0); narrower (1). Changes in scorings of Forasiepi *et al.* (2015): *Pucadelphys*, *Andinodelphys* ? > 0.

272. — **Infraspinous/supraspinous fossa width at the level of the neck (F216)**: supraspinous fossa subequal of wider (0); supraspinous fossa narrower (1). Changes in scorings of Forasiepi *et al.* (2015): *Mayulestes* 0 > 1.

273. — **Scapular notch (F217)**: more than 130° (0); between 90 and 130° (1). Changes in scorings of Forasiepi *et al.* (2015): *Mayulestes* 0 > 1; *Andinodelphys* ? > 1.

274. — **Clavicle (F218)**: present (0); absent (1). Changes in scorings of Forasiepi *et al.* (2015): *Andinodelphys* ? > 0.

275. — **Medial process or rugosity for the teres major on humeral diaphysis (F219)**: absent (0); present (1). Changes in scorings of Forasiepi *et al.* (2015): *Andinodelphys* ? > 1.

276. — **Tricipital line of humerus (F220)**: absent (0); ridge or small crest (1); massive crest continuous with deltopectoral crest (2). Changes in scorings of Forasiepi *et al.* (2015): *Andinodelphys* ? > 1.

277. — **Capitulum for radius on humerus (F221)**: spherical (0); cylindrical (1). Changes in scorings of Forasiepi *et al.* (2015): *Pucadelphys*, *Andinodelphys* 1 > 0,1.

278. — **Entepicondylar foramen (F222)**: present (0); absent (1).

279. — **Laminar supinator crest (ectepicondylar crest) (F224)**: large: proximolateral angle expanded (0); intermediate: proximolateral angle not expanded (1); absent (2). Changes in scorings of Forasiepi *et al.* (2015): *Andinodelphys* ? > 0.

*Comment: in state 0, the angle between the proximal and lateral margins of the supinator crest is subequal or inferior to 130°. In state 1, the angle is superior to 130°.*

280. — **Greater tuberosity height relative to humeral head height (F225)**: subequal or lower (0); higher (1).

281. — **Development of greater tuberosity in proximal view (F226)**: small (less than half the anteroposterior length of head) (0); large (greater than or equal to half the anteroposterior length of the head) (1). Changes in scorings of Forasiepi *et al.* (2015): *Mayulestes*, *Pucadelphys* 0 > 1; *Andinodelphys* ? > 1.

282. — **Extension of the deltoid crest (F227)**: restricted to proximal half of the humerus (0); reaches distal half of the humerus (1). Changes in scorings of Forasiepi *et al.* (2015): *Pucadelphys* 0 > 1; *Andinodelphys* ? > 1.

283. — **Distal end of deltoid crest (F228)**: merging with diaphysis (0); forming a distinct angle or process (1). Changes in scorings of Forasiepi *et al.* (2015): *Pucadelphys* 0 > 0,1; *Andinodelphys* ? > 1.

Appendix 1. — Continuation.

284. — **Relative heights of the trochlea and capitulum in anterior view (F229 modified)**: proximal extension of capitulum longer (0); subequal (1); proximal extension of trochlea longer (2). Changes in scorings of Forasiepi *et al.* (2015): *Mayulestes* 0 > 2; *Pucadelphys* 0 > 0,1. *Cladosictis* from 2 to 0 and 1; *Sipalocyon* and *Lycopsis* from 2 to 0.

285. — **Humerus medial epicondyle size (F230)**: large (0); small (1).

286. — **Humerus distal end size (F231)**: large (0); small (1). Changes in scorings of Forasiepi *et al.* (2015): *Andinodelphys* ? > 0.

*Comment: this character is based on the ratio, transverse width of distal epiphysis without entepicondyle/transverse width of proximal epiphysis. A Ratio > 0.9 is large (state 0); a ratio < 0.9 is small (state 1) (Horovitz & Sánchez-Villagra 2003; Forasiepi 2009).*

287. — **Lateral extension of capitulum (F232 modified)**: absent: capitulum rounded and regularly sloping laterally (0); present: straight with a flat shelf and/or a salient crest (1). Changes in scorings of Forasiepi *et al.* (2015): *Mayulestes*, *Pucadelphys* 0 > 1; *Andinodelphys* ? > 1.

288. — **Depth of humeral trochlea (intercondylar notch) (F233)**: wide and relatively shallow concave (0); narrow and concave posteriorly (1).

289. — **Curvature of posterior border of the humeral shaft (F234)**: curved (0); straight (1).

290. — **Medial development of ulnar anconeal process (F235)**: does not protrude beyond medial border of olecranon process (0); medially protruding (1). Changes in scorings of Forasiepi *et al.* (2015): *Andinodelphys* ? > 0,1.

291. — **Medial curvature of the ulna (F236 modified)**: present (0); absent (1). Changes in scorings of Forasiepi *et al.* (2015): *Andinodelphys* ? > 0.

292. — **Posterior border of the proximal half of the ulna (F237)**: convex posteriorly (0); straight or concave posteriorly (1).

293. — **Shape of articular facet for the humerus on the radius (F238)**: anteroposteriorly compressed (0); circular (1).

294. — **Distal shaft of the radius (F239)**: oval (wider than long) (0); rounded (almost as wide as long) (1). Changes in scorings of Forasiepi *et al.* (2015): *Pucadelphys*, *Andinodelphys* ? > 0.

295. — **Prepollex (F240)**: absent (0); present (1).

296. — **Distolateral process of scaphoid (F241)**: absent (0); present but does not separate lunate from magnum (1); present but separates lunate from magnum (2). Changes in scorings of Forasiepi *et al.* (2015): *Andinodelphys* ? > 0.

297. — **Number of plantar tubercles (distal heads) on trapezium (F242)**: two (0); one (1).

298. — **Angle between transverse axis of proximal and distal epiphyses of metacarpal V (F243)**: absent (0); present (1). Changes in scorings of Forasiepi *et al.* (2015): *Mayulestes* 0 > 1; *Pucadelphys*, *Andinodelphys* ? > 1.

299. — **Orientation of ilium relative to ischium in lateral view (F244)**: deflected dorsally (0); aligned with ischium (1). Changes in scorings of Forasiepi *et al.* (2015): *Pucadelphys* 1 > 0 and 1; *Andinodelphys* ? > 1.

300. — **Tuberosity for the rectus femoris muscle (F245)**: absent (0); protuberance (1); depression (2).

301. — **Length of the iliac neck (F246)**: long, 15% or more the total pelvis length (0); short, less than 15% the total pelvis length (1). Changes in scorings of Forasiepi *et al.* (2015): *Mayulestes* 0 > 1.

302. — **Greater sciatic notch (F247)**: obtuse angle (0); right or acute angle (1). Changes in scorings of Forasiepi *et al.* (2015): *Pucadelphys* 1 > 0.

303. — **Iliac and gluteus fossae (F248)**: no fossa (0); two fossae subequal in size (1); gluteous fossa larger (2). Changes in scorings of Forasiepi *et al.* (2015): *Mayulestes* 1 > 2; *Andinodelphys* ? > 2.

304. — **Epipubic bones (F249)**: present (0); absent (1). Changes in scorings of Forasiepi *et al.* (2015): *Andinodelphys* 1 > 0.

305. — **Proximal size of epipubic bones (F250)**: short (0); long (1). Changes in scorings of Forasiepi *et al.* (2015): *Andinodelphys* – > 0.

306. — **Torsion between proximal and distal epiphyses of femur (F251)**: present (0); absent (1). Changes in scorings of Forasiepi *et al.* (2015): *Mayulestes* 0 > 1; *Pucadelphys* 1 > 0; *Andinodelphys* ? > 0.

*Comment: The scoring of* Mayulestes *is not simple because the distal epiphysis of the left femur is incomplete and the right is known by its distal epiphysis only. Furthermore, in distal view, the elevation of the lateral trochlear crest is misleading. Therefore, a reference line for the distal epiphysis could be the line joining the attachment area of the lateral and medial femorotibial ligaments. The attachment of the femorotibial ligament is not preserved on the left femur of the holotype, but it is present on*

APPENDIX 1. — Continuation.

*the distal extremity of the right bone. Its position can thus be estimated on the left femur. Given that, there is apparently no significant torsion in* Mayulestes*, which is scored 1.*

307. — **Height of greater trochanter relative to femoral head (F252)**: lower or subequal in height (0); higher (1). Changes in scorings of Forasiepi *et al.* (2015): *Andinodelphys* 1 > 0.

308. — **Lesser trochanter of femur (F253)**: present, large and blade-like (0); knob-like or absent (1).

309. — **Femoral condyles (F254)**: lateral condyle wider than medial (0); subequal (1); medial condyle wider than lateral (2). **Ordered**.

310. — **Ossified patella (F255)**: absent (0); present (1).

311. — **Parafibula (F256)**: present (0); absent (1). Changes in scorings of Forasiepi *et al.* (2015): *Andinodelphys* ? > 1; *Sminthopsis* ? > 0.

312. — **Femorofibular articulation (F257)**: present (0); absent (1). Changes in scorings of Forasiepi *et al.* (2015): *Andinodelphys* ? > 0.

313. — **Tibial length relative to femur length (F258)**: subequal to longer (0); shorter (1).

314. — **Proximal dimensions of tibia (F259)**: larger mediolaterally than anteroposteriorly (0); subequal (1); larger anteroposteriorly than mediolaterally (2). Changes in scorings of Forasiepi *et al.* (2015): *Pucadelphys* 0 > 1; *Andinodelphys* ? > 1. **Ordered**.

315. — **Tibia shape (F260)**: sigmoid (0); straight (1). Changes in scorings of Forasiepi *et al.* (2015): *Andinodelphys* ? > 1.

316. — **Torsion between proximal and distal epiphyses of tibia (F261)**: present (0); absent (1). Changes in scorings of Forasiepi *et al.* (2015): *Pucadelphys*, *Andinodelphys* ? > 1.

317. — **Tibia, distal articulation type (F262)**: sagittal (0); spiral (1).

*Comments: in state 0, the lateral tibioastragalar facet is curved medially and turns around the medial malleolus. Such a condition allows for some rotation of the pes during flexion-extension movements of the ankle, which tend to give a medial orientation of the plantar face of the pes. In state 1, the lateral tibioastraglar facet is anteroposteriorly oriented and allows for flexion-extension movements in sagittal plane only and the plantar face of the pes faces plantarly or posteroplantarly.*

318. — **Posterior extension of the lateral astragalotibial facet of tibia in distal view (F263)**: does not extend posteriorly beyond the medial astragalotibial articulation (0); extends posteriorly beyond the medial astragalotibial articulation (1). Changes in scorings of Forasiepi *et al.* (2015): *Pucadelphys* 0 > 0,1.

319. — **Orientation of the lateral edge of the lateral astragalotibial articular facet (in lateral view)**: parallel to epiphyseal suture of the tibia (0); oblique to epiphyseal suture of the tibia (1).

320. — **Anteroposterior length of the of the medial malleolus of the tibia at base relative to the greatest anteroposterior length of the distal epiphysis (as seen in distal view)**: subequal (0); medial malleolus much shorter (1).

321. — **Distal malleolus of tibia (F264)**: absent or weak (0); distinct (1). Changes in scorings of Forasiepi *et al.* (2015): *Andinodelphys* ? > 1.

322. — **Astragalus, angle between medial and lateral astragalotibial facets (F265)**: 90° (0); intermediate (1); 180° (2). Changes in scorings of Forasiepi *et al.* (2015): *Andinodelphys* ? > 0. **Ordered**.

323. — **Astragalus, astragalonavicular facet extends onto ventromedial side of head (F266)**: absent (0); present (1).

324. — **Astragalus, width and height of navicular facet in distal view (F267)**: transverse diameter > dorsoplantar diameter (0); transverse diameter < dorsoplantar diameter (1). Changes in scorings of Forasiepi *et al.* (2015): *Andinodelphys* ? > 0.

325. — **Astragalus, visibility of medial plantar tuberosity of the astragalus in dorsal view (F268)**: not visible (0); visible (1). Changes in scorings of Forasiepi *et al.* (2015): *Eodelphis* ? > 1; *Didelphodon* ? > 0; *Mayulestes* 1 > 0; *Didelphis, Monodelphis* 0 > 1; *Lycopsis* ? > 1.

326. — **Astragalus, angle between lateral tibial and fibular facets (F269)**: no angle (0); with angle (1).

327. — **Astragalus, medial extent of sustentacular facet (F270)**: does not reach the medial edge of the neck (0); reaches the medial edge of the neck (1). Changes in scorings of Forasiepi *et al.* (2015): *Mayulestes* 0 > 1.

328. — **Astragalus, astragalar canal (F271)**: present (0); absent (1).

329. — **Astragalus, width of astragalar neck (F272)**: neck wider than head (0); neck narrower or as wide as head (1).

330. — **Malleolar shelf of the astragalus (F274)**: absent (0); present (1). Changes in scorings of Forasiepi *et al.* (2015): *Pucadelphys* 0 > 1; *Andinodelphys* ? > 1.

APPENDIX 1. — Continuation.

331. — **Astragalus, dorso-distal tuber of the head (F275)**: absent (0); present (1). Changes in scorings of Forasiepi *et al.* (2015): *Mayulestes*, *Pucadelphys*, *Andinodelphys* ? > 1.

*Comments: this structure was termed "astragalo-distal tuber" by Forasiepi (2009). We rather use here the term "dorso-distal tuber of the head", which we regard as more descriptive. A dorsal tuber is present on an astragalus* (MHNC 8398) *referred to* Mayulestes ferox *because its size and articular calcanear facets perfectly fit the condition oberved on the calcaneus of the holotype (CM pers. obs.). Furthermore, a distinct dorsal tuber is also observed in* Pucadelphys *and* Andinodelphys.

332. — **Astragalus, connection between astragalo-navicular (or cuboid) facet and sustentacular facet (F276)**: present (0); absent (1).

333. — **Astragalo-cuboid facet on astragalar head**: present (0); absent (1).

334. — **Calcaneus, longest dimension of ectal facet (F277 modified)**: anteromedial-posterolateral (0); anteroposterior (1); transverse (2); anterolateral-posteromedial (3).

335. — **Calcaneus, orientation of the calcaneoastragalar (ectal) facet (F278)**: mostly medial (0); intermediate (1); mostly dorsal (2). Changes in scorings of Forasiepi *et al.* (2015): *Mayulestes* 0 > 1; *Pucadelphys* 0 > 1. **Ordered**.

336. — **Calcaneal peroneal process (F279 modified)**: present as a salient and dorsoplantarly thick protuberance (0); present but reduced to a thin crest (1) absent or faint (2). **Ordered**.

337. — **Calcaneus, position of the peroneal process (F280)**: at the level of the edge of the cuboid facet (0); proximal to the level of the edge of the cuboid facet (1).

338. — **Calcaneal peroneal groove for the peroneous longus (F281)**: indistinct or weakly developed (0); distinct and deeply grooved (1). Changes in scorings of Forasiepi *et al.* (2015): *Mayulestes*, *Pucadelphys* 0 > 1; *Andinodelphys* ? > 1.

339. — **Calcaneus, position of the sustentaculum (F282)**: reaches anterior end of calcaneus (0); subterminal (1). Changes in scorings of Forasiepi *et al.* (2015): *Andinodelphys* ? > 0.

340. — **Calcaneus, outline of sustentacular process (F283)**: triangular or rounded (0); rectangular (1). Changes in scorings of Forasiepi *et al.* (2015): *Mayulestes*, *Pucadelphys* 0 > 1; *Andinodelphys* ? > 1.

341. — **Calcaneus, orientation of sustentacular facet in distal view (F284)**: mostly medial (0); mostly dorsal (1). Changes in scorings of Forasiepi *et al.* (2015): *Andinodelphys* ? > 0.

342. — **Calcaneus, orientation of sustentacular facet in medial view (F285)**: fully dorsal (0); *c.* 45° dorsodistally (1). Changes in scorings of Forasiepi *et al.* (2015): *Mayulestes*, *Pucadelphys*, *Andinodelphys* 0 > 1; *Lycopsis* ? > 1.

*Comment:* Contra *Horovitz & Sánchez-Villagra (2003), we consider that taxa scored with a medial orientation of the sustentacular facet (state 0) can perfectly be scored on the anteroposterior orientation of the sustentacular facet.*

343. — **Calcaneus, sustentacular facet morphology (F286)**: slightly concave or flat (0); posteriorly convex (1). Changes in scorings of Forasiepi *et al.* (2015): *Andinodelphys* ? > 0.

344. — **Calcaneus, secondary distal calcaneoastragalar facet (F287)**: absent (0); present (1). Changes in scorings of Forasiepi *et al.* (2015): *Andinodelphys* ? > 0.

345. — **Calcaneus, sustentacular and posterior calcaneoastragalar facets (F288)**: separated (0); merged (1). Changes in scorings of Forasiepi *et al.* (2015): *Andinodelphys* ? > 0.

346. — **Calcaneal facet for fibula (F289)**: present (0); absent (1).

347. — **Orientation of the calcaneal facet for the fibula (F290)**: dorsal (0); lateral (1). Changes in scorings of Forasiepi *et al.* (2015): *Pucadelphys* 1 > 0.

348. — **Length of the tuber calcis (F291)**: longer than the body (0); as long as or shorter than the body (1). Changes in scorings of Forasiepi *et al.* (2015): *Andinodelphys* ? > 1.

349. — **Medial curvature of the tuber calci (F292)**: present (0); absent (1). Changes in scorings of Forasiepi *et al.* (2015): *Pucadelphys* 1 > 0; *Andinodelphys* ? > 0.

350. — **Ventral curvature of the tuber calcis (F293)**: present (0); absent (1). Changes in scorings of Forasiepi *et al.* (2015): *Mayulestes* 1 > 0.

351. — **Calcaneus, Notch for cuboid pivot on calcaneocuboid facet (F294)**: absent (0); present (1). Changes in scorings of Forasiepi *et al.* (2015): *Andinodelphys* ? > 0.

352. — **Calcaneus, angle between proximal and distal areas of calcaneocuboid facet (F295)**: no angle (0); oblique facet (1). Changes in scorings of Forasiepi *et al.* (2015): *Andinodelphys* ? > 1.

353. — **Spatial relationship between navicular and entocuneiform (F296)**: entocuneiform distal to navicular (0); entocuneiform extends proximally and medial to the distal area of the navicular (1). Changes in scorings of Forasiepi *et al.* (2015): *Andinodelphys* ? > 0.

APPENDIX 1. — Continuation.

354. — **Angle between navicular and distal metatarsal facets of ectocuneiform (F297)**: oblique (0); parallel to the distal facet (1).

355. — **Prehallux (F298)**: absent (0); present (1).

356. — **Metatarsal V proximal process (F299)**: does not extend ventral to cuboid (0); extends ventral to cuboid (1).

357. — **Proximal ends of metatarsal II and III (F300)**: subequal in length (0); Mt II extends more proximally than Mt III (1).

358. — **Ridge on proximal articular facet of metatarsal I (F301)**: absent (0); present (1).

359. — **Mt III thickness relative to that of Mt IV (F302)**: Mt III thicker or subequal to Mt IV (0); Mt III thinner (1).

360. — **Mt III thickness relative to that of Mt I (F303)**: Mt I thicker or subequal than Mt III (0); Mt III thinner than Mt I (1). Changes in scorings of Forasiepi *et al.* (2015): *Andinodelphys* ? > 1.

361. — **Median keel on palmar/plantar surface of metapodials (F304)**: sharp (0); blunt (1). Changes in scorings of Forasiepi *et al.* (2015): *Pucadelphys* ? > 0,1; *Mayulestes* ? > 0.

362. — **Foot ungual phalanx of digit IV in proximal view (F305)**: larger dorsoventrally than mediolaterally (0); larger mediolaterally than dorsoventrally (1). Changes in scorings of Forasiepi *et al.* (2015): *Pucadelphys*, *Andinodelphys* ? > 0.

363. — **Ungual phalange (F306)**: uncleft (0); cleft (1). Changes in scorings of Forasiepi *et al.* (2015): *Pucadelphys*, *Andinodelphys* ? > 1.

364. — **Dorsal border of ungual phalanges (F307)**: crest-like (0); rounded (1). Changes in scorings of Forasiepi *et al.* (2015): *Pucadelphys*, *Andinodelphys* ? > 0.

Appendix 2. — Taxon list, specimens, and references.

*Allqokirus australis*
YPFB pal 6188, 6189, 6190, MHNC 8267. Marshall & Muizon (1988), Muizon (1992).

*Amphiperatherium ambiguum*
MNHN.F.QU8215, QU8218.

*Amphiperatherium exile*
MNHN.F.PFR10356, PFR8413.

*Amphiperatherium lamandini*
MNHN.F.PFR10356, PFR8413.

*Amphiperatherium minutum*
MNHN.F.GY7912, GY681, GY683.

*Andinodelphys cochabambensis*
MHNC 8264, 8306, 8308, 8370, 13847, 13925 13927, 13928 (five sub-complete skulls and four subcomplete to partial skeletons). Marshall & Muizon (1988), Muizon (1992), Muizon *et al.* (1997), Muizon & Argot (2003).

*Arctodictis sinclairi*
MLP 85-VII-3-1. Forasiepi (2009).

*Asiatherium reshetovi*
Cast and original specimen of PIN 3907. Szalay & Trofimov (1996).

*Asioryctes nemegtensis*
Cast of ZPAL MgM-I/56 and I/98. Kielan-Jaworowska (1975a, 1977, 1981); Horovitz (2000); Horovitz & Sánchez-Villagra (2003); Wible et *al.* (2009).

*Australohyaena antiqua*
Forasiepi *et al.* (2015).

*Borhyaena tuberata*
YPM-PU 15120, 15701, MACN 2074, Sinclair (1906) Cabrera (1927), Marshall (1981), Argot (2003c).

*Callistoe vincei*
PVL 4187. Babot et *al.* (2002), Argot & Babot (2011).

*Cladosictis centralis*
MNHN.F.COL4. Marshall (1981).

*Cladosictis patagonica*
MNHN.F.SCZ143, 146, YPM-PU 15170, 15702, 15705, 15046. Sinclair (1906), Cabrera (1927), Patterson (1965), Marshall (1981), Argot (2003b)

*Dasyurus hallucatus*
MNHN.ZM.MO.1854-99, 1880-1019, A12425.

*Dasyurus maculatus*
MNHN.ZM.AC.A3295, 1994-2140, 1865-32; FMHN 119806, 119805, 119804, 119803.

*Dasyurus viverrinus*
MNHN.ZM.AC.A2626, A2627, A3315, 1882-563, 1883-1537.

*Deltatheridium pretrituberculare*
Casts of ZPAL MgM-I/102, ZPAL MgM-I/9; casts and original specimens of PSS MAE-133 and 132; Kielan-Jaworowska (1975b), Rougier et *al.* (1998).

*Deltatheroides cretacicus*
AMNH 21700, PSS-MAE 615. Gregory & Simpson (1926a, b); Rougier *et al.* (2004).

*Didelphis albiventris*
MNHN RH 24, 120, 161, MNHN RH uncat.

*Didelphodon vorax*
Cast of USNM 2136, UC 52326, UC 46946, UC 52342, UC 51419, UC 46962, UC 48189, UC48581, UC 52290, UC 47304, UC 53181, UC 52289. Clemens (1966, 1968), Fox & Naylor (1986); Wilson et *al.* (2016).

*Dromiciops gliroides*
IEEUACG 2162, 2167; FMNH 22675, 134556.

*Eodelphis browni*
Cast of AMNH 14169. Matthew (1916), Fox (1981).

*Herpetotherium cf. fugax*
PIMUZ 2613, MB.Ma 50671, 50672, SMF 2000/168, 2000/169. Horovitz et *al.* (2008, 2009).

*Herpetotherium fugax*
FMNH P25654, P25653, P15329. Fox (1983), Korth (1994), Gabbert (1998).

*Hondadelphys fieldsi*
Photos of UCMP 37960, Marshall (1976b).

*Itaboraidelphys camposi*
Casts of DGM 804-M, 814-M, 817-M, 923-M, 926-M; MNRJ 2878-V a and b; Marshall & Muizon (1984).

*Kokopellia juddi*
OMNH 26361, 34200, 33248, 33243, 27639. Cifelli (1993); Cifelli & Muizon (1997).

*Lycopsis longirostris*
Photos of UCMP 38061. Marshall (1977), Argot (2004b).

APPENDIX 2. — Continuation.

*Maelestes gobiensis*
PPS-MAE-607, Wible et *al*. (2009).

*Mayulestes ferox*
MHNC 1249 (holotype). Muizon (1994, 1998), Argot (2001, 2002, 2003a)

*Metachirus nudicaudatus*
MNHN RH 16, 81, MNHN RH uncat, MNHN. ZO.AC.2175.

*Mimoperadectes houdei*
USNM 482355. Horovitz et *al*. (2009).

*Mimoperadectes labrus*
Cast of UM 66144.

*Monodelphis brevicaudata*
MNHN.ZO.AC.258-M, 2004-317, 1995-3216, 1967-330. Wible (2003).

*Nanodelphys hunti*
Cast of AMNH 5266, 5267, Korth (1994),

*Notogale mitis*
MNHN.F.SAL94, 95, 97, 271. Patterson & Marshall (1976), Marshall (1981), Petter & Hoffstetter (1983), Muizon (1999).

*Paraborhyaena boliviana*
MNHN.F.SAL51. Petter & Hoffstetter (1983).

*Patene colhuapiensis*
Cast of AMNH 28448. Simpson (1935), Marshall (1981).

*Patene simpsoni*
MNHN.F.ITB1, cast of AMNH 49805, DGM 324-M, DGM 654-M, DGM 655-M, 657-M, DGM 659-M, 656-M, MNRJ 1331-V, 1332-V, 1341-V, 1351-V, photos of PVL 2618. Casts of uncatalogued Itaboraí specimens of DGM, with MNHN catalogue numbers: MNHN.F.ITB8, 9, 11, 63, 64. Paula Couto (1952), Marshall (1981), Goin et *al*. (1986).

*Peradectes* spp.
*P. elegans*: cast of AMNH 17383;
*P. pauli*: cast of USNM 20879;
*P. chesteri*: cast of UM 71663, USNM 19199. Krishtalka & Stucky (1983a, b, 1984); Kurz & Habersetzer (2004). Kurz (2005).

*Peratherium antiquum*
MNHN.F.PFR10363, PFR10302, PFR10314, PFR10436, PFR10440, PFR8367, PFR8392, MNHN.F.QU8214.

*Peratherium cuvieri*
MNHN.F.GY7904, GY7905, GY679.

*Peratherium elegans*
MNHN.F.RZN2, RZN4, RZN6, RZN8, RZN12, RZN19, RZN26; MNHN.F.QU8216, QU8217.

*Peratherium* sp.
MNHN.F.QU13359 to QU13373, QU8001 to QU8033, QU8035 to QU8067.

*Pharsophorus lacerans*
MNHN.F.SAL69, SAL272, YPM-PU 20551 (same individual as MNHN.F.SAL69), AMNH 29591. Cabrera (1927), Patterson & Marshall (1978), Marshall (1978).

*Prokennalestes trofimovi*
PSS-MAE 136; Kielan-Jaworowska & Dashzeveg (1989); Sigogneau-Russell et *al*. (1992); Wible *et al.* (2001).

*Prothylacynus patagonicus*
MACN 705, 707 (same individual), MACN 642, YPM-PU 15700, MACN 5931. Sinclair (1906), Cabrera (1927), Marshall (1979), Argot (2003c).

*Pucadelphys andinus*
MHNC 8265, 8266, 8365, 8376 to 8395 (all specimens include complete or partial skull and mandibles). Marshall & Muizon (1988, 1995), Muizon (1992), Marshall & Sigogneau-Russell (1995), Argot (2001, 2002, 2003a), Muizon & Argot (2003).

*Sallacyon hoffstetteri*
MNHN.F.SAL92, 93. Villarroel & Marshall (1982), Petter & Hoffstetter (1983).

*Sipalocyon gracilis*
YPM PU 15373, 15154, 15029, AMNH 9254, MACN 691, 692, Sinclair (1906), Cabrera (1927), Marshall (1981), Argot (2003b).

*Sminthopsis crassicaudata*
FMNH 60116; FMNH 104788.

*Sminthopsis* sp.
MNHN.ZM.AC.1919-30, 1892-660.

*Thylacinus cynocephalus*
MNHN.ZM.AC.A2620, A2621, A3299, A3298, A12413.

*Thylacosmilus atrox*
Cast of FMNH P 14531. Riggs (1934), Turnbull & Segall (1984), Goin & Pascual (1987), Argot (2004c).
*Acyon* Ameghino, 1887

APPENDIX 3. — List of genus and species names cited in the text with authorship and year.

*Acyon myctoderos* Forasiepi, Sánchez-Villagra, Goin, Takai, Shigehara & Kay, 2006
*Allqokirus australis* Marshall & Muizon, 1988
*Amphiperatherium* Filhol, 1879
*Amphiperatherium ambiguum* (Filhol, 1877)
*Amphiperatherium exile* (Gervais, 1848-52)
*Amphiperatherium lamandini* (Filhol, 1876)
*Amphiperatherium minutum* (Aymard, 1846)
*Andinodelphys* Marshall & Muizon, 1988
*Andinodelphys cochabambensis* Marshall & Muizon, 1988
*Arctodictis* Mercerat, 1891
*Arctodictis munizi* Mercerat, 1891
*Arctodictis sinclairi* Marshall, 1978
*Arminiheringia* Ameghino, 1902
*Asiatherium* Trofimov & Szalay, 1994
*Asiatherium reshetovi* Trofimov & Szalay, 1994
*Asioryctes* Kielan-Jaworowska, 1975
*Asioryctes nemegtensis* Kielan-Jaworowska, 1975
*Australohyaena* Forasiepi, Babot, & Zimicz, 2015
*Australohyaena antiqua* Forasiepi, Babot, & Zimicz, 2015
*Badjcinus* Muirhead & Wroe, 1998
*Bobbschaefferia* Paula Couto, 1970
*Bobbschaefferia fluminensis* Paula Couto, 1970
*Borhyaena* Ameghino, 1887
*Borhyaena tuberata* Ameghino, 1887
*Callistoe* Babot, Powell & Muizon, 2002
*Callistoe vincei* Babot, Powell & Muizon, 2002
*Caluromys* Allen, 1900
*Cladosictis* Ameghino, 1887
*Cladosictis centralis* Ameghino, 1902
*Cladosictis patagonica* Ameghino, 1887
*Crocuta* Kaup, 1828
*Dasyurus* Geoffroy Saint-Hilaire, 1796
*Dasyurus hallucatus* Gould, 1842
*Dasyurus maculatus* (Kerr, 1792)
*Dasyurus viverrinus* (Shaw, 1800)
*Deltatheridium* Gregory & Simpson, 1926
*Deltatheridium pretrituberculare* Gregory & Simpson, 1926
*Deltatheroides* Gregory & Simpson, 1926
*Deltatheroides cretacicus* Gregory & Simpson, 1926
*Didelphis* Linnaeus, 1758
*Didelphis albiventris* Lund, 1840
*Didelphodon* Marsh, 1899
*Didelphodon vorax* Marsh, 1899
*Didelphodon coyi* Fox & Naylor, 1986
*Dromiciops* Thomas, 1894
*Dromiciops gliroides* Thomas, 1894
*Eodelphis* Matthew, 1916
*Eodelphis browni* Matthew, 1916
*Epidolops* Paula Couto, 1952
*Epidolops ameghinoi* Paula Couto, 1952
*Herpetotherium* Cope, 1873
*Herpetotherium fugax* Cope, 1873
*Herpetotherium valens* Lambe, 1908
*Hondadelphys* Marshall, 1976
*Hondadelphys fieldsi* Marshall, 1976
*Itaboraidelphys Marshall & Muizon, 1984*
*Itaboraidelphys camposi Marshall & Muizon, 1984*
*Jaskhadelphys* Marshall & Muizon, 1988
*Kokopellia* Cifelli, 1993
*Kokopellia juddi* Cifelli, 1993
*Kryptobaatar* Kielan-Jaworowska, 1969
*Lycopsis* Cabrera, 1927
*Lycopsis longirostris* Marshall, 1976
*Maelestes* Wible, Rougier, Novacek, & Asher, 2007
*Maelestes gobiensis* Wible, Rougier, Novacek, & Asher, 2007
*Marmosa* Gray, 1821
*Mayulestes* Muizon, 1994
*Mayulestes ferox* Muizon, 1994
*Metachirus* Burmeister, 1854
*Metachirus nudicaudatus* Geoffroy Saint-Hilaire, 1803
*Mimoperadectes* Bown & Rose, 1979
*Mimoperadectes houdei* Horovitz, Martin, Bloch, Ladevèze, Kurz & Sánchez-Villagra, 2009
*Mimoperadectes labrus* Bown & Rose, 1979
*Monodelphis* Burnett, 1830
*Monodelphis brevicaudata* (Erxleben, 1777)
*Morganucodon* Kühne, 1949
*Nanodelphys hunti* (Cope, 1873)
*Nimbacinus* Muirhead & Archer, 1990
*Notogale* Loomis, 1914
*Notogale mitis* (Ameghino, 1897)
*Panthera* Oken, 1816
*Paraborhyaena* Hoffstetter & Petter, 1983
*Paraborhyaena boliviana* Hoffstetter & Petter, 1983
*Patene* Simpson, 1935
*Patene colhuapiensis* Simpson, 1935
*Patene simpsoni* Paula Couto, 1952
*Pediomys* Marsh, 1889
*Peradectes* Matthew & Granger, 1921
*Peradectes elegans* Matthew & Granger, 1921
*Peradectes pauli* Gazin, 1956
*Peradectes chesteri* Gazin, 1952
*Peratherium* Aymard, 1850
*Peratherium antiquum* (Blainville, 1840)
*Peratherium cuvieri* (Fischer, 1829)
*Peratherium elegans* (Aymard, 1846)
*Pharsophorus* Ameghino, 1897
*Pharsophorus lacerans* Ameghino, 1897
*Philander* Brisson, 1762
*Procaroloameghinia* Marshall, 1982
*Procaroloameghinia pricei* Marshall, 1982
*Prokennalestes* Kielan-Jaworowska & Dashzeveg, 1989
*Prokennalestes trofimovi* Kielan-Jaworowska & Dashzeveg, 1989
*Prokennalestes minor* Kielan-Jaworowska & Dashzeveg, 1989
*Prothylacynus* Ameghino, 1891
*Prothylacynus patagonicus* Ameghino, 1891
*Pucadelphys* Marshall & Muizon, 1988

APPENDIX 3. — Continuation.

*Pucadelphys andinus* Marshall & Muizon, 1988
*Sallacyon* Villarroel & Marshall, 1982
*Sallacyon hoffstetteri* Villarroel & Marshall, 1982
*Sarcophilus* Geoffroy Saint-Hilaire & Cuvier, 1837
*Sipalocyon* Ameghino, 1887
*Sipalocyon gracilis* Ameghino, 1887
*Sminthopsis* Thomas, 1887
*Sminthopsis crassicaudata* Gould, 1844
*Thylacinus* Temminck, 1824
*Thylacinus cynocephalus* (Harris, 1808)
*Thylacosmilus* Riggs, 1934
*Thylacosmilus atrox* Riggs, 1934
*Thylamys* Gray, 1843
*Varalphadon* Johanson, 1996
*Varalphadon janetae* Carneiro, 2018
*Vincelestes* Bonaparte, 1986